



Cardiff
Catalysis Institute

Sefydliad Catalysis
Caerdydd

Synthesis of Size Controlled Metal Nanoparticles using Microwave and Sonochemical Approaches

Thesis submitted in accordance with the requirements of Cardiff
University for the degree of Doctor of Philosophy by

Manuel Pedro Simplicio Grasina

School of Chemistry

Cardiff University

2019

Primary Supervisor(s)

Professor Stuart Taylor

Dr. Nikolaos Dimitratos

Abstract

This work aimed to produce using different and new microwave and ultrasound protocols monometallic metal nanoparticles of gold, palladium, silver, iridium and copper (Au, Pd, Ag, Ir and Cu) and bimetallic alloys of AuPd. The developed batch and continuous flow protocols originated from batch optimisation work mainly carried out with microwave synthesis of Au nanoparticles and were based on the sol-immobilization method with the production of stabilized colloids in water, organic solvents or a mixture of both, with PVA and PVP being used as stabilizers and ethylene glycol as the main organic solvent.

The produced metal nanoparticles will be used for improving and developing current catalytic applications and eventually will be hugely beneficial for society. To tackle this multidisciplinary project the following targets have been chosen: To develop new metal nanoparticles synthesis protocols characterised by reduced synthesis time, improved production, minimal operation cost, minimal use of toxic reagents and controlled size and shape and to utilise the synthesised materials to convert fossil and bio-renewable feedstock via sustainable catalytic processes.

This thesis could be divided into four areas: The first (chapter 3) focused on microwave synthesis of monometallic metal nanoparticles of Au, Pd, Ag, Ir and Cu and bimetallic metal nanoparticles of the alloy type of AuPd at different molar ratios (7:1, 3:1, 1:1, 1:3, 1:7). This included work carried out under batch and continuous flow regime; The second (chapter 4) focused on ultrasound synthesis of monometallic metal nanoparticles of Au, Pd and bimetallic metal nanoparticles of the alloy type of AuPd at a molar ratio of 1:1. All work was carried out under batch regime; The third (chapter 5) saw the application of several characterisation techniques (TEM, SEM/EDX, XPS and DRIFTS) to selected metal nanoparticles produced by microwave and ultrasound synthesis and supported on TiO₂, C and CeO₂. This provided important information regarding particles average size, shape, loading, composition, stabilizer traces and oxidation state; The fourth (chapter 6) focused on catalytic testing of some of the supported metal nanoparticles by using them as heterogeneous catalysts in liquid/gas phase reactions. In total seven reactions were tested, namely 4-nitrophenol reduction, carbon monoxide oxidation, propane total oxidation, furfural hydrogenation, cinnamaldehyde hydrogenation, formic acid decomposition and hydrazine decomposition;

Even though some future work is mentioned in chapter 7, the main conclusion is that the new non-conventional synthesis protocols developed for this work have already allowed to address challenging issues in the areas of green chemistry, catalysis and materials design. This positive outcome offers a potential impact in future projects relating to water purification, biomass transformation and hydrogen storage and production.

Acknowledgements

The author would like to thank the Engineering and Physical Sciences Research Council for the funding and Cardiff University and Università degli Studi di Milano for providing excellent conditions to perform the research. The author would also like to thank the internal and external supervisors Professor Stuart Taylor, Professor Graham Hutchings, Dr. Nikolaos Dimitratos, Dr. Ceri Hammond and Dr. Alberto Villa for the guidance provided throughout the research. The author is also grateful to the remaining academic and professional staff who contributed in anyway to the outcome achieved during this PhD, in particular Dr. Qian He, Dr. Michal Perdjon and Dr Thomas Davies. Finally, the author would like to thank all the research colleagues with whom has shared the office, the laboratory and the equipment on a daily basis and to whom has many times turned seeking solutions and ideas to address several research issues, in particular Davide Motta, Felipe Sanchez, Daniele Padovan and Briony Munslow.

Last but not least, I am forever grateful for the family support and all the opportunities this PhD has unlocked on a personal level. It has allowed me to meet extraordinary friends, including my girlfriend, and turn Cardiff into a home, for the present and for the future, in reality a second home as I remained and will remain divided between two countries.

"I have a friend who's an artist and has sometimes taken a view which I don't agree with very well. He'll hold up a flower and say, "look how beautiful it is," and I'll agree. Then he says, "I as an artist can see how beautiful this is but you as a scientist take this all apart and it becomes a dull thing," and I think that he's kind of nutty. First of all, the beauty that he sees is available to other people and to me too, I believe. Although I may not be quite as refined aesthetically as he is ... I can appreciate the beauty of a flower. At the same time, I see much more about the flower than he sees. I could imagine the cells in there, the complicated actions inside, which also have a beauty. I mean it's not just beauty at this dimension, at one centimetre; there's also beauty at smaller dimensions, the inner structure, also the processes. The fact that the colours in the flower evolved in order to attract insects to pollinate it is interesting; it means that insects can see the colour. It adds a question: does this aesthetic sense also exist in the lower forms? Why is it aesthetic? All kinds of interesting questions which the science knowledge only adds to the excitement, the mystery and the awe of a flower. It only adds. I don't understand how it subtracts."

Richard P. Feynman*

Table of Contents

1	Introduction.....	1
1.1	Metal Nanoparticles.....	1
1.2	Light Interaction with Metal Nanoparticles	7
1.3	Synthesis of Metal Nanoparticles	11
1.4	Sol-Immobilization Synthesis Method	16
1.4.1	Overview	17
1.4.2	Conventional Protocols	21
1.4.3	Microwave Synthesis	29
1.4.4	Ultrasound Synthesis	35
1.5	Continuous Flow Synthesis	40
1.6	Model Reactions Overview.....	43
1.6.1	4-Nitrophenol Reduction	44
1.6.2	Carbon Monoxide Oxidation	45
1.6.3	Propane Total Oxidation	46
1.6.4	Furfural Hydrogenation	47
1.6.5	Cinnamaldehyde Hydrogenation.....	48
1.6.6	Formic Acid Decomposition	49
1.6.7	Hydrazine Decomposition	50

2 Experimental, Methods and Characterisation.....51

2.1	Chemicals, Materials, Products and Equipment	51
2.2	Analytical and Characterisation Techniques	56
2.2.1	Ultraviolet–Visible Spectroscopy (UV-Vis).....	56
2.2.2	Dynamic Light Scattering (DLS).....	59
2.2.3	Transmission Electron Microscopy (TEM)	61
2.2.4	Scanning Electron Microscopy and Energy Dispersive X-ray (SEM/EDX).....	63
2.2.5	X-ray Photoelectron Spectroscopy (XPS).....	64
2.2.6	Diffuse Reflectance Infrared Fourier Transform Spectroscopy (DRIFTS).....	66
2.2.7	Gas Chromatography (GC).....	67
2.2.8	Liquid Chromatography (LC).....	70
2.2.9	Nuclear Magnetic Resonance Spectroscopy (NMR)	71
2.3	Microwave Synthesis.....	73
2.4	Ultrasound Synthesis	75
2.5	Immobilisation of Metal Colloids	77
2.6	Heat Treatment	79
2.7	Model Reactions Experimental Procedure.....	80
2.7.1	4-Nitrophenol Reduction	81
2.7.2	Carbon Monoxide Oxidation	82
2.7.3	Propane Total Oxidation	84
2.7.4	Furfural Hydrogenation	85
2.7.5	Cinnamaldehyde Hydrogenation.....	87
2.7.6	Formic Acid Decomposition	89
2.7.7	Hydrazine Decomposition	90

3 Synthesis of Metal Nanoparticles by Microwave.....91

3.1	Overview	91
3.2	Au Optimisation Tests	93
3.2.1	Stirrer	96
3.2.2	Metal Concentration	97
3.2.3	Holding Time and Temperature	98
3.2.4	Acid/Base Addition	100
3.2.5	Solvent	102
3.2.6	Solvent Composition	104
3.2.7	Stabilizer	106
3.3	Mechanistic Studies	111
3.3.1	Conventional Heating vs. Microwave Heating	111
3.3.2	Au ³⁺ Reduction Behaviour and NaOH Effect	114
3.3.3	Role of Acetaldehyde as Reducing Agent	120
3.3.4	H ¹ NMR and C ¹³ NMR Analysis	123
3.3.5	Influence of Au Precursor Oxidation State.....	133
3.4	Selected Operating Conditions, Stability and Reproducibility.....	134
3.5	Metal Nanoparticles Production under Batch Regime.....	139
3.5.1	Au Nanoparticles.....	141
3.5.2	Pd Nanoparticles.....	149
3.5.3	Ag Nanoparticles.....	156
3.5.4	Ir Nanoparticles	162
3.5.5	Cu Nanoparticles.....	168
3.5.6	AuPd Nanoparticles	171

3.6	Metal Nanoparticles Production under Continuous Flow Regime	179
3.6.1	Au Nanoparticles.....	180
3.6.2	Pd Nanoparticles.....	182
3.7	Conclusions.....	184
4	Synthesis of Metal Nanoparticles by Ultrasound	185
4.1	Overview	185
4.2	Au Optimisation Tests	186
4.2.1	Wave Amplitude	190
4.2.2	Metal Concentration	191
4.2.3	Sonication Time	193
4.2.4	Solvent Composition	195
4.2.5	Stabilizer	197
4.3	Selected Operating Conditions, Stability and Reproducibility.....	200
4.4	Metal Nanoparticles Production under Batch Regime.....	202
4.4.1	Au Nanoparticles.....	204
4.4.2	Pd Nanoparticles.....	208
4.4.3	AuPd Nanoparticles	211
4.5	Conclusions.....	216

5	Catalysts Characterisation.....	217
5.1	Overview	217
5.2	Transmission Electron Microscopy (TEM)	218
5.3	Scanning Electron Microscopy and Energy Dispersive X-ray (SEM/EDX)	236
5.4	X-ray Photoelectron Spectroscopy (XPS).....	238
5.5	Diffuse Reflectance Infrared Fourier Transform Spectroscopy (DRIFTS) ..	244
6	Model Reactions Experimental Results	247
6.1	Overview	247
6.2	4-Nitrophenol Reduction.....	248
6.3	Carbon Monoxide Oxidation	253
6.4	Propane Total Oxidation.....	258
6.5	Furfural Hydrogenation.....	260
6.6	Cinnamaldehyde Hydrogenation	263
6.7	Formic Acid Decomposition.....	267
6.8	Hydrazine Decomposition.....	269
7	Conclusions and Future Work	270

1 Introduction

1.1 Metal Nanoparticles

According to Zamborini *et al.*¹ a nanoparticle is “any material with at least one dimension in the 1–100 nm range. The shape may vary (it does not have to be spherical) and the materials include metals, semiconductors, polymers and carbon-based materials”. For this PhD emphasis was given to metal nanoparticles for catalytic purposes even though they also find application in a range of different fields such as textile, electronics, biology or medicine.^{2,3}

Metal nanoparticles have properties (electromagnetic, optical, biological, thermal) dependent on their size and shape, which can greatly affect their catalytic activity. In particular, as the size decreases there is a splitting of the energy band, a density of states where electrons are delocalized over the entire particle, into discrete energy levels, similar to what is observed for a single atom, and the HOMO-LUMO gap increases (Figure 1). As a result, there will be a higher availability of electrons to form new bonds and undergo redox reactions.

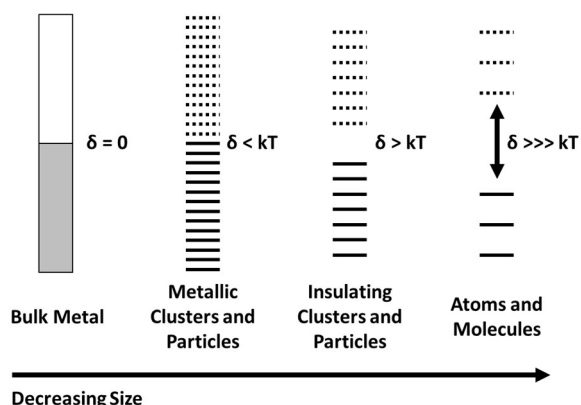


Figure 1 – Density of states and HOMO-LUMO gap (δ) as a function of the metal particle size.

(adapted from the literature)⁴

Moreover, as the metal particle size decreases the percentage of metal surface atoms becomes higher. These surface atoms are less coordinated than bulk atoms and for this reason have a higher reactivity to form new bonds in order to decrease their energy.⁴ When a support or a dopant substance is employed there are also important interactions, either because there is charge transfer, or the edge effects at the metal interface become relevant or there is a spillover effect with migration of atoms through diffusion.⁵

Introduction

1.1 Metal Nanoparticles

Typical metal particle size trends for the variation of the fraction of surface, corner and edge atoms⁶, for the thermal conductivity⁷ and for the melting point temperature⁸ are presented in Figure 2 as found in the literature. In section 1.2 the metal particle size effect on the optical properties is presented in more detail.

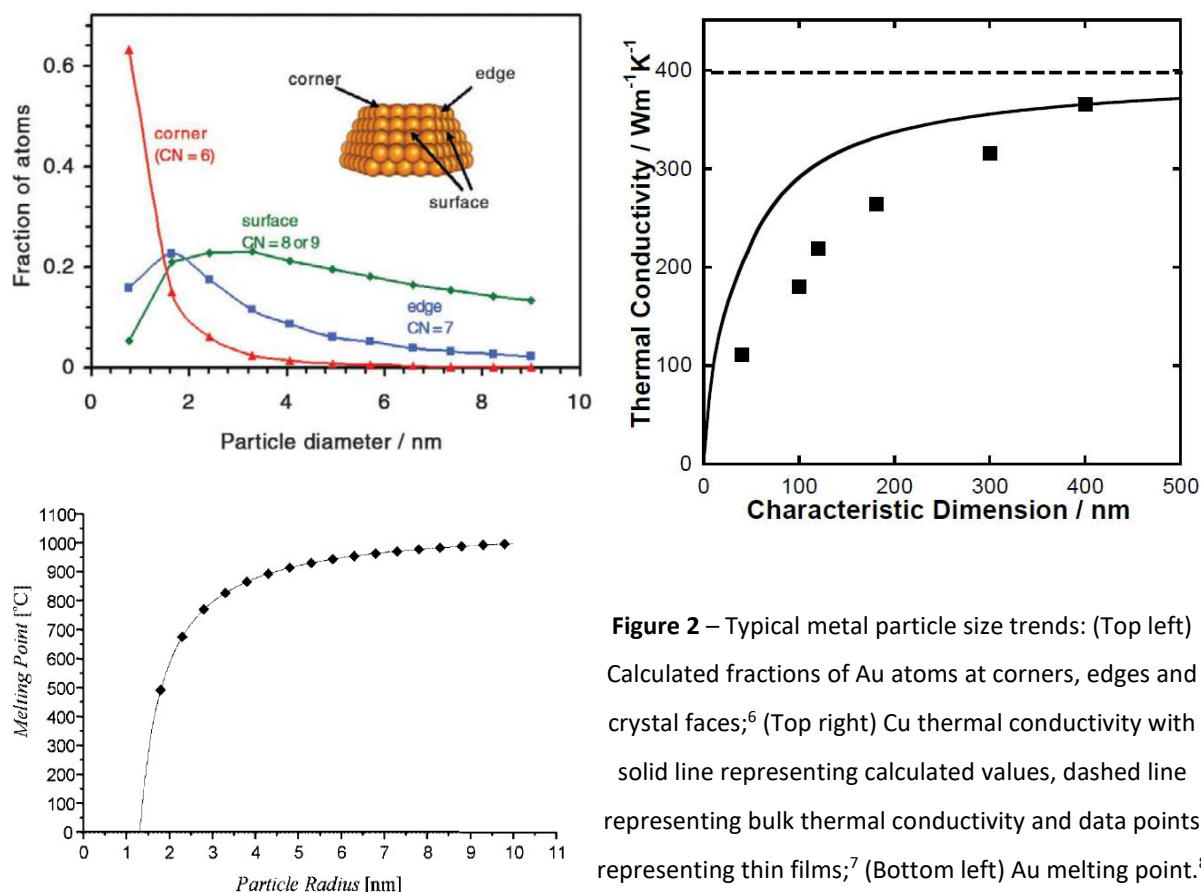


Figure 2 – Typical metal particle size trends: (Top left) Calculated fractions of Au atoms at corners, edges and crystal faces;⁶ (Top right) Cu thermal conductivity with solid line representing calculated values, dashed line representing bulk thermal conductivity and data points representing thin films;⁷ (Bottom left) Au melting point.⁸

The metal behaviour with particle size and shape explains why bulk gold, which had been regarded for a long time as an inactive catalyst, could be transformed into an excellent catalyst when moving to the nanoparticle domain. The works in the early 90's of Haruta⁹, with carbon monoxide oxidation at low temperature, and of Hutchings¹⁰, first with hydrochlorination of ethyne to vinyl chloride and later with direct synthesis of hydrogen peroxide, were paramount to make gold catalysts the subject of high interest. Even though most gold catalysis publications are dominated by heterogeneous catalysis (both the two aforementioned works) there were also recent developments in the homogeneous catalysis field with a good example being the work of Hashmi *et al.*¹⁰ who were able to extend from alkynes to alkenes the intramolecular nucleophilic addition of alcohols and the intramolecular nucleophilic addition of aromatic compounds.

Introduction

1.1 Metal Nanoparticles

The catalytic applications of metal nanoparticles are vast and some of the synthesised metal nanoparticles for this PhD, mainly Au, Pd and bimetallic AuPd alloys, were supported and successfully tested in seven reactions, namely:

- a) Aqueous 4-Nitrophenol reduction (liquid phase);
- b) Carbon monoxide oxidation (gas phase);
- c) Propane total oxidation (gas phase);
- d) Furfural hydrogenation (liquid phase);
- e) Cinnamaldehyde hydrogenation (liquid phase);
- f) Aqueous formic acid decomposition (liquid phase);
- g) Hydrous hydrazine decomposition (liquid phase);

The reaction schemes for these seven reactions and their importance in light of the targets defined for this PhD are presented in section 1.6.

An important consideration when working with metal nanoparticles designed for catalytic purposes relates to the interaction of the substrate/product to the catalyst surface, expressed by the adsorption energy, which should be neither too strong nor too weak (Sabatier principle). This is better understood by observing Figure 3, with a volcano plot of the activity for two different arbitrary metal species (A and B) and for an arbitrary reaction presented.

For metal A the adsorption energy is too low, making the adsorption of the substrate to the catalyst surface more difficult and causing the activity, expressed by the turnover frequency (TOF), to be low. For metal B, there is also low activity but due to the opposite effect, *i.e.* the adsorption energy is too high, making more difficult desorption of the product from the catalyst surface.

Therefore, the choice of the right metal for a certain reaction is a crucial step, but the adsorption energy does not depend only on the type of metal, the adsorption energy is greatly affected by particle size as well, with this effect being also explained in Figure 3. When metal A has its particle size reduced (A to A*) the adsorption energy increases and the activity increases by moving to the right on the volcano plot, whereas when metal B has its particle size reduced (B to B*) even though the adsorption energy increases the activity decreases by moving to the right on the volcano plot. This effect explains why for example a bulk metal that would be very active for a certain reaction could shift its activity to lower values when it becomes a nanoparticle.

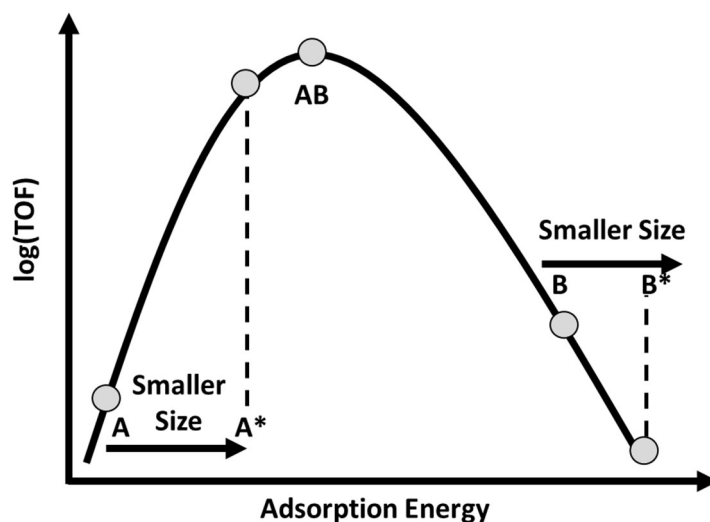


Figure 3 – Activity behaviour of mixed systems with the turnover frequency (TOF) of metals A, B and 1:1 AB alloy as a function of the adsorption energy.

(adapted from the literature)⁴

As shown in Figure 3 it is also possible to transform two catalysts presenting a low activity (A and B) into an excellent catalyst by mixing them and creating a bimetallic catalyst (AB). The total activity can be estimated by approximating the adsorption energy of the bimetallic catalyst to the average of the adsorption energies of each metal A and B. The synthesis of bimetallic catalysts, mainly AuPd alloy with 1:1 molar ratio, was also an objective for this PhD.

Bimetallic catalysts can be tuned to have not only different compositions but also different structures as shown in Figure 4, with the most common being the alloy. According to Horikoshi and Serpone¹¹ much attention has recently been paid to core-shell structures with strategies including mixing an inexpensive metal (core) with a noble metal (shell). Similar to what happens with an alloy structure, with a core-shell structure the adsorption energy also changes as shown in Figure 3 (AB) as there is an electronic transfer between the core and shell metals. At the same time the catalytic activity can also be enhanced by changing the structure from alloy to core-shell due to increased stability, for example the core metal is less likely to become inactive as it is less likely to interact with a solvent, be poisoned or change oxidation state.

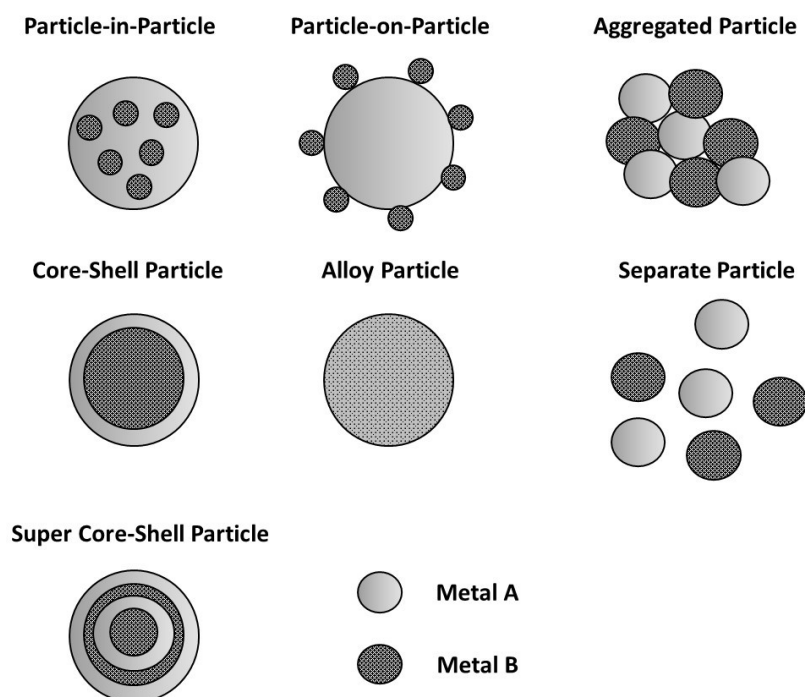


Figure 4 – Different morphologies for bimetallic nanoparticles.

(adapted from the literature)¹²

It is extensive the amount of research focused on the effect of the composition and structure of bimetallic nanoparticles on the experimental results. Even though the topics are not limited only to catalysis, but include other fields, such as sensors, electronics, energy storage and photocatalysis¹³, special interest was dedicated to the catalytic work with bimetallic AuPd nanoparticles, in particular supported on commercial P25 titanium dioxide (TiO₂), as this represents one of the main objectives for this PhD. The TiO₂ is a common support used as reference due to its well-known properties.

A model reaction that can be used to demonstrate the effect of the metal composition and structure of a bimetallic AuPd catalyst on the catalytic activity is the selective oxidation of benzyl alcohol to benzaldehyde. Silva *et al.*¹⁴ who have worked with bimetallic AuPd nanoparticles of the core-shell type, Au being the core and Pd being the shell, have obtained a Volcano-like behaviour for the catalytic activity just by changing the catalyst composition and keeping all the other operating conditions constant. For the Au:Pd molar ratio of 10:0.6 the reported benzaldehyde conversion was of 41.2 %. This conversion then increased to 87.7 % as the Pd content increased with the Au:Pd molar ratio set at 10:1. However, as the Pd content was further increased the conversion started to decrease again with a reported conversion of 17.5 % for the Au:Pd molar ratio of 10:4. For all the trials the selectivity to benzaldehyde remained similar and high, around 90 %.

Introduction

1.1 Metal Nanoparticles

Dimitratos *et al.*¹⁵ have also shown that different structures for the bimetallic AuPd nanoparticles ended up producing different results for the conversion and selectivity of the benzyl alcohol oxidation reaction, with the analysed structures including AuPd alloy, Au (core) + Pd (shell) and Au (shell) + Pd (core).

Another interesting work from Hosseini *et al.*¹⁶ focused on the toluene and propene total oxidation reactions. The previous authors have demonstrated that for the same operating conditions for both reactions the average oxidation temperature of 350 °C for Au/TiO₂ catalyst was greatly reduced to 200 °C when adding a Pd layer to the catalyst, therefore creating a bimetallic core-shell catalyst, Au being the core and Pd the shell. The previous authors have also reported different results when working with other bimetallic AuPd structures, namely of the alloy type and Au (shell) + Pd (core).

Introduction

1.2 Light Interaction with Metal Nanoparticles

1.2 Light Interaction with Metal Nanoparticles

Light interaction with all particles, regardless of size, produces different outcomes.¹⁷ The schematic representation shown in Figure 5 illustrates what happens to a beam of incident light with a certain energy, expressed by the wavelength (λ_0). Several main processes can be identified:

a) Absorption of energy from the incident light with the particle undergoing a transition to a higher energetic state followed by release of the same or different amount of energy in the form of light but propagated in several random directions. The fluorescence and thermal emission are an example of light released at a different energy level;

b) Reflection of the incident light, *i.e.* there is a change in direction from the incident light beam but the light wavelength is kept at λ_0 ;

c) Scattering of the incident light, similar to reflection but the light beam is propagated in several random directions. This process can further be divided into elastic scattering, if the wavelength of the scattered light is the same as the incident light, or inelastic scattering, if the wavelength of the scattered light is different from the incident light (Raman);

d) Refraction of the incident light, whereby the light passes through the particle but the light wavelength remains unchanged;

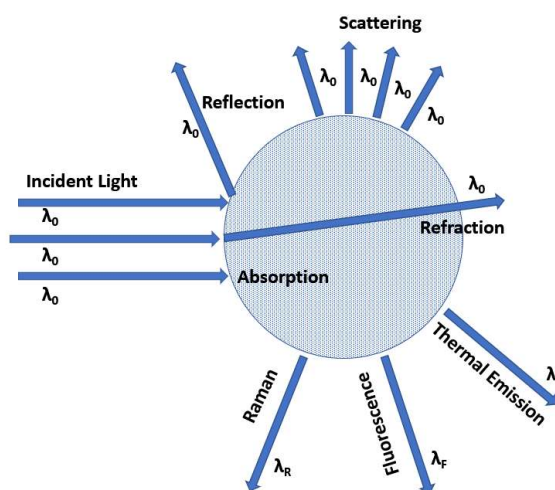


Figure 5 – Particle interaction with light.

(adapted from the literature)¹⁷

An optical property dependent on the size and shape of metal particles is the surface plasmon, which can be physically described as the collective movement of the conduction band electrons due to their interaction with an external electric field as it happens when the particles are subject to electromagnetic radiation.¹¹ A schematic representation of the surface plasmon effect is shown in Figure 6.

Introduction

1.2 Light Interaction with Metal Nanoparticles

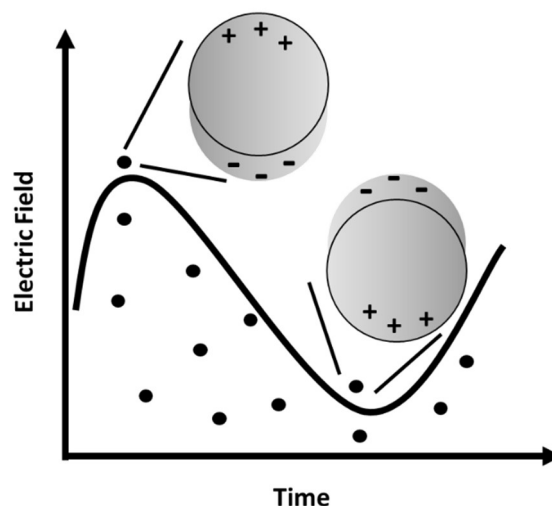


Figure 6 – Surface plasmon effect.

(adapted from the literature)¹¹

The conduction band electrons, which are constantly oscillating by trying to align with the external electric field, also produce their own electric field, which can create a resonance effect if the frequency of the two is to be equal. This effect represents a kind of polarization of the particle with the formation of an oscillating dipole.

When metal particles present sizes much smaller than the wavelength of the incident light, 400-700 nm for the visible light, as it happens with metal nanoparticles, a free electron can even be formed at the surface of the metal, causing a large resonant enhancement of the local field inside and near the nanoparticle, with strong absorption and scattering of the incident light taking place.

There is a wavelength of the electromagnetic spectrum where this surface plasmon resonance effect reaches a maximum, in most metals occurring mainly in the ultraviolet (UV) region, but in some cases, for example with Au, Ag, and Cu shifting to the visible (Vis) light domain due to electrons in the S atomic orbitals. This is the reason for the intense colour observed for colloid solutions of these metals.¹¹

The first theoretical treatment for the surface plasmon resonance effect was attempted by Rayleigh, whose theory applies for scattering of light by small spherical particles. However, this effect could be better described having in consideration the theory developed by Mie, who solved Maxwell equations for absorption and scattering of light by small spherical particle having the same frequency-dependent dielectric constant as the bulk metal. For particles presenting sizes much smaller than the incident visible light wavelength, the extinction cross section, a variable defining the energy losses in the direction of propagation of incident light due to absorption and scattering, can be approximated by Equation 1.¹⁸

Introduction

1.2 Light Interaction with Metal Nanoparticles

$$\sigma_{\text{ext}} = \frac{9 \cdot V \cdot \epsilon_m^{1.5}}{c} \frac{\omega \cdot \epsilon_2(\omega)}{[\epsilon_1(\omega) + 2 \cdot \epsilon_m]^2 + \epsilon_2(\omega)^2} \quad (1)$$

σ_{ext} is the extinction cross section (m^2), V is the nanoparticle volume (m^3), c is the speed of light in vacuum (m s^{-1}), ω is the angular frequency of incident light (rad s^{-1}), ϵ_m is the solvent dielectric constant and ϵ_1 is the nanoparticle dielectric constant. For metals the dielectric constant is dependent on the angular frequency and it is necessary to include the complex part (ϵ_2), also known as the dielectric loss.

Equation 1 is a quadratic function that returns approximately a maximum value for the extinction cross section when a wavelength is fulfilling the condition of $\epsilon_1 = -2 \cdot \epsilon_m$ and ϵ_2 is relatively small and/or constant. This wavelength represents an absorbance peak in a typical UV-Vis spectrum, commonly referred to as the plasmon peak.

Mie theory was further modified to take into account smaller particles sizes making the dielectric constant also dependent on the particle size, a more suitable approach for the modelling of metal nanoparticles. Equation 1 can even become limited as the size decreases further with the plasmon peak becoming increasingly damped. For sizes smaller than around 2 nm it has been experimentally observed the plasmon peak disappearing.¹⁸

The surface plasmon resonance effect allows a simple and fast technique such as UV-Vis spectroscopy to be employed to assess the metal nanoparticles synthesis experimental results (production, average size and size distribution). As metal nanoparticles deviate from their circular shape a second plasmon peak related to the movement of electrons along the major rod axis (longitudinal) can even appear at higher wavelengths. This second plasmon peak is particularly sensitive to changes in the aspect ratio R (longitudinal length divided by transversal length).¹⁸

More details about the correlation of the UV-Vis spectrum with the metal nanoparticles synthesis experimental results can be found in section 2.2.1. However, a typical trend for the UV-Vis spectrum of Au nanoparticles would be an increase of the plasmon peak wavelength as the average size increases. An example based on the work of Schwartzberg *et al.*¹⁹ is shown in Figure 7 (left) with the different photos at the bottom showing how the Au colloid colour varies with the position of the plasmon peak.

Introduction

1.2 Light Interaction with Metal Nanoparticles

The work of other authors²⁰ also provided insight about how the typical trend for the UV-Vis spectrum of Au nanoparticles looks like as the aspect ratio R is increased. As shown in Figure 7 (right) as the Au nanoparticles deviate more from their circular shape, an increase in the aspect ratio R, the wavelength position of the first plasmon peak is kept constant but the wavelength position of the second plasmon peak increases as the aspect ratio R increases. Again, the different photos at the bottom show how the Au colloid colour can change depending on the position of the plasmon peak.

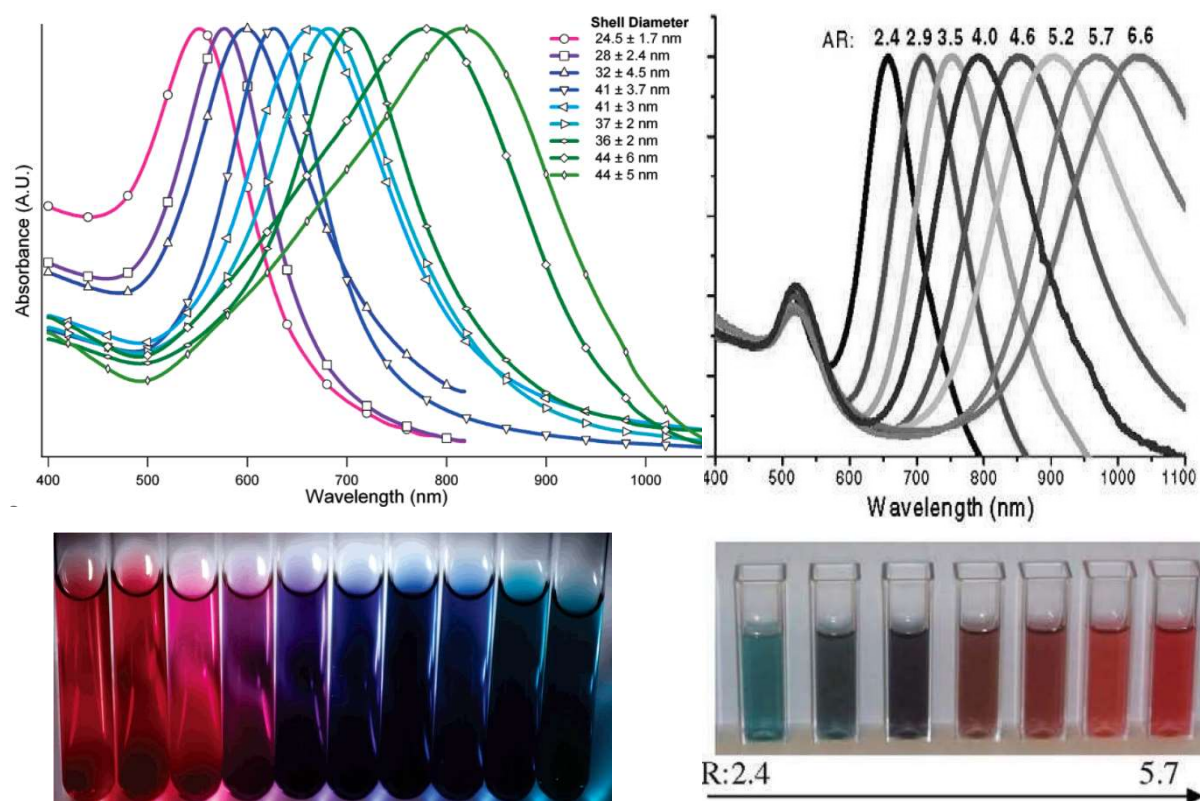


Figure 7 – Typical trends for the UV-Vis spectrum of Au nanoparticles with changes on the nanoparticles average size (left)¹⁹ and changes on the nanoparticles aspect ratio R (right)²⁰ with the colloid photos presented at the bottom.

Introduction

1.3 Synthesis of Metal Nanoparticles

1.3 Synthesis of Metal Nanoparticles

There are two main approaches regarding the synthesis of metal nanoparticles as displayed in Figure 8: one involving the division of a much larger solid (top-down); the other consisting in building the particles by aggregation of atoms (bottom-up). The latter offers a better control of the nanoparticle size, distribution and morphology.³

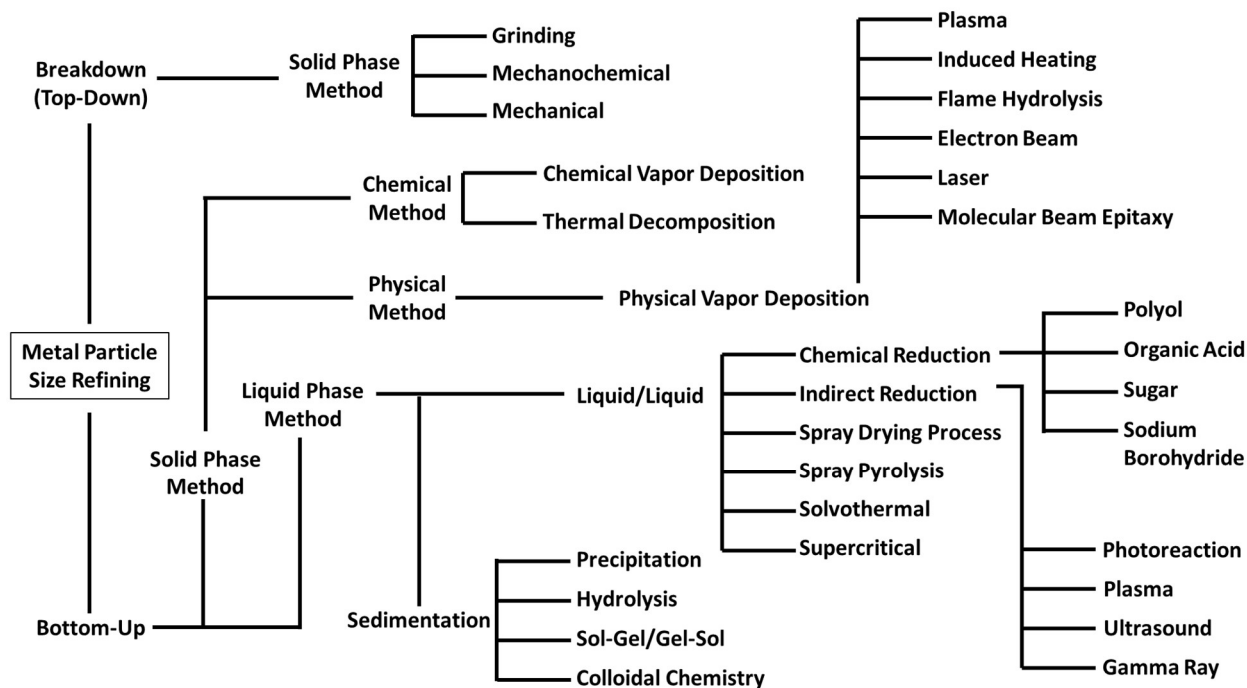


Figure 8 – Top-down and bottom-up approaches for the synthesis of nanoparticles.

(adapted from the literature)¹¹

As observed in Figure 8 each approach can be further divided into numerous other methods. According to the *Manual of Methods and Procedures for Catalyst Characterisation* published by the IUPAC in 1995²¹ the same metal nanoparticle can be prepared by more than one method but the final mechanical and catalytic properties easily end up being different as they are dependent on several operational conditions, including but not limited to:

- a) Metal precursor choice and concentration;
- b) Temperature and pH control;
- c) Stirring conditions;
- d) Shape and volume of the synthesis vessel;
- e) Sequence and duration of the operations;
- f) Interference from other chemical compounds;
- g) Solvent and support choices;

Introduction

1.3 Synthesis of Metal Nanoparticles

The most suitable synthesis method is therefore dependent on the desired application for the metal nanoparticles. As mentioned in section 1.1 there are several applications. However, some of the metal nanoparticles produced for this PhD, mainly Au, Pd and bimetallic AuPd alloys, are only meant to be used for catalytic purposes. They are meant to be supported in cheap and/or porous materials, namely titanium dioxide (TiO₂), cerium dioxide (CeO₂) or activated carbon (C) and used as heterogeneous catalysts in liquid/gas phase reactions (see section 1.6 for an overview of all the reactions, section 2.7 for the reactions experimental procedures and chapter 6 for the reactions experimental results).

The synthesis methods used for this PhD followed the bottom-up approach and were based on the metal ions reduction in solution and formation of colloids. These synthesis methods are commonly known as sol-immobilization methods and offer a better control over metal nanoparticles size and shape by performing the metal nanoparticles in the liquid phase. They are better described in section 1.4. Other commonly used synthesis methods for the production of supported metal nanoparticles to be used as catalysts include:

Impregnation

The support and metal precursor are added to a liquid solvent, dried to remove the excess of solvent, calcined to decompose the metal precursor to metal oxide which is then reduced in a furnace by usually flowing a hydrogen mixture and changing the temperature. Different operating conditions for the heat treatment based on the temperature and flowing gas flow rate and composition can be used for tuning the particle size and the metal-support interaction, therefore affecting catalyst activity and stability.

During impregnation many different and simultaneous processes take place at different rates. These processes include polymerisation of the species attached to the support, selective adsorption to the support of species by capillary action, Coulomb forces (electrostatic), Van der Waals forces and hydrogen bonds and partial dissolution and ion exchange of the support with the liquid solvent. During impregnation the properties of the solvent inside the pores are different than in the bulk and the equilibrium between the support and the solvent is slow to establish and difficult to achieve an even distribution of the species.

There are two main approaches followed with the impregnation synthesis method, one being wet impregnation and the other being incipient wetness. The main difference between those two approaches is that with incipient wetness only the necessary amount of metal precursor solution necessary to fill the support pores is added.²¹

Introduction

1.3 Synthesis of Metal Nanoparticles

Deposition Precipitation and Co-Precipitation

Precipitation involves the process by which an element in solution becomes supersaturated, usually due to addition of a precipitating agent or sudden changes in pH or temperature. It can be said that the deposition precipitation and co-precipitation are two different approaches for the production of supported metal nanoparticles using the precipitation process.

With the deposition precipitation synthesis the metal precursor is added to a solution containing the support. An example would be $\text{Ni}(\text{NO}_3)_2$ present in a solution containing the SiO_2 support with the active metal Ni starting to adsorb onto the support upon addition of the precipitating agent NH_4^+ .²¹ Another example would be the adsorption of the active metal Au onto the TiO_2 support upon changes in pH.²²

The co-precipitation synthesis is different from the previous approach in the sense that consists of the formation of one phase due to the simultaneously precipitation of two or more elements. An example being the controlled addition of the precipitating agent sodium carbonate to a solution of metal precursor nitrates of Cu, Zn and Al to form ternary Cu/ZnO/ Al_2O_3 catalysts.²³

The pH is one of the most important operating conditions affecting adsorption of the active species onto the desired support with Coulomb forces (electrostatic interaction) being the main driving force ruling adsorption of the active species. This is the case for the two aforementioned synthesis methods and the sol-immobilization synthesis method. The changes in pH contribute not only to changes on the metal precursor species present in solution but also to changes on the surface of the support. A schematic representation for the effect of pH on the adsorption of the active metal Pt onto a metal oxide support is shown in Figure 9. The PZC stands for the point of zero charge at which for a certain value of pH the net electrical charge on the surface of the support is zero.²⁴ For this PhD the metal oxides used as support are titanium dioxide (TiO_2) having a PZC in the range of 4-6 and cerium dioxide (CeO_2) having a PZC in the range of 6-7.²⁵

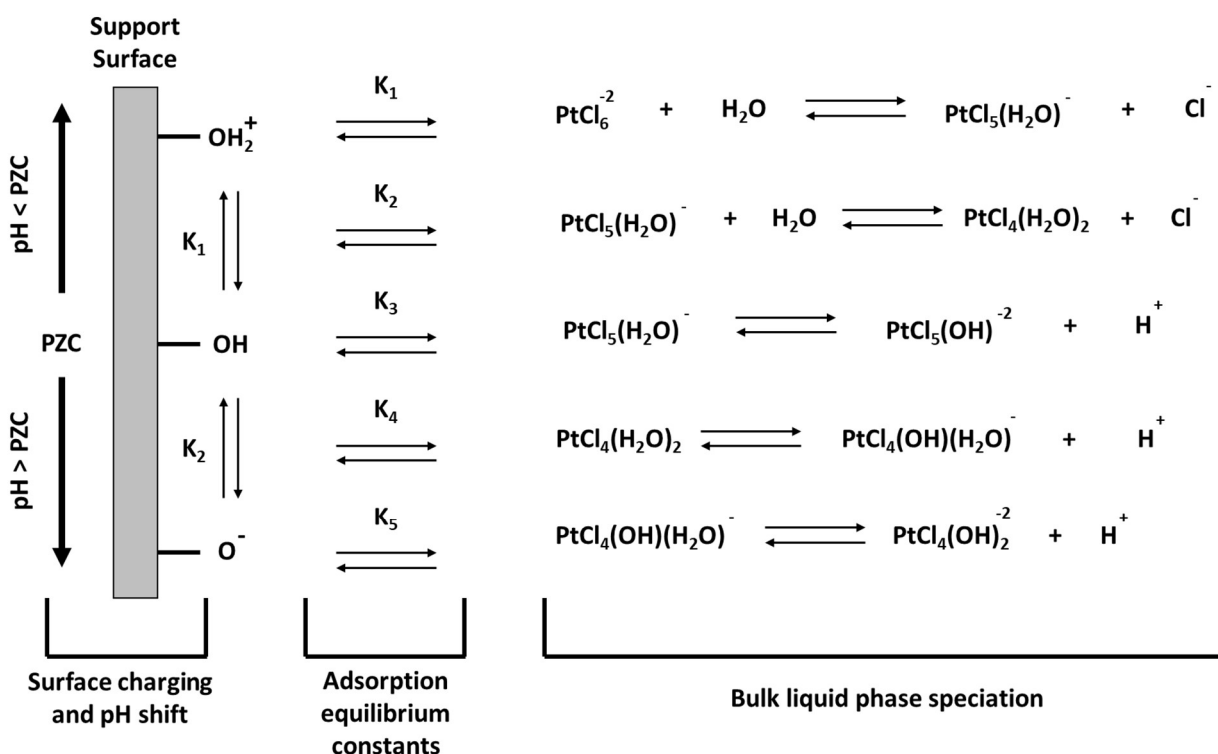


Figure 9 – Effect of pH changes on the adsorption of the active metal Pt onto a metal oxide support.

(adapted from the literature)²⁴

According to Schwarz *et al.*²⁶ the pH effect is particularly important for the deposition-precipitation synthesis method. In addition to controlling the adsorption of active species onto the desired support, if pH changes happen too fast and/or the homogeneity of the bulk of the solution is not preserved the nucleation rate for precipitation might be higher at the bulk of the solution than at the support surface, therefore compromising metal nanoparticles homogeneity and the production of small metal nanoparticles. One way of better controlling the precipitation process is to separate the steps of addition and reaction of the OH^- ions. This can be achieved by adding and using urea as a source of OH^- ions.

Moreover, Moreau *et al.*²⁷ have also demonstrated with Au nanoparticles prepared by the deposition-precipitation synthesis method and supported on TiO_2 that having the best pH in order to obtain maximum adsorption of active species (maximum loading) does not necessarily translate into the highest activity. The previous authors have achieved the highest activity for the carbon monoxide oxidation reaction when working with a pH of 9 even though the highest loading was obtained at a pH of 4. This could be linked to the adsorption of different Au species as the pH changes, with the Au species presenting the Cl^- ion producing larger Au nanoparticles, therefore being less active for the carbon monoxide oxidation.

Introduction

1.3 Synthesis of Metal Nanoparticles

An overview of the main advantages/disadvantages of some of the different synthesis methods used for the production of supported metal nanoparticles are presented in Table 1. These synthesis methods include the different approaches for the commonly used impregnation and deposition precipitation/co-precipitation synthesis methods described above, the sol-immobilization synthesis method, the method adopted for this PhD and described in section 1.4, and another less commonly used synthesis method, the antisolvent precipitation which is also used within the Cardiff Catalyst Institute.

Table 1 – Overview of the main advantages/disadvantages of different synthesis methods used for the production of supported metal nanoparticles.

Synthesis Method	Advantages	Disadvantages
Wet Impregnation	Experimentally simple Can produce high loadings	Wide particle size distribution
Incipient Wetness	Experimentally simple Can produce low loadings All metal deposited	Poor reproducibility
Sol-Immobilization	Particles homogeneity Better control of particles size Better for bimetallic structures	Traces of the stabilizer might remain on the surface of the catalyst and can hinder the catalytic activity
Deposition Precipitation	Experimentally simple Good for basic supports	Not good for acidic support
Co-Precipitation	Experimentally simple One step reaction	Not all metal on the surface
Antisolvent Precipitation	Fast precipitation Simple recovery of product Solvent can be recycled One step reaction	Supercritical fluid at high pressure Experimentally complex Not all metal on the surface

Introduction

1.4 Sol-Immobilization Synthesis Method

1.4 Sol-Immobilization Synthesis Method

This section will focus in more detail on the sol-immobilisation synthesis method, the method adopted for this PhD for the production of supported metal nanoparticles which are meant to be used for catalytic purposes. As shown in Table 1 the main advantages of this synthesis method when compared to the others are a better control of the nanoparticles size with a more homogeneous production, *i.e.* narrower particle size distribution. This synthesis method also offers better experimental results for the production of bimetallic structures. These main advantages are in line with the targets defined for this PhD.

A theoretical overview of how this synthesis method is able to produce metal nanoparticles is presented in section 1.4.1.

In section 1.4.2 some of the conventional protocols adopted with the sol-immobilization synthesis are described, namely the sodium borohydride, citrate and tetrakis(hydroxymethyl) phosphonium chloride protocols. One of those conventional protocols (sodium borohydride) has been used as reference for the work developed with microwave in chapter 3 and with ultrasound in chapter 4. In order to avoid any misunderstanding it is referred as the traditional sol-immobilization protocol.

It is also presented in section 1.4.2 some UV-Vis spectroscopy (UV-Vis) and Dynamic Light Scattering (DLS) characterisation for the metal colloids produced with the traditional sol-immobilization protocol and with the citrate protocol. These two techniques, which were intensively used during the PhD to characterise the different produced metal colloids, are described in more detail in chapter 2, the chapter focused on the experimental procedures, methods and characterisation techniques.

The working principles of the microwave and ultrasound synthesis are presented in sections 1.4.3 and 1.4.4 respectively. These were the main protocols used and optimised for this PhD with the experimental procedures described in chapter 2 and the experimental results presented in chapters 3 and 4.

Introduction

1.4 Sol-Immobilization Synthesis Method

1.4.1 Overview

With the sol-immobilization synthesis method the first step is the reduction of metal ions to individual atoms. Afterwards there is a nucleation step whereby atoms come together to form nucleus. These nuclei tend to grow in order to decrease the total surface energy. Nanoparticles formation is an extremely complex process dependent on a delicate balance between reduction, nucleation and growth mechanisms as can be observed in Figure 10.

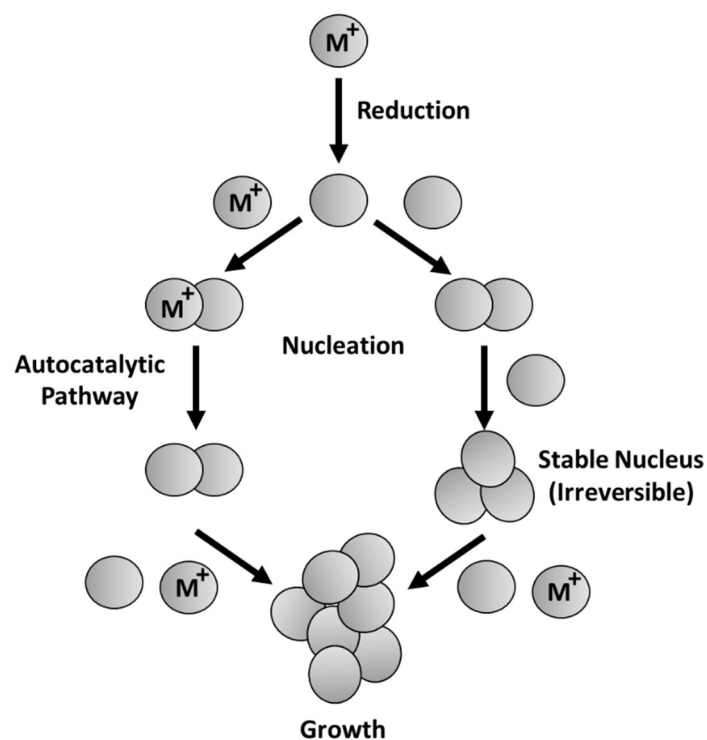


Figure 10 – Reduction, nucleation and growth mechanisms for metal nanoparticles production.

(adapted from the literature)²⁸

In the case of nucleation only homogeneous nucleation has been considered, but it is also possible to have heterogeneous nucleation if for instance there is dust contamination or if the process happens on the wall surface of reactor/beaker instead of the bulk of the solution.

The homogeneous nucleation and the growth mechanisms can be further divided into autocatalytic pathway if unreduced metal interacts first with the nucleus/particles instead of with the reducing agent. The autocatalytic pathway is the preferable path under weak reducing agents and low metal precursor concentrations conditions.²⁸

The growth mechanism is not uniform and a variety of different nanoparticles sizes and shapes can be obtained. This is usually not desired as it compromises the particles size distribution and as a result the catalytic activity.

Introduction

1.4 Sol-Immobilization Synthesis Method

In order to decrease and control the growth mechanism polymers, surfactants and other charged molecules can be used as stabilizers. They prevent interaction of nanoparticles due to steric effect of bulky ligands or by surrounding the nanoparticles with charged anions that create electrostatic repulsion (Coulomb force). The use of polyvinyl alcohol (PVA) is an example of stabilization by steric effect. In this case the PVA adsorbs to the particles surface and provides a protective layer. This prevents agglomeration of particles as the total entropy of the system would decrease so much that the Gibbs free energy would become thermodynamically unfavourable. The use of citrate is an example of stabilization by electrostatic repulsion. In this case the citrate also adsorbs to the particles surface, but agglomeration of particles is prevented by electrostatic repulsion. However, using stabilizers adds complexity to the process because at some point they will need to be separated from the final product, otherwise they might end up hindering the catalytic activity by blocking the substrate access to the active sites, *i.e.* the metal nanoparticles.²⁹⁻³⁰

According to LaMer concept of “burst nucleation” almost all the nanoparticles nucleate at the same time and will start to grow without additional nucleation. In the LaMer plot shown in Figure 11 it is observed that as the reduced metal concentration increases the saturation level is reached but there is no net nucleation yet because the energy barrier for nucleation is still too high. It is difficult to define exactly a concentration value for which nucleation begins because nucleation and redissolution can happen at any concentration, even under unsaturated conditions, but after a certain level of supersaturation (nucleation level) stable nuclei start to be formed in appreciable number and to accumulate, which in turn causes the concentration of reduced metal to decrease. These stable nuclei will then continue to growth until a final particle size is reached.

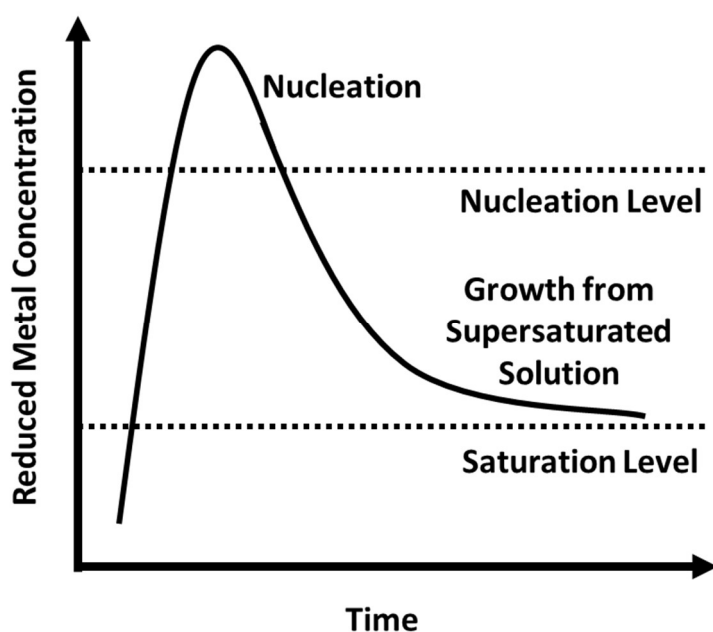


Figure 11 – LaMer plot with change of reduced metal concentration over time.

(adapted from the literature)²⁸

Introduction

1.4 Sol-Immobilization Synthesis Method

The concentration corresponding to the nucleation level can be estimated having in consideration that there is a minimum radius that will persist and not dissolve away given by Equation 2. After forming a nucleus with such radius, the nanoparticle can continuously grow while at the same time decreasing its free energy.³¹

$$r_c = \frac{2\gamma \cdot V_m}{R \cdot T \cdot \ln C} \quad (2)$$

r_c is the minimum radius (m), γ is the surface free energy per unit area (J m^{-2}), V_m is the molar volume of particle (m^3), R is the ideal gas constant ($\text{J K}^{-1} \text{mol}^{-1}$), T is temperature (K) and C is the reduced metal concentration (mol L^{-1}).

There are several operating conditions influencing the delicate balance between the mechanisms of reduction, nucleation and growth. The main operating conditions usually considered can be described as:

- a) Metal precursor choice and concentration;
- b) Reducing agent choice (weak vs. strong) and concentration;
- c) Stabilizer choice (steric vs. electrostatic) and concentration;
- d) Solvent(s) choice (polar vs. non-polar) and composition;
- e) Synthesis temperature;
- f) Synthesis time and mode (batch vs. continuous);

A schematic representation of the synthesis temperature effect on the transformation rate of the reduced metal into nanoparticles is shown in Figure 12. The total transformation rate can be considered to be the product of the growth and nucleation rates. It is possible at two different temperatures to have the same total rate of transformation. However, at one temperature the nucleation rate can be the dominant mechanism and at the other temperature the growth rate can be the dominant mechanism.

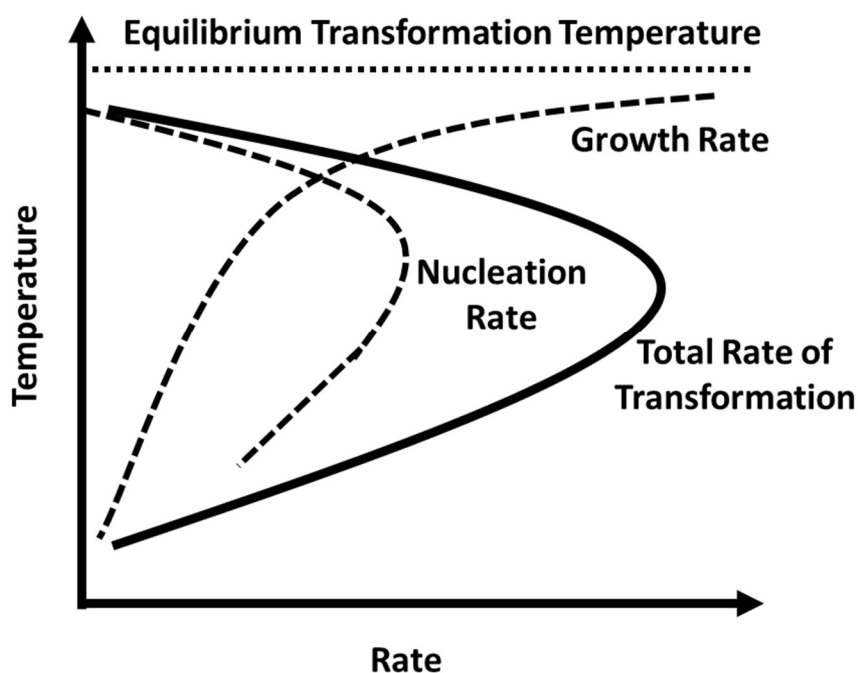


Figure 12 – Synthesis temperature effect on the metal nanoparticles nucleation and growth rates.

(adapted from the literature)³²

It is assumed with the LaMer theory that when the growth step starts the nucleation step is already finished, a condition necessary for a narrow nanoparticles size distribution.³¹ However, under the condition in which the growth rate \gg nucleation rate, the growth step will take place as soon as a nucleus is produced and at the same time as the nucleation step therefore causing broad size distributions. This represents an example of how by changing the operating conditions, in this case the temperature, metal nanoparticles of different sizes, shapes and compositions can be tailored.

Introduction

1.4 Sol-Immobilization Synthesis Method

1.4.2 Conventional Protocols

A conventional protocol for the preparation of sol-immobilised catalysts consists in adding a metal precursor, stabilizer and reducing agent to a solvent. As previously described in section 1.4.1 the reduced metal atoms will nucleate and produce metal nanoparticles with the growth mechanism being controlled by the presence of the stabilizer. The solution can then be considered a colloid. A support is added to immobilise the metal nanoparticles. For this reason, this synthesis method is called as the sol-immobilization. Three conventional protocols are described in this section.

1.4.2.1 Sodium Borohydride (Traditional) Sol-Immobilization Protocol

Intensive work with the sol-immobilization method has been carried out within Nikolaos Dimitratos research group³³⁻³⁷ who have developed a protocol with selected operating conditions for the parameters mentioned in section 1.4.1. This traditional sol-immobilization protocol was applied mainly to the production of Au, Pd and bimetallic AuPd catalysts which were then tested in several different reactions, including but not limited to glycerol oxidation³³, benzyl alcohol oxidation³⁴⁻³⁶, hydrogen peroxide synthesis and hydrogenation³⁵ and cinnamaldehyde hydrogenation.³⁷

This protocol consists in using a strong reducing agent, sodium borohydride (NaBH_4), polyvinyl alcohol (PVA) as the steric stabilizer and water as the solvent. The NaBH_4 will rapidly reduce the metal ions to individual atoms and the PVA will control the nanoparticles growth mechanism due to steric effect. For the synthesis of 1 g of catalyst of a monometallic metal with a total nominal metal weight ratio of 1 wt. % the steps are:

- a) Add 0.01 g of the metal to 400 mL of deionized water (0.025 g L^{-1});
- b) Add the PVA to the solution with a PVA/metal weight ratio of 0.65x;
- c) Add NaBH_4 to the solution with a NaBH_4 /metal molar ratio of 5 and stir for 30 min (at this point a colloid should have been formed);
- d) Add 0.99 g of support to the metal colloid and stir it for 60 min;
- e) If the support is TiO_2 add some drops of H_2SO_4 to the mixture in order to reach a pH of 1-2 (the pH will control the adsorption of the active metal onto the support as described in Figure 9);
- f) Filter the catalyst under vacuum and wash it with 1 L of deionized water;
- g) Dry the catalyst under static conditions in an oven at $110 \text{ }^\circ\text{C}$ for 16 h;

Introduction

1.4 Sol-Immobilization Synthesis Method

A schematic representation of all the aforementioned steps used for the production of Au supported monometallic nanoparticles on TiO_2 is shown in Figure 13.

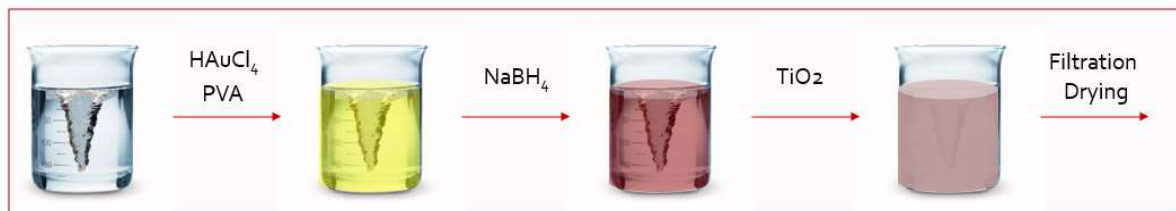


Figure 13 – Production of Au supported monometallic nanoparticles on TiO_2 by the traditional sol-immobilization protocol.

The traditional sol-immobilization protocol can also be used for the synthesis of bimetallic nanoparticles. When the bimetallic structure is of the alloy type the steps are the same as before but two metals are added instead in step a) and a PVA/metal weight ratio of 1.2x is used instead in step b). If the metal nanoparticle to be prepared is a bimetallic structure of the core-shell type one metal is used in step a), a PVA/metal weight ratio of 1.2x is used instead in step b) and after step c) the second metal is added and step c) is repeated. For the bimetallic structures of the alloy and core-shell type the total mass of the two metals is 0.01 g and the ratio of one metal to the other is adjusted according to the desired ratio.

Au/TiO_2 , Pd/TiO_2 and AuPd/TiO_2 (1:1 molar) catalysts have been synthesised by following the described traditional sol-immobilization protocol. They were tested for some of the reactions described in section 1.6 and used as benchmark against the catalysts produced by microwave and ultrasound synthesis. All the catalytic results are presented in chapter 6.

As shown in Figure 14 a strong red colour was observed when forming the Au nanoparticles colloid (top left), which changed to a light red colour after adding the TiO_2 support (top right). The Pd and AuPd (1:1 molar) colloids had a very similar brown colour, as well as a very similar grey colour after adding the TiO_2 support. Both the photos of the colloids and support addition were taken at the end of each stage. The metal precursors used were $\text{HAuCl}_4 \cdot 3\text{H}_2\text{O}$ and K_2PdCl_4 .

Introduction

1.4 Sol-Immobilization Synthesis Method



Figure 14 – Photos of the colloids formed after addition of NaBH₄ (left) and of the support addition stage with TiO₂ (right) for the synthesis of Au (top), Pd (middle), AuPd (1:1 molar) (bottom) catalysts.

Even though sodium borohydride is a strong reducing agent, an excess was still used during the nanoparticles synthesis to ensure a complete and fast metal ions reduction with a NaBH₄/metal molar ratio of 5. A suggested mechanism for the reduction of the Au precursor with sodium borohydride is presented in Equation 3.³⁸

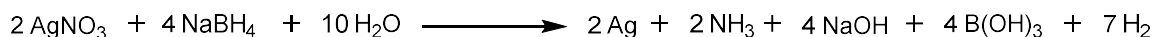


Equation 3 – Suggested mechanism for the reduction of a Au precursor with NaBH₄.³⁸

Introduction

1.4 Sol-Immobilization Synthesis Method

The mechanism by which a metal is reduced with sodium borohydride is complex and in the literature it is possible to find different mechanisms for the same metal ions reduction. This was the case of Sterling *et al.*³⁹ (Equation 4) and Solomon *et al.*⁴⁰ (Equation 5) who have both worked with the synthesis of silver (Ag) nanoparticles with sodium borohydride.



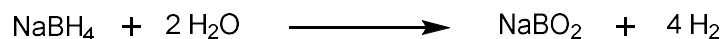
Equation 4 – Suggested mechanism by Sterling *et al.*³⁹ for the reduction of a Ag precursor with NaBH₄.



Equation 5 – Suggested mechanism by Solomon *et al.*⁴⁰ for the synthesis of a Ag precursor with NaBH₄.

From the three previous suggested mechanism for the reduction of metal precursors of Au and Ag with NaBH₄ it is observed that hydrogen (H₂) is produced, in particular for the mechanism suggested in Equation 4. The production of this gas explains the bubbles observed during the metal nanoparticles synthesis. The hydrogen bubbles are more intense immediately after addition of NaBH₄, but even after 30 min, just before the support is added, it is still possible to observe some of the bubbles. These hydrogen bubbles are particularly visible in the photo of the Au nanoparticles colloid in Figure 14 (top left).

This hydrogen generation does not result only from the previous suggested metal ions reduction mechanisms. The NaBH₄ contact with water is enough to produce hydrogen as shown in Equation 6. According to Glavee *et al.*⁴¹ this hydrogen production is further enhanced by the presence of the metal nanoparticles who act as catalysts.



Equation 6 – Hydrogen generation from NaBH₄ contact with water.⁴¹

Introduction

1.4 Sol-Immobilization Synthesis Method

The produced Au, Pd and bimetallic AuPd (1:1 molar) colloids were characterised by UV-Vis spectroscopy (UV-VIS) and Dynamic Light Scattering (DLS). The UV-Vis spectra and the DLS size distribution graphs are shown in Figure 15 for Au (top), Pd (middle) and AuPd (1:1 molar) (bottom). These two techniques were intensively used during this PhD to characterise the different produced colloids as they offer an easy and quick way of following the reduction of metal ions and the formation of metal nanoparticles with indications regarding the average size, size distribution and production. They are described in detail in chapter 2.

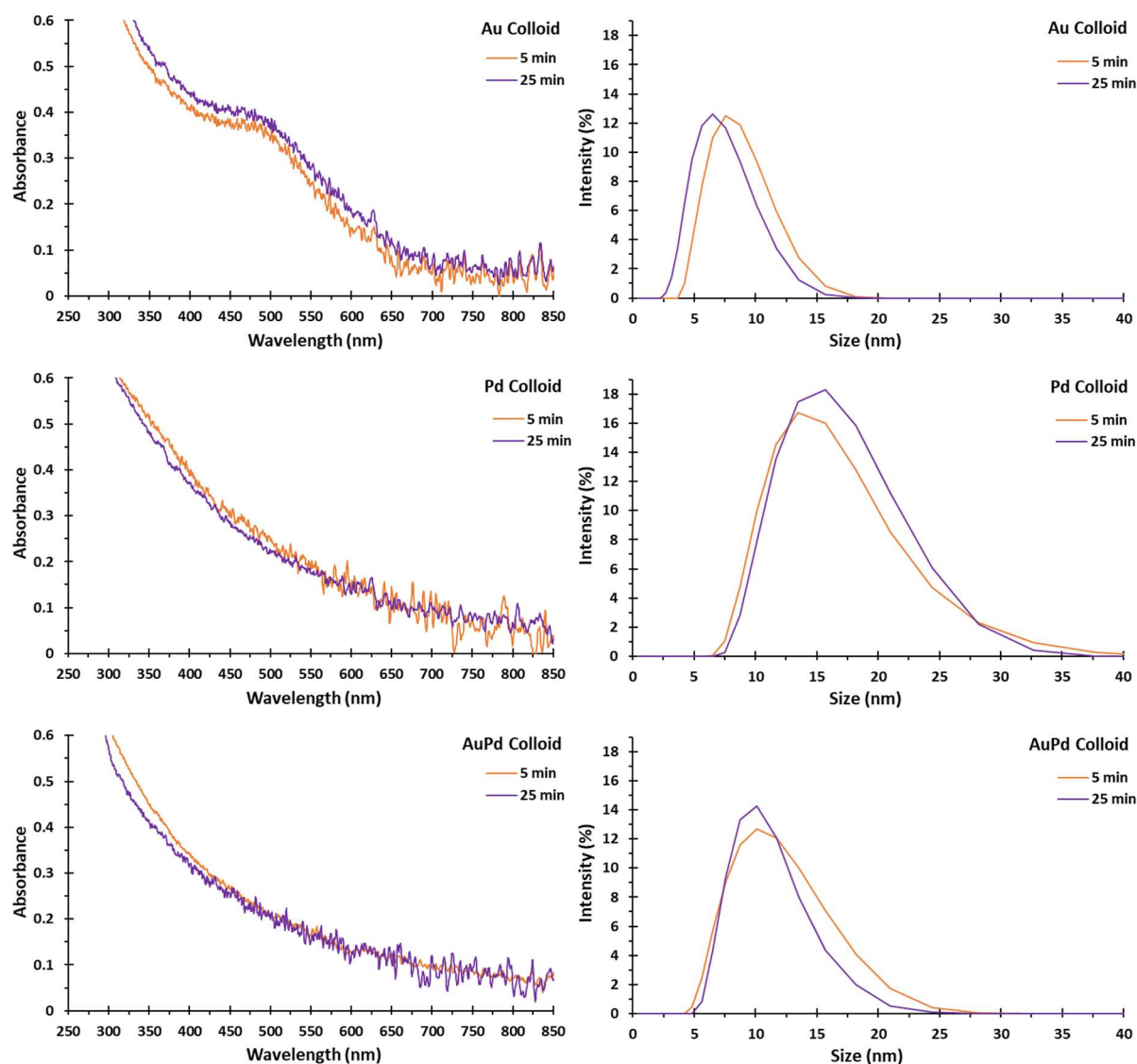


Figure 15 – UV-Vis (left) and DLS (right) analysis of Au (top), Pd (middle) and AuPd (1:1 molar) (bottom) colloids 5 and 25 min after the addition of NaBH₄.

Introduction

1.4 Sol-Immobilization Synthesis Method

A plasmon peak at around 500 nm is visible for the Au nanoparticles in Figure 15, typically observed for the synthesis of small Au nanoparticles in the range of 2-4 nm (from TEM analysis). This plasmon peak is smooth when compared to the plasmon peaks presented in Figure 7. This is a strong indication that smaller Au nanoparticles were produced and according to the trend mentioned in section 1.2, where for Au nanoparticles smaller than 2 nm the plasmon peak can even disappear.¹⁸

The Pd and AuPd UV-Vis spectra are very similar to each other and no plasmon peaks were observed. Not all the metals present a plasmon peak in this region of the electromagnetic spectrum as was explained in section 1.2. However, it is still remarkable that by creating a AuPd alloy the Au contribution to an eventual plasmon peak was completely suppressed, in agreement with the literature.⁴²

Both UV-Vis and DLS spectra did not change much between 5 and 25 min. The average sizes calculated at 25 min for Au, Pd and AuPd (1:1 molar) colloids from the DLS size distributions were 7 ± 2 nm, 16 ± 5 nm and 11 ± 3 nm. These DLS average sizes only give an indication that small nanoparticles were produced for the three colloids. As explained in section 2.2.2 the DLS measures the hydrodynamic size, which is influenced by the solvent molecules surrounding the nanoparticles and by the stabilizer.

1.4.2.2 Citrate Sol-Immobilization Protocol

Another conventional sol-immobilization synthesis protocol for the production of metal nanoparticles was also explored. This synthesis protocol consisted in using citrate, a weak reducing agent, instead of sodium borohydride. As mentioned in section 1.4.1, the citrate also acts as a stabilizer by electrostatic repulsion and PVA is not employed.

The original protocol was developed for Au nanoparticles by Turkevich *et al.*⁴³ in 1951 and later refined by Frens⁴⁴ in 1973, who was able to vary the Au nanoparticles size from 16 to 147 nm by adjusting the citrate to Au molar ratio.

As shown in Figure 16 two size ranges of 19-35 nm and 35-78 nm were produced with photos taken at 2, 15 and 30 min after the citrate addition and Au colloids were characterised by UV-Vis and DLS at 30 min after the citrate addition. The aqueous citrate solution (trisodium citrate) was only added to 50 mL of the aqueous Au solution (0.1 g L^{-1}) when the latter was already boiling. A reflux condenser was used to prevent water losses and as a result changes in the Au solution concentration. The citrate solution, with a 10 g L^{-1} concentration of citrate, acted as both the reducing agent and the stabilizer with 0.75 mL of the citrate solution added to produce Au nanoparticles in the range of 19-35 nm and 0.50 mL of the citrate solution added to produce the Au nanoparticles in the range of 35-78 nm.

Introduction

1.4 Sol-Immobilization Synthesis Method

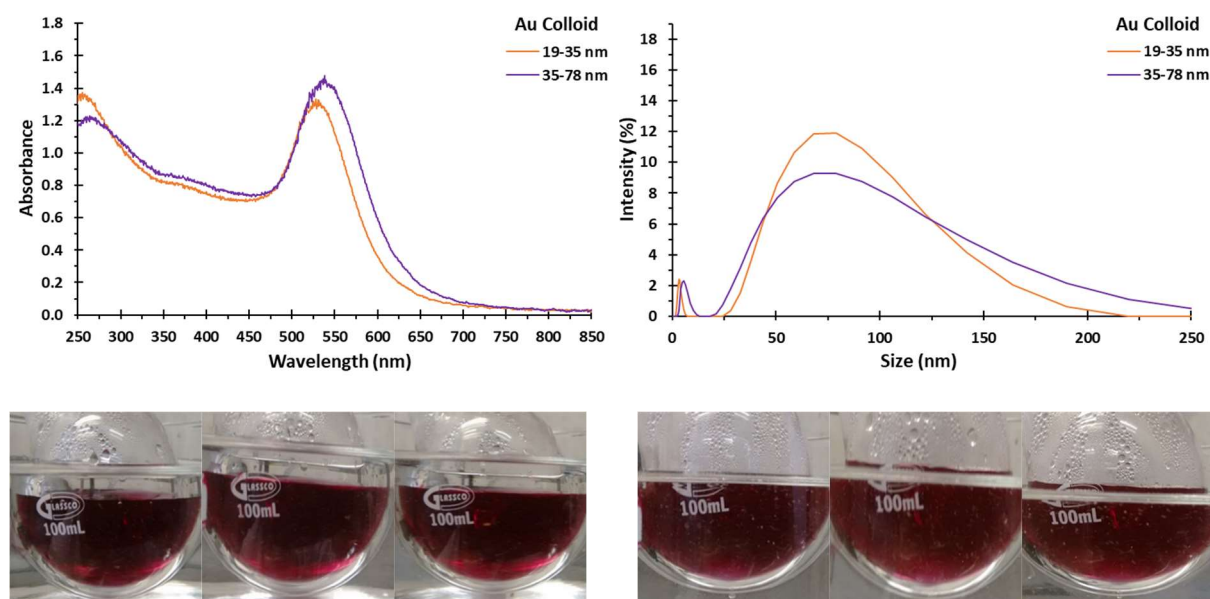


Figure 16 – UV-Vis (top left) and DLS (top right) analysis of Au nanoparticles produced by the Frens method⁴⁴ and photos of the 19-35 nm (bottom left) and 35-78 nm (bottom right) colloids at 2, 15 and 30 min.

The colour observed at 2 min for both 19-35 nm and 35-78 nm ranges did not change much at 15 and 30 min. The UV-Vis spectra showed strong plasmon peaks with the 19-35 nm range having a plasmon peak wavelength of 528 nm and the 35-78 nm range having a plasmon peak wavelength of 538 nm. As expected, this is an indication that the Au nanoparticles produced with higher content of citrate solution (0.75 mL) were smaller than the Au nanoparticles produced with less citrate solution (0.50 mL).

The plasmon peaks absorbances were significantly higher than the one observed with the traditional sol-immobilization protocol in Figure 15 (top left). This was caused by the higher initial Au solution concentration of 0.1 g L^{-1} for the citrate protocol, compared with 0.025 g L^{-1} for the traditional sol-immobilization protocol. The 4-fold increase in Au solution concentration, from 0.025 to 0.1 g L^{-1} , roughly caused a 4-fold increase in the absorbance as expected, approximately from 0.4 to 1.6.

Introduction

1.4 Sol-Immobilization Synthesis Method

1.4.2.3 THPC Sol-Immobilization Protocol

Work within Nikolaos Dimitratos research group has also been performed using the protocol developed by Duff *et al.*⁴⁵ in 1993 for the production of Au nanoparticles. For this sol-immobilization synthesis protocol tetrakis(hydroxymethyl)phosphonium chloride (THPC) is both the reducing agent and the stabilizer, similar to what happened when working with the citrate protocol.

This protocol combines the advantage of not using PVA, or similar polymers, as the stabilizer with the production of very small metal nanoparticles with a narrow particle size distribution. However, for this protocol sodium hydroxide (NaOH) is also added in order to generate formaldehyde. The formaldehyde is formed by alkaline elimination caused by the THPC reaction with OH⁻. Under alkaline conditions the THPC is also able to promote reduction of water to produce hydrogen. The formaldehyde and hydrogen enhance the Au ions reduction rate and the formation of Au nanoparticles. This synthesis protocol was also successfully extended to the production of other metal nanoparticles⁴⁶ and tested for the preparation of catalysts using different supports.⁴⁷

Introduction

1.4 Sol-Immobilization Synthesis Method

1.4.3 Microwave Synthesis

An important part of the metal nanoparticles produced during this PhD were obtained using heating from microwave radiation. This type of electromagnetic radiation is in the spectrum region between radio waves and infrared. The microwave synthesis aimed to deliver the targets defined for this PhD, in particular the elimination of toxic reducing agents, reduced synthesis time and better control over size and shape of the produced metal nanoparticles.

Typically, a commercial device is regulated to operate at 2450 MHz and its working principle is related to an oscillating magnetic and electric field interacting with charged molecules or molecules presenting a dipolar moment. The solvent molecules try to align with the oscillating field but their movement will create friction forces resulting in heat generation.¹¹ Details about the microwave synthesis experimental procedure can be found in section 2.3.

The degree of interaction between the solvent molecules and the electromagnetic radiation is expressed by the dielectric constant (ϵ_1), related to how well the molecule can be polarised, and by the dielectric loss (ϵ_2), related to how well energy is converted into heat.⁴⁸ The dielectric constant and dielectric loss were previously used in Equation 1 in section 1.2 when introducing the surface plasmon resonance effect induced by light interaction with metal nanoparticles. It is shown in Figure 17 how the dielectric constant and dielectric loss change with temperature and wavelength for the water molecule.

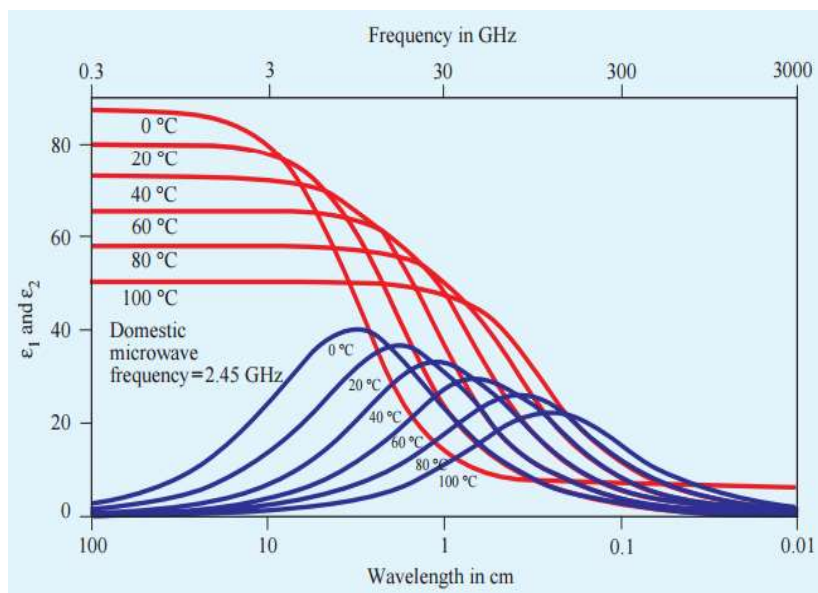


Figure 17 – Temperature and wavelength dependency for water dielectric constant (red) and dielectric loss (blue).⁴⁹

Introduction

1.4 Sol-Immobilization Synthesis Method

According to Equation 7 the dielectric constant, the dielectric loss and the wavelength of the incident radiation are used to estimate for a certain medium the penetration depth (D_p) after which the power density has fallen to 36.8% of its initial value.⁵⁰ The penetration depth will have the same units as the wavelength (usually cm). Both Figure 17 and Equation 7 explain why microwave commercial devices operate at 2450 MHz. At this frequency the dielectric constant is very high when compared to the dielectric loss, which causes the penetration depth to be large enough (order of cm) so that food, mainly composed of water, becomes warm not only on the surface but also in the interior.

$$D_p = \frac{\lambda}{2\pi\sqrt{2\varepsilon_1}} \frac{1}{\sqrt{\left[1 + \left(\frac{\varepsilon_2}{\varepsilon_1}\right)^2\right]^{0.5} - 1}} \quad (7)$$

A microwave device offers thermal advantages by providing a rapid and more homogeneous way of heating when compared to the conventional heating where there is heat transfer by convection and conduction due to a gradient of temperatures between two regions. These two advantages can be observed in Figure 18 that compares for two tubes containing water the temperature profiles after 60 s of heating. For the microwave heating (left) only the liquid inside the tube is warm with the temperature being homogeneously distributed whereas for the conventional heating (right) the tube walls are warmer than the liquid, which presents two shades of blue, an indication of a low and bad temperature distribution.

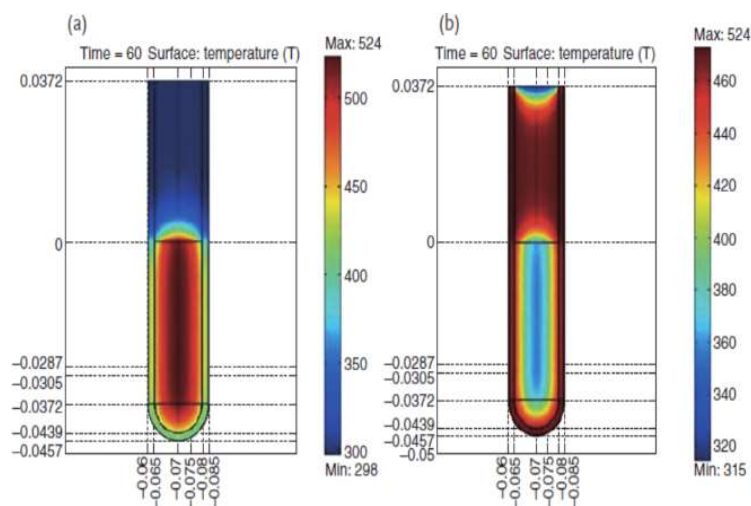


Figure 18 – Water temperature profile after 60 s of microwave heating (a) and conventional heating (b).¹¹

Introduction

1.4 Sol-Immobilization Synthesis Method

According to Galema⁴⁸, who reviewed several authors working with microwave heating, it is claimed that the advantages are only thermal and the enhancement effects observed in the work of other authors were due to poor temperature monitoring and control. It is also stressed that unlike microwave spectroscopy carried out in gas phase, for microwave heating no molecules can be excited to a higher and discrete energy level. Nevertheless, the previous author also assumes that the debate about microwave heating providing a special effect, such as lowering the activation energy of a reaction, is not yet closed.

Microwave heating has proved to be an effective tool for several applications found in different fields of chemistry as shown in Table 2.

Table 2 – List of chemical applications for microwave heating.¹¹

Chemical Field	Applications	Chemical Field	Applications
Organic Chemistry	Rapid synthesis Solid-phase synthesis Non solvent process Non catalytic process Organometallic complex Combinatorial chemistry	Analytical Chemistry	Carbonization processing Acid and alkali treatment High speed concentration High speed extraction High speed degradation
Biochemistry	Enzyme reactions PCR DNA dyeing	Polymers	Vulcanization of rubber Higher synthesis selectivity Heat processing of plastics Size control of polymers
Catalysis	Environmental catalysis Heterogeneous catalysis Homogeneous catalysis Catalysts synthesis Supports synthesis	Photochemistry	Electrodeless lamps UV hardening of coatings Photochemical synthesis
Inorganic Materials	Artificial bones synthesis Crystallinity control Drying of extruded ceramics Heat treatment of glass	Metal Chemistry	Metallic powder metallurgy Iron manufacturing Particulate coating

Introduction

1.4 Sol-Immobilization Synthesis Method

Microwave heating is far from being restricted to the traditional chemical industry. In Table 3 some applications for microwave heating in other industrial areas are also listed.

Table 3 – List of industrial applications for microwave heating.¹¹

Industry	Applications	Industry	Applications
Environmental	Sintering of asbestos Exhaust treatment Waste treatment Biomass processing Metal recycling	Food	Sterilization Processing Defrosting High-speed cooking Enzyme activation Yeast activation
Medicinal	Sterilization Hyperthermia Cutting of blood vessels Muscular warming	Ink and Paint	Drying of paint Drying of printing ink
Film and Paper	Sintering of electronic wiring Selective heating	Agriculture	Wood treatment Extermination of insects Extraction of contaminants Degradation of contaminants

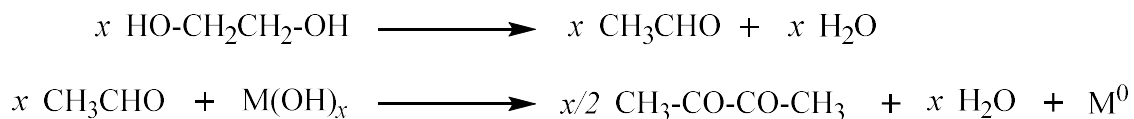
As listed in Table 2 microwave heating finds application in non-solvent synthesis as using a solvent is not required for heat conduction. This represents an advantage not only from the environmental and economic point of view, but also an advantage for the process design by avoiding a separation stage and an unwanted system overpressure.

For the metal nanoparticles synthesis dry medium conditions are not common practice. A solvent(s) needs to be present to act as the reducing agent for the metal ions and to provide a good absorption of the electromagnetic radiation followed by the dissipation of energy as heat. However, compared to the traditional sol-immobilization protocol, when using microwave heating the need to employ a toxic reducing agent (NaBH_4) is eliminated.

As shown in Equation 8, Komarneni *et al.*⁵¹ presented the general mechanism for metal ions reduction when ethylene glycol, a common solvent in microwave synthesis, is to be used.

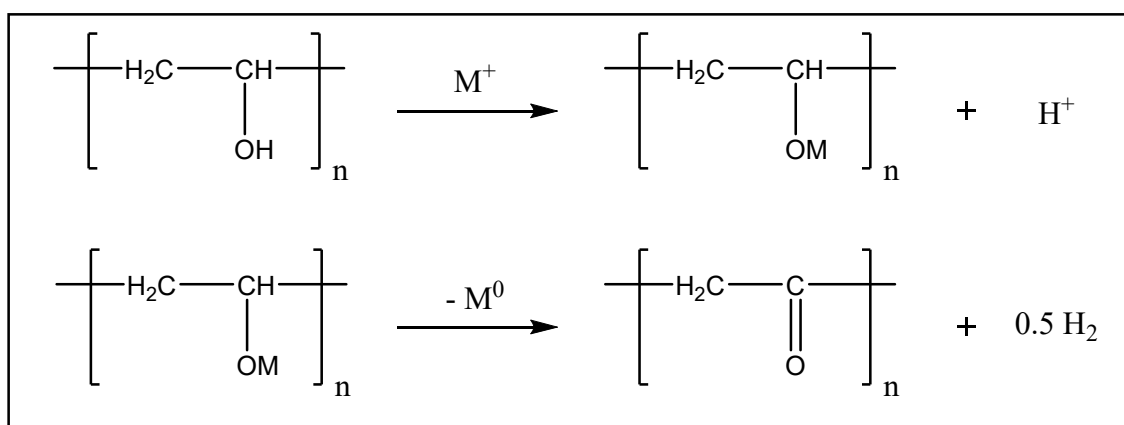
Introduction

1.4 Sol-Immobilization Synthesis Method



Equation 8 – General mechanism for metal ions reduction (M) with ethylene glycol.⁵¹

Likewise, under specific operating conditions of temperature, polyvinyl alcohol (PVA), which was only used as a stabilizer for the traditional sol-immobilization protocol, can also act as a mild reducing agent⁵² by the mechanism shown in Equation 9. Moreover, contrary to the traditional sol-immobilization protocol, where sodium borohydride quickly reduced the metal ions, with microwave synthesis metal ion reduction is slow and the hydrogen produced during the second step of the reaction is able to reduce metal ions as well. This would be a similar mechanism to what was described for the THPC method in section 1.4.2.3.



Equation 9 – General mechanism for metal ions reduction (M) with PVA.⁵³

The role of the stabilizer is even more important with microwave synthesis than with the traditional sol-immobilization protocol as the PVA is now able to act as the reducing agent. For this reason, modifications to the stabilizer, either by decreasing its amount, ideally even eliminating it, or by replacing the standard PVA by a different stabilizer, were also investigated.

Polyvinylpyrrolidone (PVP) a common stabilizer for the metal nanoparticles synthesis, presenting a protective value one order of magnitude higher than PVA²⁸ was the selected stabilizer for benchmarking purposes against PVA. This extra stabilization is due to the donation of a lone pair of electrons from the nitrogen or carbonyl oxygen.⁵⁴

Introduction

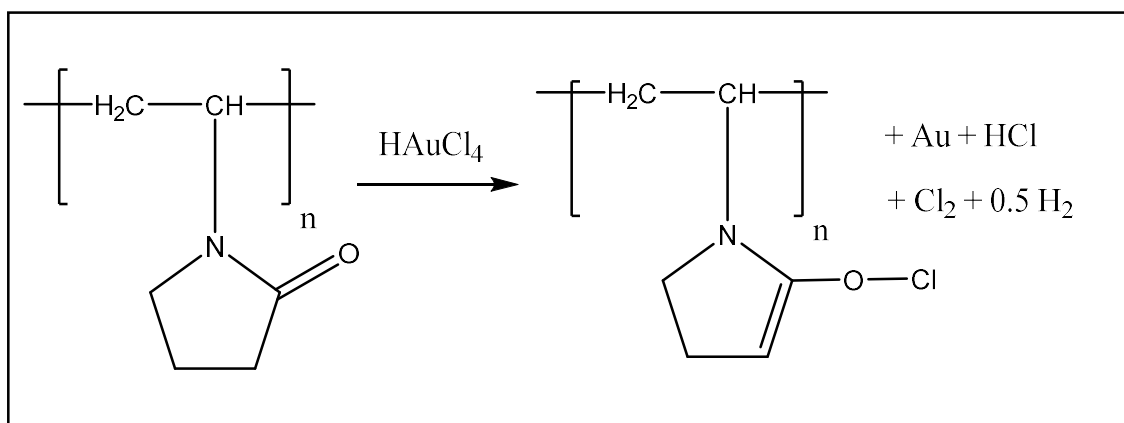
1.4 Sol-Immobilization Synthesis Method

The PVP stabilizer under specific operating conditions of temperature has also been shown to be capable of acting as a mild reducing agent by Wu *et al.*⁵⁵ who worked with the synthesis of silver nanoparticles. According to Zhang *et al.*⁵⁶ there is more than one possible mechanism by which PVP can reduce the metal ion:

a) One mechanism related to the terminal OH groups of the PVP chains, a similar mechanism to what was observed with PVA in Equation 9;

b) One mechanism related to the formation of free radical intermediates with the abstraction of hydrogen from the linear carbons;

c) One mechanism related to the formation of a complex between the metal precursor and the C=O group with the chloroauric acid example shown in Equation 10;



Equation 10 – Complex formation mechanism for chloroauric acid reduction with PVP.⁵⁶

Introduction

1.4 Sol-Immobilization Synthesis Method

1.4.4 Ultrasound Synthesis

Some of the metal nanoparticles produced during this PhD were obtained by subjecting metal precursor solutions to ultrasonic waves. The ultrasound synthesis aimed to deliver the targets defined for this PhD, in particular the elimination of toxic reducing agents, reduced synthesis time and better control over size and shape of the produced metal nanoparticles.

Contrary to the microwave heating effect which is caused by electromagnetic waves, the ultrasonic effect is caused by mechanical waves. Mechanical waves can be described as pressure waves oscillating at a certain frequency travelling through a medium and causing compressing and decompressing effects within that medium. Ultrasonic mechanical waves are in the frequency range of 20 kHz to 500 MHz, above the typical frequency range for human audition of 20 Hz to 20 kHz.⁵⁷

The ultrasonic equipment used to produce metal nanoparticles during this PhD was regulated to operate at 20 kHz. Details about the ultrasound synthesis experimental procedure can be found in section 2.4.

Frequency is not the only parameter used to characterise a mechanical wave. The waveform, phase, medium density, speed and amplitude are also important parameters. Contrary to the electromagnetic waves the mechanical waves are not described by quantum mechanics and the energy level is not exclusively and linearly dependent on the frequency. It is not even possible to talk about energy levels and as shown in Equation 11 the energy content of a mechanical wave is expressed by the intensity (I_w), dependent on the medium density, wave frequency, velocity and amplitude.⁵⁸

$$I_w = 2 \cdot \pi^2 \cdot \rho \cdot f^2 \cdot v \cdot A^2 \quad (11)$$

I_w is the wave energy intensity (W m^{-2}), ρ is the medium density (Kg m^{-3}), f is the wave frequency (Hz or s^{-1}), v is the wave velocity (m s^{-1}) and A is the wave amplitude (m).

A decibel scale (dB) has been introduced in the beginning of the 20th century with the objective of quantifying losses on communications lines over distances. The International Organization for Standardization under the ISO 80000-3 regulations defines quantities and units for space and time, including the decibel scale (dB) as shown in Equation 12.

Introduction

1.4 Sol-Immobilization Synthesis Method

$$dB = 10 \cdot \log_{10} \left(\frac{I_w}{I_r} \right) \quad (12)$$

dB is the decibel scale, I_w is the wave energy intensity ($W m^{-2}$) previously described in Equation 11 and I_r is a reference energy level of $10^{-12} W m^{-2}$ based on the lowest energy intensity the human being is able to detect.

It can be said the decibel scale is a logarithmic scale that tries to provide a translation between the energy intensity of a mechanical wave and the human perception of loudness. For every increase in 10 dB the human perception of loudness doubles. For example, when the energy intensity of a mechanical wave with 20 dB has a 10-fold increase the decibel scale will have increased to 30 dB, according to Equation 12, and the perception of loudness will have increased to the double.

The decibel scale can be further modified in order to improve the accuracy if corrected for the human perception of frequency. The human ear does not perceive all frequencies with the same loudness. For example, as shown in Equation 11 it is possible to have two mechanical waves with the same energy intensity but different frequencies. The decibel scale would then also be the same for the two waves. However, the human perception of loudness would be different from one wave to the other.

When a liquid medium is irradiated with ultrasound mechanical waves the compressing and decompressing effects caused by oscillating pressure waves contributes to the formation of small and localized regions of low pressure. Within these small and localized regions, the vapour pressure of the liquid exceeds the surrounding pressure causing the liquid to flash and to form bubbles.⁵⁸ These bubbles are commonly called cavitation bubbles. The cavitation bubbles can be further divided into:

- a) Stable cavities, which form and oscillate around a mean radius during several acoustic cycles and may never collapse;
- b) Transient cavities, which exist only during a few acoustic cycles, growing their mean radius from one acoustic cycle to the other and eventually collapse;

The collapse of a transient cavity is associated with a concentrated amount of energy being released in a very short period of time. This phenomenon causes small and localized regions within the liquid medium to reach temperatures as high as 5000 °C and pressures of 1000 bar. These regions are known as hotspots.⁵⁹

Introduction

1.4 Sol-Immobilization Synthesis Method

The extreme conditions of temperature and pressure last less than a nanosecond as there is fast heat and mass transfer between the hotspot and the bulk of the liquid. Still, this is enough to cause the bulk of the liquid to increase its temperature and energy can even be released by light emission, a phenomenon called sonoluminescence.⁶⁰

A schematic representation for the formation and collapse of a transient cavity is shown in Figure 19.

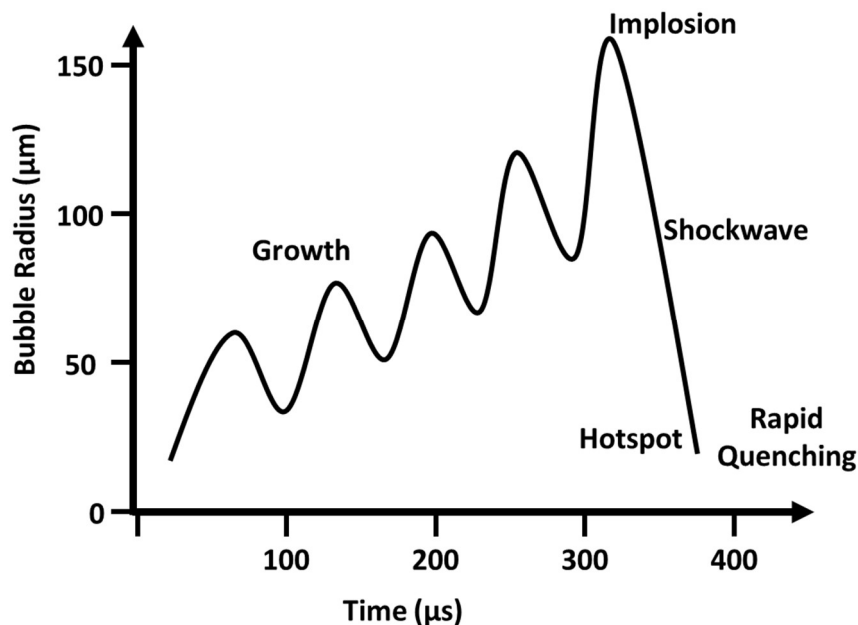


Figure 19 – Formation and collapse of a transient cavity within a liquid medium irradiated by ultrasonic mechanical waves.

(adapted from the literature)⁵⁹

The wave energy intensity expressed by Equation 11 influences the bubbles collapse intensity, *i.e.* the extreme temperature and pressure conditions that can be obtained for the hotspot. At a fixed frequency the higher the wave energy intensity the more intense should be the bubbles collapse and more extreme temperature and pressure conditions should be obtained. However, it is also described in the literature that too much energy intensity can end up compromising the experimental results as bubbles will start to accumulate near the ultrasound probe and block the transmission of waves into the liquid medium.⁶¹⁻⁶² Several other factors influence as well the hotspot temperature and pressure conditions:⁵⁸

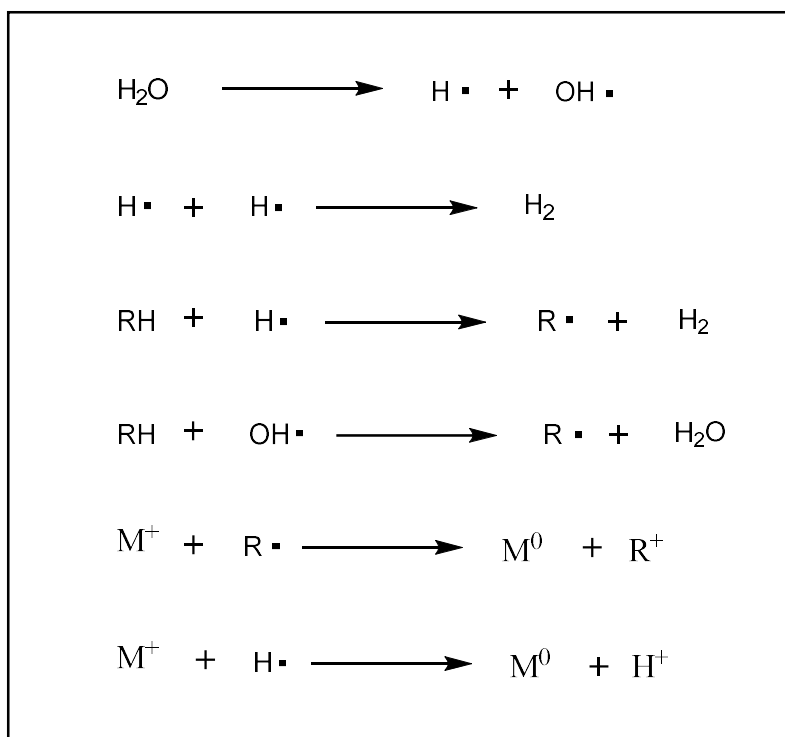
- a) Presence and nature of dissolved gases in the liquid medium;
- b) Ambient temperature will affect the liquid vapour pressure;
- c) Ambient pressure will affect the bubble implosion;
- d) Solvent(s) choice affects vapour pressure, viscosity and surface tension;
- e) The wave frequency affects the growth cycle described in Figure 19;

Introduction

1.4 Sol-Immobilization Synthesis Method

Even though extreme temperature conditions of 5000 °C can be obtained for the hotspot, the bulk of the liquid remains at a temperature of the same order of magnitude than the initial room temperature, before any irradiation with ultrasound waves takes place. Therefore, with ultrasound synthesis, and contrary to the microwave synthesis, it is not the direct effect of the temperature that causes a solvent to act as the reducing agent as described for the microwave synthesis with ethylene glycol in Equation 8. Instead, the extreme temperature and pressure conditions will cause the solvent to produce radicals.

According to Bang and Suslick⁵⁹ the general mechanism for metal ion (M^+) reduction in water is caused by generation of hydrogen radicals ($H\cdot$) as shown in Equation 13. An organic solvent is often added, an example being a water and ethylene glycol mixture. Hydrogen and hydroxyl radicals will react with the organic solvent and generate secondary radical species. Therefore, by choosing different solvents it is possible to vary the nature and concentration of organic and hydrogen radicals, and as a consequence the metal ion reduction and the formation of metal nanoparticles. Metal ion reduction is also accomplished by the presence of hydrogen, which can be formed when two hydrogen radicals react.



Equation 13 – General mechanism for metal ions reduction (M) with hydrogen (H), hydroxyl (OH) and organic (R) radicals.⁵⁹

Introduction

1.4 Sol-Immobilization Synthesis Method

Further to the cavitation effect the ultrasound mechanical waves can also interact with solid objects to produce imaging, including internal imaging. This is accomplished with ultrasound mechanical waves of low energy intensity and high frequency (3-30 MHz).⁶³

Similar to microwave heating, the ultrasound effects have been successfully applied in different fields of chemistry, not only for the production of supported metal nanoparticles for catalytic purposes. Ultrasound is also far from being restricted to the traditional chemical industry, other major industries being food and medicinal. A list of some of the ultrasound general applications, without differentiating by a specific industry, is presented in Table 4.

Table 4 – General applications of ultrasound.⁵⁸

General Applications	
Fatigue testing	Drilling
Abrasion	Cutting
Cleaning	Erosion
Imaging	Sterilization
Defoaming	Dissolution
Welding	Emulsification

Introduction

1.5 Continuous Flow Synthesis

1.5 Continuous Flow Synthesis

Increasing the production of metal nanoparticles has been defined as one of the targets for this PhD. This target is usually accomplished by either scaling-up production under batch regime by increasing the reactor volume or by moving the production from batch regime to continuous flow regime.

For the same production a better control over the metal nanoparticles average size, size distribution and shape can be achieved when adopting the continuous flow regime option. The continuous flow regime offers enhanced heat and mass transfer, therefore causing a better process homogeneity, opposed to the option of scaling-up production under batch regime as the larger the batch reactor volume the more difficult it is to control the process homogeneity.¹¹ Moreover, synthesis under continuous flow regime allows to manipulate and control additional parameters not possible under batch regime. This is the case of the flow rate and the ability to cease the reaction as soon as a small volume of product is formed. Working under continuous flow regime is also less complex and advantageous for the health and safety control of the entire synthesis process by decreasing the amount of chemicals that need to be transported, stored and handled during operation.⁶⁴

Two general configurations for continuous flow reactors can be adopted. One configuration where the properties of the reaction mixture are constant at any point of the mixture volume and equal to the outlet conditions. This configuration is called continuous stirred tank reactor (CSTR). For the other continuous flow configuration, the properties of the reaction mixture change axially along the reactor volume. This configuration is called plug flow reactor (PFR). Several CSTR reactors placed in series will approach the results of a PFR with the same total volume, eventually the two results will become equal as the volume of each of the CSTR reactors is decreased and the number of CSTR reactors is increased.⁶⁵ A schematic representation of the PFR configuration is shown in Figure 20 and of the CSTR configuration is shown in Figure 21.

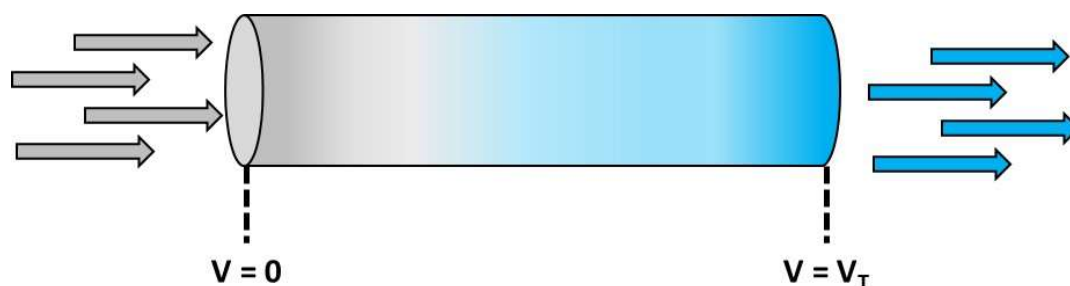


Figure 20 – Plug flow reactor configuration with changes to the reaction mixture properties represented by the colour gradient changing axially.

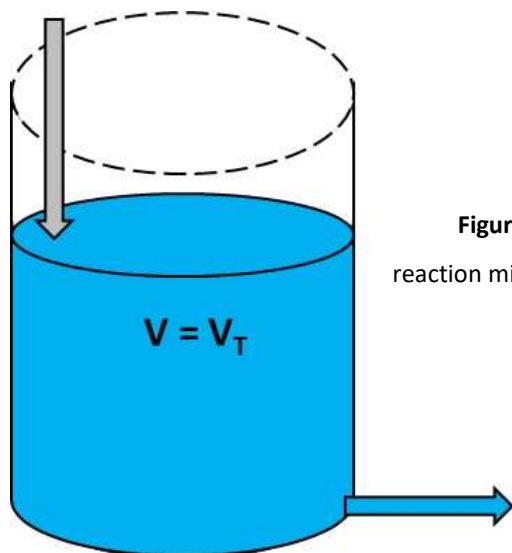


Figure 21 – Continuous stirred tank reactor with changes to the reaction mixture properties represented by the two different colours of the inlet stream and of the total mixture volume.

For this PhD an attempt to move the microwave synthesis of Au and Pd nanoparticles from the batch regime to the continuous flow regime is described in section 3.6. The reactor used was of the CSTR type configuration and supplied by the microwave device manufacturer. The experimental procedure is presented in section 2.3.

Control over the metal nanoparticles average size, size distribution and shape can be further enhanced by working with a continuous flow microreactor. Microreactors can be modelled as long plug flow reactors of small channel diameter (< 1 mm). These microreactors often contain a large number of channels in parallel in order to increase the production.⁶⁶ The main advantages of working with a small channel diameter include:

a) Possibility of achieving better heat and mass transfer coefficients due to a large surface area to volume ratio;

b) The smaller the channel the higher the flow velocity that can be used without entering into turbulent flow regime. The use of higher flow velocities is advantageous from the process point of view since it reduces the fouling phenomenon inside the channels.⁶⁷

A turbulent flow regime is characterised by a chaotic mixing where mass transfer by advection dominates over diffusion. A turbulent flow regime would hinder the synthesis of metal nanoparticles due to enhanced agglomeration. The degree of turbulence of a given flow is measured by the Reynolds number, dependent on the channel diameter and the fluid density, viscosity and velocity. The higher the Reynolds number the higher the degree of turbulence;

Introduction

1.5 Continuous Flow Synthesis

c) A large channel diameter presents significant axial dispersion. This causes the local velocity at the centre of the channel to be considerable different from the velocity near the wall of the channel. The axial flow velocity follows a parabolic profile as described by the Hagen-Poiseuille equation. This effect is particularly relevant for the metal nanoparticles size distribution and can be minimized when working with small channel diameters;

Microreactors to produce nanoparticles can be considered a recent technique. A search conducted on the database *Scopus* indicates that approximately 92 % of the articles concerning this subject were produced after 2005 (search for *microreactor* and *nanoparticles* on 9th September 2018 returned 577 results). The massification of the 3D printing technology to small consumers, which provides a higher degree of freedom when designing the reactor, has been an important driving force.⁶⁸

Introduction

1.6 Model Reactions Overview

1.6 Model Reactions Overview

As mentioned in section 1.1 there are several applications for the metal nanoparticles. However, for this PhD emphasis is only given to catalytic applications. Some of the produced metal nanoparticles by microwave and ultrasound, mainly Au, Pd and bimetallic AuPd alloys, were supported in cheap and/or porous materials, namely titanium dioxide (TiO_2), cerium dioxide (CeO_2) or activated carbon (C) and used as heterogeneous catalysts in liquid/gas phase reactions.

In total seven reactions were tested. In this section the seven reactions are presented and their importance in light of the targets defined for this PhD is described. The experimental procedures for each of the seven reactions can be found in section 2.7 and the experimental results are presented in chapter 6. Some of the experimental results were benchmarked against experimental results obtained with a commercial catalyst and with catalysts produced by the traditional sol-immobilization protocol, previously described in section 1.4.2.1.

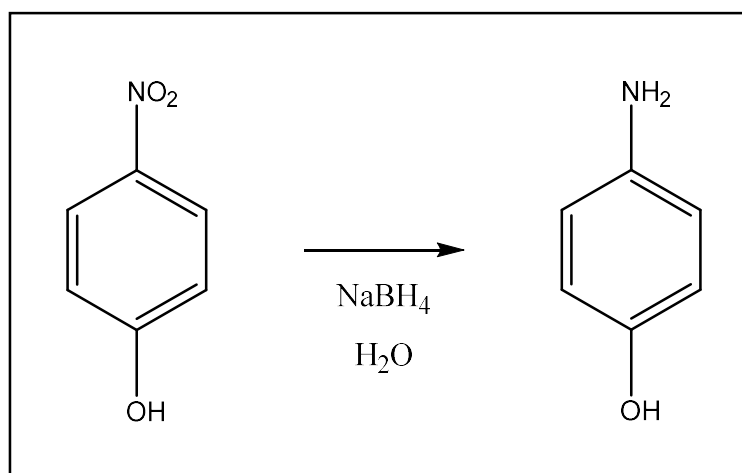
These seven reactions were only used as model reactions. The objective was never to optimise the reactions operating conditions, but rather to use the reactions as a tool to catalytically characterise the produced metal nanoparticles, in this case by calculating conversions and selectivities and comparing them. For this reason, the adopted experimental procedures were the same as the ones from previous work carried out within the Cardiff Catalysis Institute, in particular within the Nikolaos Dimitratos research group. The catalysts characterisation techniques described in detail in section 2.2 with experimental results presented in chapter 5 explain the different conversions and selectivities in terms of the metal nanoparticles average size, size distribution, loading, composition, shape, oxidation state, contamination and type of metal active site. Ultimately, the catalytic activity results can give insight into which one of the developed microwave and ultrasound sol-immobilization protocols for the synthesis of metal nanoparticles are more interesting and where future research should focus on.

Introduction

1.6 Model Reactions Overview

1.6.1 4-Nitrophenol Reduction

The 4-nitrophenol is known to be an anthropogenic pollutant with toxic and inhibitory effects if released in nature. Therefore, the removal of 4-nitrophenol from waste water is considered a beneficial application. This pollutant removal can be accomplished by reducing the 4-nitrophenol to 4-aminophenol using sodium borohydride in aqueous medium with the reaction scheme shown in Equation 14. Moreover, 4-aminophenol is a useful chemical with applications including photographic developer of black and white films, corrosion inhibitor, dyeing agent and the manufacture of analgesic and antipyretic drugs.⁶⁹



Equation 14 – 4-Nitrophenol reduction with sodium borohydride in water.

The 4-nitrophenol reduction is an interesting model reaction for the screening of metal nanoparticles with different properties. This is due to its fast kinetics at room temperature. Full conversions are usually achieved within minutes with small amounts of catalysts necessary. Therefore, it is a fast reaction that allows the screening of several catalysts in a short period of time. Moreover, the fact that there is only one product makes the experimental results easier to analyse. The experimental set-up is also easy to assemble as the concentration of the 4-nitrophenol over time is monitored with UV-Vis spectroscopy.

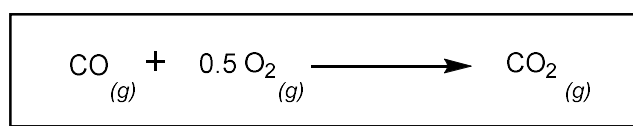
The reaction was carried out in a UV-Vis cuvette under batch regime and full details about the sodium borohydride and the 4-nitrophenol concentrations, the catalyst amount and the experimental set-up can be found in section 2.7.1. The experimental results are presented in section 6.2.

Introduction

1.6 Model Reactions Overview

1.6.2 Carbon Monoxide Oxidation

Carbon monoxide is a colourless, odourless and tasteless gas that is toxic to humans as it is able to strongly bond to the haemoglobin present in the blood cells thereby competing with and hindering the transport of oxygen throughout the body. Carbon monoxide is usually a secondary product formed when there is not enough oxygen to lead to a complete combustion. An example would be the internal combustion engine and the release of small amounts of carbon monoxide through the car exhaust. In order to tackle this environmental issue catalysts are used to oxidize carbon monoxide with oxygen to carbon dioxide with the reaction scheme shown in Equation 15.



Equation 15 – Carbon monoxide oxidation with oxygen.

Besides maintenance of clean air through emission treatment it is also important to remove residual carbon monoxide from industrial gases as it might end up compromising the downstream applications. An example would be the purification of produced hydrogen gas to be used as a fuel source. Commonly used catalysts are usually efficient at temperatures higher than 120 °C. Therefore, research is still focused in producing catalysts able to efficiently conduct this reaction at lower temperatures, ideally at room temperature.⁷⁰

As a model reaction the carbon monoxide oxidation was tested under continuous flow regime at room temperature using a mixture of carbon monoxide and synthetic air with the carbon monoxide to carbon dioxide conversion over time monitored by gas chromatography as described in section 2.7.2. The experimental results are presented in section 6.3.

Introduction

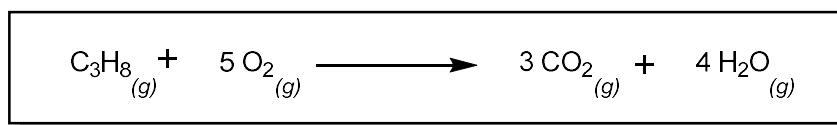
1.6 Model Reactions Overview

1.6.3 Propane Total Oxidation

Similar to the previous carbon monoxide example other chemical compounds may end up being released to the atmosphere. Of particular interest are a class of compounds known as volatile organic compounds or VOCs. According to the United States Environmental Protection Agency VOCs can be described as:

“any compound of carbon, excluding carbon monoxide, carbon dioxide, carbonic acid, metallic carbides or carbonates and ammonium carbonate, which participates in atmospheric photochemical reactions...organic chemical compounds whose composition makes it possible for them to evaporate under normal indoor atmospheric conditions of temperature and pressure”

The emission of VOCs to the atmosphere can have natural causes due to the activity of animals, volcanos, swamps and forests. However, anthropogenic effect constitutes a major source of VOCs emission with important industries comprising petrochemical, transportation and solvents and paints. VOCs toxicity to humans is not the only environmental concern. Some VOCs are able to act as greenhouse gases, cause ozone depletion and contribute to the formation of undesired ground ozone. Similar to the carbon monoxide reaction, one solution to control the emission of VOCs is the catalytic oxidation with oxygen to produce carbon dioxide and water. Catalytic oxidation is a process more complex than thermal oxidation but a higher selectivity towards carbon dioxide is obtained, less NO_x and other harmful secondary products are produced and the operation cost is lower as lower temperatures are required. Propane is an example of a VOC with the reaction scheme shown in Equation 16.⁷¹⁻⁷²



Equation 16 – Propane total oxidation with oxygen.

The propane total oxidation was tested under continuous flow regime at several temperatures using a mixture of propane and synthetic air with the propane conversion and the carbon dioxide selectivity measured by gas chromatography as described in section 2.7.3. The experimental results are presented in section 6.4.

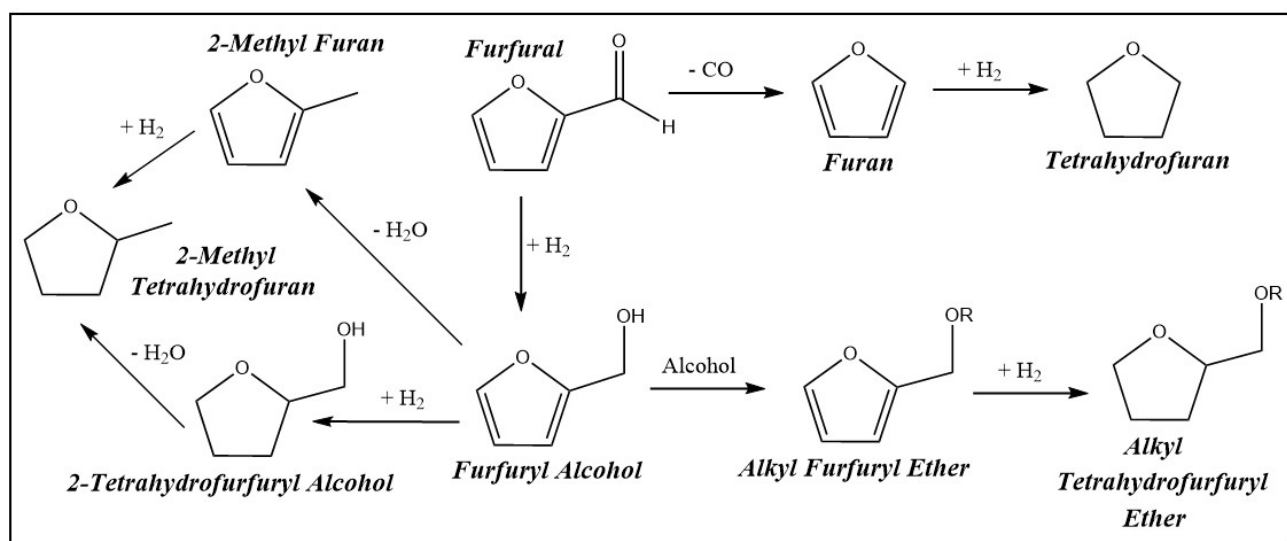
Introduction

1.6 Model Reactions Overview

1.6.4 Furfural Hydrogenation

In recent years intensive research has focused in replacing fossil fuels and their derivatives using renewable biomass feedstocks. Some examples of biomass feedstocks are cereals, wood, grass and algae. There are similarities between biomass feedstocks and fossil fuels as both of them are initially a complex mixture which need to be processed in order to isolate essential building blocks which can then be used in the synthesis of multiple chemical compounds. Therefore, biomass feedstocks can initially be considered a complex mixture of starch, hemicellulose, cellulose, lignin, oils and proteins. According to the United States Department of Energy one of the most valuable building blocks that can be obtained from biomass feedstocks is furfural.⁷³

Furfural can take part in several reactions such as aldol condensation, reductive etherification, acetalization and Grignard reactions. Moreover, furfural can be modified by reduction, hydrodeoxygenation, reductive amination and decarbonylation. For this PhD some of the produced catalysts were tested for the hydrogenation of furfural. The presence of different unsaturated bonds also promotes the production of several products as shown in the reaction scheme in Equation 17 and control of selectivity is a key aspect for this reaction.⁷⁴⁻⁷⁵



Equation 17 – Furfural hydrogenation in 2-propanol with the different possible pathways.

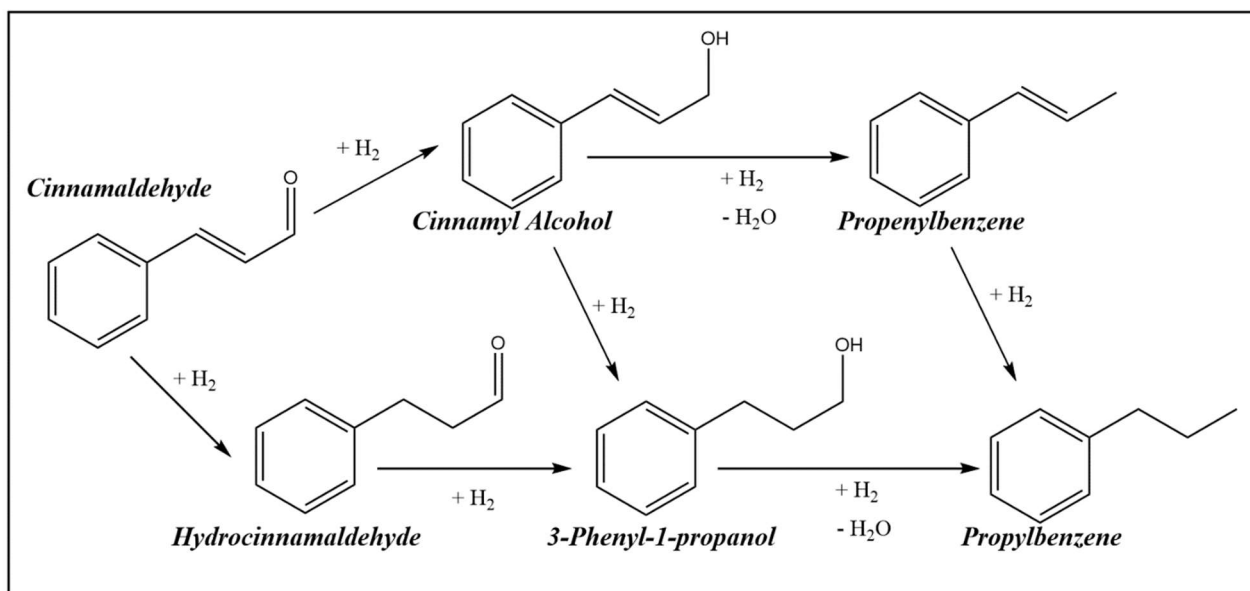
The furfural was dissolved in 2-propanol and the hydrogenation was performed under batch regime at 50 °C inside an autoclave with the conversion and selectivity measured by gas chromatography as described in section 2.7.4 with main products formed being furfuryl alcohol and 2-tetrahydrofurfuryl alcohol. The experimental results are presented in section 6.5.

Introduction

1.6 Model Reactions Overview

1.6.5 Cinnamaldehyde Hydrogenation

Similar to the furfural hydrogenation, another reaction that focused in converting renewable biomass feedstocks into more valuable chemical products was the hydrogenation of cinnamaldehyde. This compound occurs naturally as the trans isomer and can be extracted from the oil of plants. It is an important element used as a fragrant and also as a polymerisation and corrosion inhibitor. The hydrogenation of cinnamaldehyde will also lead to the production of several products as shown in the reaction scheme in Equation 18 and again control of selectivity is a key aspect for this reaction. These several products can be considered as fine chemicals of increased commercial value which are mainly used in the fragrance and pharmaceutical industry.^{37,76}



Equation 18 – Cinnamaldehyde hydrogenation in toluene with the different possible pathways.

The cinnamaldehyde was dissolved in toluene and the hydrogenation was performed under batch regime at 100 °C inside a closed round bottom flask with the conversion and selectivity measured by gas chromatography as described in section 2.7.5 with main products formed being hydrocinnamaldehyde and 3-phenyl-1-propanol. The experimental results are presented in section 6.6.

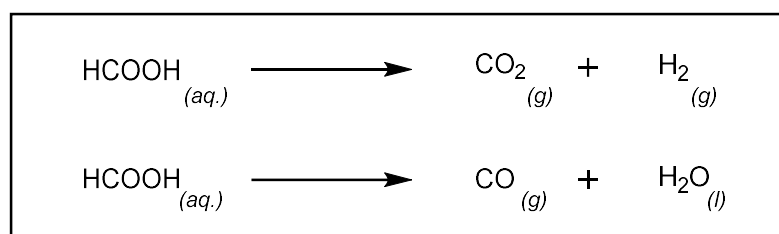
Introduction

1.6 Model Reactions Overview

1.6.6 Formic Acid Decomposition

Worldwide the energy supply sector is making a smooth transition from nuclear and fossil fuels generation sources into renewable sources, with the most important sources being the wind, the solar and the hydroelectric. In the case of fossil fuels this transition constitutes an important step into a decarbonized society, where mankind plays a minimal role on climate changes. In the case of nuclear energy this transition will ensure that no accidents like the ones in Chernobyl, Ukraine or in Fukushima, Japan will ever happen again and that no nuclear waste will need to be treated. However, even though real time grid energy supply is making the aforementioned transition the storage of energy still remains an issue. For this reason, fossil fuels are still dominant within the transportation industry. One of the solutions to this problem could be the combination of hydrogen storage with a fuel cell in order to meet transportation energy demand whenever necessary.

Hydrogen is one of the most abundant elements on earth. However, it is mainly found bonded to other elements. As shown in Equation 19, the decomposition of formic acid can be considered as an alternative source of hydrogen instead of using the conventional steam reforming of methane. Moreover, storing liquid formic acid and generating hydrogen *in-situ* could also solve one of the biggest hurdles of current hydrogen solutions, *i.e.* the safety and technical issues associated with the storage of pure hydrogen at high pressures.⁷⁷⁻⁷⁸



Equation 19 – Formic acid decomposition in water.

As observed in Equation 19 there are two pathways for the formic acid decomposition. One pathway producing hydrogen and carbon dioxide and the other producing carbon monoxide and water. The first pathway is the thermodynamically favourable reaction but some of the formic acid is also expected to follow the second pathway. This second pathway is highly undesired and needs to be rigorously controlled as carbon monoxide can end up poisoning the fuel cell.⁷⁹

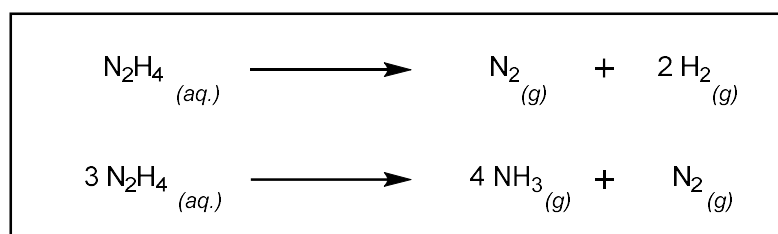
For this PhD the formic acid decomposition was only used as a model reaction and only conversions were calculated without any gas analysis being performed. An aqueous formic acid solution was tested under batch regime at 50 °C inside a round bottom flask with the conversion measured by liquid chromatography as described in section 2.7.6. The experimental results are presented in section 6.7.

Introduction

1.6 Model Reactions Overview

1.6.7 Hydrazine Decomposition

Formic acid is far from being the only liquid source for hydrogen storage. Other examples include ammonia borane, methanol and sodium borohydride (previously mentioned in Equation 6). Another promising hydrogen source is hydrazine, which presents a hydrogen content of 12.5 wt. % vs. the 4.4 wt. % of formic acid. Hydrazine can be used as a monopropellant for rockets due to its explosive action when in contact with metals. This explosive action is the result of the fast decomposition of hydrazine under liquid state into several molecules of gas as shown in the reactions scheme in Equation 20. For this safety reason, work was carried out with monohydrate hydrazine, still containing a large amount of hydrogen at around 8.0 wt. %.⁷⁹



Equation 20 – Hydrazine decomposition in water.

Similar to the formic acid decomposition, the hydrazine decomposition can also follow two pathways. The first pathway producing nitrogen and hydrogen and the other producing ammonia and nitrogen. However, contrary to the formic acid decomposition, with the hydrazine decomposition the undesired second pathway is the thermodynamically favourable reaction with an enthalpy of reaction of -157 kJ mol^{-1} vs. $-95.4 \text{ kJ mol}^{-1}$ for the first pathway. Eventually, if the temperatures are high enough, above $400 \text{ }^\circ\text{C}$, the ammonia will also decompose into hydrogen and nitrogen.⁸⁰ However, hydrazine decomposition is meant to be carried out at temperature conditions as similar as possible from room temperature and research for catalysts that can favour the first pathway is paramount.

Again, for this PhD the hydrazine decomposition was only used as a model reaction and only the amount of produced gas was analysed. The monohydrate hydrazine aqueous solution was tested under batch regime at $50 \text{ }^\circ\text{C}$ inside a closed round bottom flask with the produced gas accumulating in a graduated cylinder where the displaced volume was measured over time as described in section 2.7.7. The experimental results are presented in section 6.8.

2 Experimental, Methods and Characterisation

2.1 Chemicals, Materials, Products and Equipment

A list of all the chemicals, materials, products and equipment used during this PhD is presented in Table 5.

Some of the items therein presented were ordered from new, others were already present in the laboratory (if ordered from new identified in description with letter *N*). This is important as the item properties might change with time.

Some of the items therein presented were exclusively used for this PhD, others were shared with other research projects (if shared identified in description with letter *S*). This is important as the item might be affected by cross-contamination.

Table 5 – Description and supplier/source of chemicals, materials, products and equipment used in this PhD.

Item	Description	Supplier/Source
H ₂ AuCl ₄ .3H ₂ O	Gold (III) precursor (99.99 %) (<i>N</i>)	Alfa Aesar (36400)
AuCl	Gold (I) precursor (99.99 %) (<i>N</i>)	Alfa Aesar (40432)
K ₂ PdCl ₄	Palladium (II) precursor (99.99 %) (<i>N</i>)/(<i>S</i>)	Alfa Aesar (11885)
AgNO ₃	Silver (I) precursor (99.9+ %) (<i>S</i>)	Alfa Aesar (11414)
CuCl ₂ .2H ₂ O	Copper (II) precursor (99+ %) (<i>N</i>)	Alfa Aesar (12458)
H ₂ IrCl ₆	Iridium (IV) precursor (99 %) (<i>S</i>)	Alfa Aesar (11031)
5 % wt. Pd/C	Commercial palladium catalyst (<i>N</i>)	Sigma-Aldrich (205680)
(C ₂ H ₄ O) _n	Polyvinyl alcohol stabilizer (Mw 9,000-10,000) (<i>N</i>)	Sigma-Aldrich (360627)
(C ₆ H ₉ NO) _n	Polyvinylpyrrolidone stabilizer (PVP) (<i>N</i>)	Sigma-Aldrich (PVP10)
TiO ₂	Titanium (IV) dioxide P25 used as catalysts support (<i>S</i>)	Fisher Scientific (10646903)
CeO ₂	Cerium (IV) dioxide used as catalysts support (<i>S</i>)	Sigma-Aldrich (544841)
C	Activated carbon used as catalysts support (<i>S</i>)	Cabot (VXC72R)
H ₂ O	Deionised water for synthesis, cleaning and reactions	Veolia Purelab Pulse

Experimental, Methods and Characterisation

2.1 Chemicals, Materials, Products and Equipment

Item	Description	Supplier/Source
C ₂ H ₆ O ₂	Ethylene glycol for nanoparticles synthesis (> 99 %) (N)	Sigma-Aldrich (102466)
C ₃ H ₈ O ₂	1,3-Propanediol for nanoparticles synthesis (98 %) (N)	Fisher Scientific (10041410)
C ₃ H ₈ O ₂	1,2-Propanediol for nanoparticles synthesis (99 %) (N)	Sigma-Aldrich (134368)
C ₃ H ₈ O ₃	Glycerol solution for nanoparticles synthesis (86-89 %) (N)	Sigma-Aldrich (49781)
C ₂ H ₅ OH	Ethanol for nanoparticles synthesis (S)	Fisher Scientific (12337163)
CH ₃ OH	Methanol for nanoparticles synthesis (S)	Fisher Scientific (10675112)
C ₆ H ₈ O ₆	Ascorbic acid for nanoparticles synthesis (99 %) (S)	Fisher Scientific (10152370)
NaOH	Sodium hydroxide solution 0.1 M (N)	Sigma-Aldrich (319481)
H ₂ SO ₄	Sulfuric acid solution 0.5 M (N)	Fisher Scientific (10734761)
C ₃ H ₆ O	Acetone used as a cleaning agent (N)(S)	Sigma-Aldrich (650501)
Hotplate	Magnetic hotplate with stirrer control (N)(S)	Fischer Scientific (10414452)
Micropipettes	100, 1000 and 5000 µL micropipettes (S)	Fischer Scientific (10315622)
200 µL	Micropipette tip (N)(S)	Fisher Scientific (11933426)
1250 µL	Micropipette tip (N)(S)	Fisher Scientific (11548442)
5000 µL	Micropipette tip (N)(S)	Fisher Scientific (11648138)
Microwave	Microwave device for nanoparticles synthesis (N)(S)	CEM Discover SP
Flow Cell	Microwave flow cell for continuous flow synthesis (N)	CEM (908910)
Pump	Peristaltic tubing pump 50-300 rpm (N)	Cole-Parmer (WZ-77122-24)
Pump Tubing	Masterflex Tygon E-Lab ID-2.54 mm (N)	Cole-Parmer (OU-06460-46)
Ultrasound	Ultrasound device for nanoparticles synthesis	Hielscher UIP2000hdT
Sound Box	Acoustic box for the ultrasound transducer and probe	Cardiff University Workshop
Foam	Acoustic foam for the ultrasound sound box (N)	RS Components (479-8199)

Experimental, Methods and Characterisation

2.1 Chemicals, Materials, Products and Equipment

Item	Description	Supplier/Source
Flask	10 and 25 mL Volumetric flask (<i>N</i>)	Sigma-Aldrich (Z326712)
Cylinder	100 mL Graduated cylinder (<i>S</i>)	Fisher Scientific (11547832)
Flask	100 mL Two neck round bottom flask (<i>N</i>)	Fisher Scientific (12478966)
Condenser	Condenser used with the round bottom flask (<i>N</i>)/(<i>S</i>)	Fisher Scientific (12000073)
Beaker	150 and 400 mL Beakers for nanoparticles synthesis (<i>N</i>)	Fisher Scientific (11916528)
Funnel	Buchner funnel for the filtration of catalysts	Fisher Scientific (12075113)
Flask	1 and 2 L Erlenmeyer for the filtration of catalysts	Fisher Scientific (15449103)
Agate Mortar	Mortar and pestle used to crush and grind catalysts (<i>N</i>)	Fisher Scientific (11735146)
Sieve	0.25 mm Sieve to reduce catalysts particles size (<i>S</i>)	Fisher Scientific (12934215)
NaBH ₄	Sodium borohydride used as reducing agent (> 96 %) (<i>N</i>)	Sigma-Aldrich (71320)
Spatula	PTFE Coated spatula to use with metal precursors (<i>N</i>)	Fisher Scientific (11553502)
Boat	Coors combustion boat for catalysts heat treatment (<i>N</i>)	Sigma-Aldrich (Z561746)
Tube	Furnace tube for catalysts heat treatment (<i>N</i>)/(<i>S</i>)	Sigma-Aldrich (Z655031)
Furnace	Furnace for catalysts heat treatment (<i>S</i>)	Carbolite
Cuvette	Hellma quartz cuvette 100-QS for UV-Vis analysis (<i>N</i>)	Sigma-Aldrich (Z600091)
Oil Bath	Temperature control of reactions (<i>S</i>)	Fisher Scientific (08-741C)
Reaction Set-up	Flasks for cinnamaldehyde hydrogenation reaction (<i>S</i>)	Radleys Reaction Station
U-Tube	Carbon monoxide oxidation reaction tube (<i>N</i>)	GPE Scientific (SP4908)
H ₂	Hydrogen used for hydrogenation reactions (<i>S</i>)	University Network
CO (5000 ppm)	Carbon monoxide in air for oxidation reaction (<i>S</i>)	University Network
C ₃ H ₈ (5000 ppm)	Propane in air for oxidation reaction (<i>S</i>)	University Network
Air	Air used for catalysts calcination treatment (<i>S</i>)	University Network
5% H ₂ /Ar	Hydrogen used for catalysts reduction treatment (<i>S</i>)	University Network

Experimental, Methods and Characterisation

2.1 Chemicals, Materials, Products and Equipment

Item	Description	Supplier/Source
C ₄ H ₆ O ₂	2,3-Butanedione for microwave optimisation (97 %) (N)	Sigma-Aldrich (B85307)
C ₂ H ₂ O ₄	Oxalic acid for microwave optimisation (> 99 %) (N)	Sigma-Aldrich (75688)
C ₂ H ₄ O ₃	Glycolic acid for microwave optimisation (99 %) (N)	Sigma-Aldrich (124737)
C ₂ H ₂ O ₃	Glyoxylic acid solution for microwave optimisation (50 %) (N)	Sigma-Aldrich (260150)
C ₂ H ₂ O ₂	Glyoxal solution for microwave optimisation (40 %) (N)	Sigma-Aldrich (128465)
C ₂ H ₄ O	Acetaldehyde solution for microwave optimisation (40 %) (N)	Sigma-Aldrich (W200379)
CH ₃ COOH	Acetic acid for microwave optimisation (> 99 %) (N)	Sigma-Aldrich (A6283)
D ₂ O	Deuterium oxide for NMR analysis (N)	Sigma-Aldrich (633178)
C ₃ H ₈ O	2-Propanol as a solvent for the furfural reaction (99.5 %) (S)	Sigma-Aldrich (278475)
C ₆ H ₅ CH ₃	Toluene as a solvent for the cinnamaldehyde hydrogenation reaction (99.8 %) (S)	Sigma-Aldrich (244511)
C ₉ H ₈ O	Trans-cinnamaldehyde for the hydrogenation reaction (99 %) (N)	Sigma-Aldrich (C80687)
HCOOH	Formic acid for the decomposition reaction (> 95 %) (S)	Sigma-Aldrich (F0507)
C ₆ H ₅ NO ₃	4-Nitrophenol for the reduction reaction (> 99 %) (S)	Sigma-Aldrich (241326)
NH ₂ NH ₂ .H ₂ O	Hydrazine monohydrate for the decomposition reaction (98 %) (S)	Sigma-Aldrich (207942)
C ₅ H ₄ O ₂	Furfural for the hydrogenation reaction (99 %) (S)	Sigma-Aldrich (319910)
C ₄ H ₆ O ₄	Succinic acid as calibration standard for the formic acid reaction (>99 %) (S)	Sigma-Aldrich (797987)
CH ₃ (CH ₂) ₁₁ OH	Dodecanol as calibration standard for the furfural hydrogenation reaction (> 98 %) (S)	Sigma-Aldrich (44095)
C ₆ H ₄ (CH ₃) ₂	<i>o</i> -Xylene as calibration standard for the cinnamaldehyde hydrogenation reaction (S)	Sigma-Aldrich (95660)
TEM Grid	Holey carbon film 300 mesh Cu for TEM analysis (N)	TAAB (C062/C)
UV-Vis	Ultraviolet and visible spectroscopy for colloids characterisation and reaction analysis (S)	Avantes Avalight-DH-S-BAL
DLS	Dynamic light scattering for colloids characterisation (S)	Malvern Zetasizer Nano ZS
TEM/EDX	Transmission electron microscopy with energy dispersive X-ray for colloids and catalysts characterisation (S)	JEOL JEM-2100 and Oxford Inst. X-Max ^N 80

Experimental, Methods and Characterisation

2.1 Chemicals, Materials, Products and Equipment

Item	Description	Supplier/Source
SEM/EDX	Scanning electron microscopy with energy dispersive X-ray for catalysts characterisation (S)	Hitachi TM3030PLUS
SEM/EDX	Scanning electron microscopy with energy dispersive X-ray for catalysts characterisation (S)	TESCAN MAIA3 and Oxford Inst. X-Max ^N 80
XPS	X-ray photoelectron spectroscopy for catalysts characterisation (S)	Thermo Scientific K-Alpha
DRIFTS	Diffuse reflectance infrared Fourier transform spectroscopy for catalysts characterisation (S)	Agilent 4000
GC	Gas chromatography for reaction analysis (S)	Agilent (several models)
LC	Liquid chromatography for reaction analysis (S)	Agilent 1220 Infinity
NMR	Nuclear magnetic resonance for the microwave optimisation tests (S)	Bruker (500 MHz)
pH Meter	pH measurements of the metal solutions and produced colloids (S)	Mettler Toledo

2.2 Analytical and Characterisation Techniques

This section introduces the basic theory and experimental procedure of the several analytical and characterisation techniques used during this PhD. Some of those techniques were used to characterise metal colloids, this was the case for UV-Vis (2.2.1), DLS (2.2.2) and TEM (2.2.3). TEM was also used to characterise the catalysts, same as SEM/EDX (2.2.4), XPS (2.2.5) and DRIFTS (2.2.6). Moreover, UV-Vis was also used as an analytical technique in order to measure the conversion in the 4-nitrophenol reduction reaction. Other analytical techniques included GC (2.2.7) and LC (2.2.8). Finally, the NMR technique (2.2.9) was mainly employed in the microwave optimisation tests in section 3.3.

2.2.1 Ultraviolet–Visible Spectroscopy (UV-Vis)

This technique uses the principle that ultraviolet and visible light interacts with matter, not only with particles as described in Figure 5, but also with solvents and solutions. The degree of interaction of light with matter is dependent on the concentration and can be represented by the Beer-Lambert law as shown in Equation 21. This light interaction with matter can take place by the same processes previously identified in Figure 5, namely by absorbance, scattering, reflection and refraction/transmission.

$$A = \log_{10} \left(\frac{I_0}{I} \right) = \epsilon LC \quad (21)$$

A is the absorbance, a dimensionless unit that measures how much light interacts with matter, the higher the absorbance the more the light is interacting. I_0 and I are related to the energy intensity of the light before (I_0) and after (I) passing through the sample. ϵ is an absorption coefficient ($\text{L m}^{-1} \text{mol}^{-1}$) which is dependent on the matter being analysed. For this reason, it is always necessary to trace a calibration curve of absorbance vs. solute concentration when testing different solvents even if the solute is kept constant. L is the length that the light travels through the sample (m) and C is the matter concentration (mol L^{-1}).

The measured absorbance values are not absolute. Instead these values are measured against a reference sample. In the case of the 4-nitrophenol reduction reaction the reference sample was water. When working with the synthesis of nanoparticles other solvents were also considered, mainly ethylene glycol. A schematic representation of a typical UV-Vis set-up is shown in Figure 22.

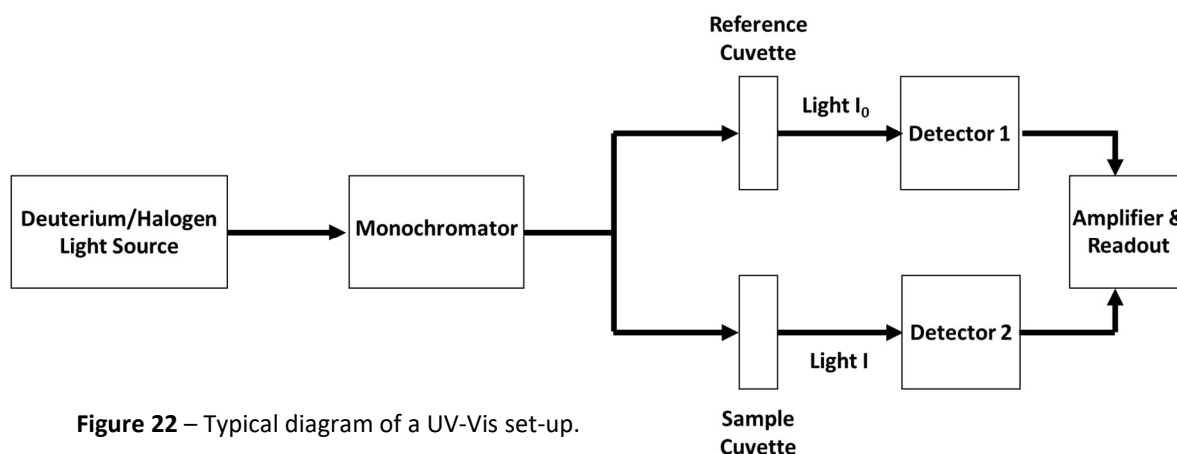


Figure 22 – Typical diagram of a UV-Vis set-up.

As described in section 1.2 some metal nanoparticles present a surface plasmon resonance effect. This allows UV-Vis, a simple and fast technique, to be employed with the produced metal colloids in order to assess trends for the reduction rate and the experimental results (production, average size and size distribution) just by analysing the plasmon peak in the UV-Vis spectrum.

Correlations between plasmon peak and the metal nanoparticles production, average size and size distribution are as follows: the higher the plasmon peak absorbance the more nanoparticles are produced, a decrease in the plasmon peak wavelength is an indication of a smaller nanoparticles average size and a narrower plasmon peak (smaller wavelength range) is an indication of a narrower nanoparticles size distribution.

A schematic representation is shown in Figure 23 for a better understanding of how the plasmon peak absorbance, the plasmon peak wavelength and the wavelength range are extracted from the UV-Vis spectrum.

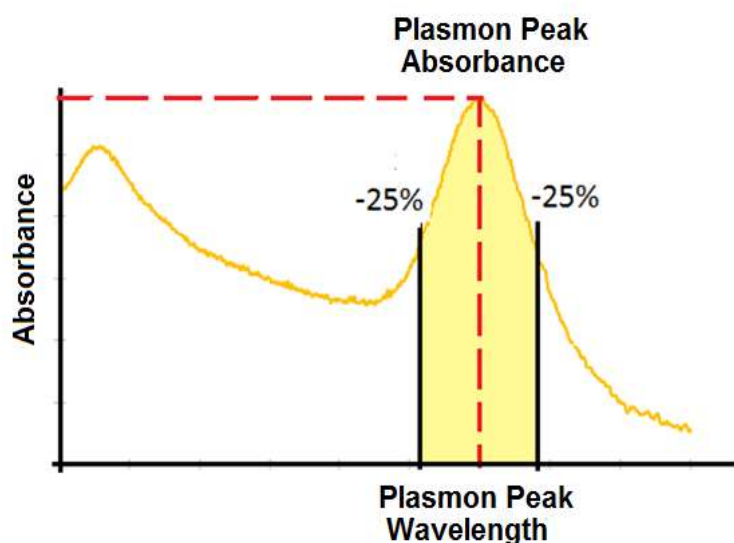


Figure 23 – Plasmon peak absorbance is read on y-axis, plasmon peak wavelength (nm) is read on x-axis and wavelength range (nm) comprises the coloured area.

Experimental, Methods and Characterisation

2.2 Analytical and Characterisation Techniques

It should be stressed that the size distribution was not measured by the normal standard deviation because many of the UV-Vis spectra were far from following a normal distribution and even among the different UV-Vis spectra different types of distribution were observed. Instead, a similar concept was implemented but based on the wavelength range associated with -25 % of the plasmon peak absorbance. As observed in Figure 23 the narrower the wavelength range is the narrower the size distribution.

From the UV-Vis spectrum the plasmon peak absorbance was calculated using *Excel* function $MAX(A_1)$ and the plasmon peak wavelength was calculated using *Excel* function $INDEX(A_2, MATCH(A_3, A_1, 0), 1)$, where A_1 is the absorbance column, A_2 is the wavelength column and A_3 is the plasmon peak absorbance.

2.2.2 Dynamic Light Scattering (DLS)

Another technique used to characterise colloidal metal nanoparticles is DLS. Similar to the UV-Vis technique described in section 2.2.1, the DLS also relies on the interaction of light with the metal nanoparticles due to the surface plasmon resonance effect. However, with DLS the sample cuvette is only irradiated with a fixed light wavelength of 633 nm and the detector measures the light scattered by the metal nanoparticles, not the refracted/transmitted light as it happens with UV-Vis.

Another difference between UV-Vis and DLS relates to the metal nanoparticles experimental results that can be assessed. As shown in Figure 23 UV-Vis gives an indirect measurement of the metal nanoparticles production, average size and size distribution, whereas with DLS a size distribution curve is calculated by applying Stokes-Einstein equation and no indication about the nanoparticles production is given.

It can be said that DLS is a more complex technique than UV-Vis as there are more factors affecting the experimental results:

- a) The calculated average size is the hydrodynamic size, which is influenced by the solvent molecules surrounding the nanoparticles;
- b) Experimental results present poor reproducibility;
- c) The average size is affected by the presence of a stabilizer, the nanoparticles shape and the nanoparticles degree of aggregation in the liquid;
- d) DLS is an intensity-weighted particle size measurement instead of a mass or number weighted particle size measurement. The amount of scattered light is strongly proportional to the particle size. As an example, one 10 nm nanoparticle would have an intensity signal 10^6 stronger than one 1 nm nanoparticle;

For all the above reasons it can be said that the DLS technique only provides an indication about the metal nanoparticles average size and size distribution and direct comparisons with other techniques should be avoided.⁸¹

Experimental, Methods and Characterisation

2.2 Analytical and Characterisation Techniques

The refractive index and extinction coefficient used in the DLS analysis were respectively 0.18 and 3.43 for Au⁸², 0.30 and 5.25 for Pd⁸³, 0.30 and 4.46 for Ag⁸³, 2.32 and 4.20 for Ir⁸⁴ and 0.27 and 3.41 for Cu.⁸² The calculation of a refractive index and extinction coefficient for a mixture is not linear.⁸⁵ However, for the bimetallic AuPd at different molar ratios the refractive index and extinction coefficient were assumed to be the weighted average based on the molar composition of each metal.

The nanoparticles average size (\bar{X}) and the size distribution, usually known as the standard deviation (σ), were calculated by applying Equation 22, which is valid when working with frequency data, with x_i being the size (nm) and I_i being the intensity (%). The calculated sample standard deviation was approximated to the population standard deviation as the sample was considered large enough.

$$\bar{X} = \frac{\sum x_i I_i}{\sum I_i} \quad \text{and} \quad \sigma = \sqrt{\frac{\sum I_i (x_i - \bar{X})^2}{\sum I_i}} \quad (22)$$

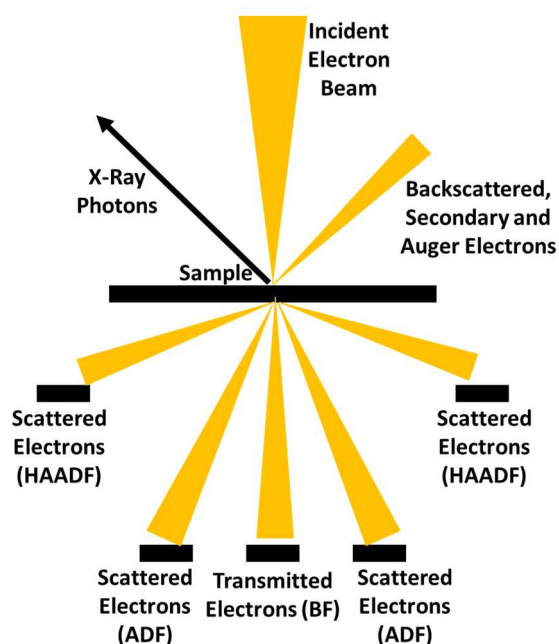
2.2.3 Transmission Electron Microscopy (TEM)

The previously described UV-Vis and DLS techniques allowed the characterisation of the metal nanoparticles in terms of production, average size and size distribution by analysing the produced metal colloids. This section introduces the TEM technique, which allows the characterisation of the metal nanoparticles in terms of average size and size distribution by analysing the metal colloids and/or the supported metal nanoparticles.

The metal colloids characterisation by UV-Vis, DLS and TEM was important to optimise and fully understand the experimental results obtained with the microwave and ultrasound synthesis methods as shown in chapters 3 and 4. However, when working with the model reactions in chapter 6 the metal nanoparticles average size and size distribution that should be linked to the catalytic activity are the ones obtained for the supported metal nanoparticles, which can only be obtained using TEM. During support addition stage metal nanoparticles can be excluded because of their size and/or shape. Moreover, changes can also happen during the drying stage at 110 °C for 16 h and during the heat treatments.

Contrary to UV-Vis and DLS, the TEM technique relies on the formation of an image able to provide resolutions as low as 0.1 nm as predicted by de Broglie equation. In order to form the image an electron beam of high energy and intensity is directed into the sample to be analysed under high vacuum conditions. The samples should be thin (<100 nm) and the used TEM operated at 200 kV (JEOL JEM-2100). Upon contact of electrons with the sample many outcomes are possible as shown by the schematic representation in Figure 24.

The aperture position of the TEM can be adjusted to choose how the image is formed, if using the transmitted electrons hitting the bright field detector (BF) or if using the scattered electrons hitting the annular dark field detector (ADF). During this PhD when working with TEM



only the bright field detector was used. In addition to the annular dark field detector it is also possible to detect scattered electrons at higher angles with the high-angle annular dark field detector (HAADF). Electrons may also not be able to pass the sample and be backscattered or produce secondary and Auger electrons. The production of secondary and Auger electrons is associated with electronic transitions and X-ray photons are also produced.

Figure 24 – Electron beam interaction with the sample.

Experimental, Methods and Characterisation

2.2 Analytical and Characterisation Techniques

TEM analysis of the colloidal metal samples is shown in chapters 3 and 4. In total nine drops of the metal colloid were added with the 100 μL micropipette to the TEM grid. The TEM grid was then dried carefully with the laboratory paper in order to remove as much as possible non-volatile organic solvents, for example ethylene glycol.

TEM analysis of the supported metal nanoparticles samples is shown in section 5.2. The catalyst (around 1 mg) was first added to a vial with approximately 1 mL of ethanol. Afterwards, the vial was immersed for 2 min in a generic laboratory ultrasonic cleaning bath. This allowed the catalyst to be homogeneously dispersed. Using the 100 μL micropipette one drop was added to the TEM grid.

Typically, each sample was analysed with 7-10 images and the metal nanoparticles were manually counted using the *ImageJ* software. Each one of the analysed particles had two sizes measured, one on the vertical position and the other one on the horizontal position, with the two sizes passing by the centre of the particle. The metal nanoparticle size was considered to be the average of the two measured sizes. The sample average size and size distribution were then calculated by having in consideration the average size and standard deviation of all the metal nanoparticles, at least 200 metal nanoparticles in each sample. For each sample the metal nanoparticles size distribution histogram was presented providing information regarding the shape of the size distribution curve, total metal nanoparticles count and cumulative frequency.

Energy dispersive X-ray analysis (EDX) was also done to the colloid metal samples aiming to confirm the TEM results and rule out any contamination as the TEM was coupled to an EDX detector (Oxford Inst. X-MaxN 80). This EDX analysis could not be performed to the supported metal nanoparticles samples due to a saturation signal from the support. The EDX analysis uses the produced X-ray photons as shown in Figure 24 in order to identify the chemical elements and their composition in the sample.

Selected AuPd (1:1) colloidal and supported samples were sent to Lehigh University to be analysed under the supervision of Christopher Kiely and Qian He by high-resolution TEM operating at 200 kV (JEOL ARM 200CF). The used mode was STEM, which focus the electron beam into a very small spot that is scanned over the sample, and the high-angle annular dark field detector (HAADF) was used. The objective of this analysis was to confirm that the bimetallic nanoparticles were of the alloy type and that no individual Au or Pd nanoparticles had been produced.

2.2.4 Scanning Electron Microscopy and Energy Dispersive X-ray (SEM/EDX)

Similar to the TEM analysis, the SEM analysis also uses the outcome of the interaction of an electron beam with the sample to produce an image as shown in Figure 24. In the case of the SEM image this is due to the backscattered and secondary electrons and only supported metal nanoparticles samples were analysed. Compared to the TEM, the SEM operates at a lower voltage and offers an image with more detailed information about the morphology of the surface of the catalyst but with a lower resolution.

Two SEM devices have been used during this PhD. The most used was the Hitachi TM3030PLUS operating at 5kV or 15kV and incorporating an EDX detector. This device was only used in order to perform EDX analysis to the supported metal nanoparticles samples and identify the chemical elements and their composition in the bulk of the catalyst as shown in section 5.3. Several milligrams of catalyst were necessary to prepare a sample. They were first deposited on a clean surface and squeezed against a copper tape producing a thick layer. This copper tape was then placed on the SEM stub and moved inside the SEM chamber to perform the analysis.

Another SEM device used during this PhD was the TESCAN MAIA3 operating between 5-30 kV. This device was only used with TiO₂ supported metal nanoparticles samples when a clear image could not be produced by the TEM analysis. This was the case when metal nanoparticles had sizes larger than 10-12 nm, of the same order of magnitude than the TiO₂ particles, therefore making the contrast between the support and the metal nanoparticles very difficult. The incident electron beam for this SEM was produced with a field emission gun providing a brighter (more monochromatic) and stable electron source than with the LaB₆ filament used with the TEM. The samples to be analysed by this SEM were prepared in the same way as described for the TEM analysis in section 2.2.3.

2.2.5 X-ray Photoelectron Spectroscopy (XPS)

Another characterisation technique employed with the supported metal nanoparticles was XPS. Similar to the EDX technique, the XPS technique also provides information about the chemical elements and their composition in the catalyst. However, XPS provides information for the catalyst surface rather than the catalyst bulk as it is limited to a depth of approximately 5 nm, depending on the XPS device. The used XPS (Thermo Scientific K-Alpha) uses aluminium K-alpha X-rays presenting a photon energy of 1486.6 eV and a wavelength of 0.834 nm. According to Mane and Patil⁸⁶ almost 95 % of the electrons emitted from the catalyst surface are from atoms within a depth of three times the wavelength of the incident X-ray, *i.e.* 2.5 nm in the case of the used XPS. Moreover, XPS provides information about the binding energy allowing to understand the oxidation state and in which compound form the chemical element is present. XPS analysis is also used to provide insight about the surface coverage of the metal. It can be said that XPS is a surface analysis tool particularly important to link the catalyst surface state to the catalytic activity of the several reactions presented in chapter 6 as adsorption of the substrates to the active sites is a surface phenomenon. The XPS analysis of the produced catalyst is shown in section 5.4.

The XPS working principle is different from that of TEM, SEM and EDX, which is represented in Figure 24. In the case of XPS the sample is not subjected to an incident electron beam, but rather to a controlled monochromatic X-ray beam with a specific energy making use of the photoelectric effect under ultra-high vacuum conditions. The photoelectric effect was theorized at the 19th century and beginning of 20th century by scientists such as Hertz, Planck and Einstein. This effect states that the action of removing an electron from an atom is dependent on the energy of the incident photon and not of the total energy (intensity).

When using the XPS (Thermo Scientific K-Alpha) with X-rays having a photon energy of 1486.6 eV all electrons whose removal energy, mainly expressed by the binding energy, is less than 1486.6 eV are able to be removed from the atom. The excess of energy is converted into kinetic energy for the removed electron. A detector is then able to measure the kinetic energy of the removed electrons and present a correlation between intensity of detected electrons (counts per second) and binding energy (eV). The electron removal energy is not equal to the binding energy as it is necessary to take into account the spectrometer work function. Therefore, the binding energy can be considered as the energy necessary to bring an electron from its core level to the Fermi level. The binding energy should also be corrected with the surface charge energy. This is usually done by calibrating the XPS instrument with C1s at 285 eV. A schematic representation is shown in Figure 25.

$$\text{Binding Energy} = 1486.6 \text{ (eV)} - \text{Kinetic Energy} - \text{Spectrometer Work Function} - \text{Surface Charge Energy}$$

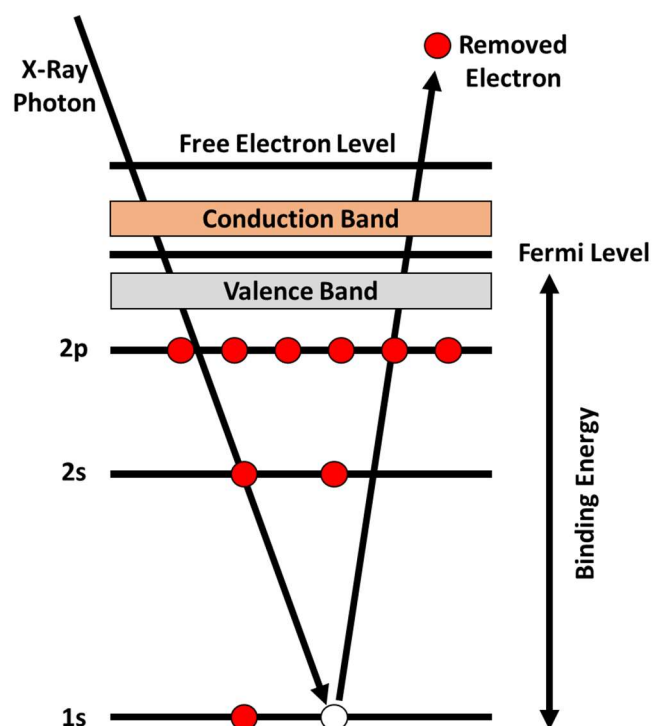


Figure 25 – X-ray photon interaction with electrons from the sample.

(adapted from the literature)⁸⁶

All the XPS results were analysed with the *CasaXPS* (v2.3.20) software.

The Pd peaks were analysed in the Pd 3d region (binding energy of around 335.0 eV for metallic Pd and of around 336.7 eV for Pd²⁺). The two Pd peaks due to spin-orbit splitting (Pd 3d_{5/2} and 3d_{3/2}) are separated by 5.26 eV. Some interference from Au 4d can be observed in this region of the energy spectrum.

The Au peaks were analysed in the Au 4f region (binding energy of around 84.0 eV for metallic Au). The two Au peaks due to spin-orbit splitting (Au 4f_{7/2} and Au 4f_{5/2}) are separated by 3.7 eV. Some interference from TiO₂ can be observed in this region of the energy spectrum.

The Ir peaks were analysed in the Ir 4f region (binding energy of around 60.9 eV for metallic Ir and of around 61.5 eV for Ir⁴⁺). The two Ir peaks due to spin-orbit splitting (Ir 4f_{7/2} and Ir 4f_{5/2}) are separated by 3.0 eV.

Full details about the XPS parameters can be found in the literature⁸⁷, including for other chemical elements analysed in this PhD, namely Ti, Ce, C, O, Cl, S and K. Some of the metal peak fittings for different catalysts can be found in section 5.4.

2.2.6 Diffuse Reflectance Infrared Fourier Transform Spectroscopy (DRIFTS)

Similar to UV-Vis and DLS, the DRIFTS technique also relies on the interaction of light with matter to produce an absorption spectrum, in this case using infrared light. The infrared light is capable of promoting molecular vibrational transitions with the energy associated with these transitions dependent on the probe molecule used and on the type and strength of the molecule bond to the catalyst active sites. Some common probe molecules for metal active sites include hydrogen, nitrogen oxide and carbon monoxide. When working with acid and basic active sites some common probe molecules include ammonia, pyridine and carbon dioxide as well as carbon monoxide.

For this PhD some of the supported metal nanoparticles were analysed with DRIFTS by probing the interaction of carbon monoxide with the metal nanoparticles active sites. Depending on the type of metal active site the carbon monoxide adsorbs differently to the surface. The carbon monoxide can adsorb with a hollow configuration ($1800\text{-}1900\text{ cm}^{-1}$), a bridge configuration ($1910\text{-}2000\text{ cm}^{-1}$) or a linear configuration ($2040\text{-}2120\text{ cm}^{-1}$).⁸⁸ The DRIFTS absorbance spectra can be found in section 5.5.

Ultimately, the objective was to understand if the different catalytic activities observed in chapter 6 for the same metal, for example AuPd produced by microwave vs. AuPd produced by ultrasound, could be explained by the presence of different types of metal active sites.

The experimental procedure with this technique consisted in placing first several milligrams of the catalyst inside the sample cup, compressing the catalyst with a spatula so that the flowing of gases would not cause any powder to be dragged away. The sample cup was then moved inside the DRIFTS chamber and 50 mL min^{-1} nitrogen was supplied with the vacuum pump turned on. This was done in order to remove as much as possible other adsorbed species to the catalyst. When no more changes were detected to the infrared absorbance spectrum the baseline was recorded. The vacuum valve was then closed and the supplied gas was changed to 50 mL min^{-1} of a 20 % carbon monoxide in nitrogen mixture. The infrared spectrum was recorded at the beginning and then at every minute until carbon monoxide saturation had been reached. All the work was carried out at $30\text{ }^{\circ}\text{C}$.

2.2.7 Gas Chromatography (GC)

The conversions and selectivities for several of the reactions presented in chapter 1 were obtained using GC analysis in order to calculate the concentration of reactants and products. This was the case for the carbon monoxide oxidation, for the propane total oxidation, for the furfural hydrogenation and for the cinnamaldehyde hydrogenation.

The working principle of GC analysis consists in injecting liquid and gas samples into a column. When analysing liquid samples, the injector presenting temperatures as high as 200-300 °C is able to immediately vaporize the liquid sample. The sample is carried across the column by a carrier gas, for example helium.

Each of the components of the sample interacts differently with the column. The component with the strongest interaction with the column will present the highest retention time. The component with the weakest interaction with the column will present the lowest retention time. All the other components will have intermediate retention times. The column is placed inside an oven and different temperatures can be selected in order to also influence the mobility of the different components.

As the components are carried across the column, they should be fully separated by the time they reach the detector. The detector placed at the end of the column is able to measure a signal proportional to the amount of component, usually rendering a symmetric peak in a detector signal vs. retention time plot. The total area of the peak is proportional to the total amount of the component. A schematic representation of a typical GC set-up is shown in Figure 26.

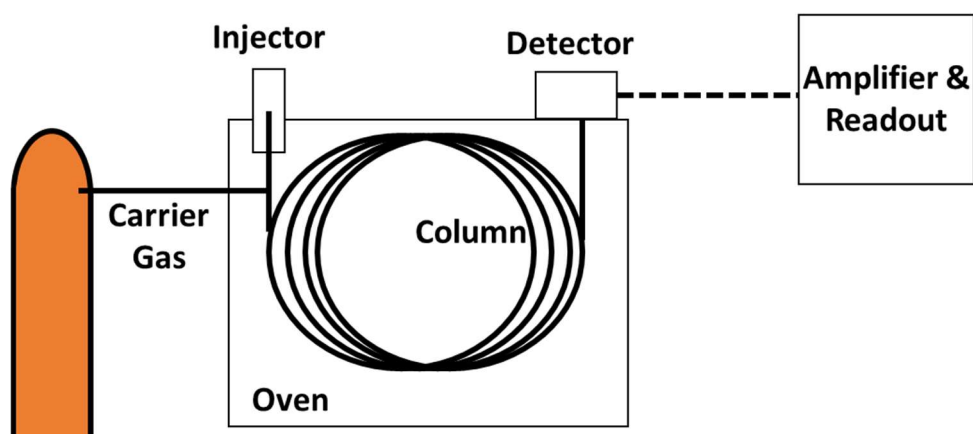


Figure 26 – Typical diagram of a GC set-up.

Experimental, Methods and Characterisation

2.2 Analytical and Characterisation Techniques

Unlike other analytical techniques, the GC analysis is dependent on several operating parameters that can be defined by the user. The set of all the operating conditions defines what is usually known as the GC method. However, it is not possible to talk about a right method for a specific GC analysis. As long as there is a good separation (resolution) between the different peaks of the different components the method should be considered correct as the objective of quantifying the reactants and products can be achieved. Some of the most important GC operating parameters can be summarized as follows:

a) GC column: There are several types of column that can be installed. During this PhD only capillary columns were used. This type of column presents a stationary phase coating on the inner wall of the column instead of being packed in the entire column. The polarity of the column is an important factor affecting the interaction with the components. The working temperature should also be taken into account when selecting the GC column. Other important factors that can be selected include the column length and diameter;

b) Injector temperature: According to the Agilent GC manufacturer the injector temperature should be selected in order to immediately vaporize the entire sample, 50 °C above the boiling point of the less volatile component. However, it is necessary to make sure that high temperatures will not cause degradation of any of the components in the sample;

c) Split/splitless injection: it is possible to tune the amount of injected sample that goes into the column by selecting different ratios between the purged carrier gas and the carrier gas going to the column. Splitting the amount of injected sample should produce better peaks;

d) Flow rate: as a rule of thumb the total flow inside the column should be adjusted to obtain velocities of around 40-50 cm/s;

e) Oven temperature: different temperature profiles can be created and as a rule of thumb the initial oven temperature should start at a temperature 20 °C below the boiling point of the sample solvent. Choosing a right temperature profile is paramount to prevent an unnecessary long GC method;

The GC detectors used during this PhD included:

a) FID: flame ionisation detector that measures the intensity of ions produced by combustion when passing the components by a hydrogen generated flame. This detector is not suitable to all components, for example water;

b) TCD: thermal conductivity detector that can be used with all sort of components and measures changes in the thermal conductivity of the carrier gas due to the components;

c) MS: mass spectrometer that can be used with all sort of components and measures the intensity and the mass/charge ratio of different ions produced by ionizing the components;

Experimental, Methods and Characterisation

2.2 Analytical and Characterisation Techniques

The GC analysis is not limited to the creation of a suitable GC method. Often it is also necessary to create a calibration curve for each one of the components that are going to be analysed, this is valid for both the reactants and for the expected products.

A calibration curve can be described as the correlation between the peak area produced by the GC detector and the quantity of the component. The quantity of the component can be expressed in either mol or mass. This method is called the external standard method as it compares peak areas in an unknown sample with areas produced by a known amount of the same component in a standard sample.⁸⁹

When working with the liquid phase reactions of cinnamaldehyde hydrogenation and furfural hydrogenation an additional component, not a reactant nor an expected product but a component with similar physical and chemical properties, was always added to any sample that was analysed by GC, whether standard samples used for the calibration curve or samples of unknown concentration. Adding this fixed amount of an additional component is called the internal standard method. This method aims to improve the accuracy of the GC analysis by correcting for volume errors due to sample preparation, evaporation or injection errors. The internal standard can be added either before or after the reaction. The calibration curve becomes then a correlation between the ratio of peak areas and the ratio of quantities.⁸⁹⁻⁹⁰

A calibration curve for a generic component with the external standard method is shown in Equation 23 and with the internal standard method is shown in Equations 24a and 24b. Equation 24 is split into two in order to show that calibration curves can also directly incorporate the concentration values even though the GC detector only measures a component quantity. All the differences end up being reflected in the *Rf* value. The *Rf* stands for response factor and is obtained from the linear regression calculated by the GC analysis of the standard samples. During this PhD each calibration curve was performed by measuring peak areas of at least six standard samples.

$$\text{Amount Component A} = Rf_1 * \text{Peak Area Component A} \quad (23)$$

$$\frac{\text{Amount Component A}}{\text{Amount Internal Standard}} = Rf_2 * \frac{\text{Peak Area Component A}}{\text{Peak Area Internal Standard}} \quad (24a)$$

$$\frac{\text{Concentration Component A}}{\text{Concentration Internal Standard}} = Rf_3 * \frac{\text{Peak Area Component A}}{\text{Peak Area Internal Standard}} \quad (24b)$$

2.2.8 Liquid Chromatography (LC)

LC analysis was used with the formic acid reaction. The working principle of this analytical method is similar to the GC, previously described in Figure 26. However, instead of vaporizing the sample and using a carrier gas, with the LC analysis the sample remains in the liquid form and is carried across the column by a liquid carrier. Compared to the GC analysis, the LC analysis is more suitable when:

- a) The components to be analysed present a very high boiling point (> 300 °c);
- b) The different components in the sample present boiling points very similar to one another and therefore there is no advantage in using GC as changes in mobility will not be obtained by changing the oven temperature;
- c) The components to be analysed are very sensitive to temperature degradation;
- d) The used solvent is water, which is more likely to damage GC columns;

During this PhD the used LC device was an HPLC Agilent 1220 Infinity with a reversed phase column. The HPLC stands for high pressure LC, which means the sample analysis is faster than if using standard LC analysis. The LC columns are packed and a reversed phase column means that the column is non-polar and the carrier liquid is moderately polar. The used carrier liquid was an aqueous solution of phosphoric acid (0.1 wt. %). The HPLC detector was an UV-Vis working at a fixed wavelength.

2.2.9 Nuclear Magnetic Resonance Spectroscopy (NMR)

NMR analysis was mainly performed in the microwave optimisation tests in section 3.3 with the objective of identifying possible compounds formed during the synthesis of the colloidal metal nanoparticles and with the objective of checking stability of known compounds before and after the microwave synthesis by monitoring any changes to the NMR spectrum.

The main advantage of using NMR analysis over another suitable analytic technique considered during this PhD (GC-MS) is that there is no need to separate the metal nanoparticles present in the colloids, which are non-volatile and would damage the GC column. It is also a more suitable technique to analyse the non-volatile stabilizers PVA and PVP present in the colloids, which would otherwise decompose. Other NMR advantages include a more flexible approach to create a method with good resolution by analysing different nuclei, with the most common nuclei being ^1H and ^{13}C . NMR can also be considered as a non-destructive technique.

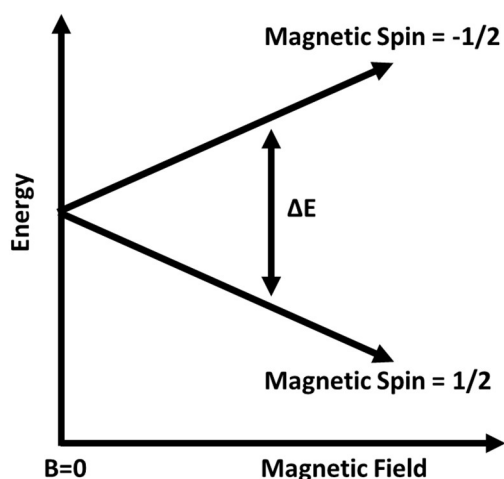


Figure 27 – External magnetic field effect on the energy level of nuclei with magnetic spin of $\pm 1/2$.

The working principle of NMR relies in the interaction of a strong and constant external magnetic field with the nuclei of the molecules. The nuclei need to present a nuclear magnetic spin. This is the case for nuclei with an odd number of protons and/or neutrons. During this PhD only ^1H and ^{13}C NMR analysis was performed with both elements having a magnetic spin of $\pm 1/2$. As the magnetic field (B) strength is increased so is the energy gap (ΔE) between the two magnetic spin states. A schematic representation is shown in Figure 27. The energy gap is a characteristic of each nucleus and is associated with the emission of radio frequency (60-1000 MHz) according to the Planck-Einstein relation. An NMR spectrum can then be created by plotting the intensity signal of the emitted radio frequency as a function of the radio frequency. Equation 25 gives the correlation between the emitted frequency and the magnetic field.

$$f = \frac{\gamma(B - B_e)}{2\pi} \quad (25)$$

Experimental, Methods and Characterisation

2.2 Analytical and Characterisation Techniques

f is the emitted radio frequency (Hz), $\gamma/2\pi$ is the gyromagnetic ratio a characteristic of each nucleus (Hz T^{-1}) and B is the magnetic field (T).

The strength of the external magnetic field is usually decreased by the presence of neighbouring electrons creating a shielding effect. This is represented in Equation 25 by the B_e factor. Moreover, splitting effects in the NMR peaks can be often observed as the emitted radio frequency by a nucleus is also affected by the presence of neighbouring nuclei of the same kind. These unique features create different frequencies for the same nuclei therefore making NMR a very important tool to understand the structure of complex molecules.

As the emitted radio frequency is dependent on the strength of the magnetic field it is necessary to create a universal scale so that measurements in two different NMR devices can be compared. This is achieved using a chemical shift scale (δ expressed in ppm) and using a reference compound, usually tetramethylsilane. As shown in Equation 26 the radio frequency emitted by the desired nucleus in a specific NMR device is always compared to the radio frequency of the reference compound obtained in the same NMR device.

For the NMR analysis 0.1 mL of the desired sample was mixed with 0.6 mL of deuterium oxide inside the NMR tube.

$$\delta = \frac{f - f_{reference}}{f_{reference}} * 10^6 \quad (26)$$

2.3 Microwave Synthesis

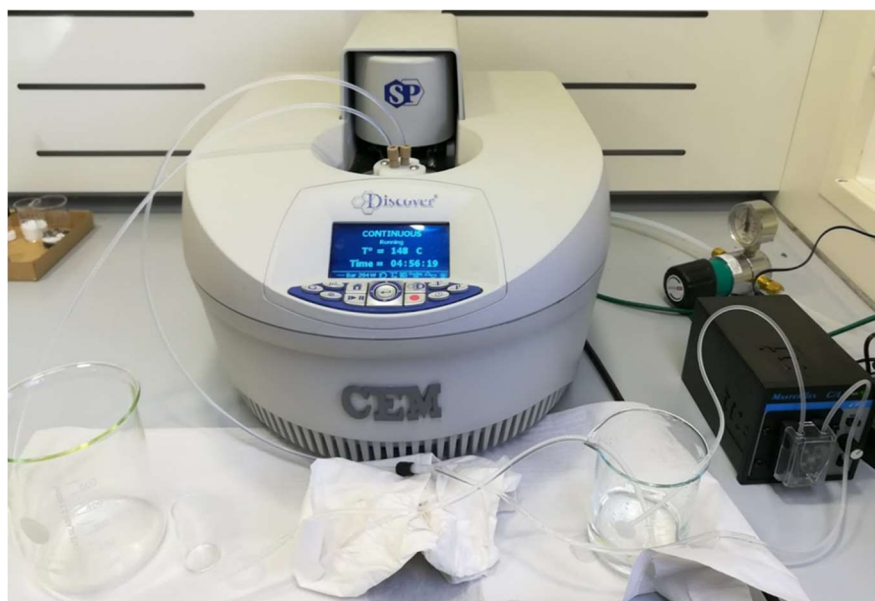


Figure 28 – Microwave synthesis experimental set-up used under continuous flow regime.

The microwave synthesis of metal nanoparticles was tested at several operating conditions as presented in chapter 3. The microwave synthesis was carried out both under batch and continuous flow regime with the microwave device operating under continuous flow regime shown in Figure 28.

Typically, Au, Pd, Ag, Ir and Cu aqueous/organic solutions were prepared in 10 mL volumetric flasks and used no more than 4-5 weeks after their preparation. The same was applied for the stabilizer solutions of polyvinyl alcohol (PVA) and polyvinylpyrrolidone (PVP). If necessary mild temperature ($\approx 50\text{ }^{\circ}\text{C}$) and stirring were applied to make sure the solutes were properly dissolved. Due to their sensitivity in being reduced when exposed to light Au and Ag solutions were protected by aluminium foil. All the prepared solutions were stored in glass vials.

A micropipette (1000 μL) was usually used to measure the desired volume of each one of the solutions and prepare the final synthesis solution. This final synthesis solution was prepared just moments before the microwave synthesis. Before each microwave synthesis a 2 mL sample of the final synthesis solution was analysed by UV-Vis in a quartz cuvette. This was done to ensure that there were no deviations from the expected concentration and that no changes due to undesired reduction were occurring to the metal stock solution over time.

Experimental, Methods and Characterisation

2.3 Microwave Synthesis

When working under batch regime a total volume of 20 mL of the synthesis solution was used and placed inside a 35 mL microwave vessel. Due to safety reasons indicated by the microwave manufacturer the full 35 mL could not be used.

After each microwave synthesis 2 mL samples of the produced colloidal metal nanoparticles were analysed by UV-Vis in a quartz cuvette with the experimental results assessed as described in section 2.2.1. Photos of the colloids were also taken. For some trials, sodium borohydride, a strong reducing agent used for the traditional sol-immobilization protocol (section 1.4.2.1), was added to the cuvette with no major changes expected if metal ions reduction had been completed. Selected metal colloids were characterised by DLS and TEM so that the metal nanoparticles average sizes and size distribution could be calculated.

When working under continuous flow regime a total volume of 200 mL of the synthesis solution was used and placed inside a beaker as shown in Figure 28. The synthesis solution was fed by a single channel Cole-Parmer Masterflex C/L 300 rpm peristaltic pump to a 10 mL flow cell present inside the microwave device.

The produced colloidal metal nanoparticles were then collected in a different beaker. The metal colloids were analysed over time by UV-Vis analysis (at $t=0$, 30 and 60 min) to monitor stability and assess the experimental results as described in section 2.2.1. The rest of the experimental procedure was exactly the same as the one described for batch regime.

A magnetic stirrer supplied by the microwave manufacturer was placed inside the 35 mL vessel or the 10 mL flow cell and cleaned with *aqua regia* after each microwave trial. This was done to ensure only homogeneous nucleation would take place, therefore achieving smaller nanoparticles average size and narrower size distribution and better reproducibility from one trial to another. Ensuring only homogeneous nucleation is particularly important when the metal ions reduction is slow as it is the case with microwave synthesis (see section 1.4.1 for more details).

2.4 Ultrasound Synthesis



Figure 29 – Ultrasound synthesis experimental set-up used under batch regime.

The ultrasound synthesis was carried out under batch regime. As shown in Figure 29 the ultrasound transducer and probe were placed inside a sound box and the ultrasonic generator was left outside the sound box. When in operation the sound box was fully closed (Figure 29 right). This sound box was necessary in order to minimise as much as possible the loud noise produced during operation. This noise was not related to the sonication itself as the device operates at 20 kHz, above the threshold for human audition, but it was related to the cavitation effect on the synthesis solvent (water and/or ethylene glycol).

Due to safety/technical reasons the ultrasound operation was limited. This was due to the aforementioned loud noise generated during operation as even with the sound box protection measurements have indicated a sound level of 80-90 dB in the surrounding area. This meant that during the 3 years this PhD research took place the ultrasound could only be used for 1 year. This has seriously reduced the number of ultrasound experiments undertaken, in particular the ones necessary for a correct optimisation procedure, similar to what was done with the microwave. Despite this major limitation, it was still possible to observe, register and analyse interesting experimental results during the 1-year operation of the ultrasound.

The ultrasound synthesis of metal nanoparticles was tested at several operating conditions as presented in chapter 4. The wave energy intensity expressed by Equation 11 and described in detail in section 1.4.4 plays an important role on the cavitation effect responsible for the metal ions reduction. However, as the ultrasound frequency could not be changed as it was a device feature and fixed at 20 kHz the energy intensity was then changed by changing the ultrasound wave amplitude, with the device presenting an amplitude scale of 50-100 %. Most of the ultrasound trials were carried out at 60 % amplitude.

Typically, Au, Pd and Ir aqueous/organic solutions were prepared in 10 mL volumetric flasks and used no more than 4-5 weeks after their preparation. The same was applied for the stabilizer solutions of polyvinyl alcohol (PVA) and polyvinylpyrrolidone (PVP). If necessary mild temperature (≈ 50 °C) and stirring were applied to make sure the solutes were properly dissolved. Due to their sensitivity in being reduced when exposed to light Au solutions were protected by aluminium foil. All the prepared solutions were stored in glass vials.

A micropipette (1000 μ L) and a graduated cylinder (100 mL) were usually used to measure the desired volume of each one of the solutions and prepare the final synthesis solution. This final synthesis solution was prepared just moments before the ultrasound synthesis. A total volume of 75 mL of the synthesis solution was used and placed inside a beaker (100 mL). A magnetic stirrer was added to the beaker and the synthesis solution was mixed for a couple of minutes on the magnetic hotplate. The stirrer was then removed and not used during the ultrasound synthesis. This was due to space constraints inside the sound box and also because it was observed that the cavitation effect itself was enough to create intense agitation inside the beaker during operation.

Before each ultrasound synthesis a 2 mL sample of the final synthesis solution was analysed by UV-Vis in a quartz cuvette. This was done to ensure that there were no deviations from the expected concentration and that no changes due to undesired reduction were occurring to the metal stock solution over time.

After each ultrasound synthesis 2 mL samples of the produced colloidal metal nanoparticles were analysed by UV-Vis in a quartz cuvette with the experimental results assessed as described in section 2.2.1. Photos of the colloids were also taken. For some trials, sodium borohydride, a strong reducing agent used for the traditional sol-immobilization protocol (section 1.4.2.1), was added to the cuvette with no major changes expected if metal ions reduction had been completed. Selected colloids were characterised by DLS and TEM so that the metal nanoparticles average sizes and size distribution could be calculated.

2.5 Immobilisation of Metal Colloids

As explained in section 1.1 as the particle size decreases the percentage of metal surface atoms becomes higher. These surface atoms are less coordinated than bulk atoms and for this reason have a higher energy content. Thus, metal nanoparticles tend to agglomerate in order to decrease their energy content.⁴ If the metal nanoparticles are instead immobilised on a support this agglomeration effect can be greatly reduced.

Another advantage of immobilisation of metal nanoparticles is that there are important metal-support interactions due to charge transfer, due to edge effects at the metal/support interface and due to a spillover effect with migration of atoms through diffusion. All these metal-support interactions can contribute to an enhanced catalytic activity.⁵

The support also allows metal nanoparticles to be used as heterogeneous catalysts in gas/liquid phase reactions thus avoiding/making easier catalyst separation from the products.

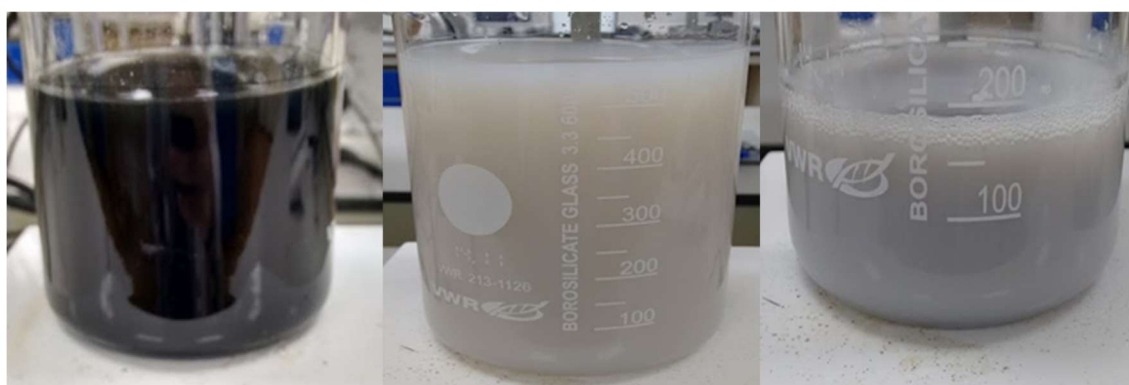


Figure 30 – Support addition stage of AuPd (1:1 molar) nanoparticles produced by microwave synthesis with carbon (left) and with TiO₂ (middle) and produced by ultrasound synthesis with TiO₂ (right).

Selected metal nanoparticles produced by microwave and ultrasound synthesis were supported in commercial supports of titanium dioxide (TiO₂), activated carbon (C), and cerium dioxide (CeO₂) by adapting the support addition stage of the traditional sol-immobilization protocol, previously mentioned in section 1.4.2.1. Photos of the support addition stage for some of the produced AuPd (1:1 molar) nanoparticles are shown in Figure 30. The adapted support addition stage is highlighted below:

- a) Add the necessary amount of the desired support to the metal colloid in order to produce a catalyst with a total nominal metal weight ratio of 1 wt. % and stir it for 60 min;
- b) If the support is TiO₂ add some drops of H₂SO₄ to the mixture in order to reach a pH of 1-2 (the pH will control the adsorption of the active metal onto the support as described in Figure 9);

Experimental, Methods and Characterisation

2.5 Immobilisation of Metal Colloids

- c) Filter the catalyst under vacuum and wash it with at least 1 L of deionized water until no traces of organic solvents are visible in the filtrate and on surface of the catalyst;
- d) Dry the catalyst under static conditions in an oven at 110 °C for 16 h;

Ethylene glycol was the most used organic solvent as described in chapters 3 and 4. When working with microwave synthesis the total volume of the metal colloid was usually around 120 mL, *i.e.* the total volume for six batch trials (6x20 mL). When working with ultrasound synthesis the total volume of the metal colloid was usually around 225 mL, *i.e.* the total volume for three batch trials (3x75 mL). However, in Figure 30 the metal colloid volume of microwave synthesis is considerable higher than the one of ultrasound synthesis. This was related to different mixture compositions. The metal colloids produced by microwave synthesis were usually a mixture with 100 % ethylene glycol, whereas the metal colloids produced by ultrasound synthesis were usually a mixture with 75 % water and 25 % ethylene glycol. In order to be consistent and to be as close as possible to the traditional sol-immobilization protocol (100 % water) the metal colloids produced by microwave synthesis were diluted to 75 % water and 25 % ethylene glycol before adding any support.

During the catalyst filtration it was sometimes necessary to recycle the first filtrate and filter it again. An example is shown in Figure 31 for the AuPd (1:1 molar) nanoparticles produced by microwave synthesis. On the left photo the first filtrate presents a visible amount of the catalyst. This first filtrate was collected and placed again inside the beaker. A new filtration was then performed with the first filtrate. As seen on the right photo the second filtrate presented now no visible amount of the catalyst. The catalyst was then washed with at least 1 L of deionized water as previously mentioned.

The clear filtrate, before adding washing water, was checked by UV-Vis spectroscopy. This was done to ensure that all the metal nanoparticles had been supported and not lost in the filtrate, therefore affecting the expected nominal metal loading of 1 wt. %.

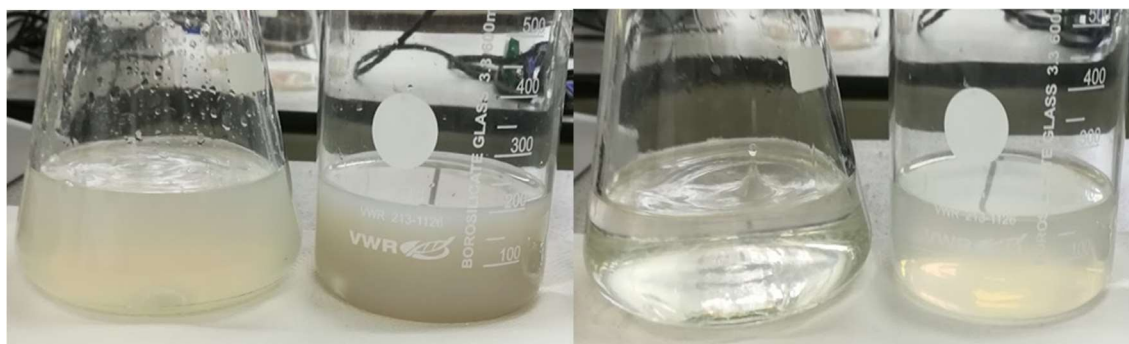


Figure 31 – Filtration of AuPd (1:1 molar) nanoparticles produced by microwave synthesis with the first filtrate (left) and after new filtration of the first filtrate (right).

2.6 Heat Treatment



Figure 32 – Photos of a Pd/TiO₂ catalyst before any heat treatment (top) and after the calcination step (middle) and of the furnace tube used for the reduction step (bottom).

Some of the produced catalysts were heat-treated in order to understand if the support-metal interactions mentioned in section 2.5 could be stronger and lead to a higher catalytic activity for the reactions described in section 1.6 with the experimental results presented in chapter 6. Another objective was to understand if the catalytic activity could also be improved by removing traces of the stabilizer still present on the catalyst surface. According to Rao *et al.*⁹¹ thermal degradation is expected for PVA above 200 °C and for PVP above 250 °C. It should be stressed that without any heat treatment all the tested catalysts showed no activity for the 4-nitrophenol reduction (section 6.2) due to metal nanoparticles leaching and no activity for the carbon monoxide oxidation (section 6.3).

The catalysts were heat-treated in two steps, first calcination in flowing air at 200, 300 or 400 °C and afterwards reduction in flowing 5% H₂ in argon at 300 or 400 °C. The most used condition was 400 °C for 3 hours for the calcination step and 300 °C for 3 hours for the reduction step. The heat treatment effect was particularly visible on the Pd/TiO₂ catalysts as shown in Figure 32. The top photo shows a catalyst before any heat treatment and the middle photo shows the catalyst after the calcination step. The colour has drastically changed due to oxidation of Pd to Pd²⁺. After the reduction step the catalyst regained its initial colour.

The bottom photo in Figure 32 shows the furnace tube used for the reduction step. This tube was usually contaminated with catalysts from other users even though it was fairly new. For this reason, a lot of effort was put into cleaning this tube in order to avoid any cross-contamination. The furnace tube used for the calcination step was not shared and cross-contamination was never an issue.

2.7 Model Reactions Experimental Procedure

In total seven reactions were tested during this PhD with the catalysts produced by microwave and ultrasound synthesis. An overview for each one of these reactions can be found in section 1.6, where the reaction schemes are presented and their importance in light of the targets defined for this PhD is described. All the experimental results are presented in chapter 6. Some of the experimental results were benchmarked against experimental results obtained with a commercial catalyst and with catalysts produced by the traditional sol-immobilization protocol, previously described in section 1.4.2.1.

In this section the experimental procedures for the seven reactions are presented. These seven reactions were only used as model reactions. The objective was never to optimise the reactions operating conditions, but rather to use the reactions as a tool to catalytically characterise the produced metal nanoparticles, in this case by calculating conversions and selectivities and comparing them. For this reason, the adopted experimental procedures were the same as the ones from previous work carried out within the Cardiff Catalysis Institute, in particular within the Nikolaos Dimitratos research group. Therefore, all the reactions were considered to be free of mass transport limitations (internal and external) as this had already been checked in previous works. Under this condition the kinetic regime is the limiting step as it presents the slowest rate and therefore the observed rate is the true reaction rate. In any case, it is important to stress that all the prepared catalysts during this PhD were sieved (cut-off particle size at 0.25 mm) which helped to guarantee that the reactions were carried out under kinetic regime.

Some of the reactions were tested by other research colleagues. This was the case of the propane total oxidation, which was tested by Parag Shah, and of the hydrazine decomposition, which was tested by Davide Motta. The 4-nitrophenol reduction was carried out with the help of Briony Munslow and the formic acid decomposition with the help of Thomas Hall. The furfural hydrogenation was carried out in an external university (Università degli Studi di Milano) within Dr. Alberto Villa research group who have optimised the operating conditions.

2.7.1 4-Nitrophenol Reduction

The 4-nitrophenol reduction reaction was carried out in liquid phase under batch regime inside a quartz cuvette with the concentration monitored by measuring the absorbance over time with UV-Vis spectroscopy. The used solvent was water with the temperature kept at 30 °C. All reaction operating conditions can be found in Table 6.

Table 6 – Operating conditions for the 4-nitrophenol reduction.

Parameter	Value
Solvent	Water
Reaction Temperature	30 °C
Reaction Volume	3 mL
4-Nitrophenol Concentration	0.126 mM
Substrate/Metal Molar Ratio	1.85
Stirring Speed	0-250 rpm
Absorption Coefficient (ϵ L)	17242 mol ⁻¹
NaBH ₄ Concentration	3.9 mM

The substrate/metal molar ratio of 1.85 means that the necessary amount of catalyst with a metal loading of 1 wt. % was very small and difficult to measure accurately (4.0 mg for Au catalysts, 3.1 mg for AuPd (1:1 molar) catalysts and 2.2 mg for Pd catalysts). For this reason, the catalyst amount was also weighted directly into the quartz cuvette in order to minimise potential losses with the process of moving the catalyst into the quartz cuvette.

A stock solution of 4-nitrophenol (0.01 M) was initially prepared and used for all the trials. The volume of 4-nitrophenol necessary to reach a concentration of 0.126 mM was measured and added to the quartz cuvette with the catalyst inside.

The UV-Vis cuvette was moved inside the UV-Vis device presenting temperature control with the 30 °C temperature reached within a couple of minutes. The stirring speed was adjusted accordingly (0-250 rpm region) just until the point that the amount of catalyst inside the cuvette would not interfere anymore with the UV-Vis measurements by scattering the light.

A fresh 0.04 M solution of NaBH₄ was prepared and the volume necessary to reach a concentration of 3.9 mM was measured and added to the quartz cuvette. This was considered the initial time for the reaction. UV-Vis measurements were then performed every 5 seconds. An excess of NaBH₄ was used to achieve a pseudo-first order reaction. The NaBH₄ acts as a Lewis base and instantaneously causes 4-nitrophenol to change to 4-nitrophenolate, which presents a UV-Vis peak at around 400 nm. This was the peak that was followed with UV-Vis spectroscopy. A calibration curve with six standard samples was initially performed according to the Beer-Lambert law shown in Equation 21 with a calculated absorption coefficient of 17242 mol⁻¹.

2.7.2 Carbon Monoxide Oxidation



Figure 33 – Carbon monoxide oxidation reaction experimental set-up.

The carbon monoxide oxidation reaction was tested under continuous flow regime with a bottle of 5000 ppm carbon monoxide in air used to feed 20 mL min^{-1} to a glass tube where the catalyst was present and compacted within a glass wool bed. A mass flow controller was used to regulate the flow rate. The glass tube was placed inside an oil or water bath with two temperatures being tested, $30 \text{ }^\circ\text{C}$ and $50 \text{ }^\circ\text{C}$. The experimental set-up is shown in Figure 33.

The reaction focused in testing mainly AuPd/TiO₂ (1:1 molar) catalysts and in each trial 19.3 mg were used. A range of Au/TiO₂ and Pd/TiO₂ catalysts were also tested in order to confirm trends and the catalyst amount was adjusted accordingly so that for all trials the same number of metal active sites had been used. Therefore, 25.0 mg were used for Au/TiO₂ catalysts and 13.5 mg for Pd/TiO₂ catalysts.

The carbon monoxide to carbon dioxide conversion was monitored over time by analysis of the outlet gas with a GC with two thermal conductivity detectors and two channels, one channel having a 10 m molecular sieve 5 Å capillary column with a peak for nitrogen at 0.47 min, a peak for oxygen at 0.53 min and a peak for carbon monoxide at 0.79 min, the second channel having a 10 m PPQ capillary column with a peak including nitrogen, oxygen and carbon monoxide all together at 0.39 min, a peak for carbon dioxide at 0.45 min and a peak for water at 0.61 min. Each trial ran for 3 hours with GC analysis every 2 minutes.

As explained in section 2.2.7 when working with GC it is not always necessary to perform a calibration curve. In this reaction the molar compositions of carbon monoxide and carbon dioxide were assumed to be equal to the ratio of their peak area to the total peak areas. This assumption is only possible if the thermal conductivities of the different gases are also the same. According to the data shown in Table 7 the thermal conductivities of the different gases are very similar in the range of temperatures of 100 K to 600 K.

Experimental, Methods and Characterisation

2.7 Model Reactions Experimental Procedure

Table 7 – Thermal conductivity of the gases at different temperatures.

Gas	Thermal Conductivity ($\text{mW m}^{-1} \text{K}^{-1}$)						Ref.
	100 K	200 K	300 K	400 K	500 K	600 K	
Oxygen	9.1	18.2	26.5	34.0	41.0	47.7	092
Nitrogen	9.4	18.3	26.0	32.8	39.0	44.8	93
Carbon monoxide			25.0	32.3	39.2	45.7	93
Carbon dioxide		9.6	16.8	25.2	33.5	41.6	94
Water			18.6	26.1	35.6	46.2	95

The inlet molar composition of carbon monoxide was not considered constant as the different gases have different densities causing the gas mixture in the bottle to not be perfectly homogeneous with the heaviest gas, namely carbon monoxide, to be less concentrated at the top of the bottle than at its bottom. Therefore, the initial molar composition of carbon monoxide was considered to be equal to the sum of the molar composition of the carbon monoxide in the outlet gas plus the amount of carbon monoxide molar composition used to yield the carbon dioxide observed. The reaction conversion was then calculated using the values for the initial and outlet molar compositions of carbon monoxide.

Other assumptions used for the carbon monoxide oxidation included:

- When the reaction was being performed a portable carbon monoxide detector was used to check for leaks in most of the connections and if no changes were observed on the carbon monoxide detector level the all system was considered leak free;
- The peaks of nitrogen, oxygen and carbon monoxide observed in the channel having the molecular sieve column were free of carbon dioxide and water interference;
- The amount of nitrogen and water in the outlet gas was the same as in the inlet gas and any carbon dioxide present was only due to the carbon monoxide oxidation reaction;
- In order to make sure that the inlet gas was at the desired temperature before contacting the catalyst, the gas was fed to the side of the glass tube without the catalyst bed;
- Total molar flow rate can be considered a constant;

2.7.3 Propane Total Oxidation

The experimental procedure for the propane total oxidation was very similar to the carbon monoxide oxidation already described in section 2.7.2. This reaction was tested under continuous flow regime with a bottle of 5000 ppm propane in air used to feed 20 mL min^{-1} to a glass tube where the catalyst was present and compacted within a quartz wool bed. A mass flow controller was used to regulate the flow rate. The catalyst amount was adjusted accordingly so that for all trials the same number of active sites had been used. Therefore, 25.0 mg were used for the Au/TiO₂ catalysts, 13.5 mg for the Pd/TiO₂ catalysts and 19.3 mg for the AuPd/TiO₂ (1:1 molar) catalysts.

However, contrary to the carbon monoxide oxidation, with the propane total oxidation the glass tube was different to the one shown in Figure 33 and a fixed bed laboratory microreactor was used instead with the temperature control able to reach temperatures as high as 600 °C. The propane conversion was monitored over time by analysis of the outlet gas with a GC with one thermal conductivity detector (TCD) and one flame ionization detector (FID) and two channels, one channel having a 10 m molecular sieve 5 Å capillary column and connected to the TCD, the second channel having a 10 m PPQ capillary column and connected to the FID.

Another major difference is related to the objective of the experiment, with the carbon monoxide oxidation the objective was to check the catalyst stability over time at a fixed temperature, whereas with the propane total oxidation the objective was to understand at which temperature a certain propane conversion could be achieved. In this work that level has been set at a propane conversion of 50 %. The reaction temperature ranged between 200 °C and 600 °C with increases of 50 °C. The GC analysis was performed three times for each temperature and the average value was used.

Even though carbon dioxide is the main product the carbon monoxide generation was also monitored with the selectivities being calculated.

2.7.4 Furfural Hydrogenation



Figure 34 – Furfural hydrogenation reaction experimental set-up.

The furfural hydrogenation was carried out in liquid phase under batch regime inside an autoclave with the concentration analysis performed by a GC with one FID detector and a CP8690-Sil 5 CB capillary column. Samples were taken at 0, 15, 30, 60, 120, 240 and 360 min. The used solvent was 2-propanol with the temperature kept at 50 °C. The experimental set-up is shown in Figure 34 and all reaction operating conditions can be found in Table 8.

The substrate/metal molar ratio of 500 means that the necessary amount of catalyst with a metal loading of 1 wt. % was 118 mg for Au catalysts, 91 mg for AuPd (1:1 molar) catalysts and 64 mg for Pd catalysts. The main catalysts used were AuPd (1:1 molar) and Pd. The Au catalyst is not effective for this reaction and was only tested as a blank reaction.

Whenever a sample was taken the autoclave was first cooled down in flowing water in order to stop the reaction and minimize the loss of chemical compounds to the atmosphere. The autoclave was then depressurized and once open around 0.2 mL of the reaction mixture were collected with a Pasteur pipette. The sample was centrifuged to separate the catalyst from the reaction solution. The GC sample was prepared by adding 0.1 mL of the reaction solution and 0.1 mL of a dodecanol solution. The dodecanol was used according to the internal standard method described in section 2.2.7 with the concentrations (M) calculated using Equation 24b. The GC analysis parameters can also be found in Table 8.

For each sample a carbon balance was calculated by adding the concentrations of all the compounds in that sample and dividing that value by the initial furfural concentration calculated for the sample at $t=0$ min.

After collecting the sample, the autoclave was closed and first flushed with nitrogen so that all the oxygen could be removed. The autoclave was then connected to the hydrogen line and pressurized again at 3 bar(g). The autoclave was placed inside the heating chamber as shown in Figure 34 and stirring was turned on at 1200 rpm. The reaction time was resumed.

Experimental, Methods and Characterisation

2.7 Model Reactions Experimental Procedure

Table 8 – Operating conditions for the furfural hydrogenation.

Parameter	Value
Solvent	2-Propanol
Reaction Temperature	50 °C
Reaction Volume	10 mL
Furfural Concentration	0.30 M
Substrate/Metal Molar Ratio	500
Stirring Speed	1200 rpm
Hydrogen Pressure	3 bar(g)
Internal Standard	Dodecanol
Internal Standard Concentration	0.2 M
Total GC Sample Volume	0.2 mL
Internal Standard in Sample	0.1 mL
Reaction Solution in Sample	0.1 mL
Furfural Response Factor	4.4515
FA Response Factor	3.3908
THF Alcohol Response Factor	2.9292
Other Peaks Response Factor	3.5905

2.7.5 Cinnamaldehyde Hydrogenation



Figure 35 – Cinnamaldehyde hydrogenation reaction experimental set-up.

The experimental procedure for the cinnamaldehyde hydrogenation was very similar to the furfural hydrogenation already described in section 2.7.4. This reaction was tested in liquid phase under batch regime inside Radleys flasks, with as many as five trials performed simultaneously. The concentration was monitored by a GC with one FID detector and a 30 m HP-5 capillary column. The used solvent was toluene with the temperature kept at 100 °C. The experimental set-up is shown in Figure 35 and all reaction operating conditions can be found in Table 9.

The substrate/metal molar ratio of 2000 means that the necessary amount of catalyst with a metal loading of 1 wt. % was 39 mg for Au catalysts, 30 mg for AuPd (1:1 molar) catalysts and 21 mg for Pd catalysts. The main catalysts used were AuPd (1:1 molar) and Pd. The Au catalyst is not effective for this reaction and was only tested as a blank reaction.

Contrary to the furfural hydrogenation, when seven samples for each trial were analysed, with the cinnamaldehyde hydrogenation only one sample for each trial was analysed at the end of the reaction. The reaction times considered were 1 and 2 hours. The hydrogen line was disconnected from the Radleys reaction station and the flask cooled down in an ice/water bath in order to stop the reaction and minimize the loss of chemical compounds to the atmosphere. Around 1 mL of the reaction mixture was collected with a Pasteur pipette. The sample was centrifuged to separate the catalyst from the reaction solution. The GC sample was prepared by adding 0.5 mL of the reaction solution and 0.5 mL of a *o*-xylene solution. The *o*-xylene was used according to the internal standard method described in section 2.2.7 with the concentrations (M) calculated using Equation 24b. The GC analysis parameters can also be found in Table 9.

For each sample a carbon balance was calculated by adding the concentrations of all the compounds in that sample and dividing that value by the initial cinnamaldehyde concentration of 0.72 M.

Experimental, Methods and Characterisation

2.7 Model Reactions Experimental Procedure

Table 9 – Operating conditions for the cinnamaldehyde hydrogenation.

Parameter	Value
Solvent	Toluene
Reaction Temperature	100 °C
Reaction Volume	5.5 mL
Cinnamaldehyde Concentration	0.72 M
Substrate/Metal Molar Ratio	2000
Stirring Speed	1000 rpm
Hydrogen Pressure	1 bar(g)
Internal Standard	o-Xylene
Internal Standard Concentration	0.7 M
Total GC Sample Volume	1.0 mL
Internal Standard in Sample	0.5 mL
Reaction Solution in Sample	0.5 mL
Cinnamaldehyde Response Factor	0.9299
HCAL Response Factor	1.0585
3-phenyl-1-propanol Response Factor	1.1297
Cinnamyl Alcohol Response Factor	1.101
Propylbenzene Response Factor	1.1433
Other Peaks Response Factor	1.07248

2.7.6 Formic Acid Decomposition

The formic acid decomposition was carried out in liquid phase under batch regime inside a 100 mL two neck round bottom flask with the concentration monitored by HPLC analysis with a UV-Vis detector and a MetaCarb 87H 250x4.6 mm reversed column. Samples were taken at 0, 5, 15, 30, 60, 90 and 120 min. The used solvent was water with the temperature kept at 50 °C by placing the round bottom flask inside an oil bath. A water condenser was used in order to minimize the loss of chemical compounds to the atmosphere. The experimental set-up is shown in Figure 36 and all reaction operating conditions can be found in Table 10.

The substrate/metal molar ratio of 2000 means that the necessary amount of catalyst with a metal loading of 1 wt. % was 38 mg for AuPd (1:1 molar) catalysts and 27 mg for Pd catalysts. Au catalysts were not tested as they had been shown to not be active for this reaction and no blank reaction was necessary as this reaction had already been intensively tested within the Nikolaos Dimitratos research group.

Samples were collected without stopping the reaction by opening one neck of the round bottom flask and using the 1000 μ L micropipette to collect 0.3 mL of the reaction mixture. The sample was centrifuged to separate the catalyst from the reaction solution. The HPLC sample was prepared by adding 0.1 mL of the reaction solution and 0.1 mL of a succinic acid solution to 9.8 mL of water. The succinic acid was used according to the internal standard method described in section 2.2.7 with the concentrations (M) calculated using Equation 24b. HPLC analysis parameters can also be found in Table 10.



Figure 36 – Formic acid decomposition reaction experimental set-up.

Table 10 – Operating conditions for the formic acid decomposition.

Parameter	Value
Solvent	Water
Reaction Temperature	50 °C
Reaction Volume	10 mL
Formic Acid Concentration	0.5 M
Substrate/Metal Molar Ratio	2000
Stirring Speed	750 rpm
Internal Standard	Succinic Acid
Internal Standard Concentration	0.2 M
Total GC Sample Volume	10 mL
Internal Standard in Sample	0.1 mL
Reaction Solution in Sample	0.1 mL
Formic Acid Response Factor	1.4109

2.7.7 Hydrazine Decomposition

The monohydrate hydrazine decomposition was carried out in liquid phase under batch regime inside a closed round bottom flask. The used solvent was water with the temperature kept at 50 °C by placing the round bottom flask inside an oil bath. Sodium hydroxide was added to the reaction solution with a final concentration of 0.5 M being achieved. All reaction operating conditions can be found in Table 11. The substrate/metal molar ratio of 250 means that the necessary amount of catalyst with a metal loading of 1 wt. % was 76 mg for Ir catalysts. Only three Ir/CeO₂ were tested with this reaction.

This reaction was still at an early stage within the Nikolaos Dimitratos research group and the protocol to fully quantify the hydrazine and the gas products was still being developed. Therefore, the closed round bottom flask was connected to a graduated cylinder full of water where the gas was accumulating as the reaction progressed. The displaced volume of water was measured over time and considered to be equal to the volume of the produced gas in the reaction. The volume of the produced gas could be converted to an amount (mol) using the ideal gas law equation. However, as shown in Equation 20, the hydrazine decomposition can follow two pathways. The first pathway producing nitrogen and hydrogen and the other producing ammonia and nitrogen. For this reason, it is useless to convert the volume of the produced gas to an amount (mol) as it would not be possible to calculate concentrations and selectivities. In any case, measuring the volume of the produced gas is a good indication for the activity of the catalyst and comparisons can be made.

Table 11 – Operating conditions for the hydrazine decomposition.

Parameter	Value
Solvent	Water
Reaction Temperature	50 °C
Reaction Volume	8 mL
Hydrazine Concentration	0.13 M
Substrate/Metal Molar Ratio	250
Stirring Speed	900
NaOH Concentration	0.5 M

3 Synthesis of Metal Nanoparticles by Microwave

3.1 Overview

This chapter presents all the experimental results associated with the microwave synthesis of colloidal metal nanoparticles, namely Au, Pd, Ag, Ir, Cu and bimetallic alloys of AuPd at different molar ratios (7:1, 3:1, 1:1, 1:3 and 1:7). The working principle of the microwave synthesis is presented in section 1.4.3 and the microwave synthesis experimental procedure is described in section 2.3.

Most of the produced colloidal metal nanoparticles were characterised by UV-Vis, DLS and TEM analysis. All samples analysed by TEM were also analysed by EDX in order to rule out any contamination. Some work was also performed with H^1 and C^{13} NMR and GC-MS. Detailed information about these techniques can be found in section 2.2. The metal nanoparticles identified as having the potential to produce good catalytic results for the reactions presented in chapter 1 were further characterised and analysed after being supported as shown in chapter 5.

In section 3.2 the microwave standard operating conditions are defined based on the traditional sol-immobilization protocol (section 1.4.2.1) and on work found in the literature. The next step consisted in optimising the operating conditions for the production of Au nanoparticles. The optimisation tests studied the effect of stirrer, metal concentration, holding time and temperature, acid/base addition, type of solvent, solvent composition and type and concentration of stabilizer. Usually for each test only one operating condition was varied and all the others were kept at standard operating conditions. The experimental results of each test were then evaluated against the microwave standard operating conditions experimental results. When compared to other metals Au is a good starting model to understand new experimental protocols due to:

- a) More control over particle size and shape by changing the operating conditions;
- b) Au nanoparticles present a plasmon peak wavelength at around 500 nm and a simple, fast and cheap technique like UV-Vis spectroscopy can be used to detect changes;
- c) Au is one of the easiest metals to be reduced among the metals normally used for catalytic purposes as observed in Table 12. For this reason, it was easier to understand the effect of small operating conditions changes in the experimental results;

Synthesis of Metal Nanoparticles by Microwave

3.1 Overview

Table 12 – Standard reduction potential (E°) of some common metals used as catalysts (298.15 K and 1 atm).⁹⁶

Reaction	E° (V)	Reaction	E° (V)
$\text{Ag}^{1+} + \text{e}^- \leftrightarrow \text{Ag}^0$	1.498	$\text{Ir}^{3+} + 3\text{e}^- \leftrightarrow \text{Ir}^0$	1.156
$\text{Au}^{3+} + 3\text{e}^- \leftrightarrow \text{Au}^0$	1.692	$\text{Ni}^{2+} + 2\text{e}^- \leftrightarrow \text{Ni}^0$	-0.257
$\text{Au}^{1+} + \text{e}^- \leftrightarrow \text{Au}^0$	0.7996	$[\text{PdCl}_4]^{2-} + 2\text{e}^- \leftrightarrow \text{Pd}^0 + 4\text{Cl}^-$	0.591
$\text{Cu}^{2+} + 2\text{e}^- \leftrightarrow \text{Cu}^0$	0.3419	$\text{Pd}^{2+} + 2\text{e}^- \leftrightarrow \text{Pd}^0$	0.951
$\text{Cu}^{1+} + \text{e}^- \leftrightarrow \text{Cu}^0$	0.521	$\text{Pt}^{2+} + 2\text{e}^- \leftrightarrow \text{Pt}^0$	1.18
$\text{Co}^{2+} + 2\text{e}^- \leftrightarrow \text{Co}^0$	-0.28	$\text{Rh}^{3+} + 3\text{e}^- \leftrightarrow \text{Rh}^0$	0.758
$[\text{IrCl}_6]^{2-} + 4\text{e}^- \leftrightarrow \text{Ir}^0 + 6\text{Cl}^-$	1.6365	$\text{Ru}^{2+} + 2\text{e}^- \leftrightarrow \text{Ru}^0$	0.455

In section 3.3 the microwave work focus on several mechanistic studies:

- Comparison of conventional heating with microwave heating for the production of Au nanoparticles;
- The study of Au^{3+} reduction behaviour and NaOH effect in terms of reduction power;
- The acetaldehyde reducing power;
- H^1 and C^{13} NMR analysis of different metal colloids, not only Au, and of the stabilizer stability during microwave synthesis;
- Au oxidation state effect on the production of nanoparticles;

In section 3.4 the best microwave synthesis operating conditions were defined by having in consideration the Au optimisation experimental results from section 3.2 and the mechanistic studies from section 3.3. The stability and reproducibility of microwave synthesis was also analysed.

In section 3.5 the microwave synthesis was extended to the remaining metals mentioned above. All experimental results are presented and analysed and were obtained at the best microwave synthesis operating conditions.

In section 3.6 the microwave work attempted to move from batch synthesis to continuous flow synthesis with experimental results for the production of Au and Pd nanoparticles presented and analysed.

Synthesis of Metal Nanoparticles by Microwave

3.2 Au Optimisation Tests

3.2 Au Optimisation Tests

Some of the standard operating conditions adopted for microwave synthesis were based on the traditional sol-immobilization protocol (section 1.4.2.1). Therefore, the metal concentration (0.025 g L^{-1} or 0.13 mM) and the PVA/metal weight ratio (0.65) were kept constant. However, the 400 mL volume was scaled-down, with a new value set at 20 mL, less than the microwave cell volume (35 mL) as recommended by the microwave manufacturer.

The time for which the microwave continued heating after reaching the final temperature was set at 5 min (holding time). Even though it is not unanimous that microwave heating offers special effects⁴⁸, the air cooling was turned on at 1 bar(g) during the holding time of 5 min so that the delivered microwave power would be higher.

The other standard operating conditions were adopted based on literature work. Abarques *et al.*⁹⁷ have produced Au nanoparticles in short-chain alcohol medium (methanol, ethanol, 1-propanol, 2-propanol and *tert*-butanol) with best results obtained with methanol, but the reducing power was mainly attributed to the stabilizer (PVA) action. Tu and Liu⁹⁸ used a methanol/water mixture for the production of Au nanoparticles. They have also used ethylene glycol for the synthesis of Pt nanoparticles reporting at around $150 \text{ }^\circ\text{C}$ colour changes for the Pt solution, an indication of nanoparticle production. Analysing other works⁹⁹⁻¹⁰⁰ with Pt, Ru and Ag, ethylene glycol at $150 \text{ }^\circ\text{C}$ has also been identified as a good microwave synthesis solvent. For these reasons and due to concerns related to overpressure and toxicity when working with methanol outside the fume hood ethylene glycol has been selected as the standard solvent. Moreover, ethylene glycol presents both a high dielectric constant/loss and boiling point. In any case, trials with other solvents, including methanol, were also performed during the optimisation tests. The microwave standard operating conditions selected for the Au nanoparticles optimisation tests are summarized in Table 13.

Table 13 – Standard operating conditions for the Au nanoparticles microwave optimisation.

Parameter	Value
Power	300 W
Solvent	Ethylene Glycol
Temperature	$150 \text{ }^\circ\text{C}$
Holding Time	5 min
Stirrer	High
Volume of Solution	20 mL
PVA/Au Weight Ratio	0.65
Au Concentration	0.025 g L^{-1} or 0.13 mM
Precursor	HAuCl_4

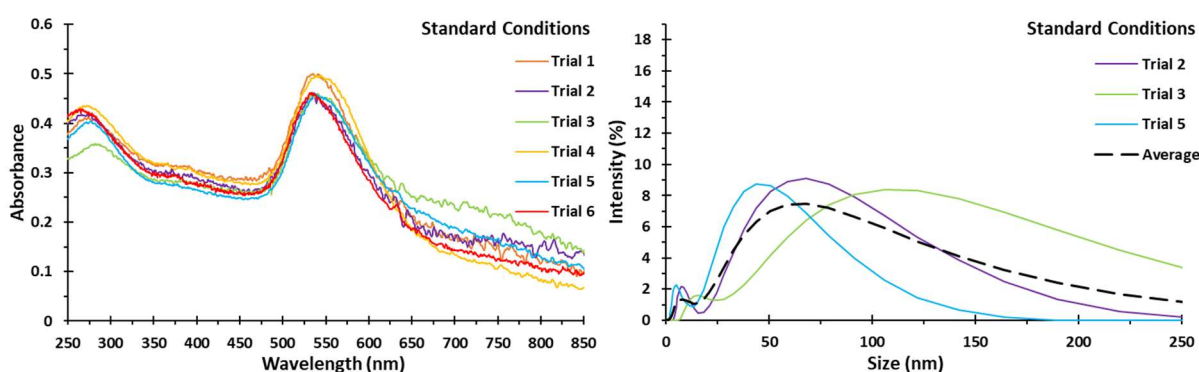
Synthesis of Metal Nanoparticles by Microwave

3.2 Au Optimisation Tests

From the several trials performed at the microwave standard operating conditions a UV-Vis selection of the six most reproducible trials is presented in Figure 37 with average values for the plasmon peak absorbance (0.47), plasmon peak wavelength (537 nm) and wavelength range (82 nm) calculated.

Photos of the six produced Au colloids are also shown, with small colour differences observed between trials, such as between trial 5 (S5) and trial 2 (S2) even though both UV-Vis spectra are very similar. Environmental light can affect the colour perception in each photo rendering comparisons based in colour alone inaccurate. For this reason, the metal colloids photos should serve merely as an indication, only UV-Vis comparisons are reliable enough.

Three of the trials were characterised by DLS. An average DLS size distribution having two peaks was calculated with average sizes for the first peak of 8.0 ± 3.9 nm and for the second peak of 84 ± 59 nm. Similar to the citrate protocol (section 1.4.2.2) it is not clear why two peaks were observed. However, as mentioned in section 2.2.2 the DLS results are affected by the presence of a stabilizer, the nanoparticles shape and the nanoparticles degree of aggregation. Moreover, the first peak is the most relevant as DLS is an intensity-weighted particle size measurement instead of a mass or number weighted particle size measurement with the amount of scattered light strongly proportional to the particle size.

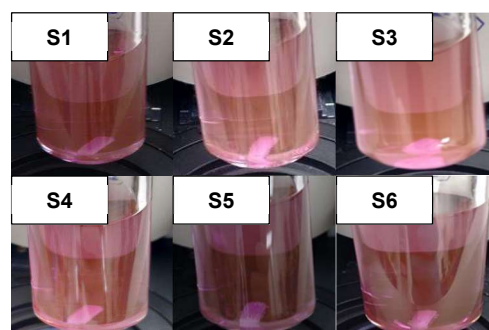


Plasmon Peak Absorbance = 0.47 ± 0.02

Plasmon Peak Wavelength = 537 ± 3 nm

Wavelength Range = 82 ± 7 nm

Figure 37 – Au nanoparticles produced at standard operating conditions with UV-Vis (top left) and DLS (top right) analysis and photos for the different trials (bottom).



Synthesis of Metal Nanoparticles by Microwave

3.2 Au Optimisation Tests

The average plasmon peak wavelength of 537 nm is higher than the 500 nm observed for Au nanoparticles produced by the traditional sol-immobilization protocol and similar to the 538 nm observed for Au nanoparticles produced by the citrate protocol with sizes in the 35-78 nm range (section 1.4.2). However, direct comparisons for the Au nanoparticles average size are not possible as two different solvents were used. For the traditional sol-immobilization and citrate protocols the solvent was water, dielectric constant of around 80,⁴⁹ whereas for the microwave synthesis the solvent was ethylene glycol, dielectric constant of around 37.¹⁰¹ According to Equation 1, the extinction cross section σ_{ext} , a measure of the light absorbance and scattering, is dependent on the solvent dielectric constant. This equation indicates that:

- a) For the same nanoparticles average size the plasmon peak appears at higher wavelengths when solvent is changed from water to ethylene glycol;
- b) For the same nanoparticles average size the absorbance values are slightly higher when solvent is changed from water to ethylene glycol;

After the trials at standard operating conditions the work moved to the Au optimisation tests in order to understand the effect of the stirrer, metal concentration, holding time and temperature, acid/base addition, type of solvent, solvent composition and type and concentration of stabilizer. Usually, for each test only one parameter was varied and all the others were kept as shown in Table 13. The experimental results were compared with the average of the six UV-Vis spectra and with the average of the three DLS spectra presented in Figure 37 and with the photo of trial 6 (S6). However, DLS analysis was not performed to all trials as it is not able to detect very small trends in the nanoparticles average size.

Synthesis of Metal Nanoparticles by Microwave

3.2 Au Optimisation Tests

3.2.1 Stirrer

The stirrer control of the CEM Discover-SP is not very precise offering only four available options: none, low, medium and high.

As observed in Figure 38, the worst results for the Au nanoparticles production and size distribution were obtained when no stirrer was used as indicated by UV-Vis analysis (low plasmon peak absorbance and not even possible to calculate a wavelength range). The Au nanoparticles production and size distribution improved when the stirrer was turned on (low) and continued to improve as the stirrer speed increased.

These observations show that the stirrer effect is an important parameter and should be turned on at maximum setting. This is consistent with the penetration depth calculated from Equation 3. As the dielectric loss (ϵ_2) of ethylene glycol is similar to its dielectric constant (ϵ_1), the penetration depth is one order of magnitude smaller than for water. A small penetration depth only causes heating to ethylene glycol near the 35 mL vessel wall. The normal boiling point temperature was then exceeded which caused unusual build-up of pressure, 20 bar(g) measured by the pressure sensor. As the stirrer is turned on and increased, the ethylene glycol inside the 35 mL vessel is mixed and a homogeneous temperature is achieved.

All UV-Vis spectra together with the Au colloids photos can be observed in Figure 38 and the experimental results are presented in Table 14.

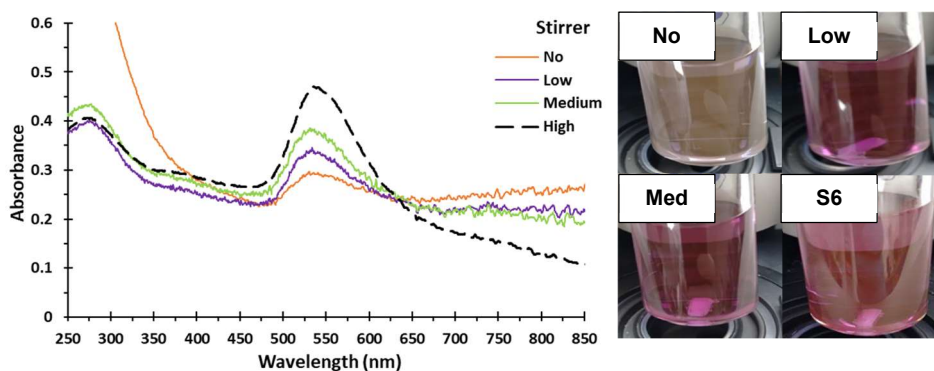


Figure 38 – Au nanoparticles produced at different stirrer settings with UV-Vis analysis (left) and photos for no stirrer (No), low stirrer (Low), medium stirrer (Med) and high stirrer (S6) (right).

Table 14 – Au nanoparticles experimental results at different stirrer settings.

Stirrer	Plasmon Peak Absorbance	Plasmon Peak Wavelength (nm)	Wavelength Range (nm)
No	0.30	530	-
Low	0.35	534	102
Medium	0.39	531	92
High (standard)	0.47	537	82

Synthesis of Metal Nanoparticles by Microwave

3.2 Au Optimisation Tests

3.2.2 Metal Concentration

The UV-Vis spectra in Figure 39 and the experimental results in Table 15 suggest that it is still possible to work with higher concentrations of Au and increase the nanoparticles production, measured by the plasmon peak absorbance.

However, the plasmon peak absorbance does not present a directly proportional trend with the Au concentration. For instance, a 10-fold increase in Au concentration from 0.065 mM to 0.65 mM is only followed by approximately a 5-fold increase in the plasmon peak absorbance from 0.24 to 1.1. At high enough Au concentration (1.3 mM) the production can even be worse than at a lower Au concentration (0.65 mM).

Moreover, the size distribution is negatively affected by the Au concentration increase, with the 1.3 mM trial presenting a UV-Vis spectrum too broad to even calculate a wavelength range. The Au nanoparticles average size also started to increase with a plasmon peak wavelength of 564 nm observed for the Au concentration of 0.65 mM.

All these results indicate that the agglomeration effect is progressively enhanced when working at higher Au concentrations. This is according to the principle that metal nanoparticles growth rate is strongly dependent on metal concentration, with an order of reaction higher than the metal nanoparticles nucleation rate.

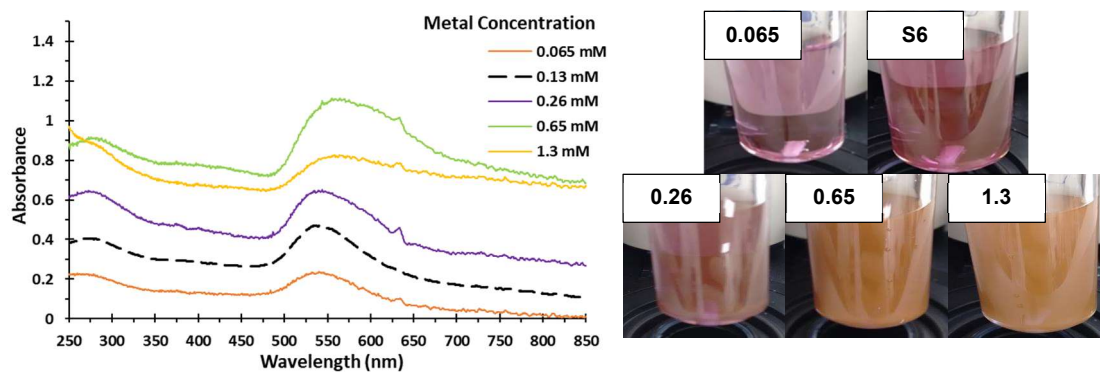


Figure 39 – Au nanoparticles produced at different Au concentrations with UV-Vis analysis (left) and photos for 0.065, 0.13 (S6), 0.26, 0.65 and 1.3 mM (right).

Table 15 – Au nanoparticles experimental results at different Au concentrations.

Au Concentration (mM)	Plasmon Peak Absorbance	Plasmon Peak Wavelength (nm)	Wavelength Range (nm)
0.065	0.24	540	70
0.13 (standard)	0.47	537	82
0.26	0.65	543	109
0.65	1.1	564	176
1.3	0.83	558	-

Synthesis of Metal Nanoparticles by Microwave

3.2 Au Optimisation Tests

3.2.3 Holding Time and Temperature

The holding time and temperature were varied having in consideration six values for both parameters: 0, 2.5, 5, 10, 15 and 20 min and 60, 80, 100, 125, 150 and 175 °C.

It was observed that only at 100 °C and 15 min Au nanoparticles started to be formed. In Figure 40 (left) the Au solution peak is gradually decreasing with holding time and only after 15 min the UV-Vis spectrum presented a plasmon peak. The photos taken at the end of each synthesis support this conclusion by showing that only for the holding time of 15 min the colour changed from transparent to a light yellow. At 100 °C, the UV-Vis spectra and the experimental results, which are presented in Table 16, indicate that Au nanoparticles production, average size and size distribution are still far from the standard scenario of 150 °C for 5 min.

Choice of a minimum holding time and temperature is paramount for the synthesis of Au nanoparticles, but above a certain threshold, in particular for temperature, it appears that all experimental results start to get worse (production, average size and size distribution). In Figure 40 (right), with the holding time fixed at 5 min, when changing from 150 to 175 °C the agglomeration effect is visible. This indicates that the agglomeration effect is progressively enhanced when working at higher holding times and temperatures and according to the principle that the metal nanoparticles growth rate is stronger dependent on the temperature than the metal nanoparticles nucleation rate as suggested by Figure 12.

All experimental results are presented in Table 16.

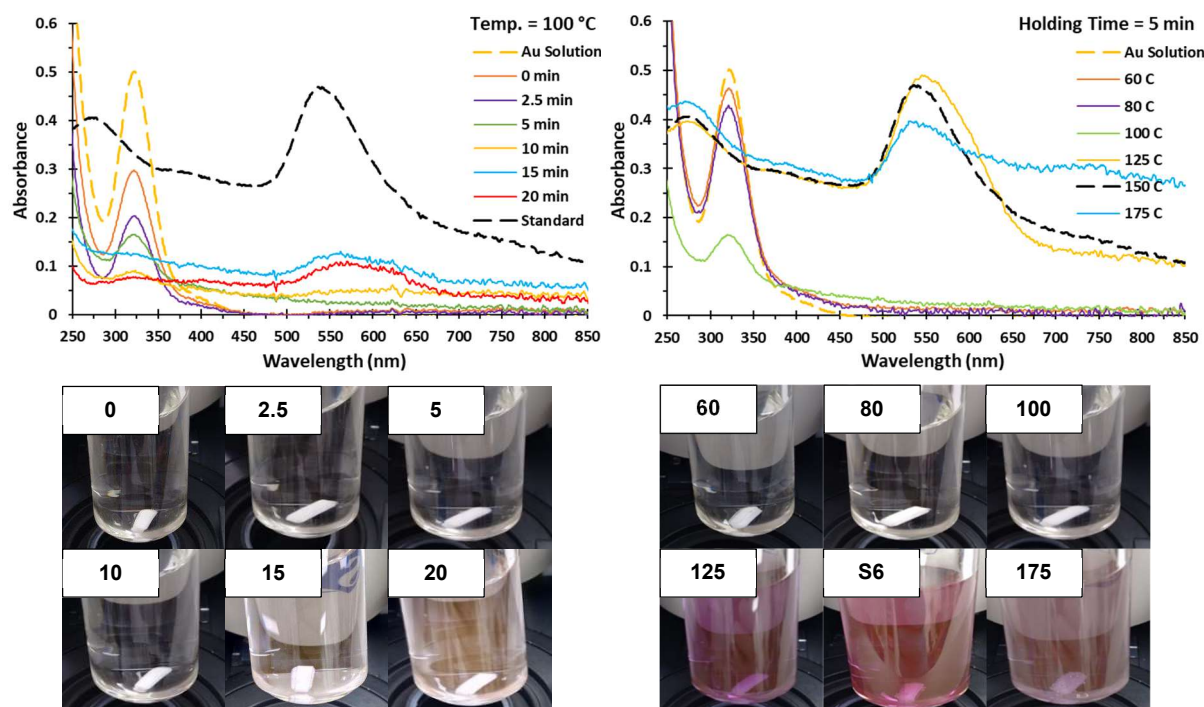


Figure 40 – Au nanoparticles produced at a temperature of 100 °C and at different holding times (left) and at a holding time of 5 min and at different temperatures (right) with UV-Vis analysis (top) and photos (bottom).

Synthesis of Metal Nanoparticles by Microwave

3.2 Au Optimisation Tests

Table 16 – Au nanoparticles experimental results at different temperatures and holding times.

	Holding Time (min)	Plasmon Peak Absorbance	Plasmon Peak Wavelength (nm)	Wavelength Range (nm)
60 °C	0, 2.5, 5, 10, 15, 20	-	-	-
80 °C	0, 2.5, 5, 10, 15, 20	-	-	-
100 °C	0, 2.5, 5, 10	-	-	-
	15	0.13	562	113
	20	0.11	570	113
125 °C	0	0.06	561	78
	2.5	0.41	547	82
	5	0.49	546	91
	10	0.47	561	99
	15	0.45	546	89
	20	0.50	539	77
150 °C	0	0.50	549	107
	2.5	0.47	547	88
	5 (standard)	0.47	537	82
	10	0.45	544	91
	15	0.45	539	87
	20	0.39	538	103
175 °C	0	0.41	543	98
	2.5	0.44	538	112
	5	0.40	531	159
	10	0.45	535	112
	25	0.46	534	101
	20	0.44	536	119

Synthesis of Metal Nanoparticles by Microwave

3.2 Au Optimisation Tests

3.2.4 Acid/Base Addition

The effect of adding a strong base or acid, NaOH and H₂SO₄, was investigated at different molar ratios between the Au and the active species OH⁻ and H⁺ assuming full dissociation of the base and acid in the non-aqueous solvent ethylene glycol. This last assumption was made because ethylene glycol is a polar solvent presenting two OH groups capable of suffering protonation/deprotonation. Variations in the pH are expected to influence the production of metal nanoparticles by affecting solubility in the solvent and the reduction, nucleation and growth rates as described in the literature.¹⁰²

As shown in Figure 41 (left) the addition of NaOH is continuously affecting the UV-Vis spectrum. In particular, at the highest concentration of 16 eq. it was even noticed a strong absorption at higher wavelengths of the visible region and a change in colour from violet to a blue shade. This is an indication of Au nanoparticles agglomeration.

The H₂SO₄ addition also impacted significantly the results but only after the concentration reached 4 eq. as observed in Figure 41 (right).

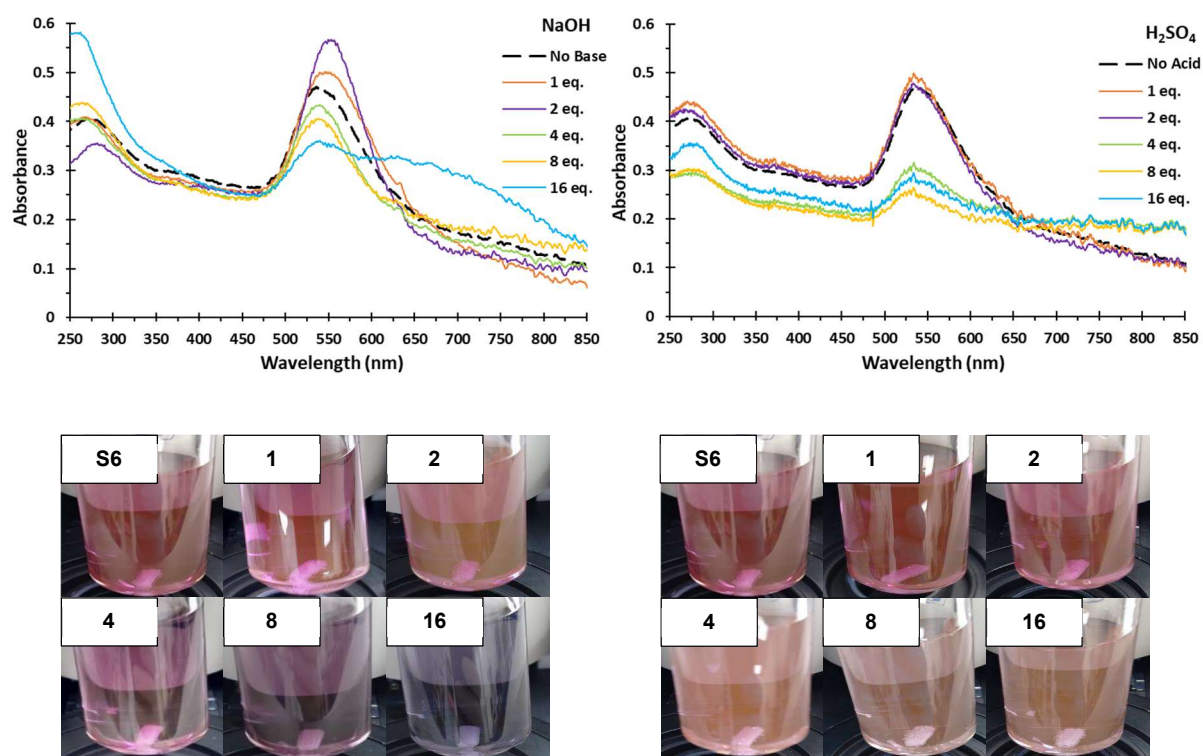


Figure 41 – Au nanoparticles produced at different concentrations of NaOH (left) and at different concentrations of H₂SO₄ (right) with UV-Vis analysis (top) and photos for no base/acid (S6), 1, 2, 4, 8 and 16 eq. (bottom).

Synthesis of Metal Nanoparticles by Microwave

3.2 Au Optimisation Tests

According to the experimental results for these two tests, presented in Table 17, there are no conditions where it is an advantage to add H₂SO₄ since the plasmon peak absorbance and the wavelength range became worse. On the other hand, controlled addition of NaOH, between 1-2 eq., could improve these two experimental results. However, the plasmon peak wavelength, which was not affected by the H₂SO₄ addition appears to have increased to around 550 nm when 1-2 eq. of NaOH were added. A mechanistic study trying to explain why NaOH addition has impacted the Au nanoparticles synthesis is presented in section 3.3.2.

Table 17 – Au nanoparticles experimental results at different NaOH/H₂SO₄ concentrations.

Acid/Base	Plasmon Peak Absorbance	Plasmon Peak Wavelength (nm)	Wavelength Range (nm)
No Base/Acid (standard)	0.47	537	82
1 eq. NaOH	0.50	549	87
2 eq. NaOH	0.57	553	64
4 eq. NaOH	0.43	539	75
8 eq. NaOH	0.41	538	81
16 eq. NaOH	0.36	539	-
1 eq. H ₂ SO ₄	0.50	533	71
2 eq. H ₂ SO ₄	0.48	533	78
4 eq. H ₂ SO ₄	0.32	534	95
8 eq. H ₂ SO ₄	0.26	533	120
16 eq. H ₂ SO ₄	0.29	533	119

Synthesis of Metal Nanoparticles by Microwave

3.2 Au Optimisation Tests

3.2.5 Solvent

As mentioned in section 1.4.3, the solvent should act as the reducing agent for the metal ions and provide good absorption of the electromagnetic radiation followed by dissipation of energy as heat. The general mechanism for metal ions reduction with ethylene glycol is presented in Equation 8. Moreover, the solvent also influences the solubility and the level of supersaturation (nucleation level) as expressed by the LaMer plot in Figure 11.

Therefore, the study of Au nanoparticles synthesis by microwave was extended to more solvents with a chemical composition similar to ethylene glycol ($C_2H_6O_2$). One of the solvents was a C_2 with one OH group (ethanol), two were a C_3 with two OH groups (1,2-propanediol and 1,3-propanediol), one was a C_3 with three OH groups (glycerol) and one had several OH groups (ascorbic acid). Ascorbic acid was first dissolved in water and a concentration of 5 mM was used, around 38x higher than the concentration of Au. Ascorbic acid has been shown to act not only as the reducing agent but also as a way of controlling the metal nanoparticles size and shape.¹⁰³

Water, the greenest possible solvent and at the same time presenting a high value for the dielectric constant (ϵ_1), and methanol, which was used by other authors, either just by itself⁹⁷ or mixed with water,⁹⁸ were also investigated. The Au nanoparticles produced in water are only the result of the stabilizer action (PVA) by the mechanism described in Equation 9.

All the UV-Vis spectra and the corresponding photos can be observed in Figure 42.

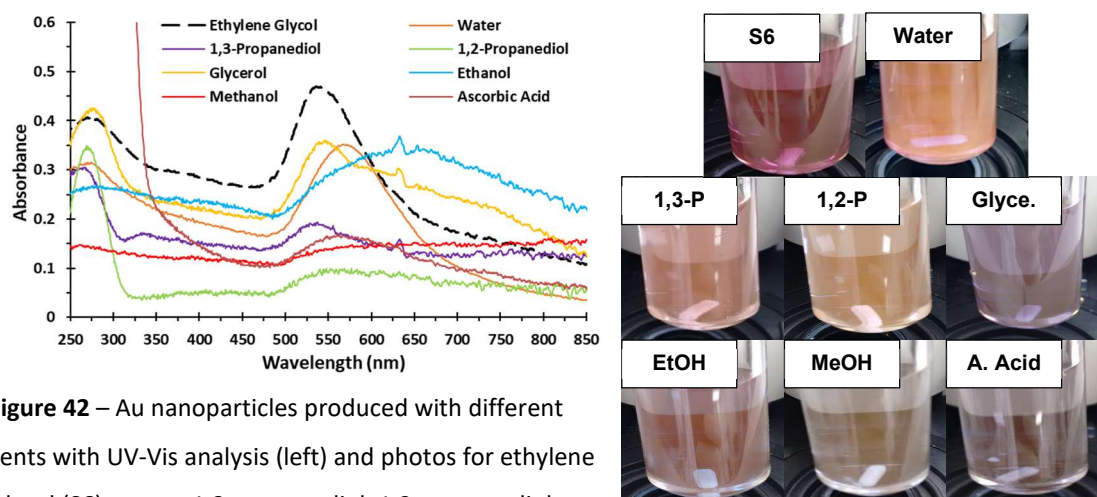


Figure 42 – Au nanoparticles produced with different solvents with UV-Vis analysis (left) and photos for ethylene glycol (S6), water, 1,3-propanediol, 1,2-propanediol, glycerol, ethanol, methanol and ascorbic acid (right).

Synthesis of Metal Nanoparticles by Microwave

3.2 Au Optimisation Tests

As shown in Table 18, the best experimental results in terms of Au nanoparticles production, average size and size distribution were obtained when ethylene glycol was used. The Au nanoparticles experimental results in water due to the PVA action were also interesting. A mechanistic study focused on this stabilizer action is presented in section 3.3.4.4 and more tests were also performed in sections 3.2.6 and 3.2.7. From the other solvents analysis only glycerol has been identified as a promising solvent but it still presented a strong absorption in the red region of the UV-Vis spectrum.

Table 18 – Au nanoparticles experimental results with different solvents.

Solvent	Plasmon Peak Absorbance	Plasmon Peak Wavelength (nm)	Wavelength Range (nm)
Ethylene glycol (standard)	0.47	537	82
Water	0.35	567	87
1,3-Propanediol	0.19	538	126
1,2-Propanediol	0.10	569	155
Glycerol	0.36	547	129
Ethanol	0.37	633	161
Methanol	-	-	-
Ascorbic acid	0.17	560	134

Synthesis of Metal Nanoparticles by Microwave

3.2 Au Optimisation Tests

3.2.6 Solvent Composition

Interaction between ethylene glycol and water was studied at different mixture compositions of 25, 50 and 75 % (Vol. H₂O/Vol. Glycol) and compared to the standard scenario of only ethylene glycol (0 %) and only water (100 %). The objective was to check for synergistic effects and also to use greener and more economic conditions for the production of metal nanoparticles by decreasing the amount of ethylene glycol.

According to the Au nanoparticles UV-Vis spectra presented in Figure 43 the addition of water (25 %) started to cause a bimodal distribution with a small new peak appearing at around 700 nm. This new peak progressively interferes with the main peak at around 537 nm as more water is added. Eventually with 100 % water only one main peak was again observed at around 567 nm. The experimental results are consistent with having one main UV-Vis peak at around 537 nm caused by the usual ethylene glycol mechanism described in Equation 8 and another main UV-Vis peak at around 567 nm caused by the stabilizer (PVA) mechanism described in Equation 9. When ethylene glycol and water mixtures are used both mechanisms take place and a bimodal distribution is even observed. As explained in section 1.2 as metal nanoparticles deviate from their circular shape a bimodal distribution can be observed.

DLS size distributions having two peaks were again observed for all the trials and compared to the average DLS size distribution for the standard conditions. The calculated average sizes were:

- 8.0 ± 3.9 nm and 84 ± 59 nm for the standard conditions with only ethylene glycol (0 %);
- 6.0 ± 2.6 nm and 68 ± 35 nm for the 25 % trial;
- 4.5 ± 1.9 nm and 60 ± 28 nm for the 50 % trial;
- 5.2 ± 1.8 nm and 78 ± 59 nm for the 75 % trial;
- 45 ± 9.7 nm and 234 ± 113 nm for the 100 % trial;

As expected DLS analysis only provided an indication about the Au nanoparticles average sizes with DLS size distributions being very similar for 0 %, 25 %, 50 % and 75 % trials. However, a strong trend was observed when working only with water (100 %). For this trial the DLS average sizes for both peaks had a significant increase. As shown in Table 19 the plasmon peak wavelength increase from 537 nm to 567 nm supports as well the idea that when working only with water (100 %) significantly larger Au nanoparticles were produced. In section 3.5, based on TEM analysis, further evidence of the Au nanoparticles average size and size distribution is presented.

Synthesis of Metal Nanoparticles by Microwave

3.2 Au Optimisation Tests

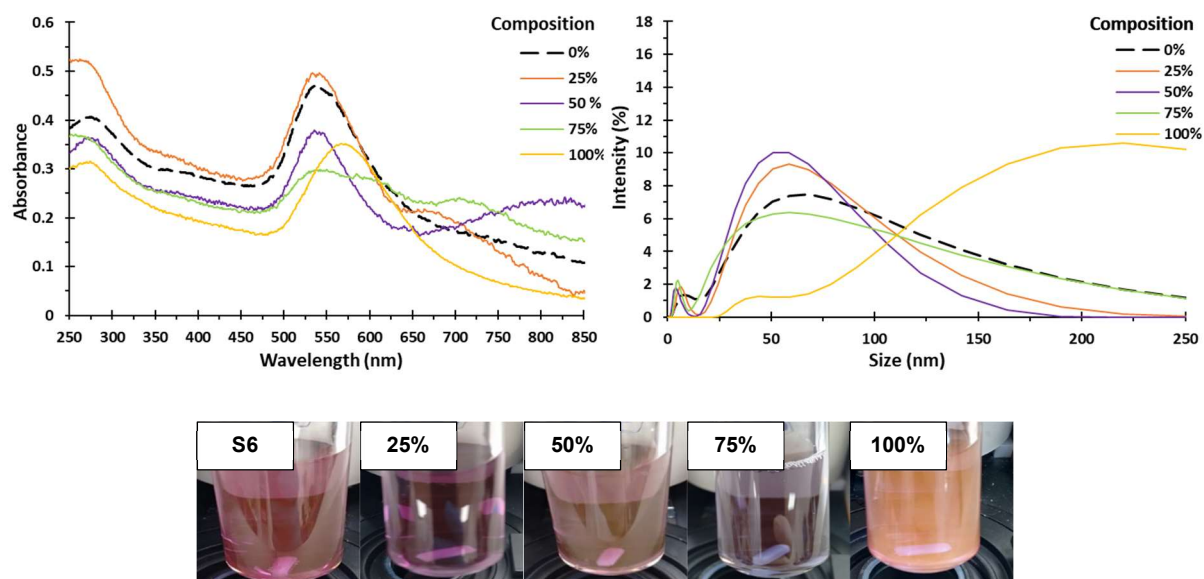


Figure 43 – Au nanoparticles produced at different compositions of water and ethylene glycol with UV-Vis (top left) and DLS (top right) analysis and photos for 0 (S6), 25, 50, 75 and 100 % (Vol. H₂O/Vol. Glycol) (bottom).

In summary, it appears that mixing ethylene glycol and water brings no synergistic effects with all experimental results becoming even worse (production, average size and size distribution) due to enhanced agglomeration and the possibility of a bimodal distribution. A mechanistic study focused on the stabilizer action and presented in section 3.3.4.4 also covers in more detail these experimental results.

Table 19 – Au nanoparticles experimental results at different water compositions.

Water Composition % (v/v)	Plasmon Peak Absorbance	Plasmon Peak Wavelength (nm)	Wavelength Range (nm)
0 (standard)	0.47	537	82
25	0.50	533	78
50	0.38	535	68
75	0.30	539	-
100	0.35	567	87

Synthesis of Metal Nanoparticles by Microwave

3.2 Au Optimisation Tests

3.2.7 Stabilizer

As explained in section 1.4.1, the stabilizers are used with the sol-immobilization synthesis method to control the growth mechanism by the steric effect of bulky ligands or by surrounding the nanoparticles with charged anions that create electrostatic repulsion (Coulomb force). During this PhD the stabilizers used were the PVA and PVP polymers that act due to the steric effect. These two polymers can also act as reducing agents under specific temperature conditions by the mechanisms shown in Equation 9 and Equation 10.

The effect of the PVA concentration was tested at different PVA/metal weight ratios of 0.325, 3.25 and 6.50 and compared to the standard scenario of 0.65 and also when no stabilizer is used. As observed in Figure 44 the UV-Vis spectra changed as the PVA/metal weight ratio changed, but small changes and without a clear trend present when considering the no stabilizer, 0.325xPVA, 0.65xPVA and 3.25xPVA trials. Only for the 6.50xPVA trial the Au nanoparticles production and size distribution have considerably improved. A stronger red colour could also be observed in the Au colloid photo.

Similar to the UV-Vis analysis, with the DLS analysis there was also not a clear trend present except for the 6.50xPVA trial, which seems to have had a considerable decrease of the Au nanoparticles average size, in particular for the first peak:

- 8.8 ± 3.5 nm and 67 ± 30 nm for no stabilizer trial;
- 4.3 ± 2.2 nm and 46 ± 22 nm for the 0.325xPVA trial;
- 8.0 ± 3.9 nm and 84 ± 59 nm for the 0.65xPVA trial (standard conditions);
- 6.1 ± 2.1 nm and 84 ± 80 nm for the 3.25xPVA trial;
- 2.6 ± 0.8 nm and 47 ± 28 nm for the 6.50xPVA trial;

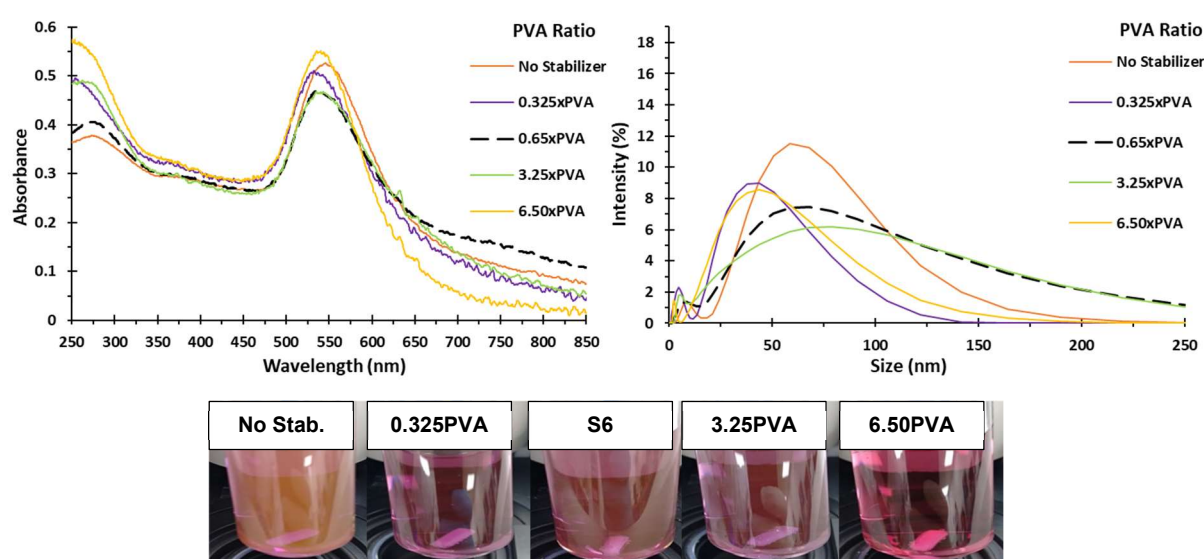


Figure 44 – Au nanoparticles produced at different PVA/metal weight ratios with UV-Vis (top left) and DLS (top right) analysis and photos for no stabilizer, 0.325xPVA, 0.65xPVA (S6), 3.25xPVA and 6.50xPVA (bottom).

Synthesis of Metal Nanoparticles by Microwave

3.2 Au Optimisation Tests

It was also investigated the PVA substitution by PVP at the same stabilizer/metal weight ratios as in the previous PVA test. The UV-Vis spectra shown in Figure 45 are also compared to the standard scenario of 0.65xPVA. Overall, better experimental results were observed for the Au nanoparticles production and size distribution when changing from the standard 0.65xPVA condition to any PVP condition. Contrary to the PVA test, it was observed a trend related to the PVP amount, with experimental results for Au nanoparticles production and size distribution improving as the PVP/metal weight ratio increased. Similar to the PVA test a stronger red colour was observed for the 6.50xPVP trial, but also for the 3.25xPVP trial.

All DLS size distributions were very similar to one another and no trends could be detected with this analysis:

- 8.0 ± 3.9 nm and 84 ± 59 nm for the 0.65xPVA trial (standard conditions);
- 7.2 ± 2.9 nm and 60 ± 28 nm for the 0.325xPVP trial;
- 7.0 ± 3.0 nm and 60 ± 24 nm for the 0.65xPVP trial;
- 5.4 ± 2.0 nm and 51 ± 23 nm for the 3.25xPVP trial;
- 5.7 ± 1.9 nm and 76 ± 47 nm for the 6.50xPVP trial;

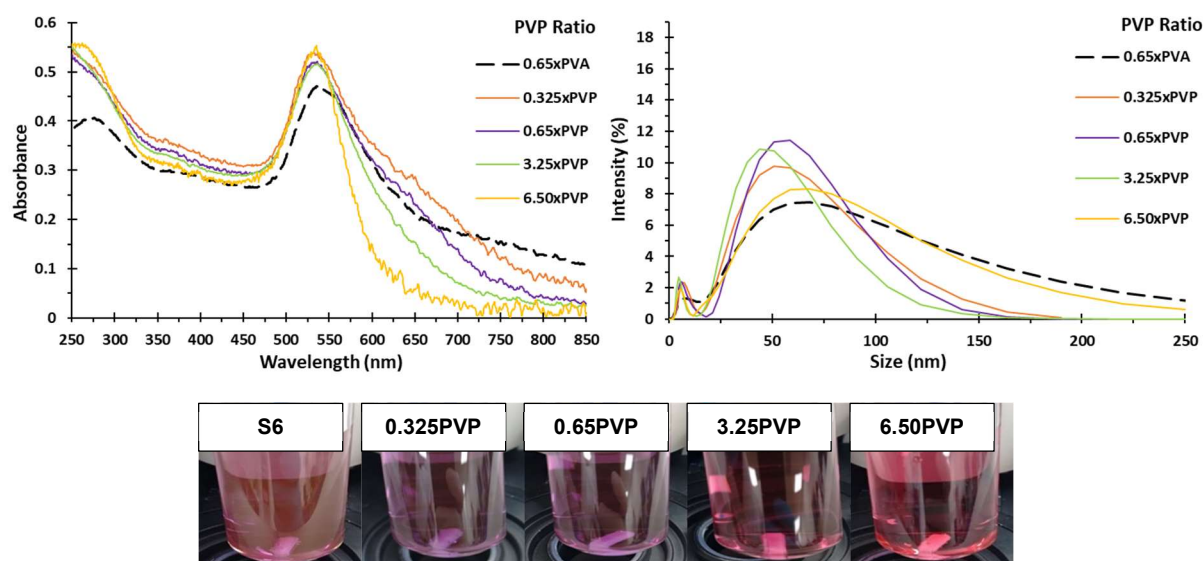


Figure 45 – Au nanoparticles produced at different PVP/metal weight ratios with UV-Vis (top left) and DLS (top right) analysis and photos for 0.65xPVA (S6), 0.325xPVP, 0.65xPVP, 3.25xPVP and 6.50xPVP (bottom).

The two previous tests for the solvent (Figure 42) and solvent composition (Figure 43) showed that water in conjugation with PVA can be used for the production of Au nanoparticles. Moreover, as already mentioned, using greener and more economic conditions for the production of metal nanoparticles are also important targets. For these reasons, stabilizer tests in water, both with PVA and PVP, were conducted to understand if any improvements to the Au nanoparticles production (0.35) average size (567 nm) and size distribution (87 nm) could be obtained by varying the stabilizer amount.

Synthesis of Metal Nanoparticles by Microwave

3.2 Au Optimisation Tests

As shown in Figure 46, tests were conducted to water (100 %) with stabilizer/metal weight ratios of 0.65xPVA, 3.25xPVA, 6.50xPVA, 0.65xPVP, 3.25xPVP and 6.50xPVP. The experimental results were compared to the standard scenario of 0.65xPVA in ethylene glycol and also when only water without any stabilizer is used.

As the amount of PVA increased the Au nanoparticles production and size distribution is expected to have considerably improved with the best experimental results obtained for the 6.50xPVA trial. However, the plasmon peak wavelength has not changed much (from 567 to 557 nm), with large Au nanoparticles still expected to have been produced. This was supported by the calculated DLS average sizes of 45 ± 9.7 nm and 234 ± 113 nm for the 0.65xPVA trial and 117 ± 56 nm for the 3.25xPVA trial.

When changing to PVP the experimental results indicate a major decline for the Au nanoparticles production, average size and size distribution with their UV-Vis spectra being all very similar. The calculated DLS average sizes of 14 ± 4.5 nm and 90 ± 44 nm for the 0.65xPVP trial and 107 ± 60 nm for the 3.25xPVP trial did not support this decline in the experimental results as strongly as the UV-Vis analysis. In any case, these calculated DLS average sizes were significantly higher than the 8.0 ± 3.9 nm and 84 ± 59 nm that could be observed for the standard scenario trial.

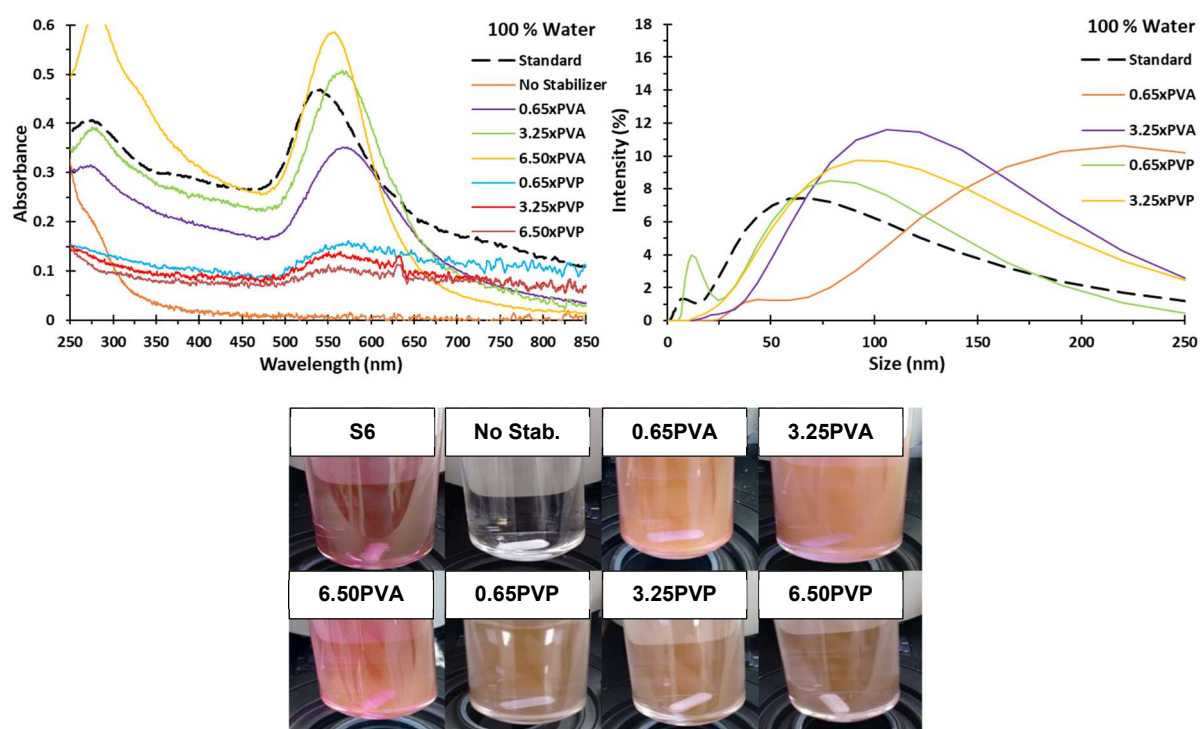


Figure 46 – Au nanoparticles produced in 100 % water at different PVA/metal and PVP/metal weight ratios with UV-Vis (top left) and DLS (top right) analysis and photos for standard conditions (S6), no stabilizer, 0.65xPVA, 3.25xPVA, 6.50xPVA, 0.65xPVP, 3.25xPVP and 6.50xPVP (bottom).

Synthesis of Metal Nanoparticles by Microwave

3.2 Au Optimisation Tests

This test at 100 % water was also important as it demonstrated that using only water (No Stabilizer trial) did not cause any changes to the Au solution UV-Vis spectrum and no Au nanoparticles were produced. Therefore, it is shown that the metal reduction action is derived only from the stabilizers action (PVA or PVP) as predicted.

As shown in Figure 47, tests were also carried out in a 25 % ethylene glycol and 75 % water mixture (v/v) (75 %) with stabilizer/metal weight ratios of 0.65xPVA, 6.50xPVA, 0.65xPVP and 6.50xPVP. The experimental results were compared to the standard scenario of 0.65xPVA in ethylene glycol.

No major improvements could be observed when increasing the PVA amount from a 0.65 to a 6.50 PVA/metal weight ratio. Contrary to the 100 % water scenario, the experimental results appear to have improved when moving from PVA to PVP with the bimodal distribution even disappearing. However, worst experimental results were observed when moving from the 0.65xPVP trial to the 6.50xPVP trial.

The calculated DLS average sizes were overall similar to the one observed for the standard conditions trial:

- 5.2 ± 1.8 nm and 78 ± 59 nm for the 0.65xPVA trial;
- 6.9 ± 3.0 nm and 123 ± 86 nm for the 6.50xPVA trial;
- 5.4 ± 2.7 nm and 85 ± 61 nm for the 0.65xPVP trial;
- 11 ± 3.9 nm and 76 ± 38 nm for the 6.50xPVP trial;

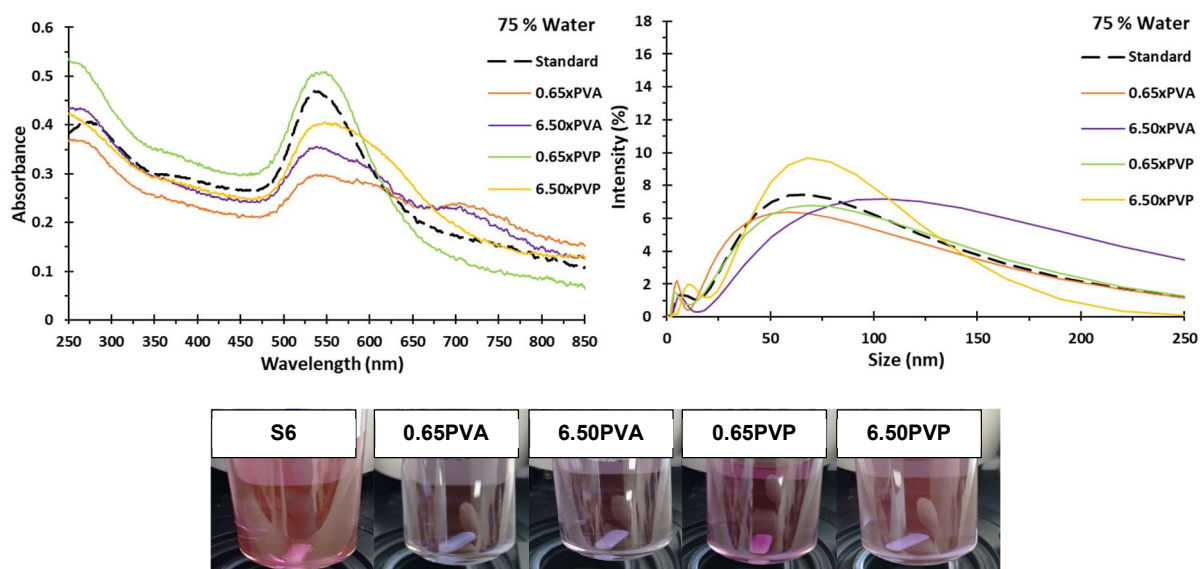


Figure 47 – Au nanoparticles produced in 75 % water at different PVA/metal and PVP/metal weight ratios with UV-Vis (top left) and DLS (top right) analysis and photos for standard conditions (S6), 0.65xPVA, 6.50xPVA, 0.65xPVP and 6.50xPVP (bottom).

Synthesis of Metal Nanoparticles by Microwave

3.2 Au Optimisation Tests

After considering all the stabilizer tests, with all the experimental results compared in Table 20, it is strongly suggested that major improvements to the standard scenario are expected when increasing the stabilizer amount. However, it was also possible to produce Au nanoparticles if using ethylene glycol without any stabilizer, as shown in Figure 44, even though the expected Au nanoparticles average size is larger with a plasmon peak wavelength of 546 nm observed.

Replacing PVA by PVP at stabilizer/metal weight ratios of 3.25 and 6.50 resulted in considerable better experimental results for the Au nanoparticles size distribution. Overall, all PVP trials presented high and similar plasmon peak absorbances and low and similar plasmon peak wavelengths.

Interesting results were observed when working only with water (100 %) and with an ethylene glycol and water mixture (75 %), but the experimental results were still far from what could be obtained when working only with ethylene glycol.

The stabilizer action is further analysed in section 3.3.4.4 where a mechanistic study is presented.

Table 20 – Au nanoparticles experimental results at different stabilizer conditions.

	Condition	Plasmon Peak Absorbance	Plasmon Peak Wavelength (nm)	Wavelength Range (nm)
Ethylene Glycol (EG)	No stabilizer	0.53	546	77
	0.325xPVA	0.51	532	80
	0.65xPVA (standard)	0.47	537	82
	3.25xPVA	0.47	540	86
	6.50xPVA	0.55	535	69
	0.325xPVP	0.54	532	77
	0.65xPVP	0.52	536	73
	3.25xPVP	0.52	535	70
	6.50xPVP	0.55	535	50
Water (W)	No stabilizer	-	-	-
	0.65xPVA	0.35	567	87
	3.25xPVA	0.51	567	74
	6.50xPVA	0.58	557	63
	0.65xPVP	-	-	-
	3.25xPVP	-	-	-
	6.50xPVP	-	-	-
75 % W 25 % EG	0.65xPVA	0.30	539	-
	6.50xPVA	0.36	539	-
	0.65xPVP	0.51	549	87
	6.50xPVP	0.41	549	134

3.3 Mechanistic Studies

Work not focused on the Au nanoparticles experimental results but rather in the mechanism by which the Au nanoparticles were produced was carried out and presented in this section. The aim is to deliver an insight of the influence of heating, NaOH addition, stabilizer, solvent and Au oxidation state on the metal nanoparticles formation mechanism, in particular on the metal reduction, nucleation and growth steps.

3.3.1 Conventional Heating vs. Microwave Heating

It was verified that Au nanoparticles production was possible if using conventional heating with a round bottom flask placed inside an oil bath. The standard conditions used for the microwave heating and described in section 3.2 were followed for the conventional heating test as well, but trials at 125 °C and without stabilizer were also carried out. Two conventional heating conditions were considered:

- a) Normal heating, where the solvent, metal and stabilizer were present inside the round bottom flask and heated from room temperature to 125 °C or 150 °C;
- b) Preheating, where the solvent and stabilizer were present inside the round bottom flask and heated from room temperature to 125 °C or 150 °C and only after the desired temperature was reached the metal was added;

Samples were taken at 5, 10, 15 and 20 min for each trial with all the analysed UV-Vis spectra and the Au colloids photos taken at 15 min shown in Figure 48 and compared to the microwave heating standard scenario.

As observed in Table 21, the experimental results for the nanoparticles production, average size and size distribution obtained with normal heating were worse than the ones obtained with microwave at standard conditions. This is according to the principle that microwave offers a thermal advantage (more homogeneous heating).

When trying to minimize the microwave thermal advantage by only adding the Au when all solvent inside the round bottom flask was already at the desired temperature (preheating condition) it was verified that the Au nanoparticles were produced faster and the experimental results improved. However, the experimental results were still worse than what could be obtained with microwave at standard conditions. This is consistent with microwave heating offering special effects and not only thermal advantages. As mentioned in section 1.4.3 these potential special effects are still a source of debate among several authors but could mean lower activation energies which would have an impact on the metal reduction rate.⁴⁸

Synthesis of Metal Nanoparticles by Microwave

3.3 Mechanistic Studies

Similar to the microwave heating scenario, in both trials with conventional heating at 125 °C and 150 °C it was also possible to produce Au nanoparticles without any stabilizer, but the experimental results were worse.

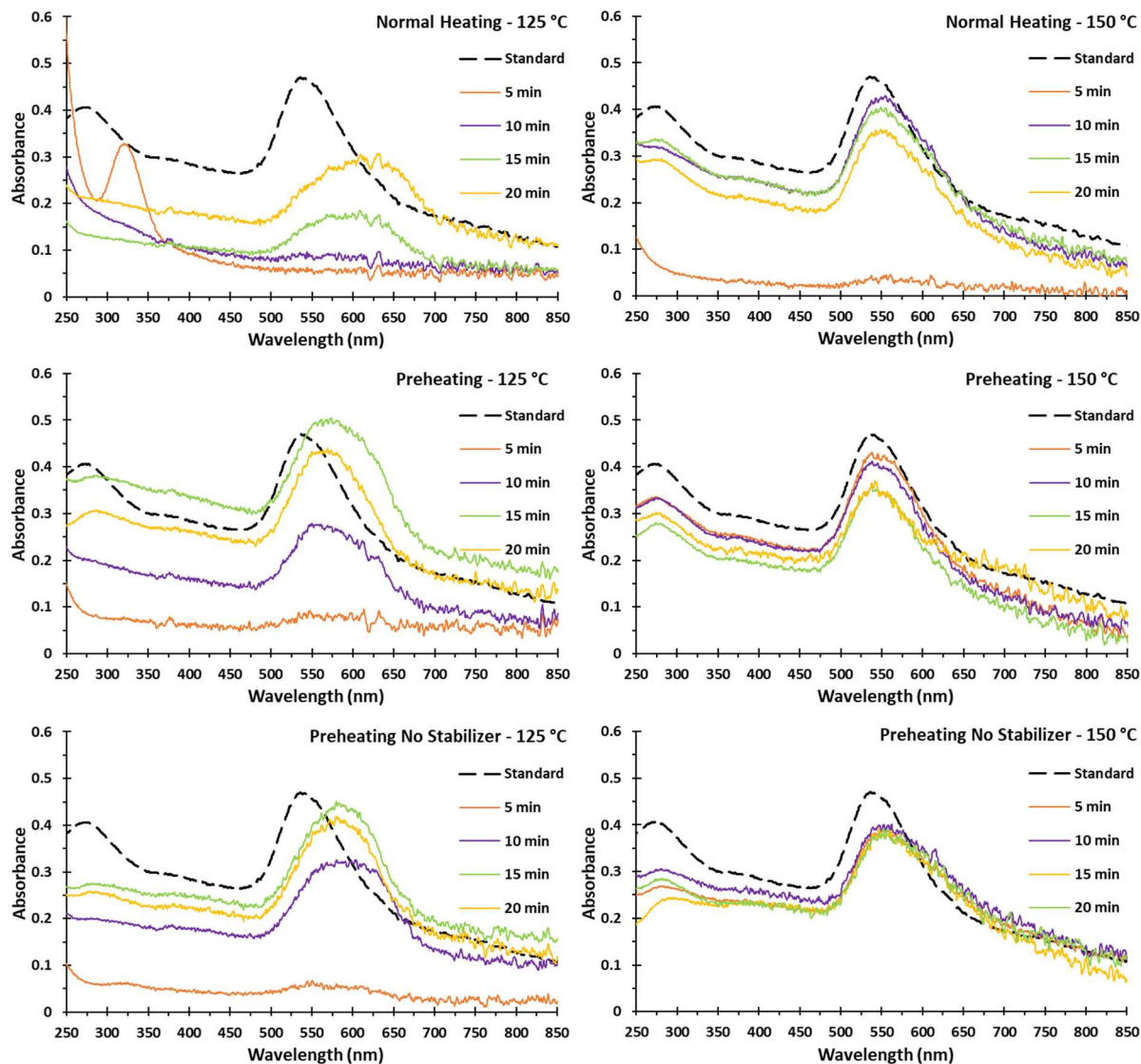


Figure 48 – Au nanoparticles produced by conventional heating at 125 °C (left) and 150 °C (right) with UV-Vis analysis and photos (bottom) for microwave standard conditions (S6) and for the colloids at 15 min at 125 °C and 150 °C with normal heating (NH), preheating (PH) and preheating no stabilizer (PHNS).

Synthesis of Metal Nanoparticles by Microwave

3.3 Mechanistic Studies

Table 21 – Au nanoparticles experimental results with conventional heating at different temperatures, holding times and heating conditions.

	Heating Condition and Holding Time (min)	Plasmon Peak Absorbance	Plasmon Peak Wavelength (nm)	Wavelength Range (nm)
125 °C	Normal Heating – 5 min	-	-	-
	Normal Heating – 10 min	-	-	-
	Normal Heating – 15 min	0.19	610	115
	Normal Heating – 20 min	0.31	634	130
125 °C	Preheating – 5 min	-	-	-
	Preheating – 10 min	0.28	551	96
	Preheating – 15 min	0.50	574	120
	Preheating – 20 min	0.44	570	96
125 °C	Preheating N Stab – 5 min	-	-	-
	Preheating N Stab – 10 min	0.33	605	119
	Preheating N Stab – 15 min	0.45	581	100
	Preheating N Stab – 20 min	0.42	581	97
150 °C	Normal Heating – 5 min	-	-	-
	Normal Heating – 10 min	0.43	556	92
	Normal Heating – 15 min	0.41	550	93
	Normal Heating – 20 min	0.36	550	86
150 °C	Preheating – 5 min	0.43	539	86
	Preheating – 10 min	0.41	539	83
	Preheating – 15 min	0.36	538	80
	Preheating – 20 min	0.37	543	77
150 °C	Preheating N Stab – 5 min	0.39	553	110
	Preheating N Stab – 10 min	0.40	554	117
	Preheating N Stab – 15 min	0.49	549	122
	Preheating N Stab – 20 min	0.39	560	100

3.3.2 Au³⁺ Reduction Behaviour and NaOH Effect

Another mechanistic study relates to the reduction behaviour of Au³⁺ in solution, initially present as the [AuCl₄]⁻ species. As observed in the holding time and temperature optimisation test in section 3.2.3 in Figure 40 at 100 °C the Au solution peak at around 325 nm gradually decreased with time, but Au nanoparticles were only detected by UV-Vis analysis after 15 min of microwave heating. Likewise, with a 5 min holding time the Au solution peak at around 325 nm gradually decreased with increasing temperature, but Au nanoparticles were only detected by UV-Vis analysis after reaching 125 °C. A schematic representation of the Au solution peak behaviour at 100 °C with microwave heating holding times of 0 and 2.5 min is displayed in Figure 49. The schematic representation suggests one of two hypotheses:

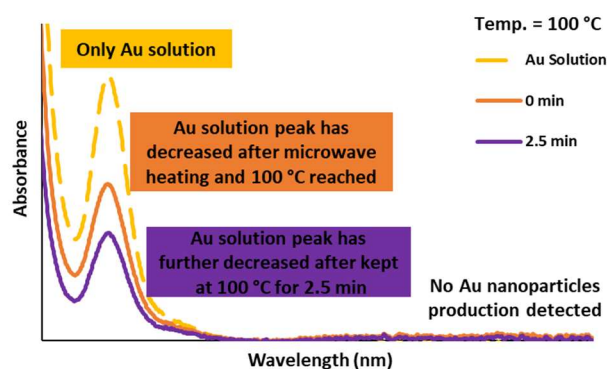


Figure 49 – Schematic representation of Au³⁺ reduction behaviour with microwave heating at 100 °C with holding times of 0 and 2.5 min and cooled to room temperature.

a) Before reduction, [AuCl₄]⁻ species are undergoing a transformation to other species, which are not detected by UV-Vis analysis, and only after Au nanoparticles are formed;

b) [AuCl₄]⁻ species are being reduced to individual Au atoms and accumulating before the nucleation process is triggered, but the Au atoms are too small to be detected by UV-Vis analysis;

According to Wang *et al*¹⁰² there are several possible Au precursor species in equilibrium with each other depending on pH of the Au solution as shown in Table 22. In fact, it is not even possible to talk about the [AuCl₄]⁻ species in solution because after contact with water it immediately undergoes hydrolysis to [AuCl₃(OH)₁]⁻. In any case, the oxidation state of Au in solution remains always unchanged at +3.

Synthesis of Metal Nanoparticles by Microwave

3.3 Mechanistic Studies

Table 22 – Speciation of Au solution at different pH values.¹⁰²

pH	$[AuCl_X(OH)_{4-X}]^-$					Average Formula
	X = 0	X = 1	X = 2	X=3	X=4	
2.91	-	-	+	+	+	$[AuCl_{2.91}(OH)_{1.09}]^-$
3.39	-	-	+	+	+	$[AuCl_{2.56}(OH)_{1.44}]^-$
4.01	-	-	+	+	+	$[AuCl_{2.46}(OH)_{1.54}]^-$
5.01	-	-	+	+	-	$[AuCl_{2.43}(OH)_{1.57}]^-$
6.16	+	+	+	-	-	$[AuCl_{1.09}(OH)_{2.91}]^-$
7.52	+	+	-	-	-	$[AuCl_{0.83}(OH)_{3.17}]^-$
8.01	+	+	-	-	-	$[AuCl_{0.67}(OH)_{3.33}]^-$
10.35	+	+	-	-	-	$[AuCl_{0.10}(OH)_{3.90}]^-$

a) – stands for absence; b) + stands for presence;

As shown in Figure 50, pH tests were conducted by adding NaOH to Au solution in water (left) and in ethylene glycol (right) in order to understand whether or not the Au solution peak decrease was due to the formation of different Au precursor species. The PVA/metal weight ratio was kept at 0.65, same condition as in the optimisation test. Different molar ratios between the active species OH⁻ and Au were considered, namely 1, 2, 4, 8 and 16 eq. and compared to the no NaOH addition scenario.

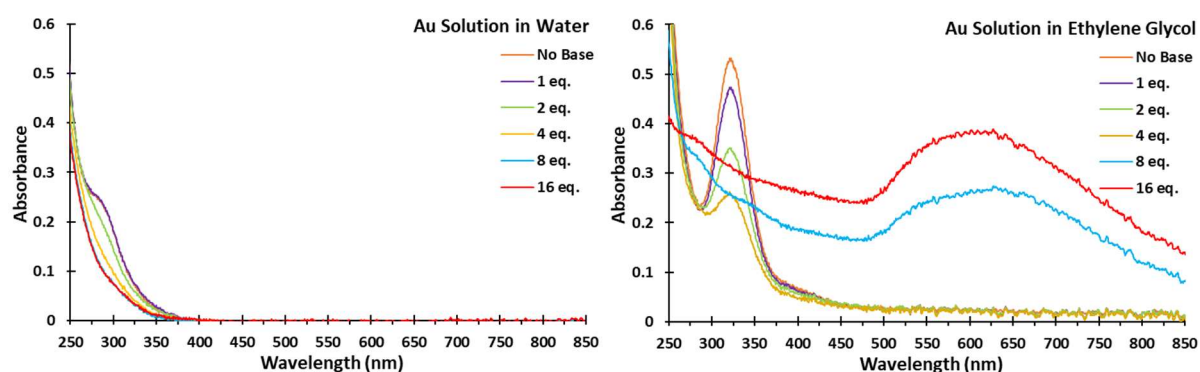


Figure 50 – UV-Vis analysis of Au solution in water (left) and in ethylene glycol (right) at different concentrations of NaOH.

As mentioned in the acid/base addition optimisation test in section 3.2.4, it is assumed full dissociation when adding a strong base or acid to the non-aqueous solvent ethylene glycol because ethylene glycol is a polar solvent presenting two OH groups capable of offering protonation/deprotonation. However, when using a pH meter in ethylene glycol solution direct comparisons should not be made between the values of water and ethylene glycol as the equipment is calibrated to perform measurements only in aqueous solutions. Therefore, the pH meter measurements in an ethylene glycol solution only provided an indication about the effect of adding NaOH. The measured pH values are presented in Table 23.

Synthesis of Metal Nanoparticles by Microwave

3.3 Mechanistic Studies

Table 23 – pH measurements of Au solution in water and in ethylene glycol at different concentrations of NaOH.

NaOH Concentration	pH in Water	pH in Ethylene Glycol
No Base	3.9	3.8
1 eq.	4.1	6.7
2 eq.	4.6	7.2
4 eq.	10.3	9.4
8 eq.	11.3	10.1
16 eq.	11.6	10.6

Both water and ethylene glycol presented a neutral pH, around 7.0. The stabilizer addition did not affect these values but upon addition of the Au precursor, namely chloroauric acid with the chemical formula $HAuCl_4$, the solvents changed to an acid pH, 3.9 for water and 3.8 for ethylene glycol. As expected, the Au precursor underwent dissociation and donated protons, becoming $[AuCl_4]^-$.

As observed in Figure 50, the UV-Vis spectra of Au solutions in water changed with the addition of NaOH. The peak at around 300 nm continuously decreased as more NaOH was added until 8 eq. concentration was reached. After 8 eq. concentration no more changes in the UV-Vis spectrum were observed and increasing the NaOH concentration to 16 eq. produced no impact. This can be explained by considering that the pH at 8 eq. and 16 eq. was very similar, 11.3 and 11.6 respectively. Furthermore, as shown in Table 22, above a 10.35 pH almost all of the Au precursor had already changed to $[AuOH_4]^-$.

A similar trend was observed when considering Au solutions in ethylene glycol. The increased addition of NaOH contributed to the reduction of the Au solution peak at 325 nm. This was exactly the same type of behaviour observed in the holding time and temperature optimisation test in section 3.2.3 in Figure 40. However, contrary to the water scenario it is wrong to link these UV-Vis changes only to the NaOH addition. When the NaOH concentration increased to 8 eq. and 16 eq. UV-Vis spectra consistent with the formation of Au nanoparticles were observed. The same test at 16 eq. NaOH was also performed without adding any stabilizer (Figure 51). This showed that the NaOH Au nanoparticles production effect was not due to interaction of NaOH with the stabilizer but instead with the ethylene glycol.

In order to confirm Au nanoparticles production DLS and TEM analysis were performed to the 16 eq. NaOH trials as shown in Figure 51. The UV-Vis and DLS analysis were also compared to the standard conditions used for the microwave heating.

Synthesis of Metal Nanoparticles by Microwave

3.3 Mechanistic Studies

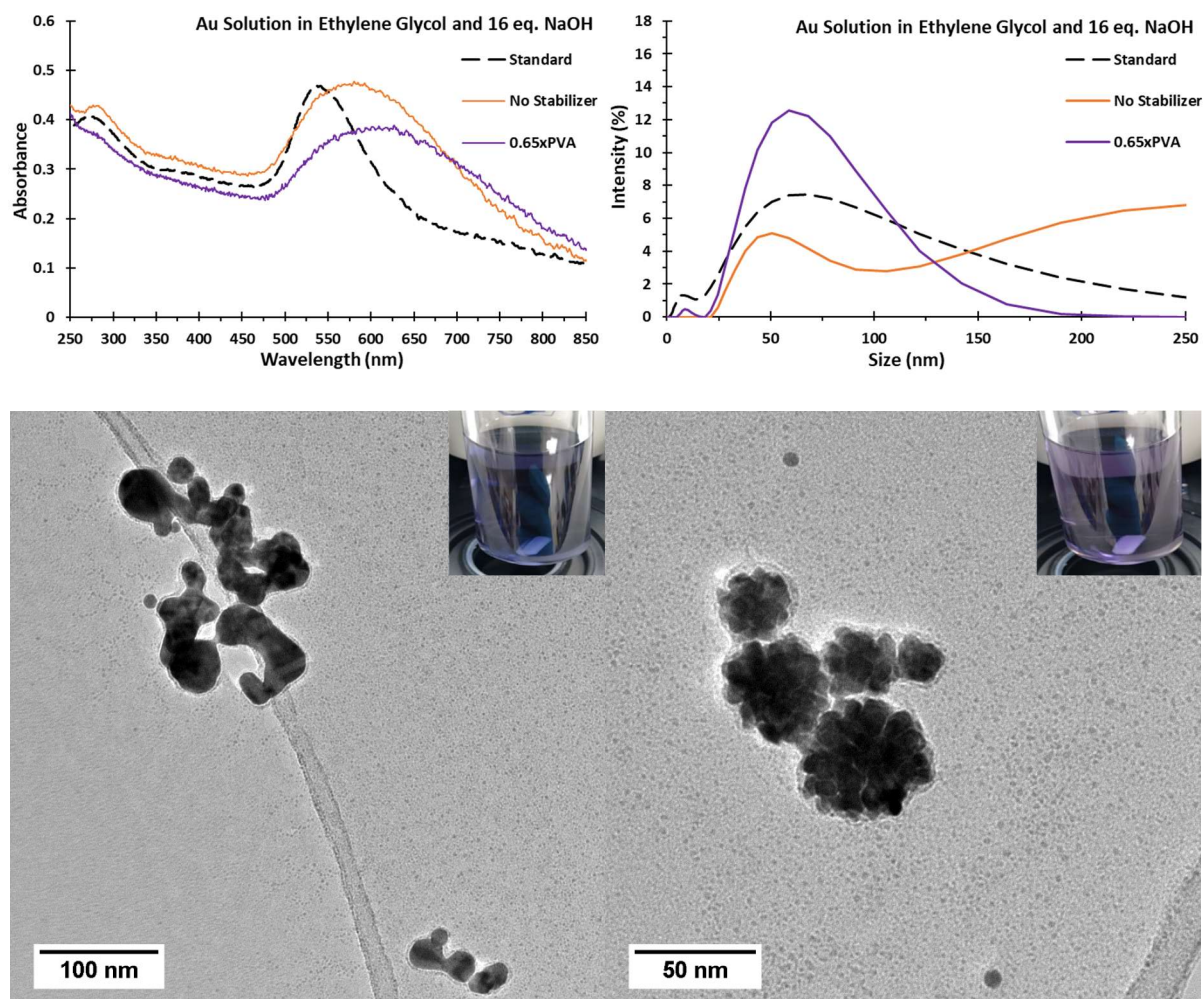


Figure 51 – Au nanoparticles produced without microwave heating by adding 16 eq. of NaOH to Au solution in ethylene glycol with no stabilizer and 0.65xPVA with UV-Vis (top left) and DLS (top right) analysis and TEM images for no stabilizer trial (bottom left) and 0.65xPVA trial (bottom right) with Au colloid photos included.

It can be said that UV-Vis, DLS and TEM analysis confirmed that adding NaOH to the Au solution in ethylene glycol was enough to produce Au nanoparticles without using any microwave heating, but the observed Au nanoparticles sizes were big.

Compared to the Au nanoparticles produced at the standard conditions the UV-Vis spectra presented a broader size distribution and a higher plasmon peak wavelength. The calculated DLS average sizes for the two peaks were also higher with 59 ± 22 nm and 320 ± 166 nm for the no stabilizer trial and 9.2 ± 2.1 nm and 66 ± 29 nm for the 0.65xPVA trial. The TEM analysis revealed a considerable degree of agglomeration with the 0.65xPVA trial presenting more circular and smaller nanoparticles when compared to the no stabilizer trial. For both trials one TEM image was analysed by EDX in order to confirm that the observed large and non-circular nanoparticles were in fact Au.

Synthesis of Metal Nanoparticles by Microwave

3.3 Mechanistic Studies

It is remarkable that Au nanoparticles could be produced only by adding NaOH to the Au solution in ethylene glycol without any microwave heating. This NaOH Au nanoparticles production effect was not detected during the acid/base addition optimisation test shown in section 3.2.4 in Figure 41. The reasons for this being:

- a) During the acid/base addition optimisation test the Au solution was not checked with UV-Vis after adding the NaOH;
- b) Colour changes to the solution could only be detected several minutes after adding the NaOH, which indicates the existence of an induction period;
- c) Slow process with the UV-Vis spectrum for a certain concentration of NaOH only becoming completely stable after several minutes;

Moreover, the NaOH Au nanoparticles production effect also provides an explanation of why for the acid/base addition optimisation test shown in section 3.2.4 in Figure 41 the controlled addition of NaOH, between 1-2 eq., could improve the experimental results. When adding 1-2 eq. of NaOH to the Au solution, an important part of the Au was already reduced before starting any microwave heating but no Au nanoparticles were formed yet. This caused the nucleation step to be faster as it was not as much limited as before by the rate of metal reduction. According to the LaMer concept, mentioned in section 1.4.1, the growth step starting only after the nucleation step is a condition necessary to obtain a narrow size distribution. The faster the nucleation step is the closer the experiment is to this ideal scenario.

However, above a certain threshold for the addition of NaOH (8-16 eq.) the Au nanoparticles started to be formed as observed in Figure 50 and Figure 51. For this reason, before starting any microwave heating an important part of the Au had already originated large and non-circular nanoparticles which led to the experimental results for the acid/base addition optimisation test shown in section 3.2.4 in Figure 41 also becoming worse. Again, the LaMer principle explains why large and non-circular Au nanoparticles were produced. The NaOH acted as a very weak reducing agent, causing the nucleation step to be even slower than when normal microwave heating was applied. Furthermore, the reduction potential measured by Wang *et al*¹⁰² indicated that when $[AuCl_4]^-$ and $[AuCl_3(OH)_1]^-$ are the dominant species in solution they can be facilely reduced whereas if $[AuCl_1(OH)_3]^-$ and $[Au(OH)_4]^-$ are the dominant species in solution they are very difficult to be reduced. As the NaOH is added the dominant species become $[AuCl_1(OH)_3]^-$ and $[Au(OH)_4]^-$.

It is also important to stress that conducting microwave trials with the addition of any amount of NaOH has a negative impact on the method reproducibility as it is more difficult to exactly reproduce the initial Au solution conditions.

Synthesis of Metal Nanoparticles by Microwave

3.3 Mechanistic Studies

In conclusion, changing from one Au species to another can modify the UV-Vis spectrum. This is clearly observed in the water trials with NaOH in Figure 50. However the big changes in the UV-Vis spectra observed in the holding time and temperature optimisation test in section 3.2.3 in Figure 40 and in the ethylene glycol trials with NaOH in Figure 50 are not explained only by the formation of different Au species.

All the evidence suggests that the nucleation step is triggered only after a certain amount of Au^{3+} is reduced and a concentration threshold is reached for the individual Au^0 reduced atoms which are not detected by UV-Vis analysis. This finding is according with the LaMer principle of burst nucleation, evidenced in the plot shown in Figure 11.

Moreover, if the UV-Vis spectra changes were only due to different Au species being formed they should be able to be reverted by changing again the pH from basic to acid conditions. However, when adding a strong acid (H_2SO_4) it was not possible to revert any of the UV-Vis spectra changes observed with the Au solution in ethylene glycol, only in water.

Finally, adding NaOH to Au solution in water did not cause the Au nanoparticles production effect. Therefore, it can be excluded that the reduction observed for Au^{3+} ions in the ethylene glycol solution without any microwave heating was only caused by NaOH. It is possible that similar to the synthesis protocol described in section 1.4.2.3, in which tetrakis(hydroxymethyl)phosphonium chloride (THPC) acts as the reducing agent in the presence of NaOH due to the formation of formaldehyde, also when combining NaOH with ethylene glycol a reducing agent is formed. Supported by the microwave heating general mechanism for metal ions reduction with ethylene glycol, shown in Equation 8, it is likely that the formed reducing agent was acetaldehyde.

Synthesis of Metal Nanoparticles by Microwave

3.3 Mechanistic Studies

3.3.3 Role of Acetaldehyde as Reducing Agent

In order to verify if acetaldehyde alone is able to reduce Au nanoparticles a trial was conducted by adding Au precursor to 1 mL of a 40 wt. % acetaldehyde solution in water and to 19 mL of water. The Au solution concentration was kept at the standard condition and no stabilizer was added.

The UV-Vis spectrum shown in Figure 52 is compared to the microwave heating standard scenario. The UV-Vis spectrum for the acetaldehyde trial shown in Figure 52 is consistent with the production of Au nanoparticles. However, the experimental results were still very far from what was obtained with the microwave heating standard scenario.

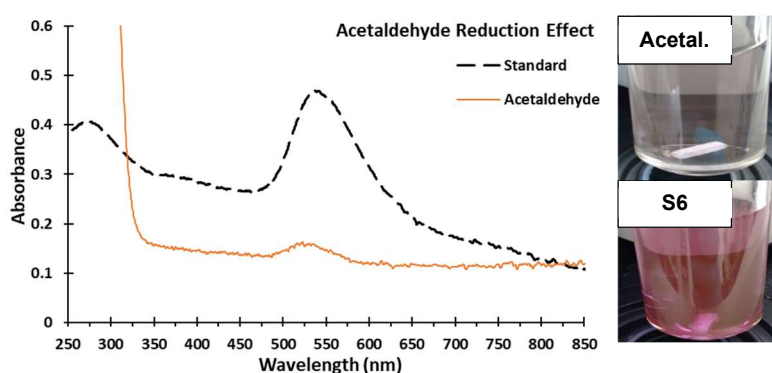


Figure 52 – Au nanoparticles produced without microwave heating in 20 mL acetaldehyde/water Au solution (1 mL of a 40 wt. % acetaldehyde solution in water added to 19 mL of water) with UV-Vis analysis (left) and photos for microwave standard conditions (S6) and acetaldehyde trial (Acetal.)

Acetaldehyde is a highly volatile compound, with normal boiling point of around 20 °C, and very easy to be detected by the pressure sensor if significant amounts are produced. When producing Au nanoparticles with microwave heating at standard conditions the system relative pressure remained low, around 1.2 bar as indicated by the pressure sensor. At the end of the microwave synthesis no changes in the system volume were observed and NMR analysis confirmed that ethylene glycol was still the only major compound detected, with ^1H NMR shown in Figure 53 (bottom) and ^{13}C NMR shown in Figure 54 (bottom).

These observations indicate that only a very low amount of ethylene glycol was converted to acetaldehyde and not much acetaldehyde is necessary to drive the Au reduction. Therefore, a low amount of acetaldehyde can be excluded as the reason for the different and much worse experimental results obtained in Figure 52. The different properties between the two solvents, water in the acetaldehyde trial and ethylene glycol in the microwave synthesis, could be the main reason. It is possible that acetaldehyde is not trapped in water as much as in ethylene glycol and easily escapes to the atmosphere without reducing much of the Au ions.

Synthesis of Metal Nanoparticles by Microwave

3.3 Mechanistic Studies

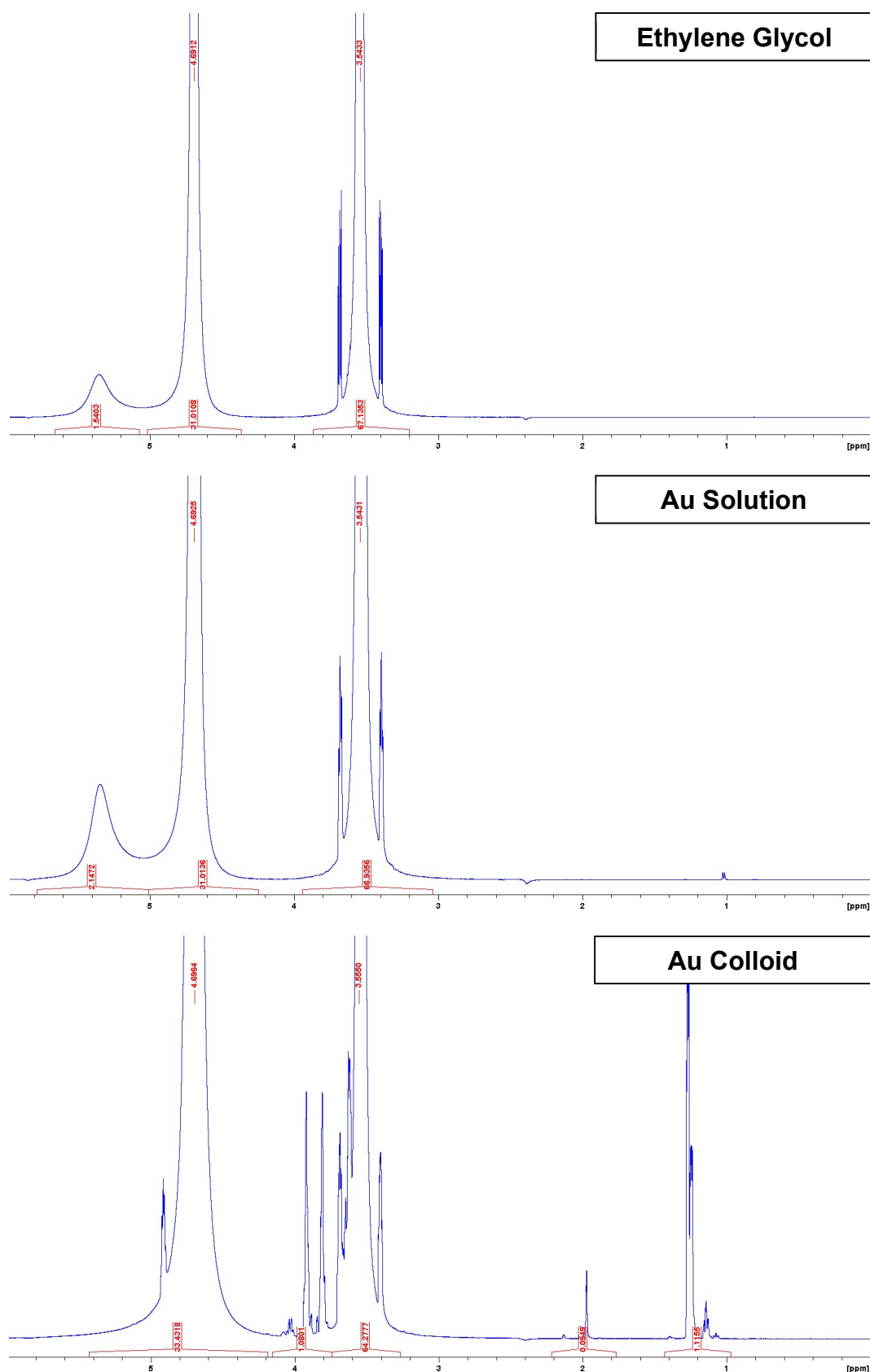


Figure 53 – ^1H NMR spectrum of ethylene glycol (top), of the Au solution at microwave heating standard conditions (middle) and of the produced Au nanoparticles colloid with the standard conditions (bottom).

Synthesis of Metal Nanoparticles by Microwave

3.3 Mechanistic Studies

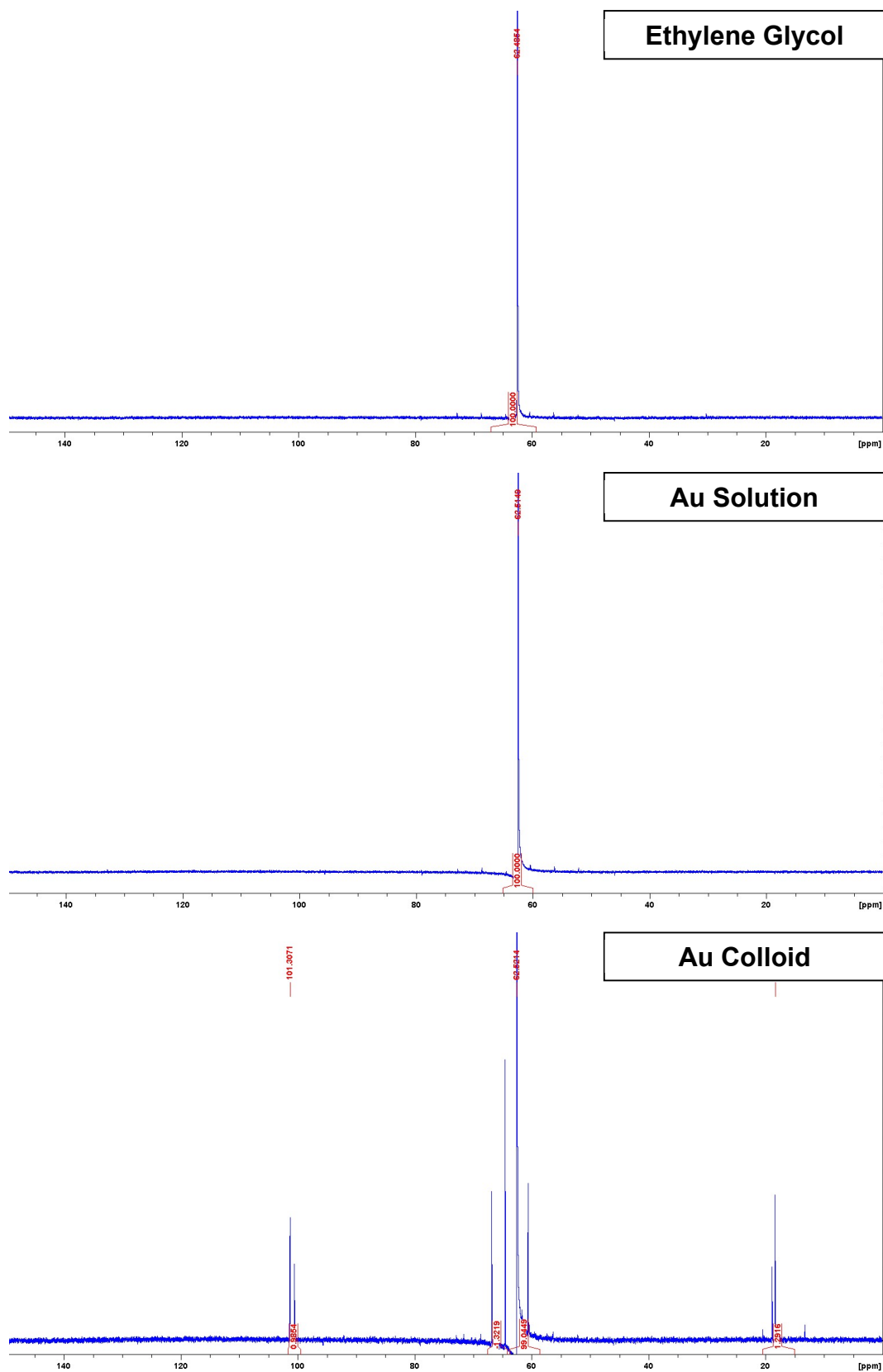


Figure 54 – ^{13}C NMR spectrum of ethylene glycol (top), of the Au solution at microwave heating standard conditions (middle) and of the produced Au nanoparticles colloid with the standard conditions (bottom).

3.3.4 H¹NMR and C¹³NMR Analysis

The NMR spectra obtained for the produced Au nanoparticles colloid at microwave heating standard conditions in Figure 53 and Figure 54 were also compared to the spectra of only ethylene glycol (top) and of the Au solution before any microwave heating (middle).

Both for the H¹NMR and C¹³NMR analysis no differences were observed between ethylene glycol and the Au solution. This means that adding the stabilizer at the standard PVA/metal weight ratio of 0.65 had a neutral effect. The produced Au nanoparticles colloid presented new NMR peaks (bottom). However, the relative areas of these new peaks were small, with 2.3 % for the H¹NMR and 3.6 % for the C¹³NMR. The produced Au nanoparticles colloid also revealed the disappearance of the small ethylene glycol peak at a chemical shift of around 5.4 ppm.

3.3.4.1 Ethylene Glycol NMR Analysis

The ethylene glycol NMR spectra were according to the expected: For the H¹NMR spectrum there were six protons from the ethylene glycol to take into consideration. Four of the protons from the two CH₂ groups, which presented a relative area very similar to the theoretical area of 66.6 %, and two of the protons from the two terminal OH groups, which presented a relative area very similar to the theoretical area of 33.3 %. The signal from the four protons from the two CH₂ groups corresponds to a triplet as each proton is also affected by two other neighbouring protons.

However, it is not completely understood what the small peak at around 5.4 ppm represents. This peak could be related to the formation of a terminal protonated group (OH₂⁺). This hypothesis was supported by pH tests as when adding NaOH to ethylene glycol, therefore eliminating the existence of any terminal protonated group (OH₂⁺), the small 5.4 ppm peak disappeared. The addition of H₂SO₄ to ethylene glycol also caused the small 5.4 ppm peak to disappear. It seems that moving to extreme acidic conditions caused the H¹NMR signal from the terminal protonated group (OH₂⁺) to merge with the signal from the terminal OH groups. This could explain the produced Au nanoparticles colloid H¹NMR spectrum in Figure 53 (bottom) not presenting this small 5.4 ppm peak. The pH meter confirmed that the initial value of 3.8 for the Au solution in ethylene glycol, as shown in Table 23, had decreased (< 2) after the Au nanoparticles colloid had been produced with microwave heating.

3.3.4.2 Au Nanoparticles Colloid NMR Analysis

The new NMR peaks observed for the produced Au nanoparticles colloid with the microwave synthesis could be related to acetaldehyde and/or 2,3-butanedione, which are formed as shown in the general mechanism for metal ions reduction with ethylene glycol presented in Equation 8. In order to test these hypotheses both the ^1H NMR and ^{13}C NMR spectra for the Au nanoparticles colloid were compared to spectra obtained for the 40 wt. % acetaldehyde solution in water and for the 2,3-butanedione.

The ^1H NMR spectra compared in Figure 55 indicated for acetaldehyde and 2,3-butanedione peaks related to the CH_3 group at around 1.3 and 2.0 ppm, a similar position for two of the new peaks observed in the Au nanoparticles colloid. However, these two new peaks presented an area ratio of around 10:1, with the 1.3 ppm peak area much larger than the 2.0 ppm peak area, whereas in the acetaldehyde and 2,3-butanedione this ratio was of around 1:1. Moreover, the two other new peaks in the 4.0-3.8 ppm region, with a similar relative area to the new 1.3 ppm peak, were not observed in the acetaldehyde and 2,3-butanedione ^1H NMR analysis. The acetaldehyde also presented a peak related to the aldehyde proton (RCOH) at high chemical shifts (>6 ppm and not shown in the spectrum in Figure 55). This aldehyde peak was never observed for the Au nanoparticles colloid. Following a similar logic, the ^{13}C NMR analysis presented in Figure 56 also returned a negative match between the Au nanoparticles colloid new peaks and the acetaldehyde and 2,3-butanedione peaks.

It can be said that the acetaldehyde and the 2,3-butanedione were produced in such small amounts during microwave synthesis that they were not even detected by the NMR analysis and that the new NMR peaks were originated by an unknown compound(s) with further analysis presented in section 3.3.4.3.

Synthesis of Metal Nanoparticles by Microwave

3.3 Mechanistic Studies

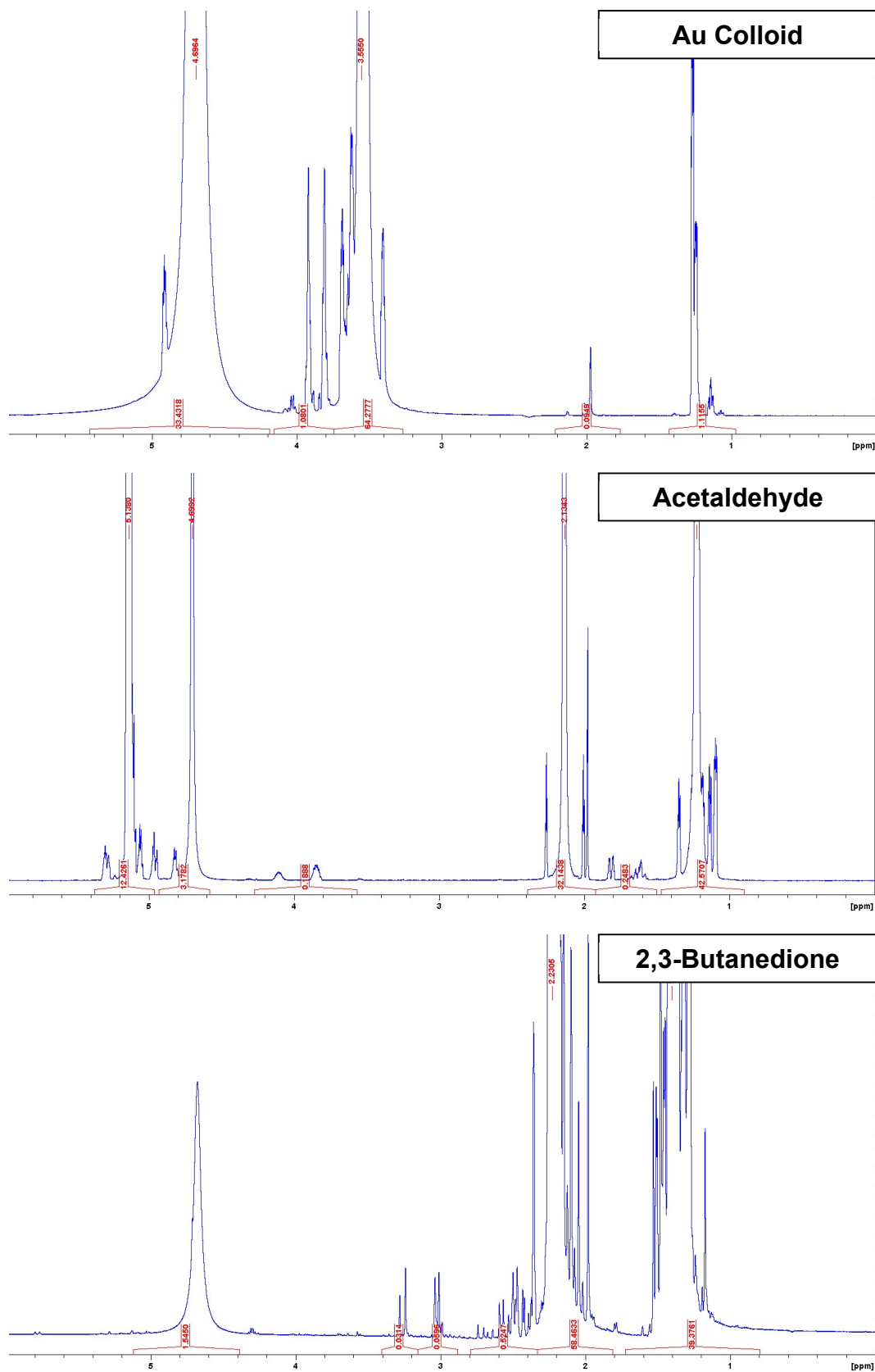


Figure 55 – ^1H NMR spectrum of the produced Au nanoparticles colloid with microwave synthesis (top), of the 40 wt. % acetaldehyde solution in water (middle) and of 2,3-butanedione (bottom).

Synthesis of Metal Nanoparticles by Microwave

3.3 Mechanistic Studies

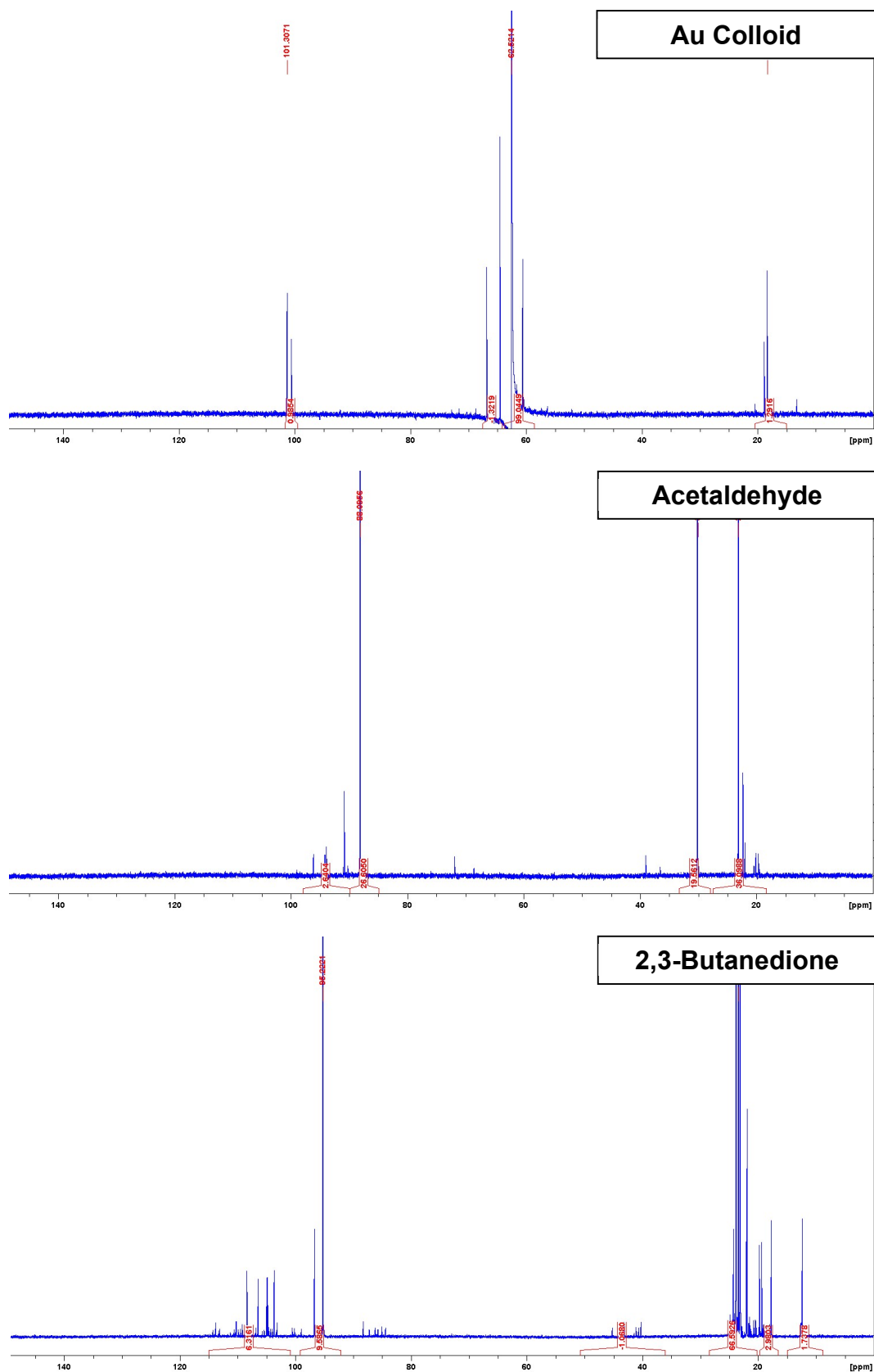


Figure 56 – ^{13}C NMR spectrum of the produced Au nanoparticles colloid with microwave synthesis (top), of the 40 wt. % acetaldehyde solution in water (middle) and of 2,3-butanedione (bottom).

3.3.4.3 Analysis of the Au Nanoparticles Colloid New NMR Peaks

The microwave synthesis was extended to the production of other metal nanoparticles, namely Pd, Ir, Ag and Cu, with detailed information presented in section 3.5. These other produced colloidal metal nanoparticles were also analysed by H^1 NMR and C^{13} NMR.

For the Pd nanoparticles colloid the NMR analysis also indicated these new peaks, but their relative areas were one order of magnitude smaller than what was observed for the Au nanoparticles colloid. For the other colloidal metal nanoparticles of Ir, Ag and Cu no new NMR peaks were detected and the NMR spectra were equal to the spectra of only ethylene glycol, shown in Figure 53 and Figure 54.

During the synthesis of the other metal nanoparticles the system relative pressure remained always at zero as indicated by the pressure sensor. It seems that the 1.2 bar relative pressure measured during the Au nanoparticles synthesis was only due to the formation of these unknown compound(s) detected by the NMR analysis and not due to the formation of acetaldehyde as initially thought.

It is possible that Au and Pd nanoparticles combined with the 150 °C microwave synthesis temperature homogeneously catalysed a reaction(s) that led to the formation of the unknown compound(s).

As shown in Figure 44 and Table 20 larger Au nanoparticles are expected to be produced when using ethylene glycol without any stabilizer as the plasmon peak wavelength increased from 537 to 546 nm. The NMR analysis of these larger Au nanoparticles colloid also indicated the new NMR peaks. However, it appears that the homogeneously catalysed reaction(s) takes place only during the initial stage of the nucleation step, when the Au nanoparticles are still small. The reason being that the NMR analysis of the 8 eq. NaOH trial of the acid/base addition optimisation test shown in section 3.2 in Figure 41 indicated no new NMR peaks before and after the microwave synthesis. As shown in section 3.3.2 in Figure 51 the addition of 8 eq. of NaOH to the Au solution in ethylene glycol caused the reduction of the Au precursor and the production of large and non-circular Au nanoparticles before any microwave heating.

Further NMR analysis was performed in order to identify these unknown compound(s) assuming that they could be originated from ethylene glycol, acetaldehyde and 2,3-butanedione. The tested compounds were acetic acid, glycolic acid, glyoxal, glyoxylic acid and oxalic acid. Again, no positive match was returned between the tested compounds NMR peaks and the new NMR peaks observed with the Au and Pd nanoparticles colloid.

Synthesis of Metal Nanoparticles by Microwave

3.3 Mechanistic Studies

A final attempt to identify the unknown compound(s) included removing from the colloid the Au nanoparticles and analysing with CG-MS the remaining liquid. The Au nanoparticles needed to be removed before any GC-MS analysis as they could damage the capillary column.

The Au nanoparticles produced when using only ethylene glycol without any stabilizer were selected as for this trial the removal from the colloid of the Au nanoparticles was the easiest. This colloid was first stored for several weeks, after which Au nanoparticles started to agglomerate and deposit at the bottom of the storage recipient (see section 3.4). Therefore, simple techniques such as filtration and centrifugation could be used. The remaining liquid was first checked with H^1 NMR and C^{13} NMR analysis in order to confirm that the unknown compound(s) were still present, which was the case.

However, it was not possible to identify with CG-MS the unknown compound(s) as only ethylene glycol could be observed. The GC-MS analysis was compromised due to the small amount of the unknown compound(s) combined with ethylene glycol overlapping the peaks as the used capillary column was probably not the most suitable for a correct separation.

3.3.4.4 PVA and PVP NMR Analysis

NMR has also been an important tool to study how the used stabilizers, both PVA and PVP, were affected by the microwave synthesis, with only H^1 NMR being considered.

However, in first place it was necessary to understand why no PVA peaks were observed during the H^1 NMR analysis of the Au solution shown in Figure 53 (middle). The lack of stabilizer NMR peaks was also observed when working with PVP, with the NMR analysis of the Au solution being equal to the NMR analysis of just ethylene glycol. When changing the solvent from ethylene glycol to water and also when working with the microwave synthesis of different metal nanoparticles using the two aforementioned solvents, both PVA and PVP remained undetected by NMR analysis.

After discarding the effect of the stabilizer, the synthesis solvent and the type of produced metal nanoparticles the work focused on the amount of stabilizer. The different trials at higher stabilizer/metal weight ratios considered during the stabilizer optimisation test shown in section 3.2.7 also returned the same NMR peaks as just ethylene glycol. Eventually it was possible to link the inexistence of the expected NMR peaks to the amount of stabilizer, but only when greatly increasing the stabilizer amount as shown in Figure 57. Two samples of only PVA in water (top) and of only PVA in ethylene glycol (middle) were prepared by first adding 0.3 g of PVA to 20 mL of water or ethylene glycol. This PVA concentration was around 1000x higher than the PVA concentration used for the production of Au nanoparticles by microwave synthesis at standard conditions as shown in Table 13.

Synthesis of Metal Nanoparticles by Microwave

3.3 Mechanistic Studies

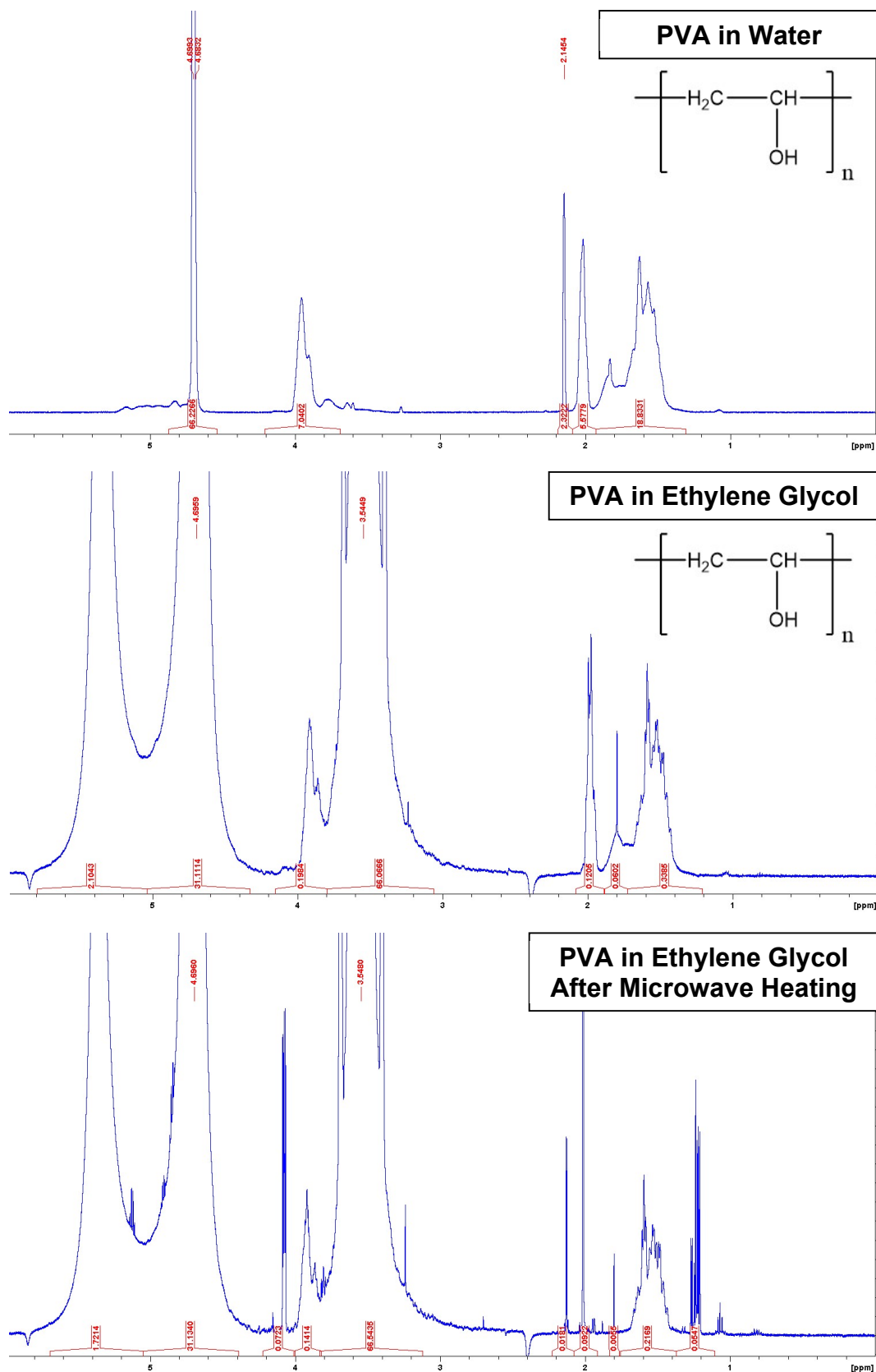


Figure 57 – ^1H NMR spectrum of PVA in water (top), of PVA in ethylene glycol (middle) and of PVA in ethylene glycol after microwave heating at the standard conditions.

Synthesis of Metal Nanoparticles by Microwave

3.3 Mechanistic Studies

It is possible to observe only the NMR peaks related to the PVA at a chemical shift of around 2 ppm for the protons of the CH₂ group and at a chemical shift of around 4 ppm for the protons of the secondary alcohol group (HOCH), with the chemical shift of these peaks being the same in both water and ethylene glycol. However, the NMR peak for the proton of the OH group of the PVA is overlapped by the solvents NMR peaks as they also present a OH group.

When applying microwave heating at the standard conditions to the previous two samples, *i.e.* 5 min at 150 °C with the stirrer at the high setting, different results were observed. In the case of PVA in water no changes were observed after the microwave heating and the H¹NMR was exactly the same as the one shown in Figure 57 (top). In the case of PVA in ethylene glycol new NMR peaks were observed as shown in Figure 57 (bottom).

These new NMR peaks can be linked to the degradation of PVA in ethylene glycol due to the high temperature of 150 °C attained during the microwave synthesis and to the formation of new compounds. Gilman *et al.*¹⁰⁴ has shown that PVA pyrolysis will start to occur as the temperature reaches 200-250 °C. Above this decomposition temperature PVA begins a rapid chain-stripping elimination of water and several other compounds can be formed according to the mechanisms presented in Figure 58.

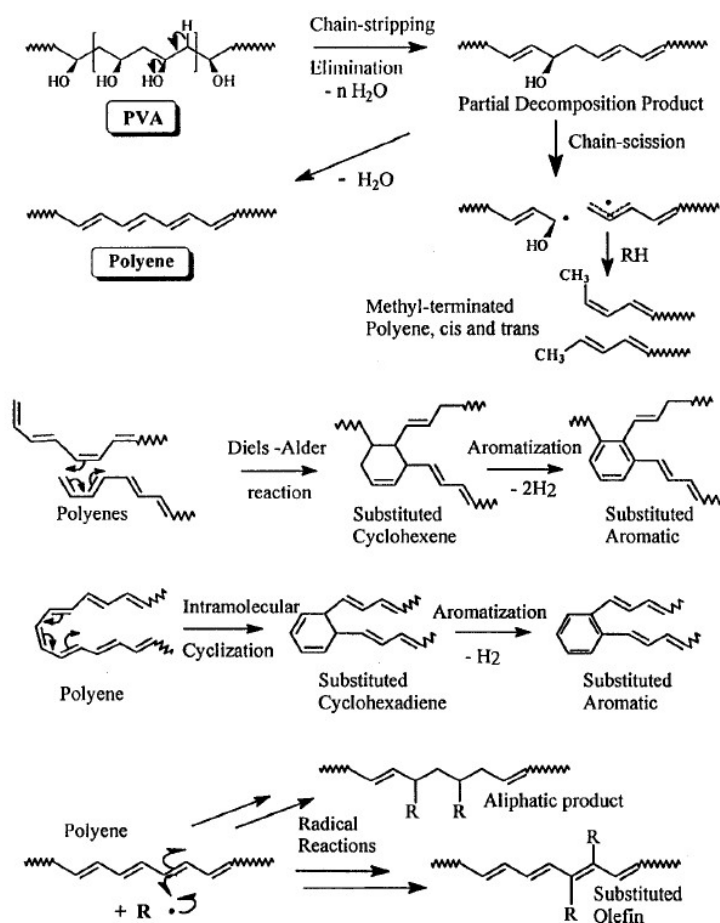


Figure 58 – Formation of new compounds due to PVA degradation with temperature.¹⁰⁴

Synthesis of Metal Nanoparticles by Microwave

3.3 Mechanistic Studies

The new formed compounds are able to cause colour changes and foam-like residues.¹⁰⁴ This is consistent with what was observed inside the 35 mL vessel after the microwave synthesis. Moreover, other authors^{91,105} have also shown that high temperatures can cause PVA degradation. It can be said that even though 200-250 °C were never reached during microwave synthesis, this control experiment of PVA in ethylene glycol without a metal has shown that a temperature of 150 °C was already enough to cause the PVA degradation.

The same type of H¹NMR analysis was also extended to the PVP stabilizer as shown in Figure 59. Again, only after greatly increasing the amount of PVP (1000x vs. standard scenario) the NMR related peaks could be observed.

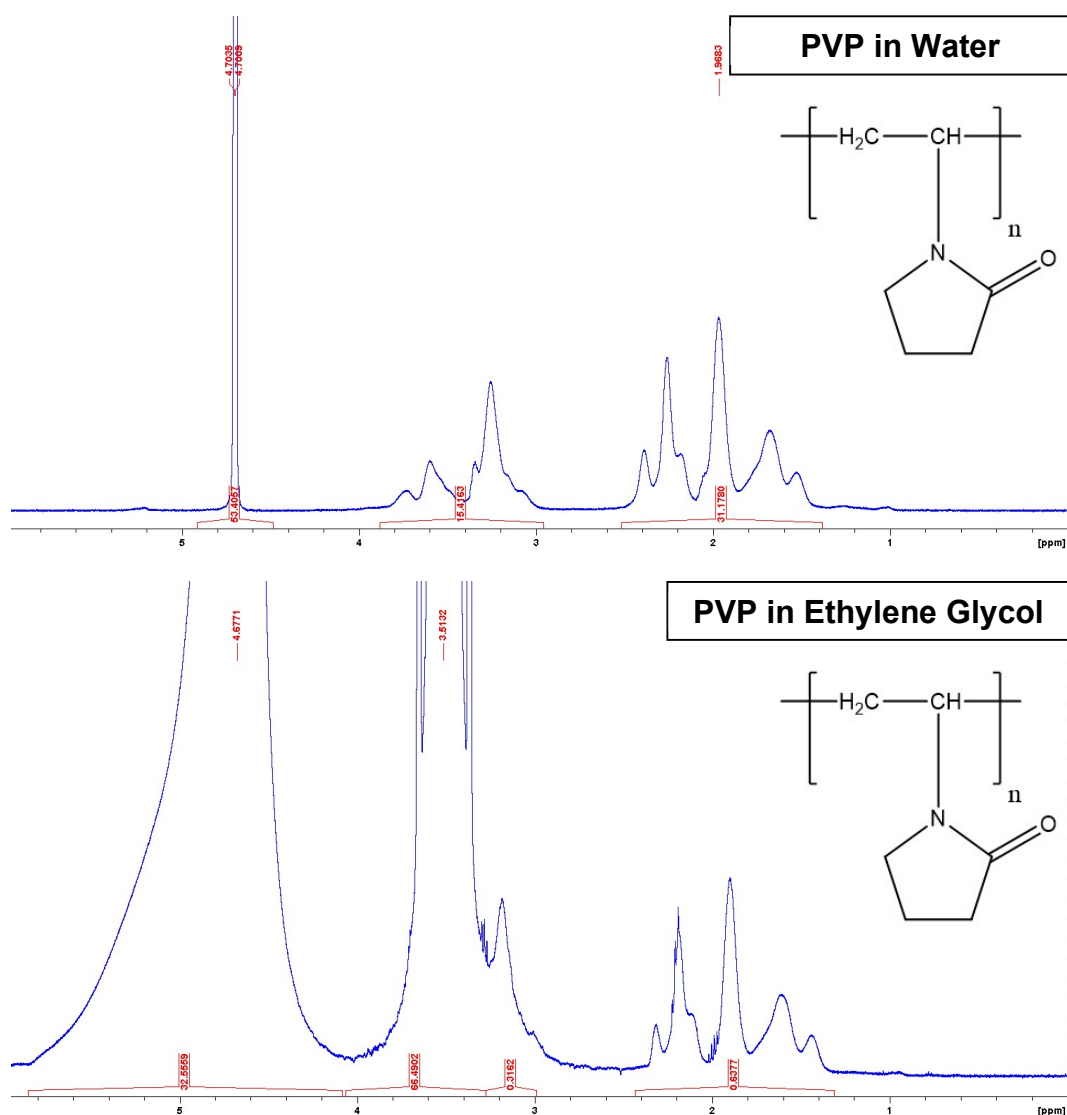


Figure 59 – H¹NMR spectrum of PVP in water (top) and of PVP in ethylene glycol (bottom).

Synthesis of Metal Nanoparticles by Microwave

3.3 Mechanistic Studies

Similar to the PVA, it is also possible to observe the NMR peaks only related to the PVP at a chemical shift in the range of 1.5-2.5 ppm for the protons of the CH₂ group from the chain and for the protons of two CH₂ groups from the ring and in the range of 3.0-4.0 ppm for the proton of the CH group from the chain bonded to the nitrogen and for the protons of the CH₂ group from the ring also bonded to the nitrogen. In total the first NMR peak represents 6 protons and the second NMR peak represents 3 protons. This is consistent with the ratio of the relative areas as the relative area of the first NMR peak (1.5-2.5 ppm) is also the double as the relative area of the second NMR peak (3.0-4.0 ppm). The lone pair of electrons in the nitrogen atom together with the oxygen allowed the formation of a resonance hybrid, thus creating a positive charge on the nitrogen atom and less electronic shielding in the surrounding protons which caused their chemical shift to increase to the 3.0-4.0 ppm range. The splitting of the NMR peaks is according to the expected. However, it is difficult to analyse them as there is strong interference from different protons, for example in the range 3.0-4.0 ppm there are protons with two other neighbouring protons (triplet) and also protons with four other neighbouring protons (quintet). Also similar to the PVA, it was observed that the PVP NMR peaks occur at the same chemical shift in both water and ethylene glycol. Contrary to the PVA, with the PVP there is no OH group present but it is still possible to observe interference from the ethylene glycol for the NMR peak in the 3.0-4.0 ppm range.

The major difference detected by the H¹NMR analysis between PVA and PVP concerns the degradation of the stabilizer in ethylene glycol after applying microwave heating. In the case of PVA it was observed the formation of new NMR peaks, consistent with a degradation pathway, whereas in the case of PVP no changes were observed.

These different results could be explained by having in consideration that PVA is not much soluble in ethylene glycol, even when applying moderate heating, contrary to the PVP, which is easily soluble even at room temperature. This was observed during the preparation of the stabilizers solutions. Therefore, it is possible that during microwave synthesis the PVA in ethylene glycol is not perfectly mixed and hotspots are formed with temperatures higher than 150 °C. This solubility effect would explain why PVA is degraded in ethylene glycol, not degraded in water and also why PVP is not degraded in both water and ethylene glycol.

This solubility effect could also explain why a bimodal distribution was observed when working with water and ethylene glycol mixtures as shown for the different trials in section 3.2. For the same reason aforementioned, it is possible that PVA is not perfectly mixed and the PVA reduction mechanism is enhanced in temporary water rich regions of the mixture.

3.3.5 Influence of Au Precursor Oxidation State

The last mechanistic study focused on changing the Au precursor oxidation state. Au(I) was tested by working with the AuCl precursor and the experimental result compared to the standard microwave condition of Au(III) with HAuCl₄ as the precursor.

As shown in Figure 60, the Au nanoparticles production became worse when changing the precursor oxidation state from Au(III) to Au(I). This could be due to the reduction potential shown in Table 12, Au(I) with 0.7996 V less likely to be reduced than Au(III) with 1.692 V.

The AuCl precursor solubility also influenced the experimental results. Both in water and in ethylene glycol some degree of AuCl precursor precipitation was observed at the bottom of the glass vial. Even when applying moderate heating to the AuCl precursor solutions or changing the pH by adding an acid no major solubility changes were observed. This solubility issue can also be observed in Figure 60, with the Au(I) solution peak much smaller than the Au(III) solution peak. Even though direct comparisons should not be made, as the UV-Vis spectrum depends on the metal oxidation state, the big absorbance gap between the two Au solutions spectra give an indication that the Au(I) concentration in solution is lower than the expected due to solubility issues.

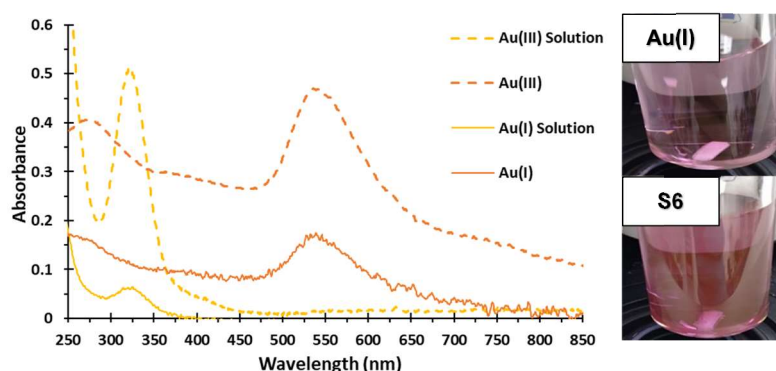


Figure 60 – Au nanoparticles produced at different Au precursor oxidation states with UV-Vis analysis (left) and photos for Au(III) (S6) and Au(I) (right).

Synthesis of Metal Nanoparticles by Microwave

3.4 Selected Operating Conditions, Stability and Reproducibility

3.4 Selected Operating Conditions, Stability and Reproducibility

This section aims to identify the best microwave synthesis operating conditions for the production of metal nanoparticles in light of the targets defined for this PhD, *i.e.* reduced synthesis time, improved production, minimal operation cost, minimal use of toxic reagents and controlled size and shape. The best microwave synthesis operating conditions were defined by taking into consideration the Au optimisation experimental results from section 3.2 and the mechanistic studies from section 3.3, which were not limited only to Au nanoparticles. The main conclusions drawn from those two sections can be summarised as follows:

- a) Best experimental results obtained with ethylene glycol;
- b) Mixing water and ethylene glycol compromised the experimental results, in particular when using PVA due to solubility problems in ethylene glycol which even caused bimodal distribution;
- c) PVP preferred in ethylene glycol as presents no major solubility issues and therefore no degradation during microwave synthesis and experimental results more reproducible;
- d) Better experimental results when increasing the stabilizer/metal weight ratio, but too much stabilizer can hinder the catalytic activity as it blocks the substrate access to the metal nanoparticles, which are the active sites;
- e) Even though working at higher metal concentrations would improve the production It would also negatively impact the metal nanoparticles average size and size distribution;
- f) Controlled addition of NaOH has the potential to decrease the metal nanoparticles average sizes but the method reproducibility is negatively impacted as it is more difficult to exactly reproduce the initial Au solution conditions before any microwave heating takes place;

As shown in Table 24 three operating conditions have been selected and can be compared to the standard microwave operating conditions shown in Table 13:

- a) The operating condition A uses no stabilizer;
- b) The operating condition B uses PVP instead of PVA and the stabilizer/metal weight ratio increases from 0.65 to 3.25;
- c) The operating condition C uses only water and the PVA/metal weight ratio increases from 0.65 to 3.25;

Synthesis of Metal Nanoparticles by Microwave

3.4 Selected Operating Conditions, Stability and Reproducibility

Table 24 – Selected operating conditions for the metal nanoparticles microwave synthesis.

Parameter	Operating Condition A	Operating Condition B	Operating Condition C
Power	300 W	300 W	300 W
Solvent	Ethylene Glycol	Ethylene Glycol	Water
Temperature	150 °C	150 °C	150 °C
Holding time	5 min	5 min	5 min
Stirrer	High	High	High
Volume of solution	20 mL	20 mL	20 mL
Stabilizer/Metal Weight Ratio	0	3.25xPVP	3.25xPVA
Metal Concentration	0.025 g L ⁻¹ or 0.13 mM	0.025 g L ⁻¹ or 0.13 mM	0.025 g L ⁻¹ or 0.13 mM

When using the operating condition B the metal nanoparticles production is expected to be the highest, the metal nanoparticles average size is expected to be the smallest and the metal nanoparticles size distribution is expected to be the narrowest. The experimental reproducibility is also expected to be the highest. When using the operating condition A worse experimental results are expected but no stabilizer is used. When using operating condition C even worse experimental results are expected but a less toxic solvent is used.

The Au nanoparticles colloids produced at these three selected operating conditions were also checked for their stability over time using UV-Vis spectroscopy. They were first checked immediately after having been produced (Day 1) and then stored in glass vials with repeated UV-Vis measurements performed regularly, namely at Days 4, 7, 14, 28 and 56. Photos of the produced colloids stored inside the glass vials were taken as well.

As shown in Figure 61, the Au nanoparticles produced using operating condition A, without any stabilizer, started to agglomerate and deposit at the bottom of the glass vial as soon as 4 days had passed. At day 14 almost all of the Au nanoparticles had been deposited at the bottom of the glass vial and the Au colloid colour had drastically changed from the initial violet shade to almost transparent, the same colour as just ethylene glycol. This result is according to what was expected as only with the presence of the stabilizers, PVA and PVP, interaction of Au nanoparticles with one another can be prevented due to the steric effect. At day 56 the UV-Vis measurement was very close to the baseline, thus indicating that only ethylene glycol was being measured. This sample, produced with operating condition A and stored in a glass vial for 56 days, was the one used for the mechanistic study presented in section 3.3.4.3 that focused in identifying with GC-MS the unknown compound(s) produced after microwave synthesis. The Au nanoparticles colloids produced with operating conditions B and C were stable over time with no major changes to the UV-Vis spectrum and photos observed.

Synthesis of Metal Nanoparticles by Microwave

3.4 Selected Operating Conditions, Stability and Reproducibility

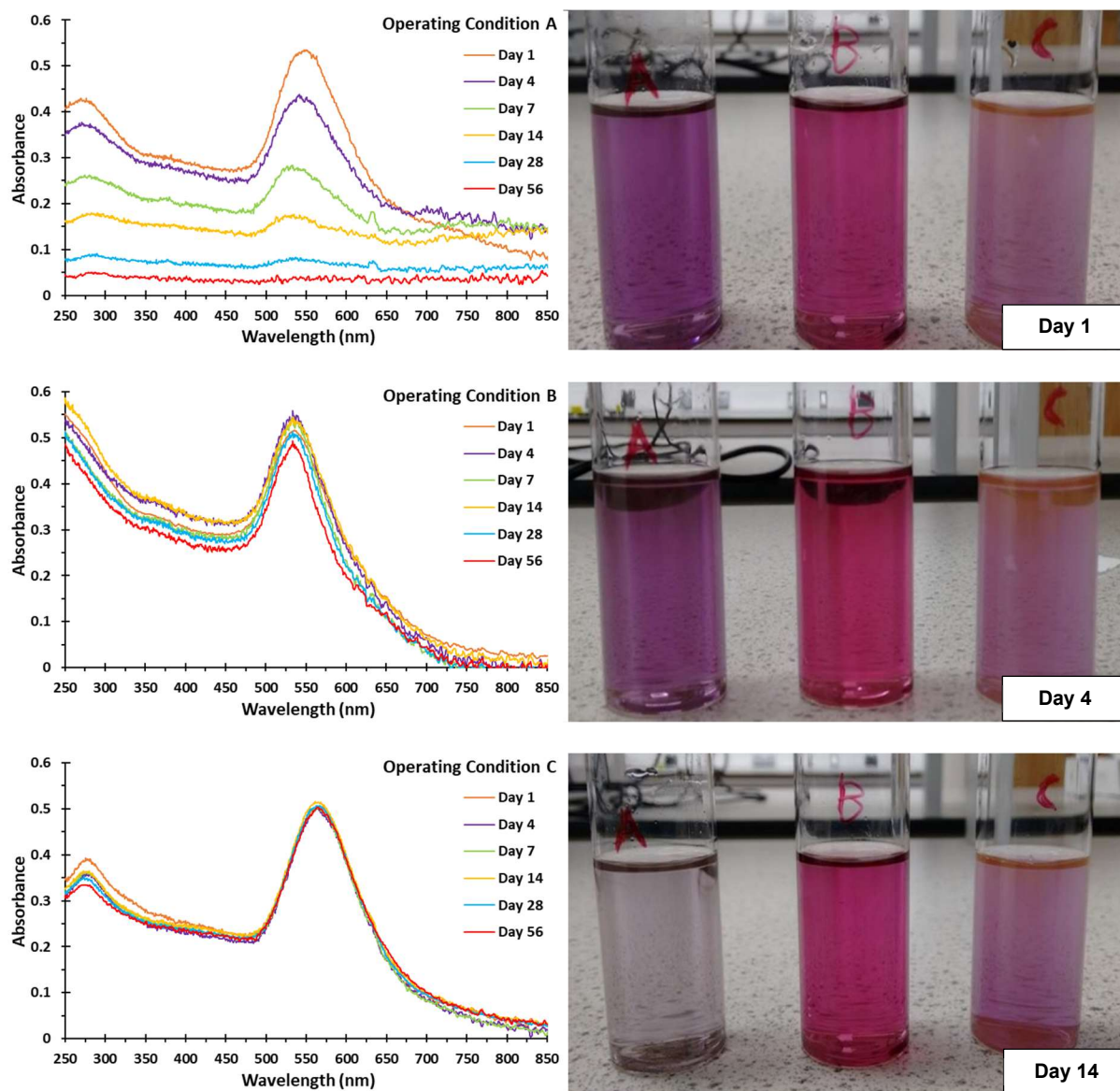


Figure 61 – UV-Vis analysis (left) of Au nanoparticles produced by microwave synthesis with the operating conditions A (top), B (middle) and C (bottom) and photos (right) of the three produced Au nanoparticles colloids at day 1 (top), day 4 (middle) and day 14 (bottom) with operating conditions written on each flask.

However, some minor changes were observed to the UV-Vis spectra over time when using PVP with operating condition B. This observation is somehow surprising as in fact the literature mentions that PVP offers an even higher protective degree than PVA.²⁸ In any case it should be mentioned that no clear trend over time was detected as it would be the case if the Au nanoparticles were agglomerating as it happened with the operating condition A. Therefore, it can be concluded that these UV-Vis spectra changes over time were related to a minor water solubility interference which is able to produce for the same sample similar but different UV-Vis spectra if the cuvette is not properly agitated or if the UV-Vis measurement is performed too long after the cuvette was agitated.

Synthesis of Metal Nanoparticles by Microwave

3.4 Selected Operating Conditions, Stability and Reproducibility

These stability tests were extremely important as they allow to understand how fast after synthesis the produced metal colloids should be supported without undergoing changes. As explained in section 2.5 the support addition stage for microwave and ultrasound synthesis only takes place after the production of several batches have rendered a reasonable volume. Therefore, for the first produced batch several hours can pass between the synthesis and the moment the metal nanoparticles are supported. Moreover, these stability tests also allow to understand the viability of storing and shipping colloidal metal nanoparticles to external research groups.

The operating conditions reproducibility was also checked by producing several trials and calculating for the six most reproducible trials the standard deviations for the plasmon peak absorbance, plasmon peak wavelength and plasmon peak range. The several UV-Vis spectra can be observed in Figure 62 with the experimental results compared in Table 25. This is a similar procedure to what was performed with the standard microwave operating conditions considered during the Au optimisation tests in section 3.2 and shown in Figure 37.

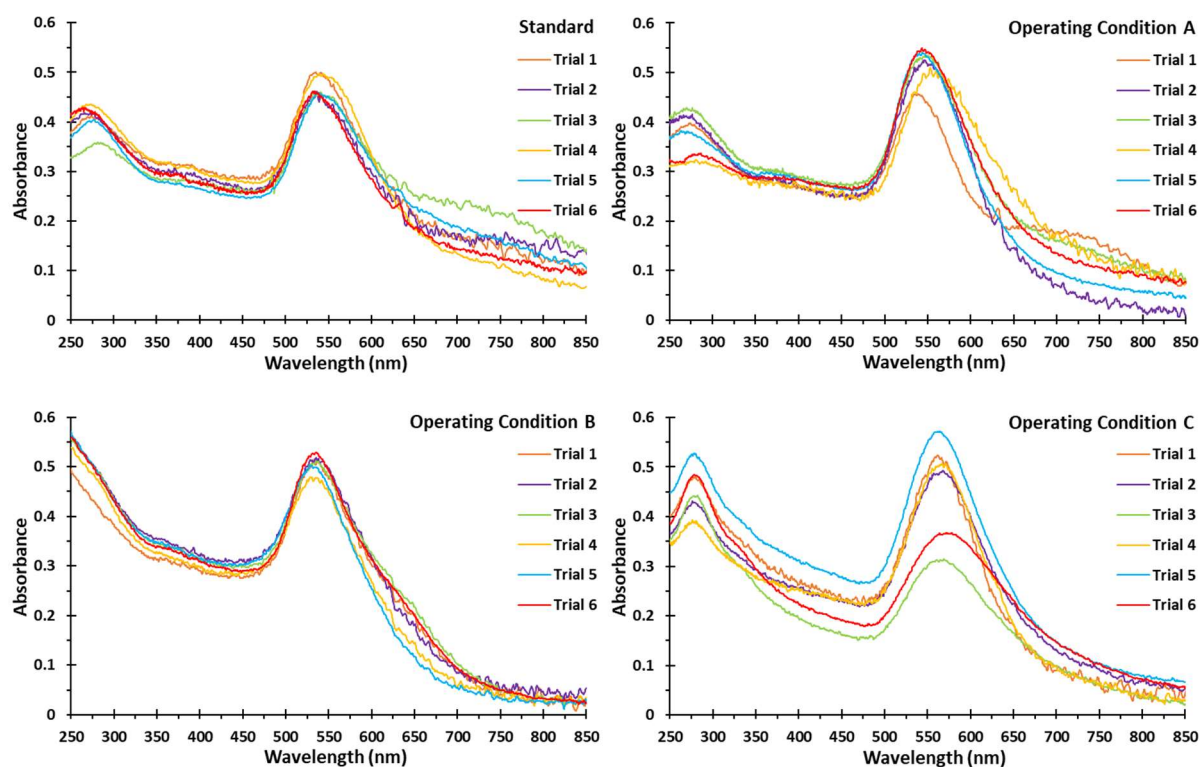


Figure 62 – UV-Vis spectra of Au nanoparticles produced by microwave synthesis at standard operating conditions (top left), with operating condition A (top right), with operating condition B (bottom left) and with operating condition C (bottom right) and with six trials for each operating condition.

Synthesis of Metal Nanoparticles by Microwave

3.4 Selected Operating Conditions, Stability and Reproducibility

Table 25 – Plasmon peak experimental results and standard deviations of Au nanoparticles produced by microwave synthesis at different operating conditions with six trials for each operating condition.

Operating Condition	Plasmon Peak Absorbance	Plasmon Peak Wavelength (nm)	Wavelength Range (nm)
Standard	0.47 ± 0.02	537 ± 3	82 ± 7
A	0.52 ± 0.03	546 ± 5	77 ± 7
B	0.51 ± 0.01	535 ± 4	76 ± 5
C	0.46 ± 0.10	567 ± 4	82 ± 13

As expected, the lowest standard deviations were obtained with operating condition B. This confirms operating condition B to be the most reproducible protocol. When working with operating condition A reproducibility is compromised by the absence of any stabilizer. The worst reproducibility is achieved with operating condition C as all reducing action is only due to the PVA stabilizer, a weak reducing agent, therefore causing slow reduction of Au³⁺ ions and the nucleation step to take place simultaneously with the growth step, which according to the LaMer concept, mentioned in section 1.4.1, can compromise the experimental results.

In conclusion, it is not possible to select only one operating condition as each of them might favour more one of the targets defined for this PhD than the others. The desired application for the metal nanoparticles might also favour more one operating condition than the other. For example, even though with the operating conditions A and C the expected metal nanoparticles average sizes are large with a broad distribution and therefore not likely to have a significant catalytic activity, it could also be interesting to produce metal nanoparticles with such features for applications other than catalysis, for example medicinal applications where large metal nanoparticles are required and/or no traces of ethylene glycol are allowed.

Therefore, it can be said that the main objective of this section was to narrow down to a reasonable number of selected operating conditions all the possible microwave parameters combinations. The three presented operating conditions were then extended to the synthesis of all the metal nanoparticles considered for this PhD, namely Au, Pd, Ag, Ir, Cu and bimetallic AuPd at different ratios. These metal nanoparticles are presented and analysed in more detail in sections 3.5 and 3.6, in particular with TEM, a more reliable technique to perform size measurements and that also allows to understand the metal nanoparticles shape.

3.5 Metal Nanoparticles Production under Batch Regime

The microwave synthesis of colloidal metal nanoparticles using the three selected operating conditions from section 3.4 is presented and analysed in detail in this section and compared to some of the microwave work found in the literature. The considered metal nanoparticles were monometallic Au, Pd, Ag, Ir, Cu and bimetallic alloys of AuPd at different molar ratios, 7:1, 3:1, 1:1, 1:3 and 1:7.

Similar to section 3.2 each sample was characterised with UV-Vis and DLS analysis and photos of the metal colloids were taken. The characterisation was further completed using TEM analysis with three selected images and the metal nanoparticles size distribution histogram being presented for each sample. The TEM histogram also provides information about the total nanoparticles count and the cumulative frequency.

Contrary to Au nanoparticles no plasmon peak in the UV-Vis region is observed for Pd, Ir and AuPd nanoparticles. Therefore, for those metal nanoparticles it is not possible to directly correlate the UV-Vis spectra with their average sizes. However, UV-Vis is still a useful technique as it is possible to observe trends as operating conditions change, quickly check for the method reproducibility and observe the metal nanoparticles stability over time.

An overview of average sizes calculated by DLS and TEM analysis for the metal nanoparticles produced at these three selected operating conditions is shown in Table 26. The calculated DLS average sizes are related to the first peak, which is the most relevant as DLS is an intensity-weighted particle size measurement as explained in more detail in section 2.2.2.

Overall it can be said that both DLS and TEM analysis are in agreement. When metal nanoparticles are calculated to be small by TEM the DLS also indicates a small size, for example Pd nanoparticles produced with the operating condition B. When metal nanoparticles are calculated to be small by TEM but also present to some degree large metal nanoparticles, which can be inferred by having the standard deviation similar to the average size, the DLS also indicates larger sizes, for example Au nanoparticles produced with the operating condition C. When metal nanoparticles are observed to be agglomerated with the TEM the DLS also indicates even larger sizes, for example Pd nanoparticles produced with the operating condition A. The TEM analysis could not be extended to all metal nanoparticles. The reasons being:

a) Some of the produced metal nanoparticles with the operating conditions A and C were just agglomerated;

b) It was not possible to reduce copper and produce nanoparticles using any of the three selected operating conditions;

Synthesis of Metal Nanoparticles by Microwave

3.5 Metal Nanoparticles Production under Batch Regime

c) Even though Ir nanoparticles were successfully produced they were rather small, below 1-2 nm, which was close to the equipment detection limit and ended up compromising the production of a meaningful nanoparticles size distribution histogram;

Table 26 – TEM and DLS average sizes of metal nanoparticles produced by microwave synthesis with the three selected operating conditions (Table 24).

Metal	Operating Condition	TEM Average Size (nm)	DLS Average Size (nm)
Au	A	50 ± 14	8.8 ± 3.5
Au	B	12 ± 3.9	5.4 ± 2.0
Au	C	18 ± 27	117 ± 56
Pd	A	Agglomeration	644 ± 180
Pd	B	3.3 ± 0.8	7.7 ± 1.2
Pd	C	Agglomeration	239 ± 60
Ag	A	Agglomeration	180 ± 64
Ag	B	13 ± 14	38 ± 9
Ag	C	Agglomeration	115 ± 8
Ir	A	Less than 1-2 nm	3.9 ± 0.9
Ir	B	Less than 1-2 nm	13 ± 9
Ir	C	Agglomeration	214 ± 85
Cu	A	No Reduction Observed	
Cu	B	No Reduction Observed	
Cu	C	No Reduction Observed	
AuPd 1:1	A	Agglomeration	181 ± 48
AuPd 1:1	B	3.0 ± 0.6	7.1 ± 1.0
AuPd 1:1	C	Agglomeration	643 ± 483
AuPd 7:1	B	9.0 ± 1.8	26 ± 8
AuPd 3:1	B	4.7 ± 1.1	18 ± 7
AuPd 1:3	B	3.2 ± 0.7	8.5 ± 1.9
AuPd 1:7	B	3.3 ± 0.8	8.7 ± 1.9

A separated and more detailed discussion for each type of metal nanoparticles can be found in the following subsections. Further to the points aforementioned it is also discussed:

a) The work with Au nanoparticles produced by replicating operating conditions found in the literature in an attempt to decrease as much as possible the Au nanoparticles average size as the minimum size obtained with the operating condition B was of only 12 ± 3.9 nm;

b) The work with NaOH in order to replicate the same nanoparticles enhanced production effect observed when working with Au nanoparticles as presented in section 3.3.2;

c) Use of high-resolution transmission electron microscopy analysis (STEM/HAADF mode), a technique with a lower detection limit than regular TEM, in order to demonstrate that produced bimetallic AuPd nanoparticles with a molar ratio of 1:1 were in fact an alloy;

Synthesis of Metal Nanoparticles by Microwave

3.5 Metal Nanoparticles Production under Batch Regime

3.5.1 Au Nanoparticles

In Figure 63 the average UV-Vis and DLS spectra and photos of the Au nanoparticles produced with the three selected operating conditions are compared.

Plasmon peak absorbances and wavelength ranges of the different Au nanoparticles are very similar indicating that Au nanoparticles production and size distribution should also be very similar. However, the plasmon peak wavelengths are significantly different indicating that Au nanoparticles average sizes should also be significantly different. The Au nanoparticles produced with the operating condition B are expected to be the smallest, plasmon peak wavelength of 535 nm, followed by the ones produced with the operating condition A, plasmon peak of 546 nm, and the ones produced with the operating condition C are expected to be the largest, plasmon peak of 567 nm. The DLS analysis also supports this trend with the calculated DLS average sizes for each operating condition reported in Table 26.

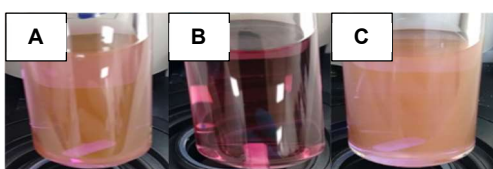
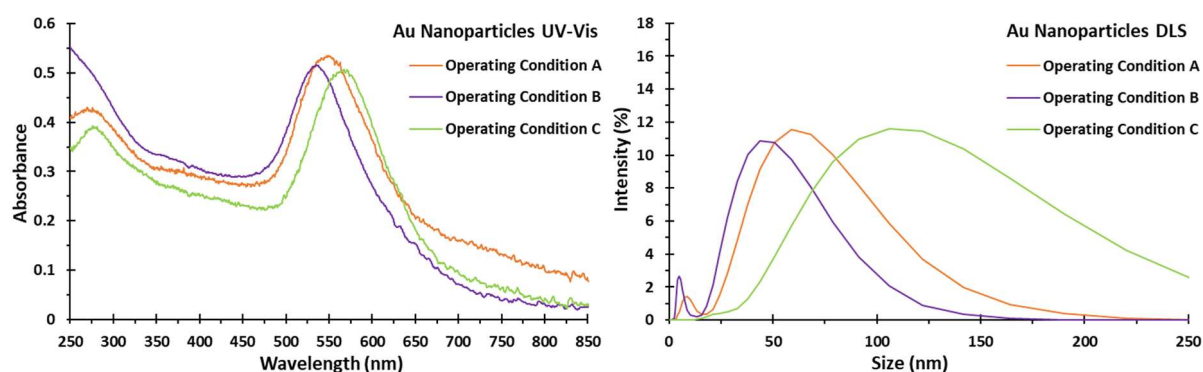


Figure 63 – Au nanoparticles produced by microwave synthesis with the three selected operating conditions (Table 24) with UV-Vis (top left) and DLS (top right) analysis and photos (bottom left).

The first sample analysed by TEM is shown in Figure 64 and concerns the Au nanoparticles produced with the operating condition A. Overall, the produced Au nanoparticles were circular but it was also observed some degree of aggregation (image 1) and agglomeration (image 2). These two effects are consistent with having in the UV-Vis spectrum higher absorbances at higher wavelengths (above 650 nm) than for the other two samples.

Synthesis of Metal Nanoparticles by Microwave

3.5 Metal Nanoparticles Production under Batch Regime

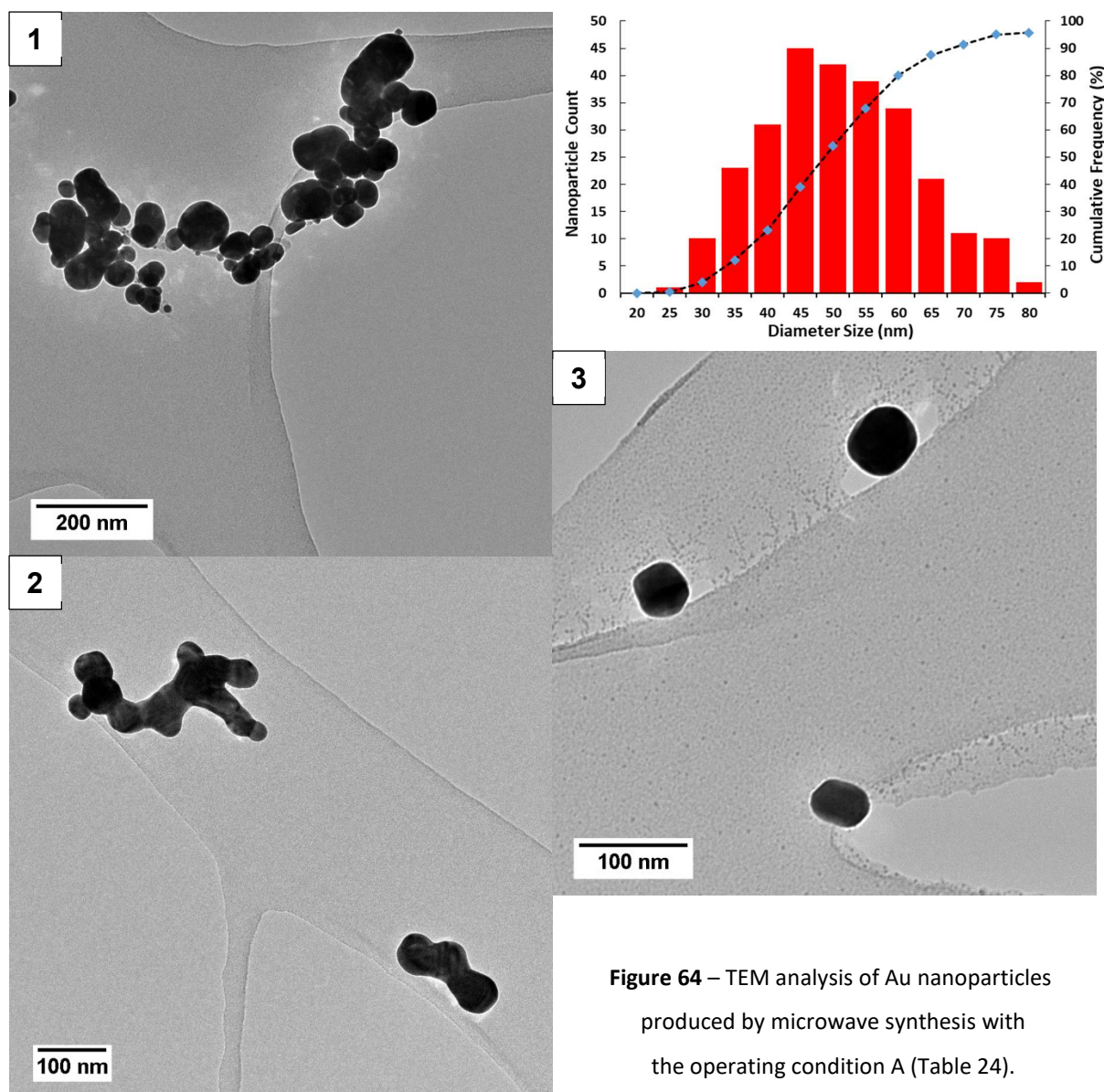


Figure 64 – TEM analysis of Au nanoparticles produced by microwave synthesis with the operating condition A (Table 24).

The TEM analysis of Au nanoparticles produced with the operating condition B is shown in Figure 65. As expected from the UV-Vis and DLS analysis, there was a major decrease of the Au nanoparticles size, from 50 ± 14 nm with the operating condition A to 12 ± 3.9 nm with the operating condition B. Circular nanoparticles continued to be clearly dominant and no relevant degree of aggregation or agglomeration was observed.

Synthesis of Metal Nanoparticles by Microwave

3.5 Metal Nanoparticles Production under Batch Regime

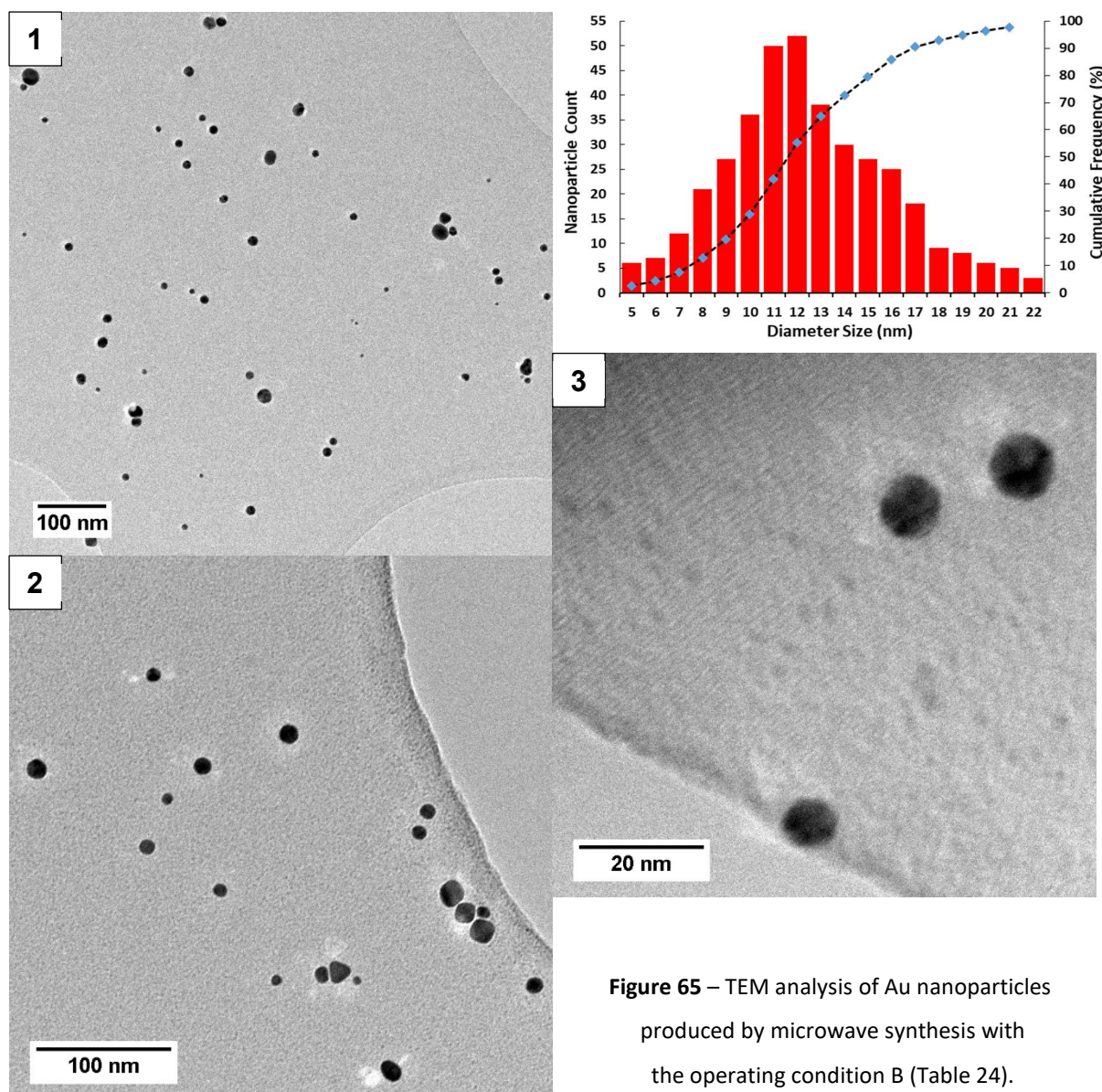


Figure 65 – TEM analysis of Au nanoparticles produced by microwave synthesis with the operating condition B (Table 24).

Contrary to what was expected from the UV-Vis and DLS analysis, the TEM average size for the Au nanoparticles produced with the operating condition C was of only 18 ± 27 nm, a value higher than what was obtained with the operating condition B but lower than what was obtained with the operating condition A.

However, the standard deviation of 27 nm is of the same order of magnitude and even higher than the calculated average size of 18 nm. This can be explained by having in consideration the TEM analysis shown in Figure 66. In all the three images it is possible to observe large Au nanoparticles, around 100 nm in size, which are surrounded by much smaller and numerous Au nanoparticles. The Au nanoparticles size distribution histogram also indicates this effect with the cumulative frequency only reaching approximately 80% at 16 nm, above the 16 nm threshold there are still 20% of larger nanoparticles to be considered.

Synthesis of Metal Nanoparticles by Microwave

3.5 Metal Nanoparticles Production under Batch Regime

It is possible that the UV-Vis plasmon peak was affected by proximity between small and large nanoparticles. Therefore, the high plasmon peak wavelength of 567 nm and the average plasmon peak range of 74 nm do not reflect properly the existence of small Au nanoparticles, only of large Au nanoparticles. The same can be said about the DLS analysis.

This sample is a good example of why UV-Vis and DLS are useful techniques but can only provide an indication and in order to obtain accurate size measurements other techniques such as TEM need to be employed. It should also be mentioned that many of the produced Au nanoparticles presented a triangular shape. This is especially visible on image 1.

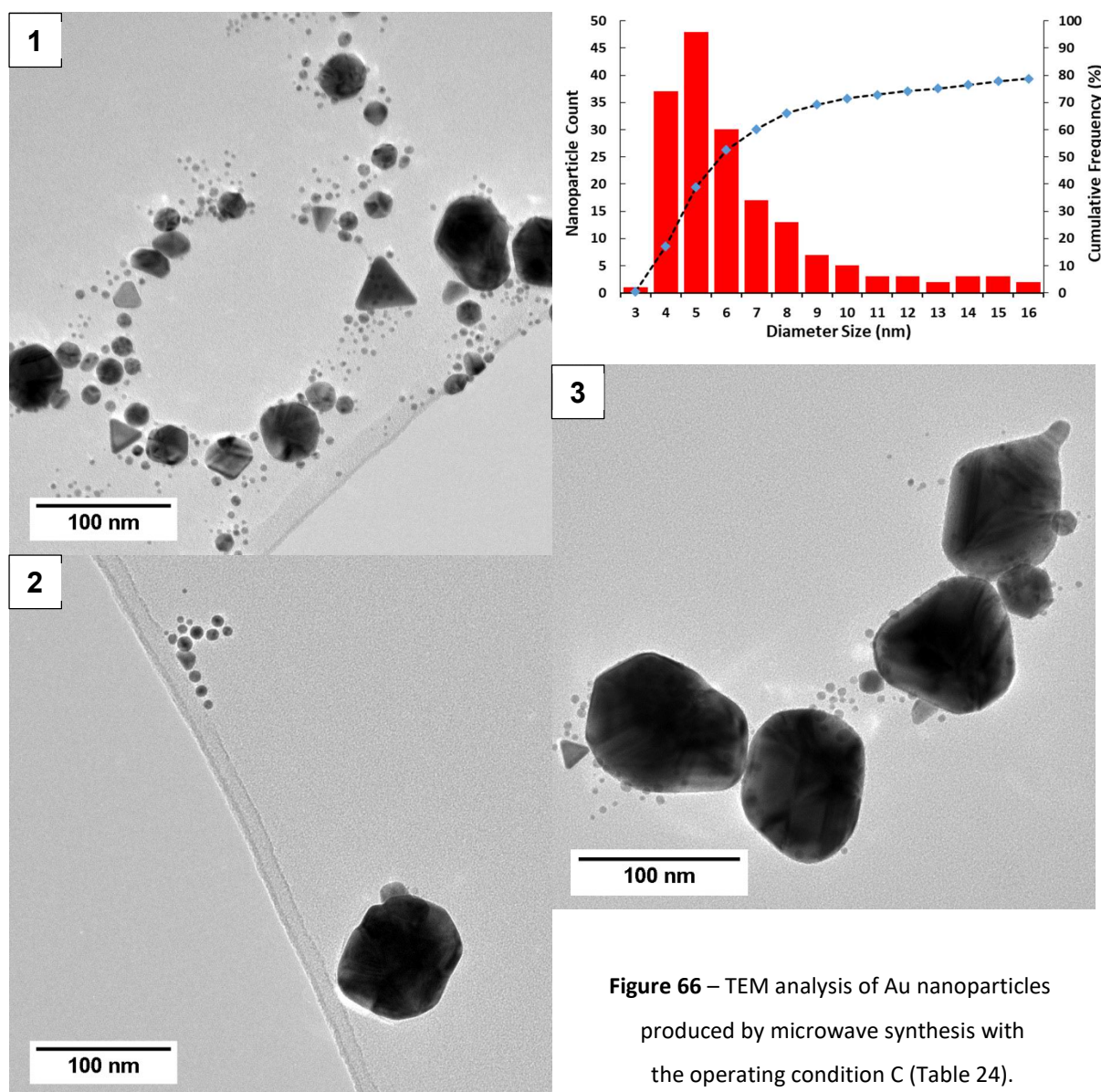


Figure 66 – TEM analysis of Au nanoparticles produced by microwave synthesis with the operating condition C (Table 24).

Synthesis of Metal Nanoparticles by Microwave

3.5 Metal Nanoparticles Production under Batch Regime

The minimum Au nanoparticles average size was of only 12 ± 3.9 nm and obtained with the operating condition B. This size is considerable higher than what could be obtained when working with the traditional sol-immobilization protocol, around 3 nm.

This difference on the average sizes can be explained by having in consideration that with the microwave synthesis the reducing agent action is much weaker than when sodium borohydride is employed. Furthermore, with microwave synthesis the Au nanoparticles are subject to higher temperatures and the growth step is favoured. The reducing agent and temperature effects on the metal nanoparticles formation mechanism is explained in more detail in section 1.4.1.

However, it was still possible to find in the literature the production of Au nanoparticles by microwave synthesis with average sizes smaller than 12 ± 3.9 nm. Tu and Liu⁹⁸ who have produced Au nanoparticles by working with the short-chain alcohol methanol in a 1:1 (v/v)

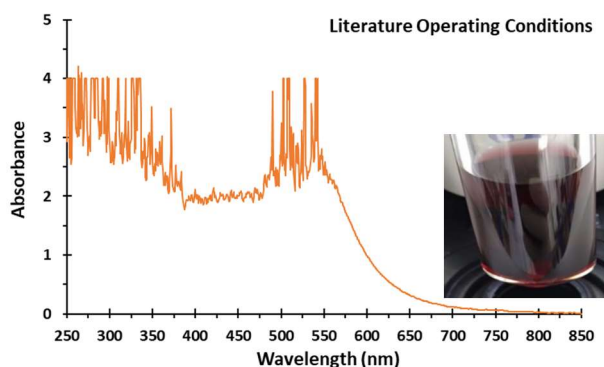


Figure 67 – UV-Vis analysis and photo of Au nanoparticles produced by microwave synthesis with the operating conditions from the work of Tu and Liu.⁹⁸

water mixture with a total volume of 20 mL and containing 0.111g of PVP and 8 eq. of NaOH have reported Au nanoparticles average sizes of 7.6 ± 1.45 nm. Some trials were then conducted in order to understand how these authors were able to achieve smaller Au nanoparticles sizes.

Firstly their operating conditions were replicated but it was verified that the high Au concentration of 1 mM caused the UV-Vis detector to saturate as shown in Figure 67 with the observed absorbances in excess of 2-3 higher than the equipment detection limit.

The 1 mM Au concentration represents approximately an 8-fold increase from the 0.13 mM Au concentration adopted for the three selected operating conditions. During the optimisation tests in section 3.2.2 it was demonstrated that the experimental results might get worse when increasing the Au concentration but not when decreasing the Au concentration, as long as there is enough Au to reach the nucleation level and trigger the nucleation step as predicted by the LaMer plot as shown in Figure 11. Therefore, it was decided to scale down the Au concentration from 1 mM to 0.13 mM but keeping the other operating conditions constant, namely the mixture composition, the total mixture volume, the PVP/metal weight ratio, the NaOH/metal molar ratio and the microwave synthesis time and temperature.

Synthesis of Metal Nanoparticles by Microwave

3.5 Metal Nanoparticles Production under Batch Regime

A quick TEM analysis, as shown in Figure 68, was consistent with their reported average size. After verifying the validity of their operating conditions, it was formulated the hypothesis that smaller Au nanoparticles were mainly produced due to the high amount of PVP stabilizer used. These authors have worked with a PVP/metal weight ratio of 28. This value represents almost a 9-fold increase from the 3.25 ratio adopted for the operating condition B and a 43-fold increase from the 0.65 ratio adopted for the traditional sol-immobilization protocol. In order to test this hypothesis a new trial was conducted with the operating condition B but instead of using the PVP/metal ratio of 3.25 it was changed to the authors ratio of 28.

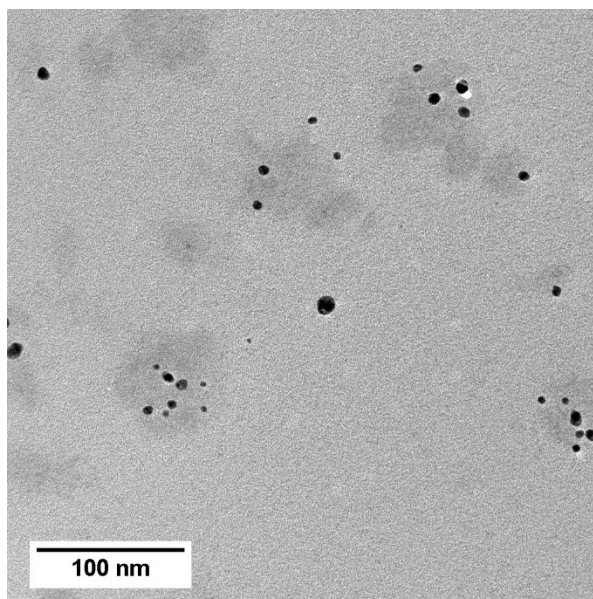


Figure 68 – TEM analysis of Au nanoparticles produced by microwave synthesis with the operating conditions adapted from the work of Tu and Liu.⁰

As shown in Figure 69 the Au nanoparticles produced with the literature operating conditions presented a plasmon peak absorbance of only 0.39, significantly lower than the 0.51 from operating condition B and the 0.49 from operating condition B with 28xPVP. The plasmon peak wavelength range was the highest when using the literature operating conditions with 90 nm, followed by the operating condition B with 76 nm and the lowest with the operating condition B with 28xPVP with 64 nm. The plasmon peak wavelengths of 535 nm and 536 nm indicate Au nanoparticles average sizes very similar for operating condition B and operating condition B with 28xPVP respectively and the plasmon peak wavelength of 531 nm indicates the smallest Au nanoparticles average size for the literature operating conditions.

As expressed by Equation 1 and mentioned in section 3.2, the plasmon peak results are dependent on the type of solvent used and direct comparisons should not be made. In this particular case methanol presents a dielectric constant very similar to ethylene glycol and therefore a direct comparison of a methanol/water mixture with ethylene glycol results in a smaller error than a direct comparison of water with ethylene glycol.

The calculated DLS average size for the literature operating conditions was contradictory with the UV-Vis plasmon peak wavelength as it indicated a value of 20 ± 6 nm, considerable higher than the calculated DLS average sizes of 5.4 ± 2.0 nm for the operating condition B and 4.1 ± 1.9 nm for the operating condition B with 28xPVP.

Synthesis of Metal Nanoparticles by Microwave

3.5 Metal Nanoparticles Production under Batch Regime

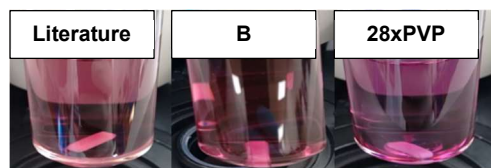
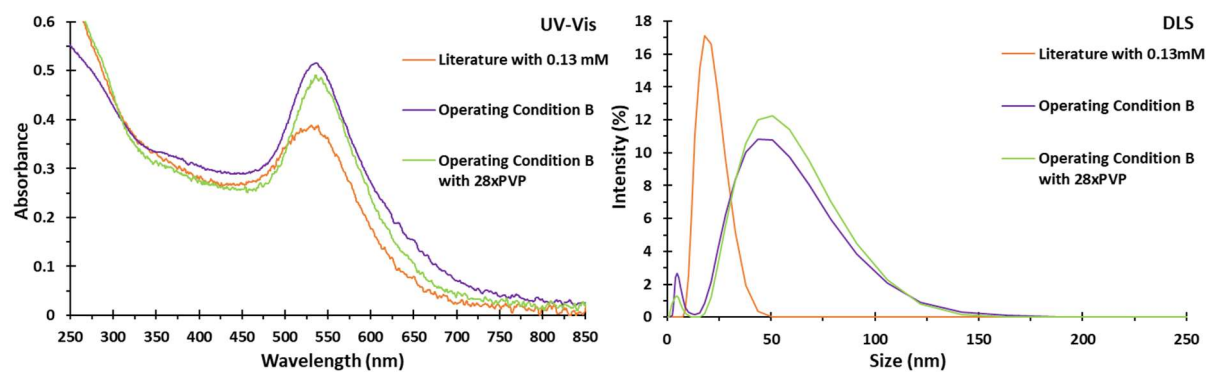


Figure 69 – Au nanoparticles produced by microwave synthesis with the operating conditions adapted from the work of Tu and Liu⁹⁸ (literature), with the operating condition B (Table 24) and with the operating condition B with 28xPVP with UV-Vis (top left) and DLS (top right) analysis and photos (bottom left).

As shown in Figure 70 the TEM analysis of the operating condition B with 28xPVP confirms that smaller Au nanoparticles were indeed produced just by increasing the PVP/metal weight ratio from 3.25 to 28. It can be concluded that the hypotheses that smaller Au nanoparticles were mainly produced due to the high amount of PVP stabilizer used was proved correct as Au nanoparticles lower than 12 ± 3.9 nm could be produced if the PVP/metal weight was to be greatly increased. The Au nanoparticles average size decreased from 12 ± 3.9 nm to 9.2 ± 1.9 nm.

This average size is still higher than the 7.6 ± 1.45 nm reported by Tu and Liu⁹⁸. However, these authors have also employed NaOH, which has been demonstrated in section 3.3.2 to enhance the Au nanoparticles production by forming acetaldehyde, capable of acting as a weak reducing agent even at room temperature. The use of NaOH could explain the still existing gap of 9.2 ± 1.9 nm to 7.6 ± 1.45 nm. However, as explained in section 3.3.2, working with NaOH presents the disadvantage of affecting the metal nanoparticles reproducibility.

Moreover, for the work developed for this PhD working at those high PVP/metal weight ratios is not desirable as the metal nanoparticles are meant to be used as catalysts and the PVP would end up blocking the substrate access to the metal nanoparticles which hinders the catalytic activity.

It should also be mentioned that the TEM images shown in Figure 70 are notoriously affected by a small contamination phenomenon. This contamination phenomenon was often observed throughout all the TEM analysis performed for this PhD and related to organic contamination, in this particular case due to the high amount of PVP used in the sample.

Synthesis of Metal Nanoparticles by Microwave

3.5 Metal Nanoparticles Production under Batch Regime

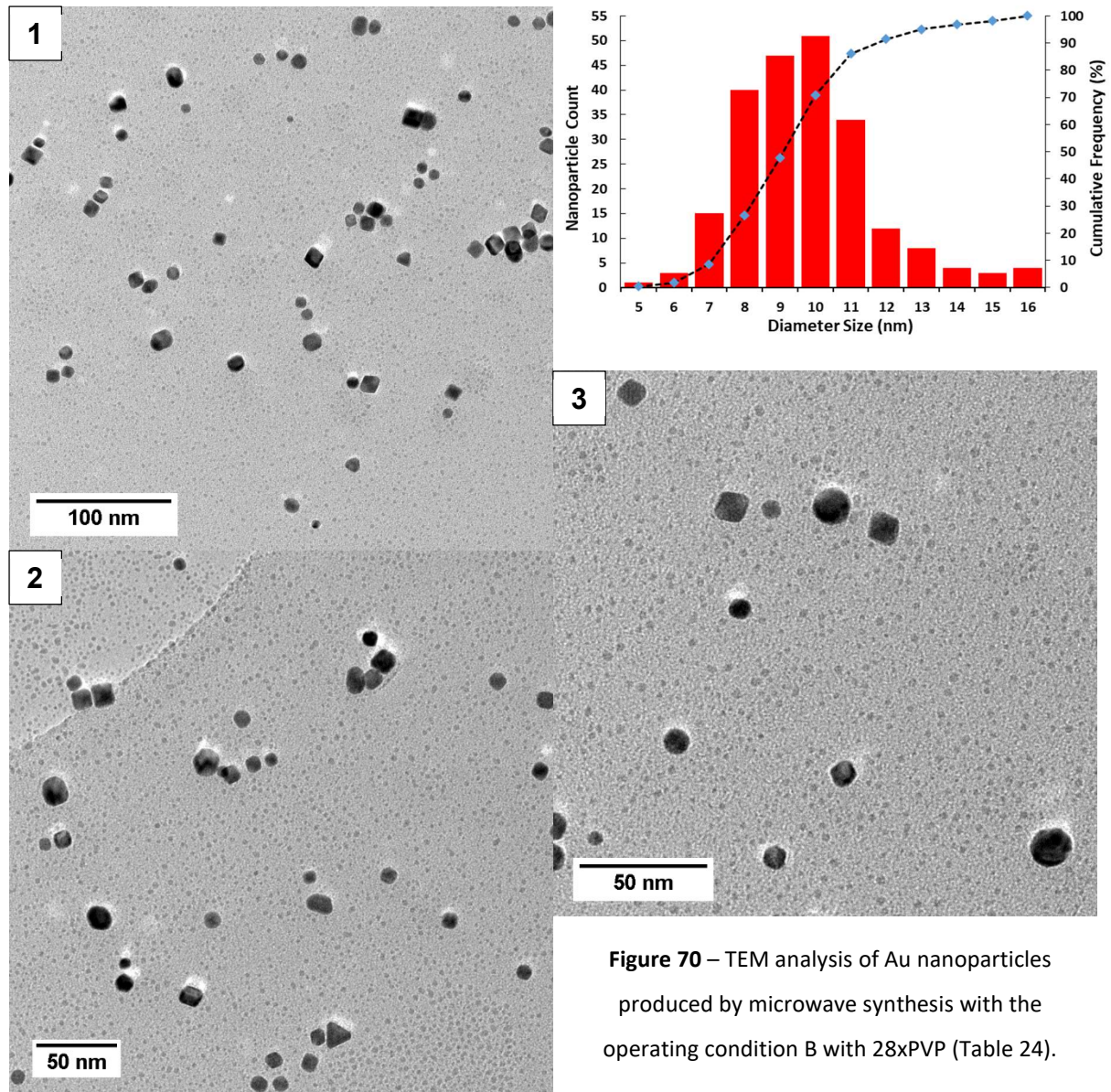


Figure 70 – TEM analysis of Au nanoparticles produced by microwave synthesis with the operating condition B with 28xPVP (Table 24).

Synthesis of Metal Nanoparticles by Microwave

3.5 Metal Nanoparticles Production under Batch Regime

3.5.2 Pd Nanoparticles

The UV-Vis and DLS spectra and photos of the Pd nanoparticles produced with the three selected operating conditions are compared in Figure 71.

The first observation that can be made is that Pd nanoparticles do not present a plasmon peak in this region of the electromagnetic spectrum. However, it is still possible to observe that the three UV-Vis spectra are different from one another. The UV-Vis spectrum of Pd nanoparticles produced with the operating condition B is actually almost identical to the UV-Vis spectrum of Pd nanoparticles produced with the traditional sol-immobilization protocol shown in Figure 15 (middle) and presenting an average size of around 3 nm. Therefore, it can also be formulated the hypothesis that Pd nanoparticles produced with the operating condition B have a similar average size. The calculated DLS average size of 7.7 ± 1.2 nm also supports this hypothesis.

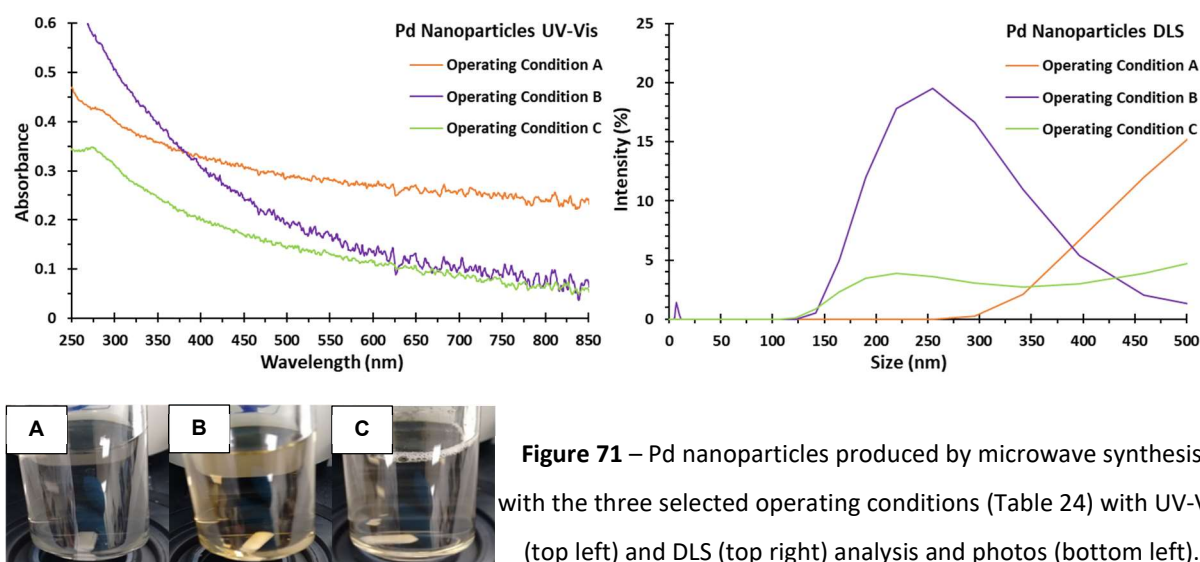


Figure 71 – Pd nanoparticles produced by microwave synthesis with the three selected operating conditions (Table 24) with UV-Vis (top left) and DLS (top right) analysis and photos (bottom left).

The TEM analysis of Pd nanoparticles produced with the operating condition A and shown in Figure 72 only revealed the agglomeration of Pd. This is according to the high value of 644 ± 180 nm calculated for the average size with the DLS analysis. Only two images are presented but more TEM images were analysed and the same agglomeration phenomenon was observed. Contrary to Au nanoparticles, the microwave synthesis with a stabilizer is paramount for the formation of Pd nanoparticles.

Synthesis of Metal Nanoparticles by Microwave

3.5 Metal Nanoparticles Production under Batch Regime

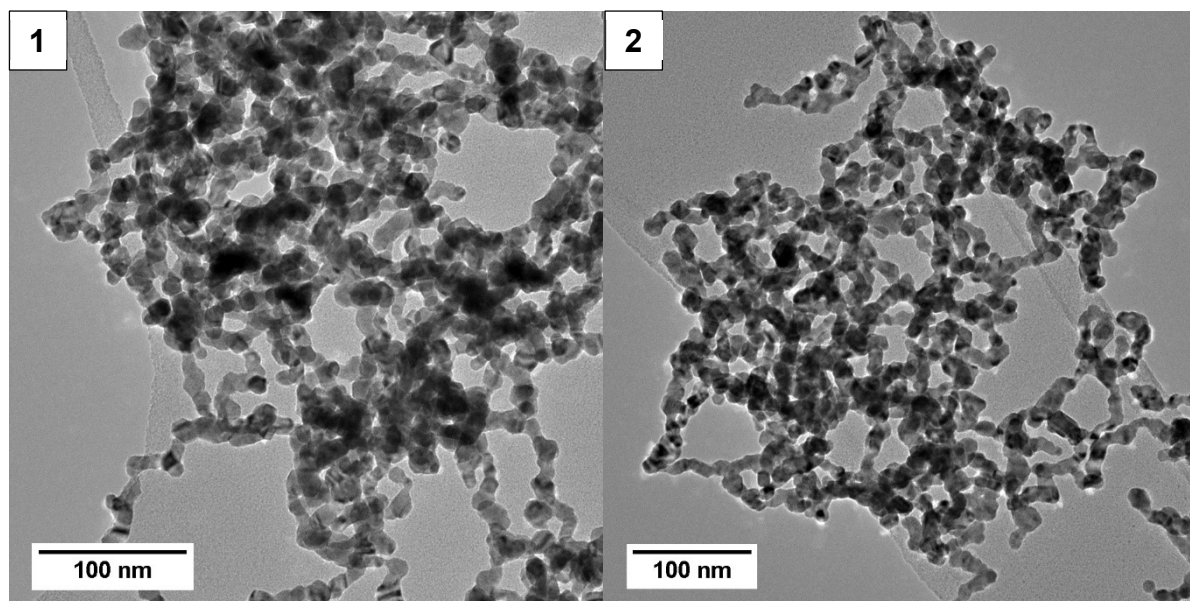


Figure 72 – TEM analysis of Pd nanoparticles produced by microwave synthesis with the operating condition A (Table 24).

The TEM analysis shown in Figure 73 validated the hypothesis that the produced Pd nanoparticles with the operating condition B were around the same range of sizes obtained when working with the traditional sol-immobilization protocol with a calculated TEM average size of 3.3 ± 0.8 nm.

The produced Pd nanoparticles were circular and aggregation and agglomeration were not observed. The low standard deviation value of 0.8 nm indicates a narrow size distribution. Similar to what was done in section 3.4 the Pd nanoparticles were stored in a glass vial and the UV-Vis spectrum was checked over time (54 days) with no major changes to the UV-Vis spectrum being detected.

When the traditional sol-immobilization protocol is employed both average sizes for the Au and Pd nanoparticles are around 3 nm. However, it is remarkable that with microwave synthesis with the operating condition B average sizes of 3.3 ± 0.8 nm could be obtained for the Pd nanoparticles whereas with Au nanoparticles the average size was of only 12 ± 3.9 nm. Some of the factors that could explain this disparity include but are not limited to:

a) PVP interaction with the Pd nanoparticles is stronger than PVP interaction with the Au nanoparticles therefore causing different growth step rates, particularly important when working at high temperatures as it is the case with the 150 °C attained during the microwave synthesis;

Synthesis of Metal Nanoparticles by Microwave

3.5 Metal Nanoparticles Production under Batch Regime

b) Even though the standard reduction potential shown in Table 12 indicates Au^{3+} with a higher tendency to be reduced than Pd^{2+} , 1.692 vs. 0.951 V, this parameter is a measure of the equilibrium, not kinetics. For this reason it is possible that with the microwave synthesis in ethylene glycol the reduction rate of Pd^{2+} is higher than the reduction rate of Au^{3+} and as a result the effect of the nucleation step taking place simultaneously with the growth step is more relevant for Au, which according to the LaMer concept, mentioned in section 1.4.1, can compromise the experimental results;

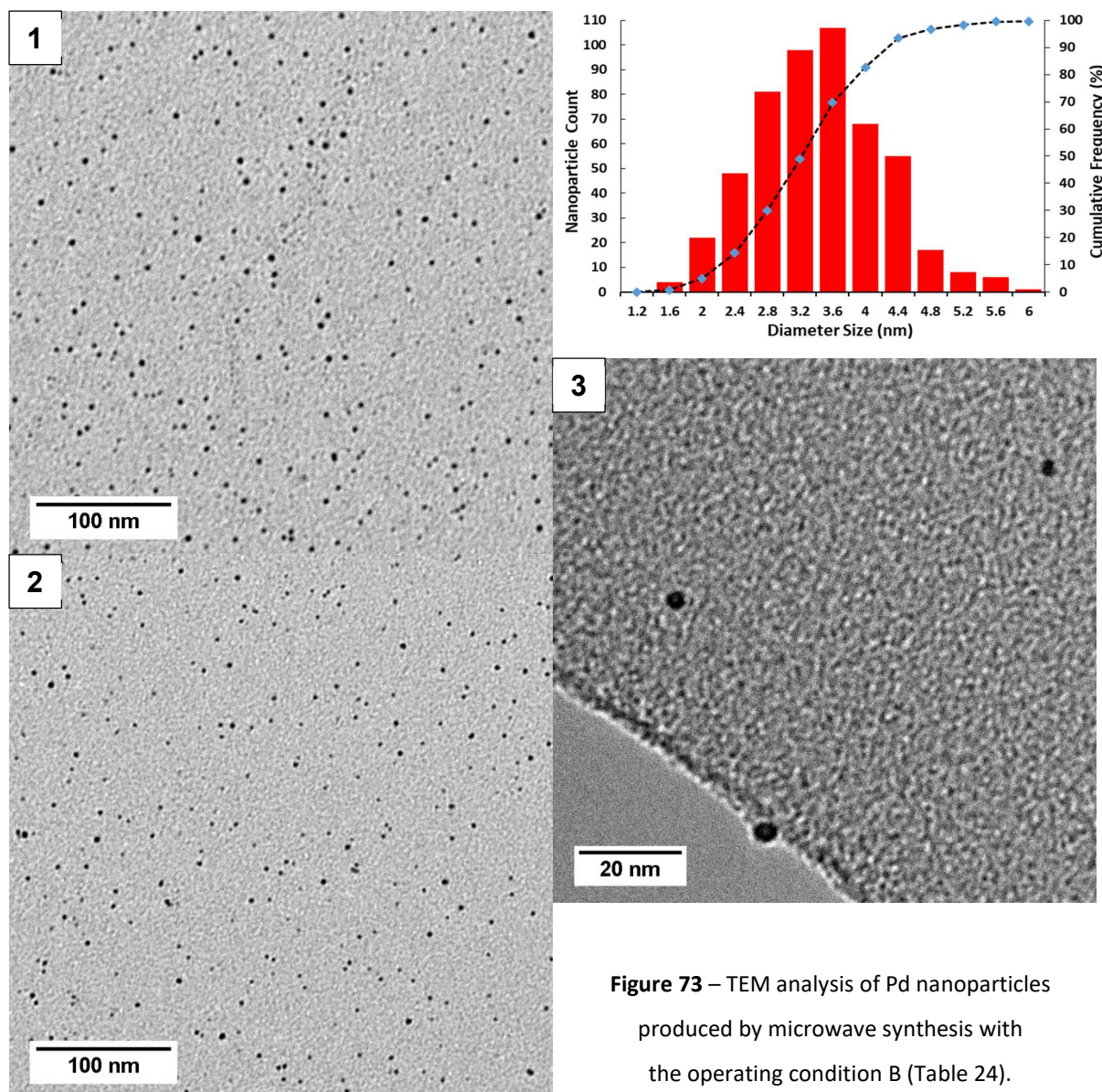


Figure 73 – TEM analysis of Pd nanoparticles produced by microwave synthesis with the operating condition B (Table 24).

Synthesis of Metal Nanoparticles by Microwave

3.5 Metal Nanoparticles Production under Batch Regime

Working with operating condition C produced only agglomeration of Pd nanoparticles as revealed by the TEM analysis in Figure 74 with two images shown, but in total more than two images were also analysed. Again, the DLS analysis is according to this agglomeration effect with a calculated average size of 239 ± 60 nm.

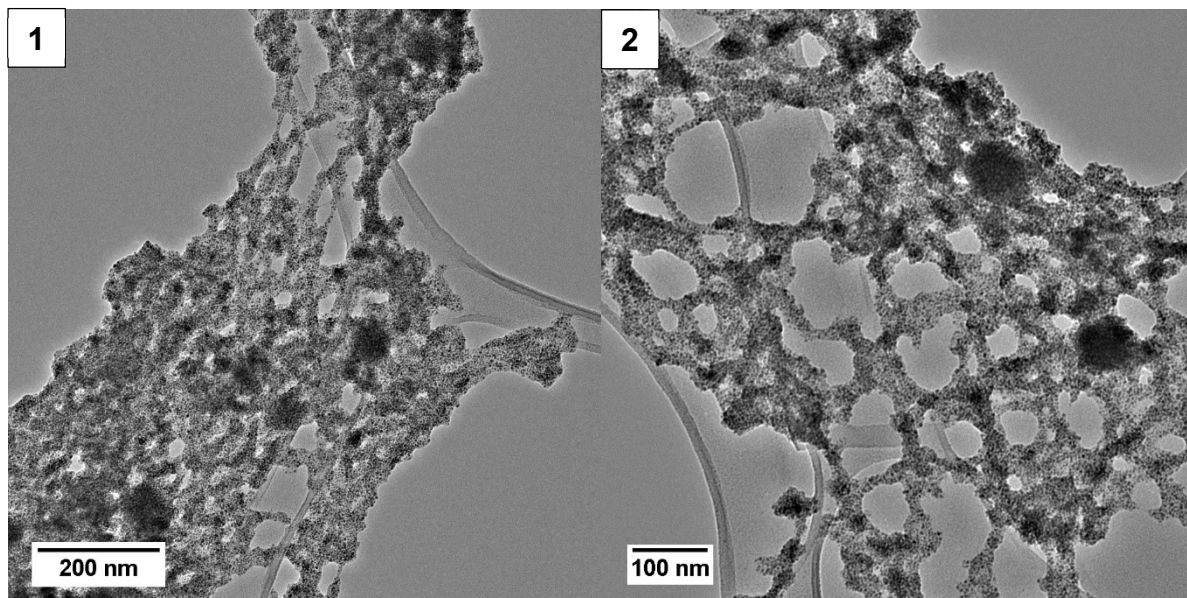


Figure 74 – TEM analysis of Pd nanoparticles produced by microwave synthesis with the operating condition C (Table 24).

As the microwave work with the Pd nanoparticles was less extensive than the work with the Au nanoparticles, which included the trials performed during the optimisation tests and the mechanistic studies, a more complete literature review was done in order to fully understand the potential Pd nanoparticles average sizes that could be produced. Pd and Au nanoparticles are particularly important for this PhD, more than Ag, Cu and Ir, as they are the main metal nanoparticles supported, heat treated and further characterised in chapter 5 and then tested in the several reactions presented in chapter 1. As shown in Table 27 by changing operating conditions the several authors were able to tailor the Pd nanoparticles average size.

Tu and Liu⁹⁸, who have reported Au nanoparticles average sizes smaller than the 12 ± 3.9 nm, have also reported Pd nanoparticles average sizes smaller than the 3.3 ± 0.8 nm obtained with the operating condition B. As demonstrated with the Au nanoparticles this was only possible by greatly increasing the amount of stabilizer. Therefore, they had to work with a PVP/metal weight ratio of 52 so that such small Pd nanoparticles could be produced. This is a similar value to the 50xPVP/metal weight ratio used by Zawadzki¹⁰⁶ who was also able to produce Pd nanoparticles with an average size smaller than 3.3 ± 0.8 nm. This author has also shown how the stabilizer/metal weight ratio influences the Pd nanoparticles average size. As the PVP/metal weight ratio decreased from 50 to 25 and then to 10 the Pd nanoparticles

Synthesis of Metal Nanoparticles by Microwave

3.5 Metal Nanoparticles Production under Batch Regime

average size increased respectively from 2.0 ± 0.18 nm to 6.1 ± 0.85 nm and then to 13.0 ± 1.01 nm. This is according with the previous finding for Au nanoparticles. As previously explained working at high PVP/metal weight ratios is not desirable as the metal nanoparticles are meant to be used as catalysts and the PVP would end up blocking the substrate access to the metal nanoparticles which hinders the catalytic activity.

An interesting green approach for the production of Pd nanoparticles has been developed by Baruwati and Varma¹⁰⁷ who have used the waste of red wine production, the commonly called pomace, as both the reducing agent and the stabilizer due to the presence of numerous polyphenolic compounds. The main disadvantage of their microwave protocol being the necessity to purify the produced metal nanoparticles with centrifugation and washing which are estimated to result in losses of around 20 %.

Overall most of the authors in Table 27 reported Pd nanoparticles average sizes higher than 3.3 ± 0.8 nm, even if working at stabilizer/metal weight ratios much higher than 3.25. The high Pd concentrations used, considerable higher than the 0.13 mM from operating condition B, could have compromised the production of small Pd nanoparticles. As shown in section 3.2.2, the Au concentration optimisation test demonstrated that the experimental results might get worse when increasing the metal concentration.

In conclusion, compared to the work of these authors it can be said that the microwave protocol developed for this PhD with the operating condition B is the best when it comes to the production of small and circular Pd nanoparticles to be used in catalytic applications.

Table 27 – Overview of Pd nanoparticles produced by microwave synthesis as found in the literature.

Average Size (nm)	Microwave Time (min)	Pd (mM)	Solvent and/or Reducing Agent	Stabilizer	Stabilizer/Pd Weight Ratio	Ref.
1.3 ± 0.27	0.5	1.0	50% Methanol (aq.)	PVP	52	98
7.0	2	1.2	Glycerol	PVP	Unknow	108
30	1	0.5	Ethylene Glycol	PVP	2.1	109
22	1	0.5	Glycerol	PVP	2.4	109
5 - 10	1	10	Grape Pomace	Grape Pomace	Unknown	107
2.0 ± 0.18	5	Unknown	Ethylene Glycol	PVP	50	106
6.1 ± 0.85	5	Unknown	Ethylene Glycol	PVP	25	106
13.0 ± 1.01	5	Unknown	Ethylene Glycol	PVP	10	106
180	5	0.3	2.5 mM Hydrazine (aq.)	Polyacrylamide	33	110
20 - 50	30	4.2	500 mM HEPES (aq.) ^a	CTAB ^b	10.2	111
9 - 10	30	4.2	500 mM HEPES (aq.) ^a	PVP	6.2	111

a) HEPES stands for (2-[4-(2-hydroxyethyl)-1-piperazinyl]ethanesulfonic acid);

b) CTAB stands for cetyltrimethylammonium bromide;

Synthesis of Metal Nanoparticles by Microwave

3.5 Metal Nanoparticles Production under Batch Regime

Some work with NaOH was also carried out. The objective was to replicate the same metal nanoparticles enhanced production effect observed when working with Au nanoparticles as presented in section 3.3.2. However, as observed in Figure 75 it was not possible to produce Pd nanoparticles only by adding NaOH to the Pd solution in ethylene glycol and without any microwave heating.

When using both 8 eq. and 16 eq. of NaOH the Pd solution UV-Vis spectrum did not change much and it was not compatible with the production of Pd nanoparticles. Similar to what was done with the Au nanoparticles it was tested the addition of NaOH without stabilizer (Figure 75 left), same as in the operating condition A, and in the presence of stabilizer with a PVP/metal weight ratio of 3.25 (Figure 75 right), same as in the operating condition B.

As mentioned in section 3.3.2 the NaOH metal nanoparticles enhanced production effect is a slow process and associated with an induction period. Therefore, even though the UV-Vis spectra in Figure 75 were recorded 30 min after adding NaOH it cannot be ruled out the possibility that the induction period for Pd is much higher than the induction period for Au.

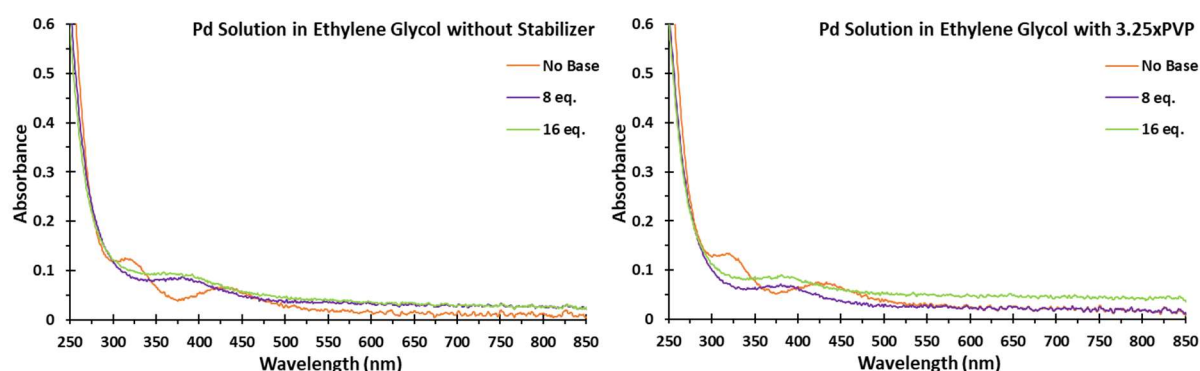


Figure 75 – UV-Vis analysis of Pd solution in ethylene glycol without stabilizer (left) and with 3.25xPVP (right) at different concentrations of NaOH.

The two aforementioned Pd solution samples with 16 eq. of NaOH, with and without stabilizer, were subject to microwave heating, same test previously done for Au in section 3.2.4 with the acid/base addition optimisation test.

The UV-Vis spectra and DLS analysis are presented in Figure 76 and compared to the operating conditions A and B, previously shown in Figure 71.

Surprisingly, after applying microwave heating the Pd nanoparticles presented a peak in the UV-Vis region that looked like a plasmon peak. This is probably related to the formation of other Pd complex as the NaBH_4 test indicated that Pd ions reduction had not been completed.

The DLS analysis also indicated a decrease in the calculated DLS average size for the trial without stabilizer with a value of 59 ± 13 nm, much lower than the 644 ± 180 nm calculated with just the operating condition A.

Synthesis of Metal Nanoparticles by Microwave

3.5 Metal Nanoparticles Production under Batch Regime

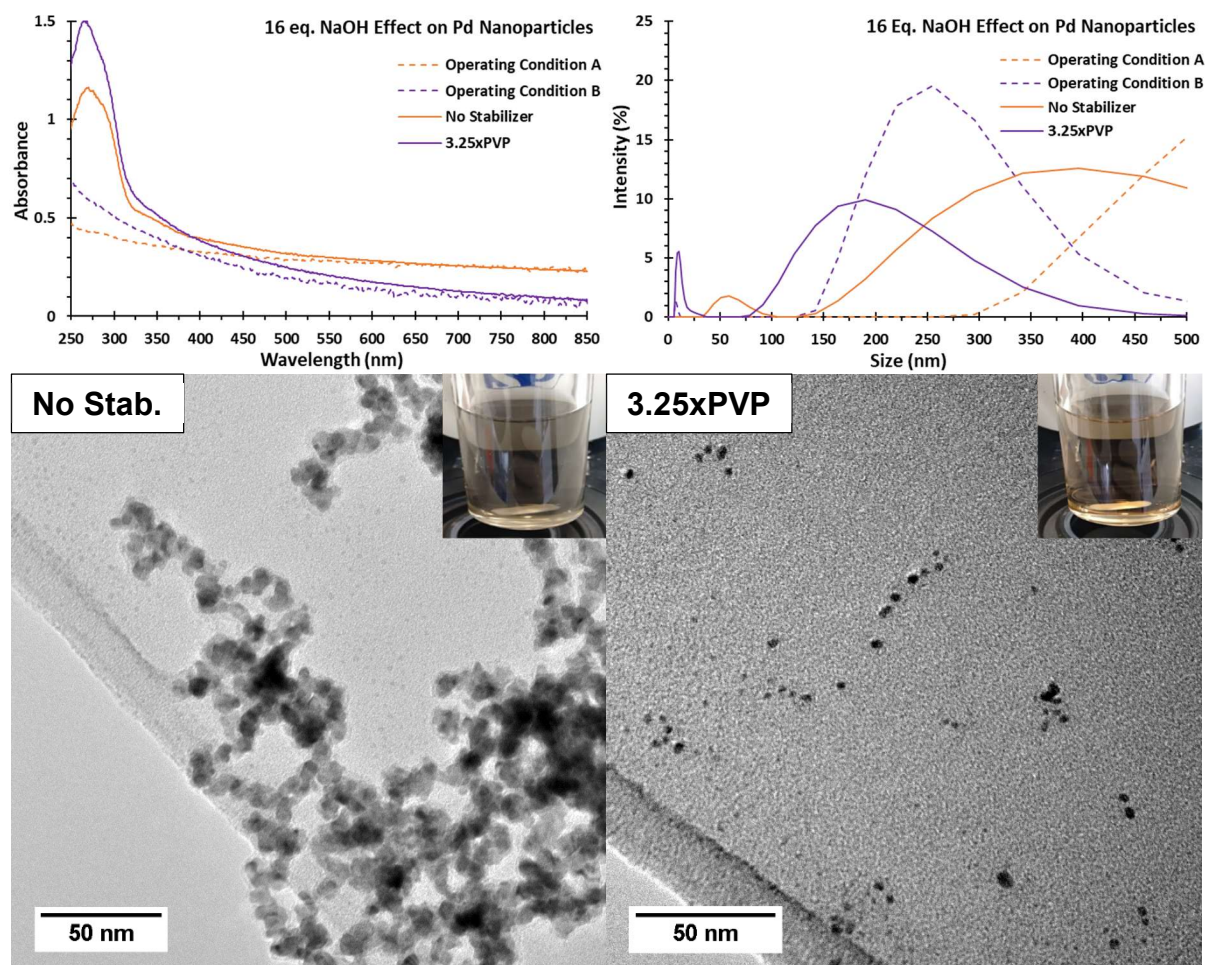


Figure 76 – Pd nanoparticles produced by microwave synthesis at 16 eq. of NaOH with UV-Vis (top left) and DLS (top right) analysis and TEM images for no stabilizer trial (bottom left) and 3.25xPVP trial (bottom right) with colloid photos included.

When analysing the Pd nanoparticles with TEM (Figure 76 bottom) it is clear that when no stabilizer was used adding 16 eq. NaOH to the Pd solution also ended up producing only agglomerated Pd nanoparticles. When 3.25xPVP were used, adding 16 eq. NaOH resulted in small Pd nanoparticles being produced, but when compared to the Pd nanoparticles produced with operating condition B (shown in Figure 73) these Pd nanoparticles were slightly larger, the size distribution was worse and the circular shape was compromised.

Therefore, it can be said that adding 8 eq. and 16 eq. of NaOH to the production of Pd nanoparticles resulted in worse experimental results. This is the same conclusion that was reached for Au in section 3.2.4 with the acid/base addition optimisation test. Moreover, the Pd reduction was now incomplete. It is also not expected that the controlled addition of 1-2 eq. of NaOH could bring any benefits. It was shown in Figure 75 that contrary to the Au scenario with Pd the NaOH addition did not contribute to reduction before starting any microwave synthesis. As explained in section 3.3.2 this was the reason why with Au the controlled addition of 1-2 eq. of NaOH was able to bring some benefits to the nanoparticles production.

Synthesis of Metal Nanoparticles by Microwave

3.5 Metal Nanoparticles Production under Batch Regime

3.5.3 Ag Nanoparticles

The UV-Vis spectra of Ag nanoparticles shown in Figure 77 indicates for the operating conditions A and B a plasmon peak at around 400 nm, which according to what is found in the literature is associated with Ag nanoparticles having average sizes of around 10-12 nm.⁴⁰ The UV-Vis spectrum for the operating condition C did not reveal a plasmon peak and large or agglomerated Ag nanoparticles are expected to have been produced.

The DLS calculated average size of 180 ± 64 nm for the operating condition A is not consistent with the expected 10-12 nm average size. The DLS calculated average size of 38 ± 9 nm for the operating condition B is higher than 10-12 nm but still within a reasonable deviation as the DLS analysis is influenced by the presence of stabilizers and it reports the average size of the hydrated nanoparticle, *i.e.* surrounded by the solvent molecules. The DLS calculated average size of 115 ± 8 nm for the operating condition C is consistent with what is expected according to the UV-Vis spectrum.

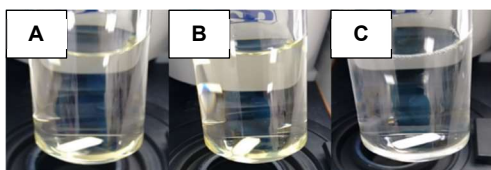
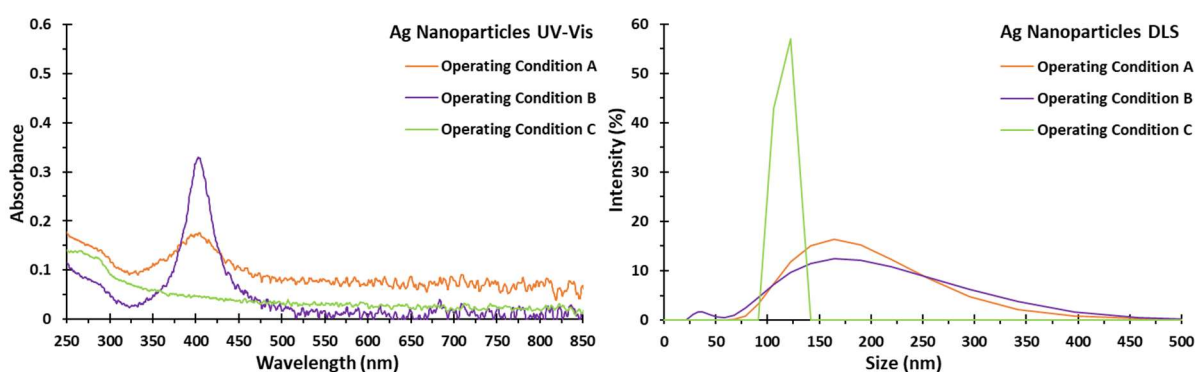


Figure 77 – Ag nanoparticles produced by microwave synthesis with the three selected operating conditions (Table 24) with UV-Vis (top left) and DLS (top right) analysis and photos (bottom left).

The Ag nanoparticles produced with the operating condition A were confirmed by the TEM analysis shown in Figure 78 to be significantly aggregated and agglomerated. A small amount of individual and circular Ag nanoparticles with average sizes in the 10-12 nm range were also observed. Only two TEM images are presented in Figure 78 but in total more than two were analysed. The aggregation and agglomeration effects explain why the plasmon peak observed in the UV-Vis analysis at around 400 nm was not as pronounced as the same plasmon peak observed for the operating condition B. These effects also explain why the DLS analysis indicated much larger Ag nanoparticles average size than 10-12 nm.

Synthesis of Metal Nanoparticles by Microwave

3.5 Metal Nanoparticles Production under Batch Regime

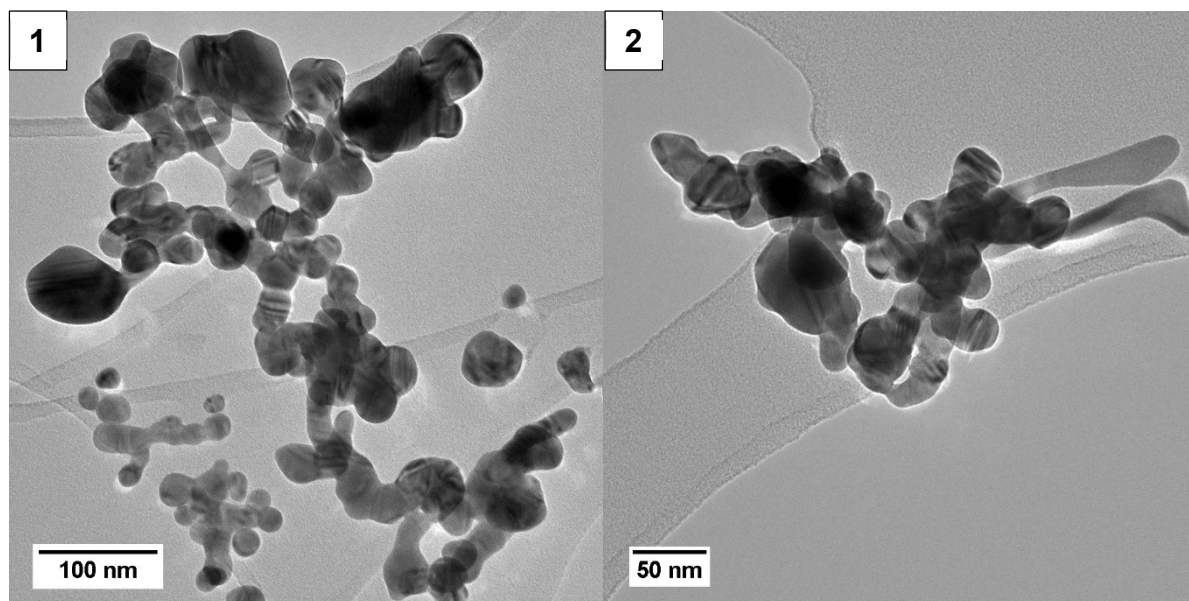


Figure 78 – TEM analysis of Ag nanoparticles produced by microwave synthesis with the operating condition A (Table 24).

As shown in Figure 79 the TEM analysis of Ag nanoparticles produced with the operating condition B revealed circular Ag nanoparticles with an average size of 13 ± 14 nm, consistent with the plasmon peak shown in the UV-Vis analysis at 400 nm and with the calculated DLS average size of 38 ± 9 nm.

The standard deviation of 14 nm was of the same order of magnitude than the calculated TEM average size of 13 nm, similar to what was observed with the Au nanoparticles produced with the operating condition C with a calculated TEM average size of 18 ± 27 nm (see Figure 66). Some considerable larger than 13 nm Ag nanoparticles are observed in image 1. However, contrary to the Au nanoparticles produced with the operating condition C, this was not the reason why the standard deviation was high. The Ag nanoparticles size distribution histogram indicates that the cumulative frequency had already reached slightly more than 90 % at 22 nm, above the 22 nm threshold there were only less than 10 % of larger Ag nanoparticles to be considered. Therefore, these larger than 13 nm Ag nanoparticles were not much relevant to the calculation of the standard deviation, without considering any Ag nanoparticles above 22 nm the standard deviation would still be in the same order of magnitude that the average size of 13 nm.

Synthesis of Metal Nanoparticles by Microwave

3.5 Metal Nanoparticles Production under Batch Regime

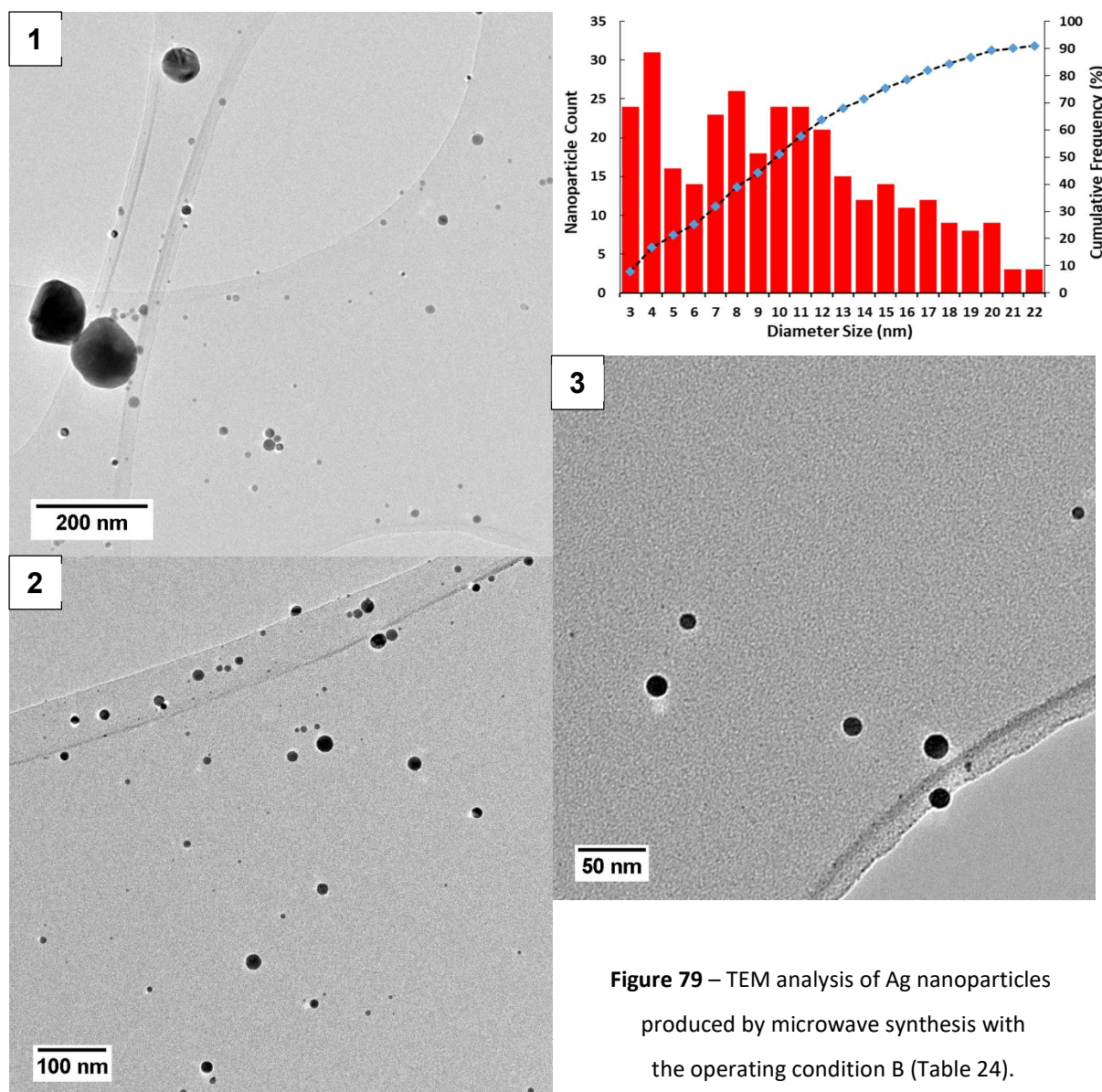


Figure 79 – TEM analysis of Ag nanoparticles produced by microwave synthesis with the operating condition B (Table 24).

On the other hand, what stands out from the TEM analysis is that the Ag nanoparticles size distribution histogram is very far from following a normal Gaussian distribution curve. As mentioned in the experimental procedure for the synthesis of metal nanoparticles (chapter 2), after each synthesis, either by microwave or ultrasound, sodium borohydride (NaBH_4) was added to the UV-Vis cuvette with no major changes expected if the reduction had been completed. As shown in Figure 80 upon addition of NaBH_4 to the UV-Vis cuvette major changes were observed and it was clear that the Ag solution had not been fully reduced.

The UV-Vis spectrum of the Ag solution is the same as the baseline with only zero absorbance observed. For this reason it was not immediately detected with the UV-Vis analysis of the sample produced with the operating condition B in Figure 77 that there was still some unreduced Ag solution.

Synthesis of Metal Nanoparticles by Microwave

3.5 Metal Nanoparticles Production under Batch Regime

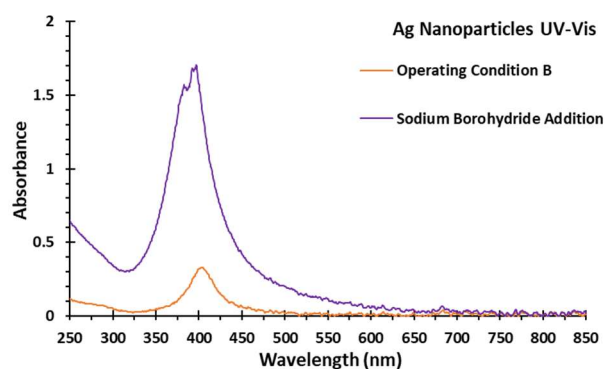


Figure 80 – UV-Vis analysis of Ag nanoparticles produced by microwave synthesis with the operating condition B (Table 24) and after adding NaBH₄ to the UV-Vis cuvette.

The incomplete reduction of the Ag solution is not exclusive of operating condition B. The same NaBH₄ test also indicated incomplete reduction of the Ag solution when working with the operating conditions A and C.

In particular, the TEM analysis of the Ag nanoparticles produced with the operating condition C was the most difficult to perform. Most of the TEM grid did not present any Ag nanoparticles, a strong indication of incomplete reduction. The few Ag nanoparticles observed with TEM analysis, with two images shown in Figure 81, were of irregular shape and presented large sizes. This is according to what was expected from the UV-Vis and DLS analysis. The incomplete reduction also explains the very low UV-Vis absorbances for the operating condition C in Figure 77.

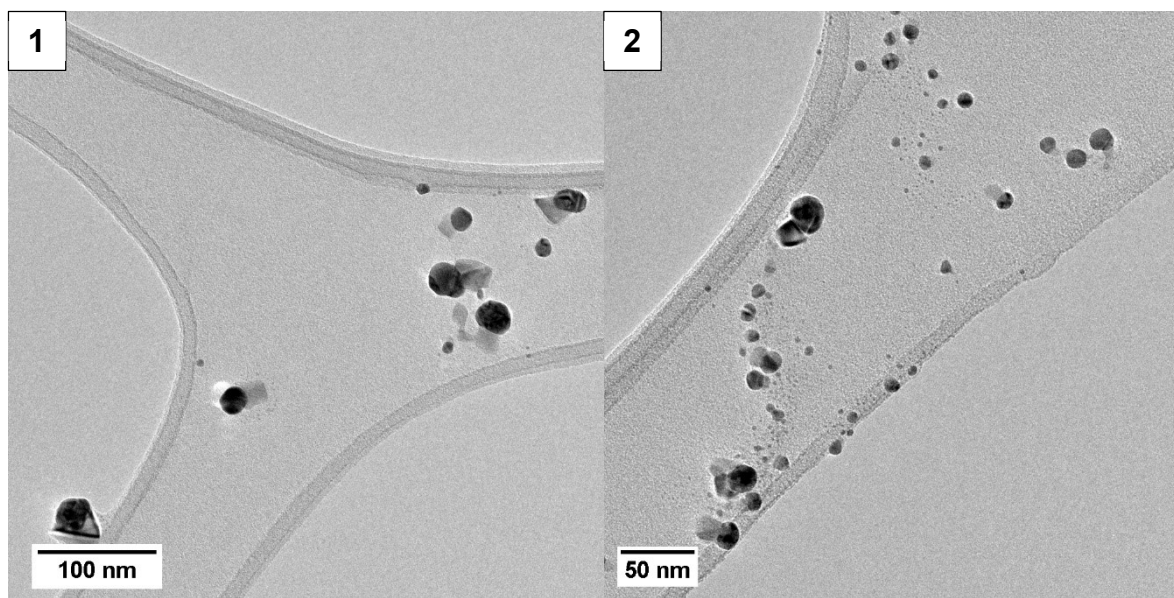


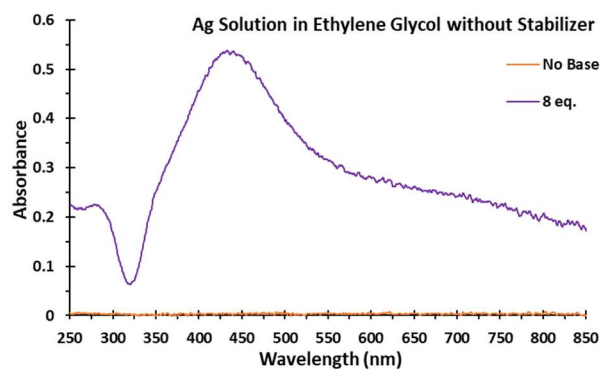
Figure 81 – TEM analysis of Ag nanoparticles produced by microwave synthesis with the operating condition C (Table 24).

Synthesis of Metal Nanoparticles by Microwave

3.5 Metal Nanoparticles Production under Batch Regime

Similar to what was done when working with the Pd nanoparticles some work with NaOH was also carried out. Again, the objective was to replicate the same metal nanoparticles enhanced production effect observed when working with Au nanoparticles as presented in section 3.3.2. Contrary to the Pd nanoparticles, it was possible to produce Ag nanoparticles only by adding NaOH to the Ag solution in ethylene glycol and without any microwave heating.

As shown in Figure 82 the addition of 8 eq. NaOH to Ag solution in ethylene glycol without stabilizer, same as in the operating condition A, caused major changes to the UV-Vis spectrum with the expected plasmon peak for Ag nanoparticles at around 400 nm observed.



Moreover, contrary to what was observed with Au nanoparticles, there was no induction period with the observed UV-Vis changes taking place almost immediately after adding the NaOH. For this reason, no test with 16 eq. NaOH was performed.



Figure 82 – Ag nanoparticles produced without microwave synthesis by adding 8 eq. of NaOH to Ag solution in ethylene glycol with no stabilizer with UV-Vis analysis (top) and colloid photo (bottom).

The aforementioned Ag solution sample with 8 eq. of NaOH and without stabilizer was subject to microwave heating, same test as previously done for Au in section 3.2.4 with the acid/base addition optimisation test. The UV-Vis spectrum presented in Figure 83 is compared to the operating condition A, previously shown in Figure 77.

It can be said that adding NaOH solved the incomplete reduction of Ag. As observed in the UV-Vis spectrum, the absorbances are considerable higher than when no NaOH was used with the operating condition A. The sample was also tested by adding NaBH_4 to the UV-Vis cuvette and no major changes were observed, an indication that reduction had been completed. However, when compared to the Ag nanoparticles produced with the operating condition A the plasmon peak slightly shifted from 400 nm to 425 nm, an indication that a greater amount of Ag nanoparticles with sizes larger than 10-12 nm were produced.

Synthesis of Metal Nanoparticles by Microwave

3.5 Metal Nanoparticles Production under Batch Regime

For the reasons explained in section 3.3.2 with the Au nanoparticles, the controlled addition of 1-2 eq. of NaOH can bring some benefits, but there is a threshold (8 eq. of NaOH) above which the experimental results will become worse (production, average size and size distribution). A similar situation is expected with the Ag nanoparticles regarding their average size and size distribution but with the difference that any NaOH concentration will always improve the Ag nanoparticles production as it will minimize the issue with the incomplete reduction of the Ag solution.

A more detailed study, with more trials at different NaOH concentrations and including the presence of stabilizer, similar to what was done for Au in section 3.2.4 with the acid/base addition optimisation test, would be necessary in order to fully understand the maximum amount of NaOH that could be added to improve the Ag nanoparticles average size and size distribution.

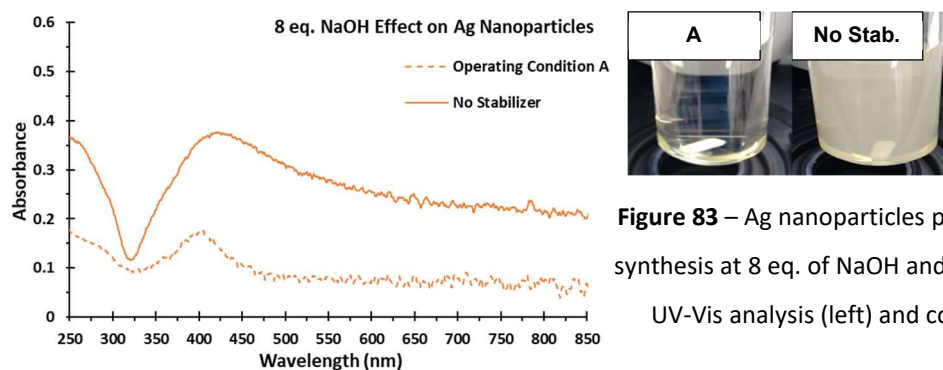


Figure 83 – Ag nanoparticles produced by microwave synthesis at 8 eq. of NaOH and without stabilizer with UV-Vis analysis (left) and colloid photos (right).

Synthesis of Metal Nanoparticles by Microwave

3.5 Metal Nanoparticles Production under Batch Regime

3.5.4 Ir Nanoparticles

The UV-Vis spectra of Ir nanoparticles shown in Figure 84 are of similar shape to the UV-Vis spectra obtained for the Pd nanoparticles in Figure 71. Particularly important is the observation that Ir nanoparticles also do not present a plasmon peak in this region of the electromagnetic spectrum.

However, contrary to the Pd nanoparticles, which presented all the three UV-Vis spectra different from one another, with Ir nanoparticles the operating conditions A and B have produced very similar UV-Vis spectra. The DLS analysis in Figure 84 also supports the hypothesis that these Ir nanoparticles are small and of similar size to each other with calculated DLS average sizes of 3.9 ± 0.9 nm for operating condition A and of 13 ± 9 nm for operating condition B. These calculated DLS average sizes are very different from the 214 ± 85 nm obtained when working with the operating condition C.

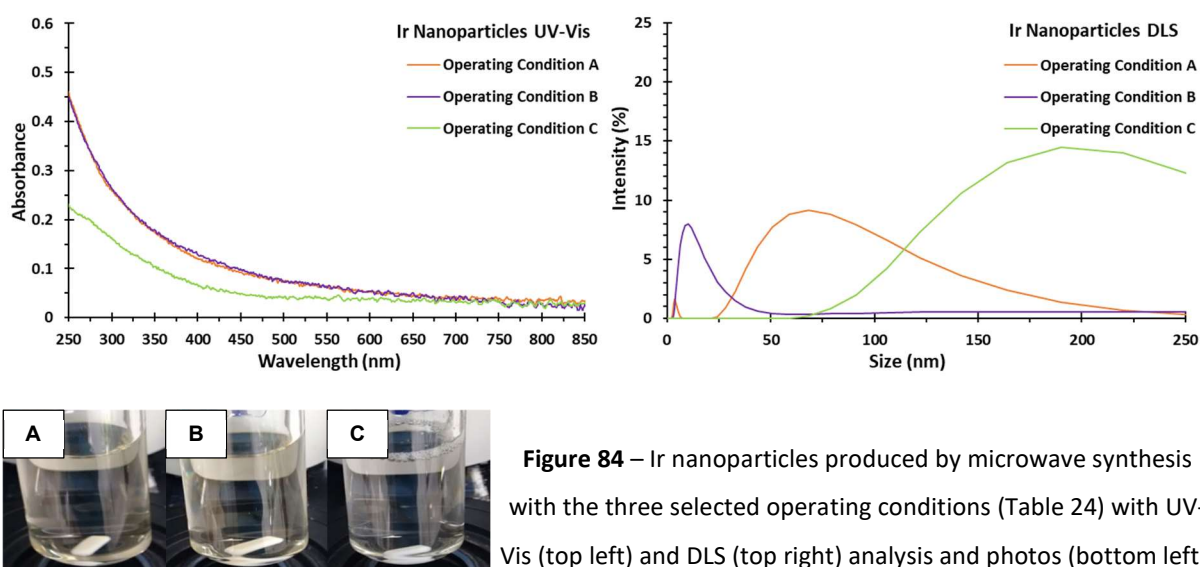


Figure 84 – Ir nanoparticles produced by microwave synthesis with the three selected operating conditions (Table 24) with UV-Vis (top left) and DLS (top right) analysis and photos (bottom left).

The TEM analysis of Ir nanoparticles produced with the operating condition A shown in Figure 85 revealed sizes smaller than 1-2 nm. This type of sizes is close to the equipment detection limit, which makes it very difficult to produce a meaningful Ir nanoparticles size distribution histogram. Two major sources of error would be expected:

- There would be undetected Ir nanoparticles not considered in the nanoparticles size distribution histogram;
- The sizes for the Ir nanoparticles would start to be in the same order of magnitude than the absolute error for each nanoparticle size measurement, estimated to be in the 0.3-0.5 nm range;

Synthesis of Metal Nanoparticles by Microwave

3.5 Metal Nanoparticles Production under Batch Regime

In any case, the TEM analysis was an important tool as it allowed to verify the production of circular and significantly small Ir nanoparticles (1-2 nm) with a very narrow size distribution being expected.

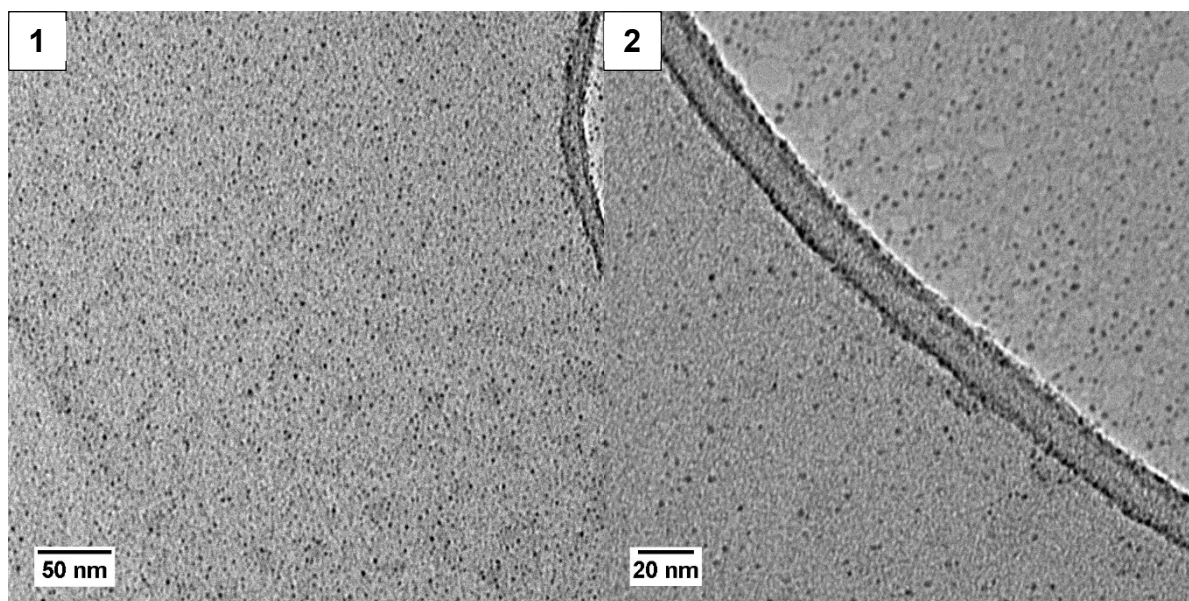


Figure 85 – TEM analysis of Ir nanoparticles produced by microwave synthesis with the operating condition A (Table 24).

As shown in Figure 86, the TEM analysis of the Ir nanoparticles produced with the operating condition B confirmed the hypothesis derived from the UV-Vis and DLS analysis that the operating conditions A and B had produced Ir nanoparticles of small size and similar to each other. Again, and for the same reasons, it would be very difficult to produce a meaningful Ir nanoparticles size distribution histogram.

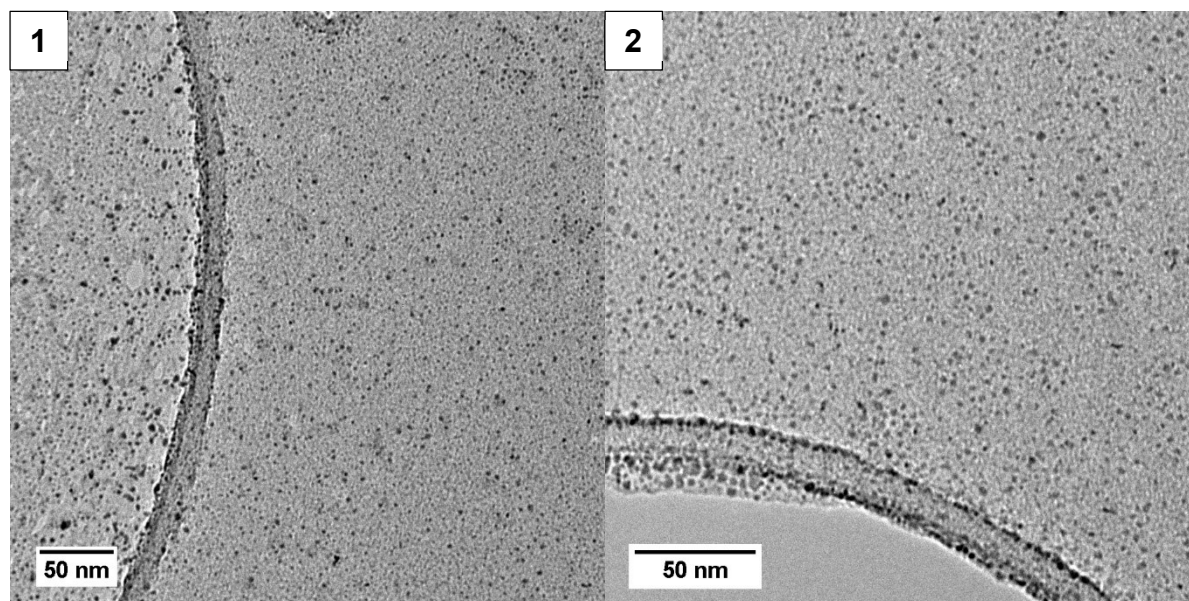


Figure 86 – TEM analysis of Ir nanoparticles produced by microwave synthesis with the operating condition B (Table 24).

Synthesis of Metal Nanoparticles by Microwave

3.5 Metal Nanoparticles Production under Batch Regime

When using the operating condition C only agglomerated Ir nanoparticles were produced as shown by the TEM analysis in Figure 87. This is similar to what happened with the Pd nanoparticles shown in Figure 74. The calculated DLS average size of 214 ± 85 nm is according to this agglomeration effect.

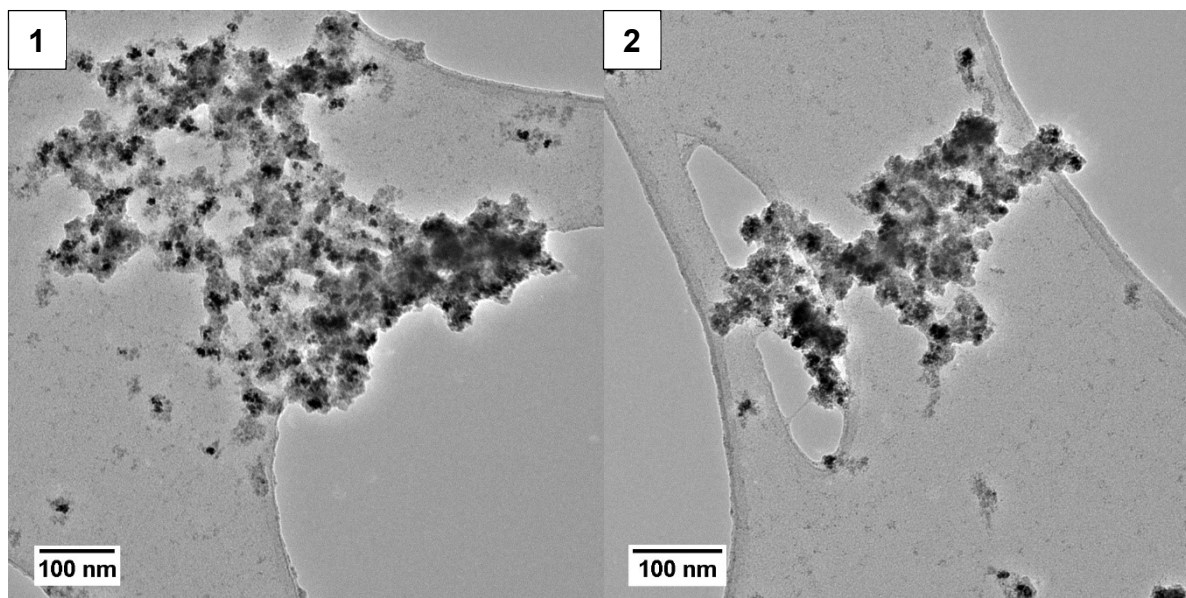


Figure 87 – TEM analysis of Ir nanoparticles produced by microwave synthesis with the operating condition C (Table 24).

Similar to what was done when working with Pd and Ag some work with NaOH was also carried out with Ir. Again, the objective was to replicate the same metal nanoparticles enhanced production effect observed when working with Au nanoparticles as presented in section 3.3.2.

As shown in Figure 75 when adding both 8 eq. and 16 eq. of NaOH to the Pd solution the UV-Vis spectrum did not change much and it was not compatible with the production of Pd nanoparticles. As shown in Figure 82 the addition of 8 eq. of NaOH to the Ag solution was enough to induce instantaneous changes to the UV-Vis spectrum compatible with the production of Ag nanoparticles.

As shown in Figure 88 it was tested the addition of 8 eq. and 16 eq. of NaOH to Ir solution in ethylene glycol without any microwave heating and without stabilizer, same as in the operating condition A, and with 3.25xPVP, same as in the operating condition B. Mixed results were observed for both situations depending on the concentration of NaOH. The addition of 8 eq. of NaOH did not cause major changes to the UV-Vis spectrum, similar to Pd, whereas with the addition of 16 eq. of NaOH major changes were observed, similar to Ag.

Synthesis of Metal Nanoparticles by Microwave

3.5 Metal Nanoparticles Production under Batch Regime

Even though at 16 eq. of NaOH major changes were observed to the UV-Vis spectrum they are still not consistent with a typical UV-Vis spectrum of Ir nanoparticles as shown in Figure 84. Moreover, the sample was tested by adding NaBH_4 to the UV-Vis cuvette and major changes were observed, an indication that reduction of Ir solution was still not complete as it would be the case if Ir nanoparticles had been produced. Therefore, it is not likely that this UV-Vis spectrum major changes were caused by the production of Ir nanoparticles, instead only by the reduction of Ir, with accumulation of Ir reduced atoms before the nucleation step could be triggered as predicted by the LaMer plot (see Figure 11).

This would be the same scenario as the one observed with the Au solution in section 3.3.2. Only after adding 8 eq. of NaOH Au nanoparticles started to be produced, before that NaOH concentration the Au solution was only being reduced but nucleation had not yet been triggered. Therefore, it might happen that with the Ir solution it is just a matter of a NaOH concentration higher than 16 eq. being necessary.

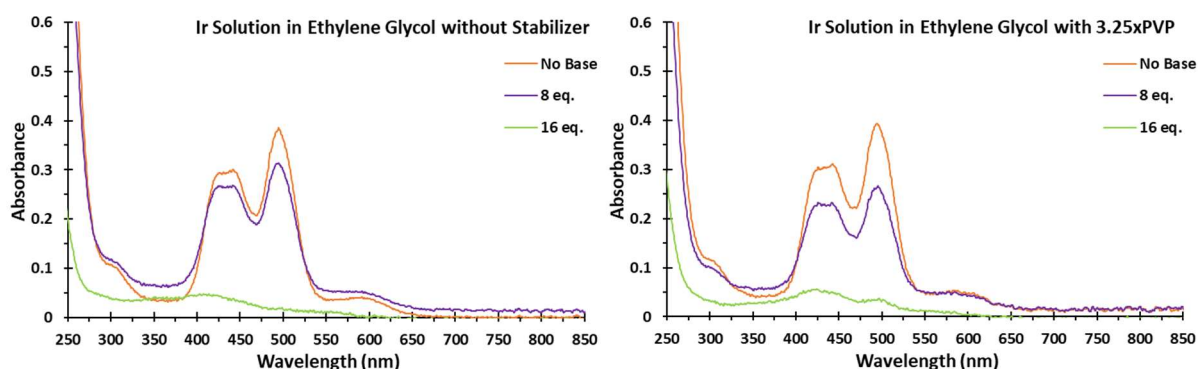


Figure 88 – UV-Vis analysis of Ir solution in ethylene glycol without stabilizer (left) and with 3.25xPVP (right) at different concentrations of NaOH.

The two aforementioned Ir solution samples with 16 eq. of NaOH, with and without stabilizer, were subject to microwave heating, same test previously done for Au in section 3.2.4 with the acid/base addition optimisation test.

The UV-Vis spectra and DLS analysis are presented in Figure 89 and compared to the operating conditions A and B, previously shown in Figure 84.

Similar to what happened with Pd nanoparticles, after applying microwave heating the Ir nanoparticles surprisingly presented a peak in the UV-Vis region that looked like a plasmon peak. This is probably related to the formation of other Ir complex as the NaBH_4 test indicated that Ir ions reduction had not been completed.

Synthesis of Metal Nanoparticles by Microwave

3.5 Metal Nanoparticles Production under Batch Regime

Similar to what happened with the operating conditions A and B the produced UV-Vis spectra with and without stabilizer were almost identical. The DLS analysis indicated a decrease in the calculated DLS average size for both samples, with the trial without stabilizer presenting a value of 0.7 ± 0.1 nm, lower than the 3.9 ± 0.9 nm calculated with the operating condition A, and with the trial with stabilizer with a value of 0.7 ± 0.1 nm, lower than the 13 ± 9 nm calculated with the operating condition B.

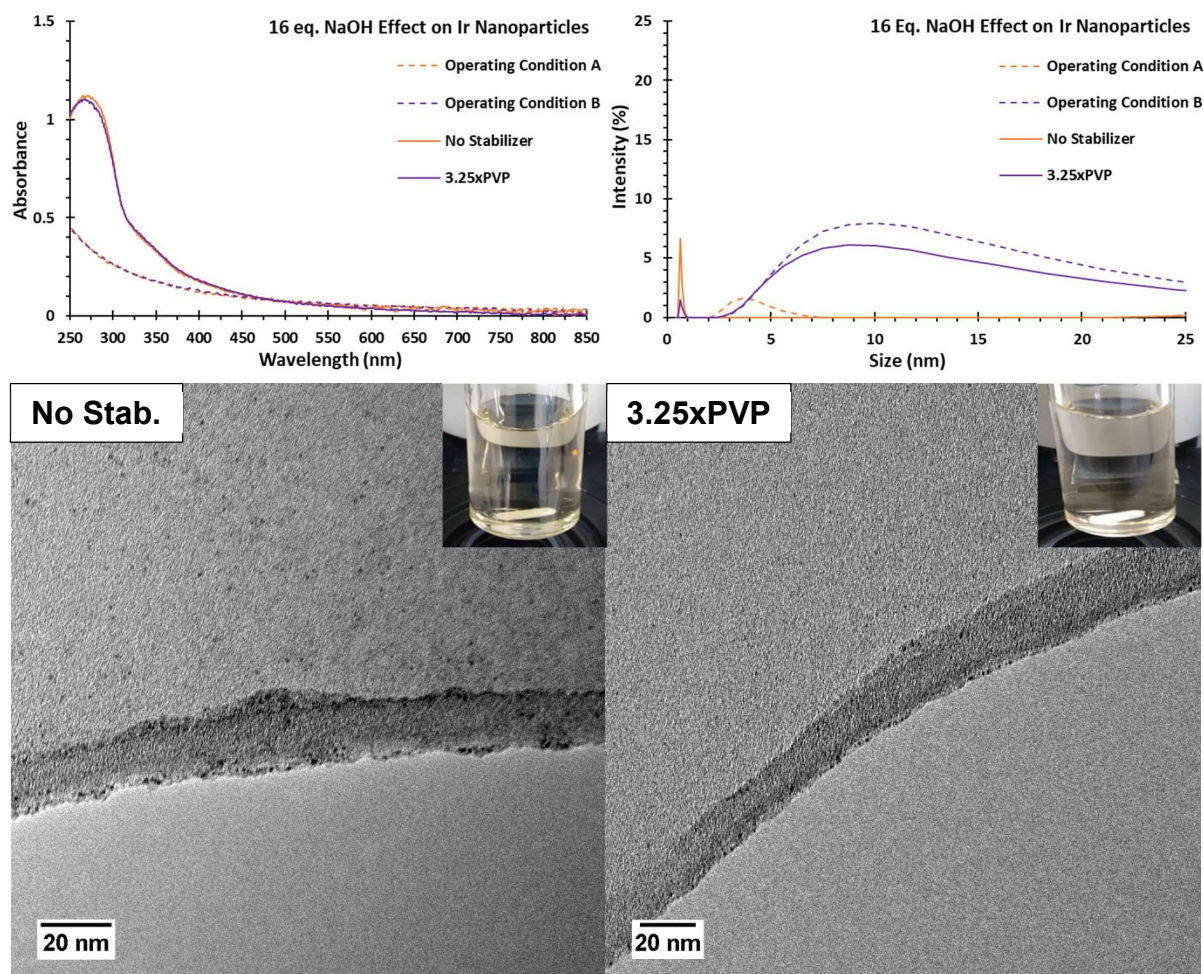


Figure 89 – Ir nanoparticles produced by microwave synthesis at 16 eq. of NaOH with UV-Vis (top left) and DLS (top right) analysis and TEM images for no stabilizer trial (bottom left) and 3.25xPVP trial (bottom right) with colloid photos included.

When analysing the Ir nanoparticles with TEM (Figure 89 bottom) it is clear that for both trials, without stabilizer and with 3.25xPVP, even smaller than 1-2 nm sizes ended up being produced, with the Ir nanoparticles almost undetected with TEM analysis. This result was in agreement with the DLS analysis. Moreover, the Ir reduction was now incomplete which caused TEM analysis to be more difficult as well.

Synthesis of Metal Nanoparticles by Microwave

3.5 Metal Nanoparticles Production under Batch Regime

It can be said that the addition of 16 eq. of NaOH can bring benefits to the production of Ir nanoparticles. This is according to what was expected based on the Au nanoparticles experimental results. As shown in section 3.2.4 with the acid/base addition optimisation test the controlled addition of 1-2 eq. of NaOH was able to bring benefits to the production of Au nanoparticles but above a certain threshold, 8 eq. of NaOH, the experimental results started to be worse. As explained in section 3.3.2 when 1-2 eq. of NaOH were added to the Au solution reduced Au atoms were produced before any microwave heating but no production of Au nanoparticles was observed. Likewise, with Ir, with 16 eq. of NaOH added to the Ir solution reduced Ir atoms were produced before any microwave heating but no production of Ir nanoparticles was observed. For the same reasons it is also expected that there will be a threshold for the NaOH concentration above which Ir nanoparticles will start to be produced before any microwave heating and the experimental results will be worse. This threshold would be above 16 eq. of NaOH. In order to determine that threshold more Ir trials with NaOH would be necessary.

Synthesis of Metal Nanoparticles by Microwave

3.5 Metal Nanoparticles Production under Batch Regime

3.5.5 Cu Nanoparticles

The three selected operating conditions were tested for the production of Cu nanoparticles. However, contrary to the results obtained with Au, Pd, Ag and Ir, with Cu no nanoparticles production was observed. In Figure 90 the UV-Vis spectra of Cu solutions at the three different operating conditions are presented. After the microwave synthesis the UV-Vis spectra remained unchanged.

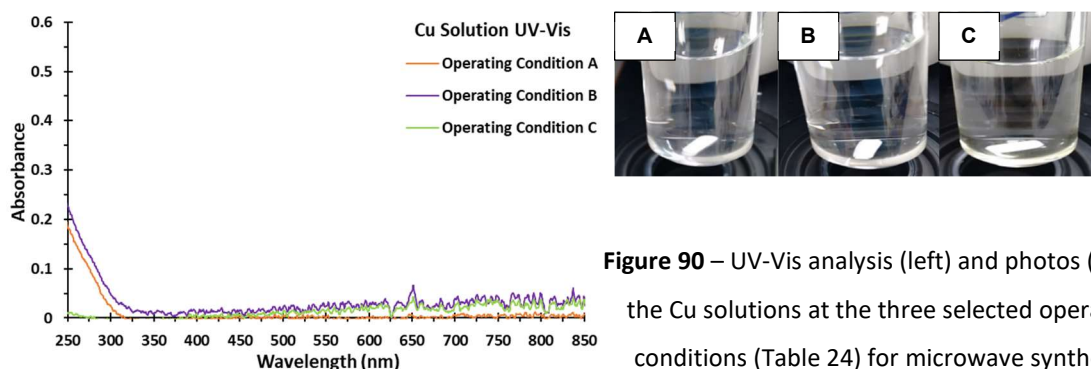


Figure 90 – UV-Vis analysis (left) and photos (top) of the Cu solutions at the three selected operating conditions (Table 24) for microwave synthesis.

These results do not mean that Cu nanoparticles cannot be produced by microwave synthesis. Horikoshi and Serpone¹¹ highlight that the synthesis of Cu nanoparticles by ethylene glycol requires several hours or even days at high temperatures. Other authors have been able to successfully produce Cu nanoparticles using microwave synthesis as shown in Table 28, but using operating conditions very different from the three selected operating conditions for this PhD.

Table 28 – Overview of Cu nanoparticles produced by microwave synthesis as found in the literature.

Average Size (nm)	Microwave Time (min)	Cu (mM)	Solvent and/or Reducing Agent	Stabilizer	Stabilizer/Pd Weight Ratio	Ref.
46 ± 9	10	16.6	Diethylene glycol	PVP	5	112
5-6	20	10	1-Heptanol	Octanoate	4.5	113
21-357	5	50	Hydrazine/Ethylene Glycol	None	None	114

As reported by Nakamura *et al.*¹¹³ Cu is more difficult to be reduced than other metals, such as Au and Ag, due to a low standard reduction potential. This is according to what is shown in Table 12 with Cu²⁺ presenting a standard reduction potential of only 0.3419 V. Therefore, larger average sizes and more extreme operating conditions are expected for the microwave synthesis of Cu nanoparticles.

Synthesis of Metal Nanoparticles by Microwave

3.5 Metal Nanoparticles Production under Batch Regime

Some work with NaOH was also carried out. The objective was to replicate the same metal nanoparticles enhanced production effect observed when working with Au nanoparticles as presented in section 3.3.2.

Similar results to what was obtained for Pd in section 3.5.2 were observed. As shown in Figure 91 it was not possible to produce Cu nanoparticles only by adding NaOH to the Cu solution in ethylene glycol and without any microwave heating. When using both 8 eq. and 16 eq. of NaOH the Cu solution UV-Vis spectrum did not change much and it was not compatible with the production of Cu nanoparticles. It was tested the addition of NaOH without stabilizer (Figure 91 left), same as in the operating condition A, and in the presence of stabilizer with a PVP/metal weight ratio of 3.25 (Figure 91 right), same as in the operating condition B.

As mentioned in section 3.3.2 the NaOH nanoparticles enhanced production effect is a slow process and it is associated with an induction period. Therefore, even though the UV-Vis spectra in Figure 91 were recorded 30 min after adding the NaOH it cannot be ruled out the possibility that the induction period for Cu is much higher than the induction period for Au.

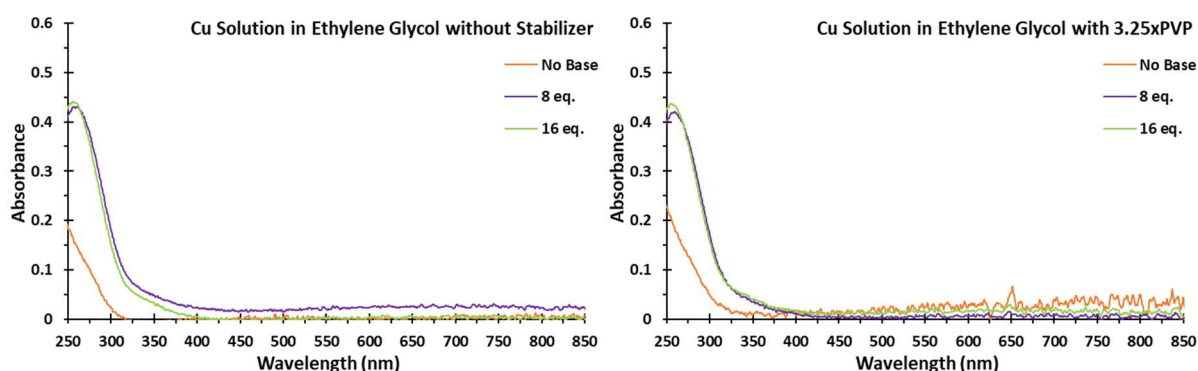


Figure 91 – UV-Vis analysis of Cu solution in ethylene glycol without stabilizer (left) and with 3.25xPVP (right) at different concentrations of NaOH.

The two aforementioned Cu solution samples with 16 eq. of NaOH, with and without stabilizer, were subject to microwave heating, same test previously done for Au in section 3.2.4 with the acid/base addition optimisation test.

The UV-Vis spectra and DLS analysis are presented in Figure 92 and compared to the operating conditions A and B, previously shown in Figure 90. Major changes to the UV-Vis spectra were observed with significant absorbance increases up to 550 nm wavelengths. Even though there was not a clear plasmon peak these changes are compatible with the production of Cu nanoparticles according to the literature.¹¹²⁻¹¹³ The DLS analysis was also consistent with the production of Cu nanoparticles with a calculated DLS average size for the trial without stabilizer of 152 ± 46 nm and for the trial with 3.25xPVP of 532 ± 227 nm.

Synthesis of Metal Nanoparticles by Microwave

3.5 Metal Nanoparticles Production under Batch Regime

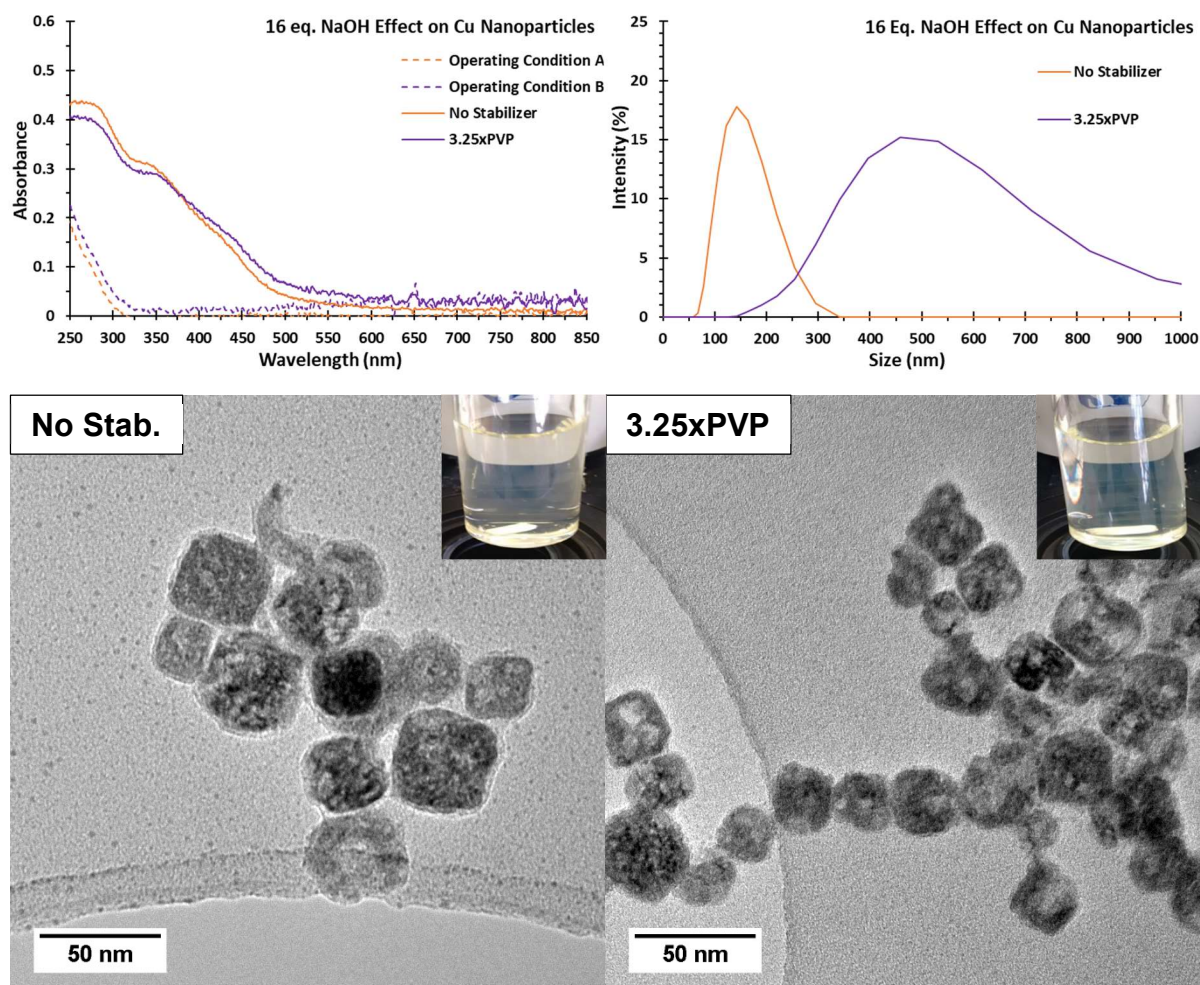


Figure 92 – Cu nanoparticles produced by microwave synthesis at 16 eq. of NaOH with UV-Vis (top left) and DLS (top right) analysis and TEM images for no stabilizer trial (bottom left) and 3.25xPVP trial (bottom right) with colloid photos included.

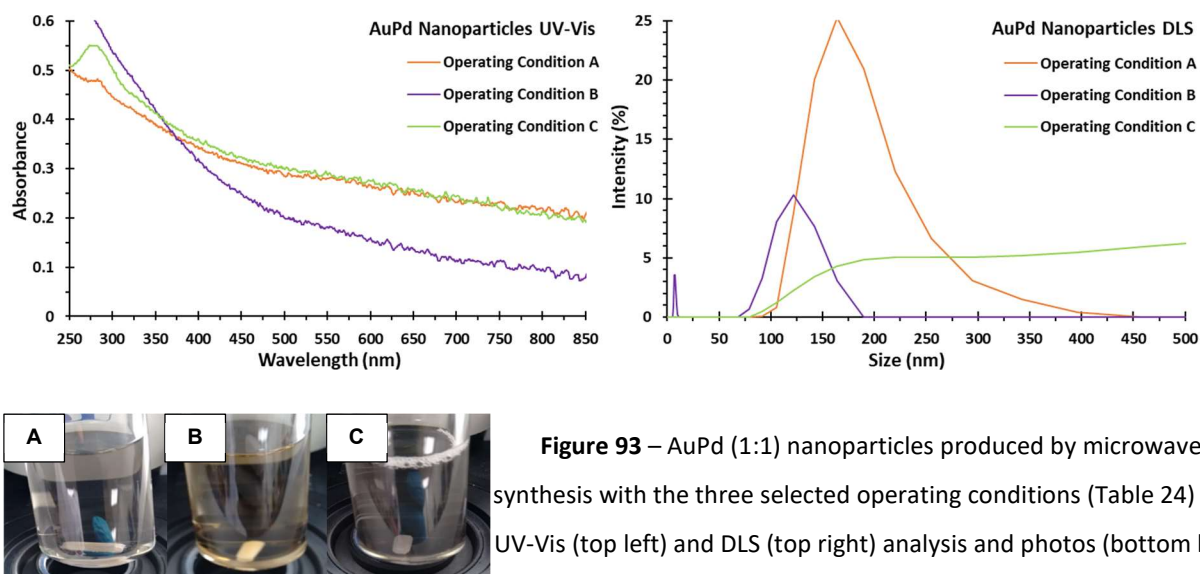
The TEM analysis confirmed for both trials the formation of Cu nanoparticles of similar size, around 50 nm. The Cu nanoparticles were mainly aggregated with a shape having a low circularity. This could explain the absence of a clear plasmon peak in the UV-Vis spectrum. However, it is still remarkable that just by adding NaOH to the Cu solution the microwave synthesis of Cu nanoparticles was now possible. The samples were also tested by adding NaBH_4 to the UV-Vis cuvette and no major changes were observed, an indication that reduction had been completed.

Synthesis of Metal Nanoparticles by Microwave

3.5 Metal Nanoparticles Production under Batch Regime

3.5.6 AuPd Nanoparticles

The UV-Vis and DLS spectra and photos of the AuPd (1:1 molar) nanoparticles produced with the three selected operating conditions are compared in Figure 93. Similar to the Pd nanoparticles also the AuPd (1:1 molar) nanoparticles do not present a plasmon peak.



The UV-Vis spectra of AuPd (1:1 molar) nanoparticles produced with the operating conditions A and C are very similar to the UV-Vis spectrum of the agglomerated Pd nanoparticles produced with the operating condition A shown in Figure 71.

As expected, the TEM analysis of AuPd (1:1 molar) nanoparticles produced with the operating condition A and shown in Figure 94 only revealed agglomerated nanoparticles. This is according to the high value of 181 ± 48 nm calculated for the average size with the DLS analysis.

Likewise, the TEM analysis of AuPd (1:1 molar) nanoparticles produced with the operating condition C and shown in Figure 95 only revealed agglomerated nanoparticles. This is also according to the high value of 643 ± 483 nm calculated for the average size with the DLS analysis.

Synthesis of Metal Nanoparticles by Microwave

3.5 Metal Nanoparticles Production under Batch Regime

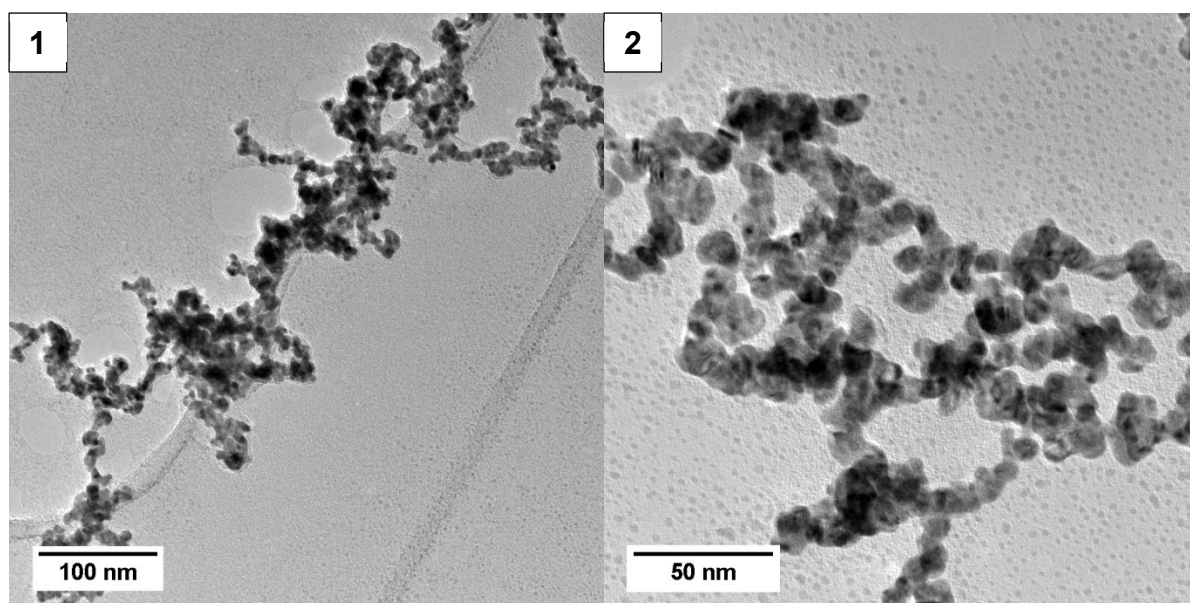


Figure 94 – TEM analysis of AuPd (1:1) nanoparticles produced by microwave synthesis with the operating condition A (Table 24).

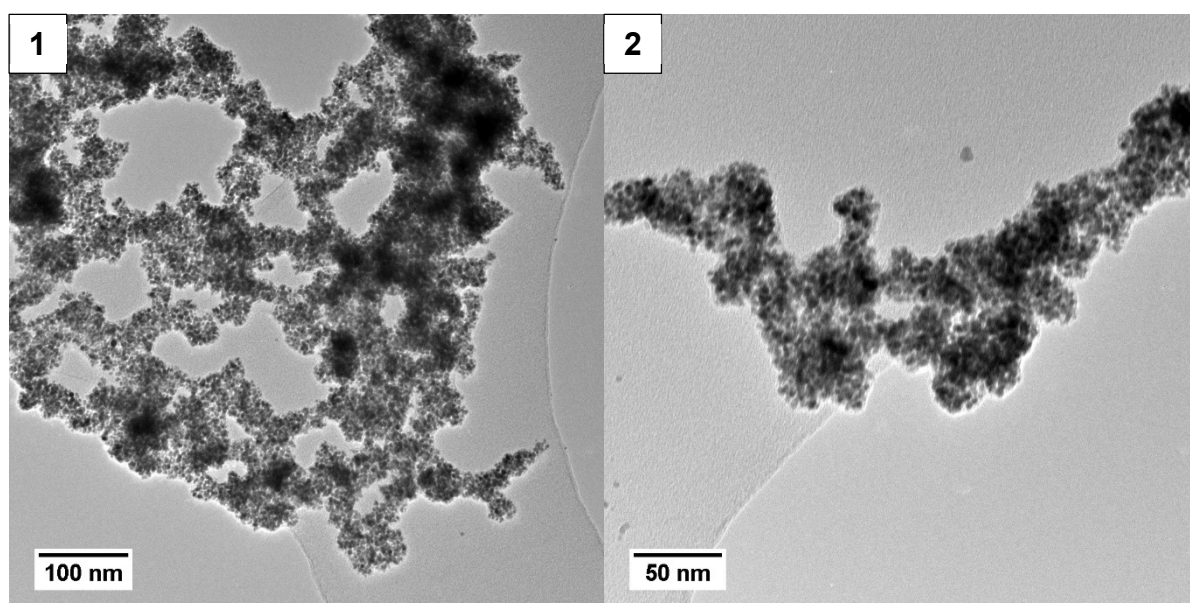


Figure 95 – TEM analysis of AuPd (1:1) nanoparticles produced by microwave synthesis with the operating condition C (Table 24).

The UV-Vis spectrum of AuPd (1:1 molar) nanoparticles produced with the operating condition B is actually almost identical to the UV-Vis spectra of Pd nanoparticles produced with the operating condition B shown in Figure 71 and AuPd/Pd nanoparticles produced with the traditional sol-immobilization protocol shown in Figure 15. All these nanoparticles present average sizes of around 3 nm. Therefore, it can also be formulated the hypothesis that AuPd (1:1 molar) nanoparticles produced with the operating condition B have a similar average size. The calculated DLS average size of 7.1 ± 1.0 nm also supports this hypothesis.

Synthesis of Metal Nanoparticles by Microwave

3.5 Metal Nanoparticles Production under Batch Regime

The TEM analysis of AuPd (1:1 molar) nanoparticles produced with the operating condition B and shown in Figure 96 confirmed the production of nanoparticles of small sizes with a calculated TEM average size of 3.0 ± 0.6 nm.

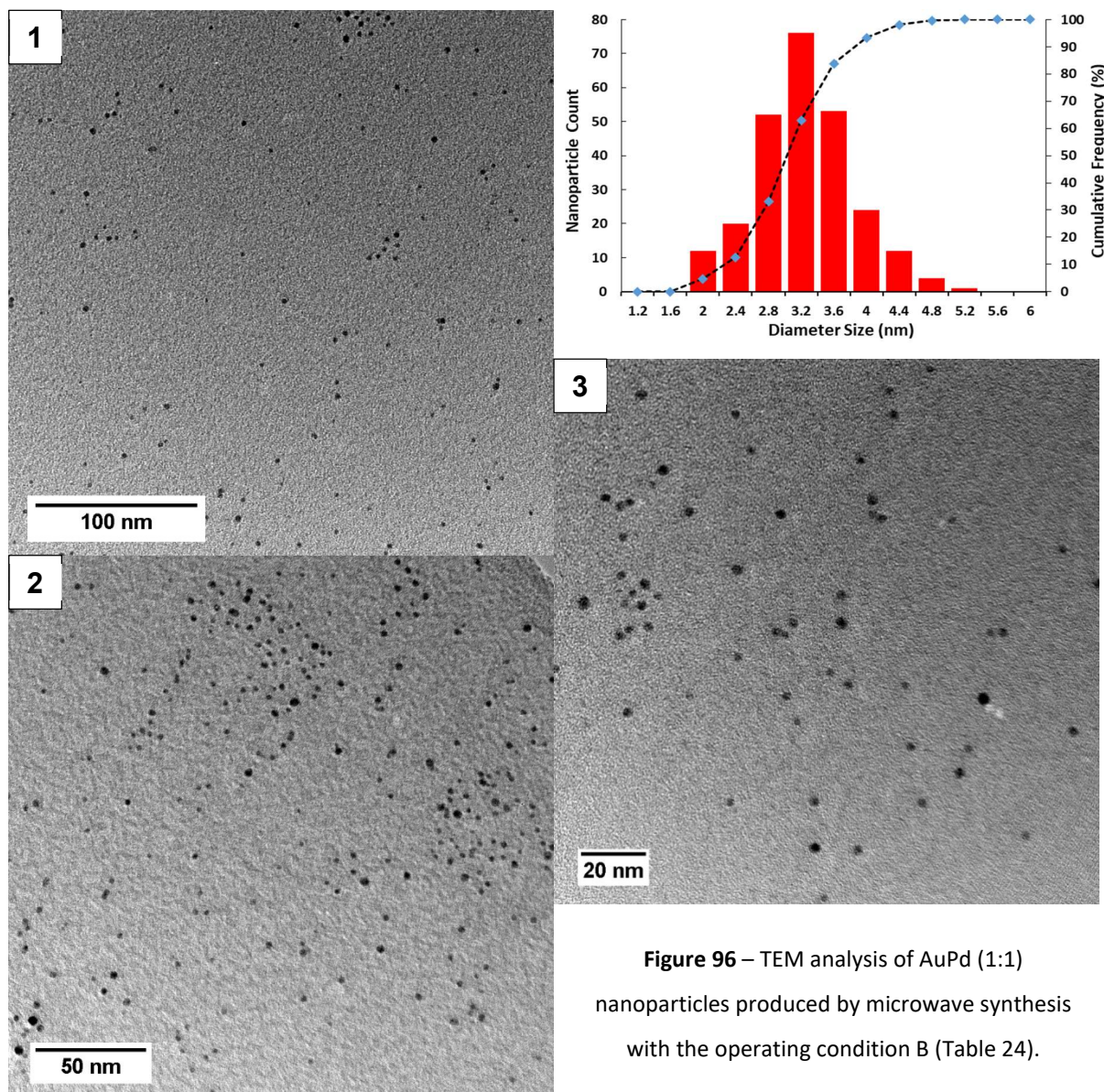


Figure 96 – TEM analysis of AuPd (1:1) nanoparticles produced by microwave synthesis with the operating condition B (Table 24).

Analysis with high-resolution TEM (STEM/HAADF mode) was also performed in order to confirm that the bimetallic nanoparticles were of the alloy type and that no individual Au or Pd nanoparticles had been produced. This high-resolution technique allowed to isolate individual AuPd nanoparticles and check their composition with EDX with compositions consistent with a 1:1 molar alloy observed. Two of the images obtained with HRTEM are shown in Figure 97.

Synthesis of Metal Nanoparticles by Microwave

3.5 Metal Nanoparticles Production under Batch Regime

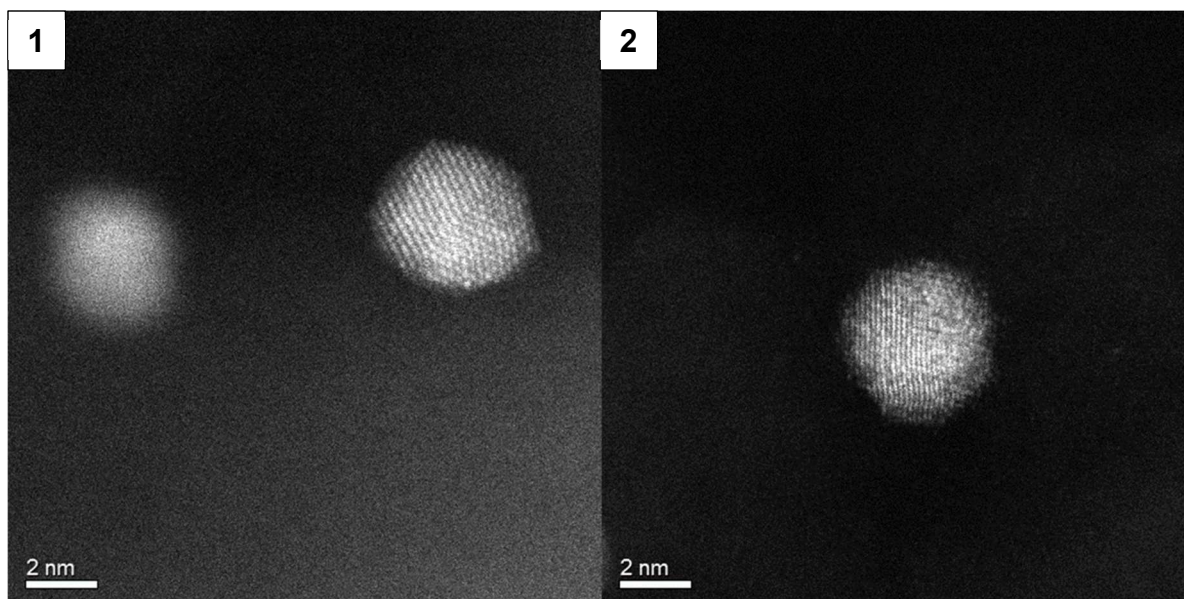


Figure 97 – High-resolution TEM (STEM/HAADF mode) analysis of AuPd (1:1) nanoparticles produced by microwave synthesis with the operating condition B (Table 24).

Moreover, lattice-fringe spacing was also according to the expected with a value of 0.233 nm calculated, between that of pure Au (0.237 nm) and that of pure Pd (0.226 nm). This lattice-fringe spacing analysis looks into creating diffraction patterns that can be observed by TEM which can then be used to estimate distance between atoms in one nanoparticle.¹¹⁵⁻¹¹⁶

The synthesis of AuPd nanoparticles with the operating condition B was also extended to different molar ratios, namely 7:1, 3:1, 1:3 and 1:7. The different UV-Vis and DLS spectra and photos can be observed in Figure 98 and are also compared to the molar ratio of 1:1.

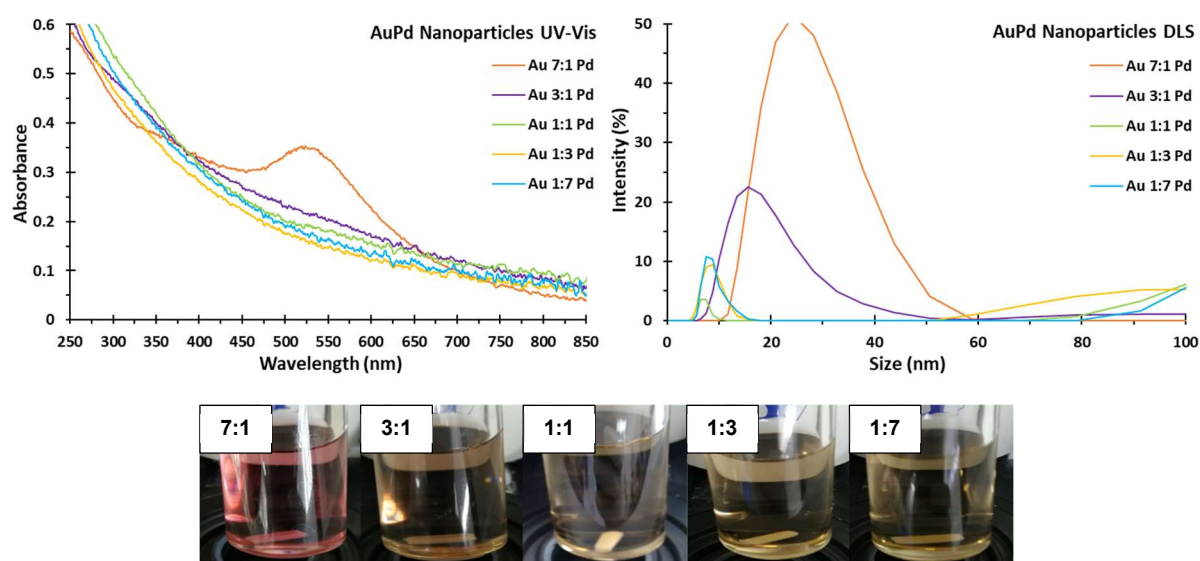


Figure 98 – AuPd nanoparticles at different molar ratios produced by microwave synthesis with the operating condition B (Table 24) with UV-Vis (top left) and DLS (top right) analysis and photos (bottom).

Synthesis of Metal Nanoparticles by Microwave

3.5 Metal Nanoparticles Production under Batch Regime

Overall the UV-Vis spectra of AuPd nanoparticles at different molar ratios were very similar to one another. The only major difference was related to the molar ratio of 7:1 with a plasmon peak in the 500-550 nm range observed. It looks like the UV-Vis spectrum of 7:1 was a hybrid of the one of pure Au in Figure 63 and the one of pure Pd in Figure 71. This could mean that the synthesis of Au 7:1 Pd alloy was unsuccessful and two types of nanoparticles were produced, pure Au nanoparticles and pure Pd nanoparticles.

The DLS analysis indicated a decrease on the average size when moving from Au rich alloys (7:1 with 26 ± 8 nm) to Pd rich alloys, but no major differences on the average sizes for the molar ratios of 1:1 (7.1 ± 1.0 nm), 1:3 (8.5 ± 1.9 nm) and 1:7 (8.7 ± 1.9 nm) are expected.

The different AuPd nanoparticles were also analysed by TEM. The first sample to be analysed was Au 7:1 Pd as shown in Figure 99.

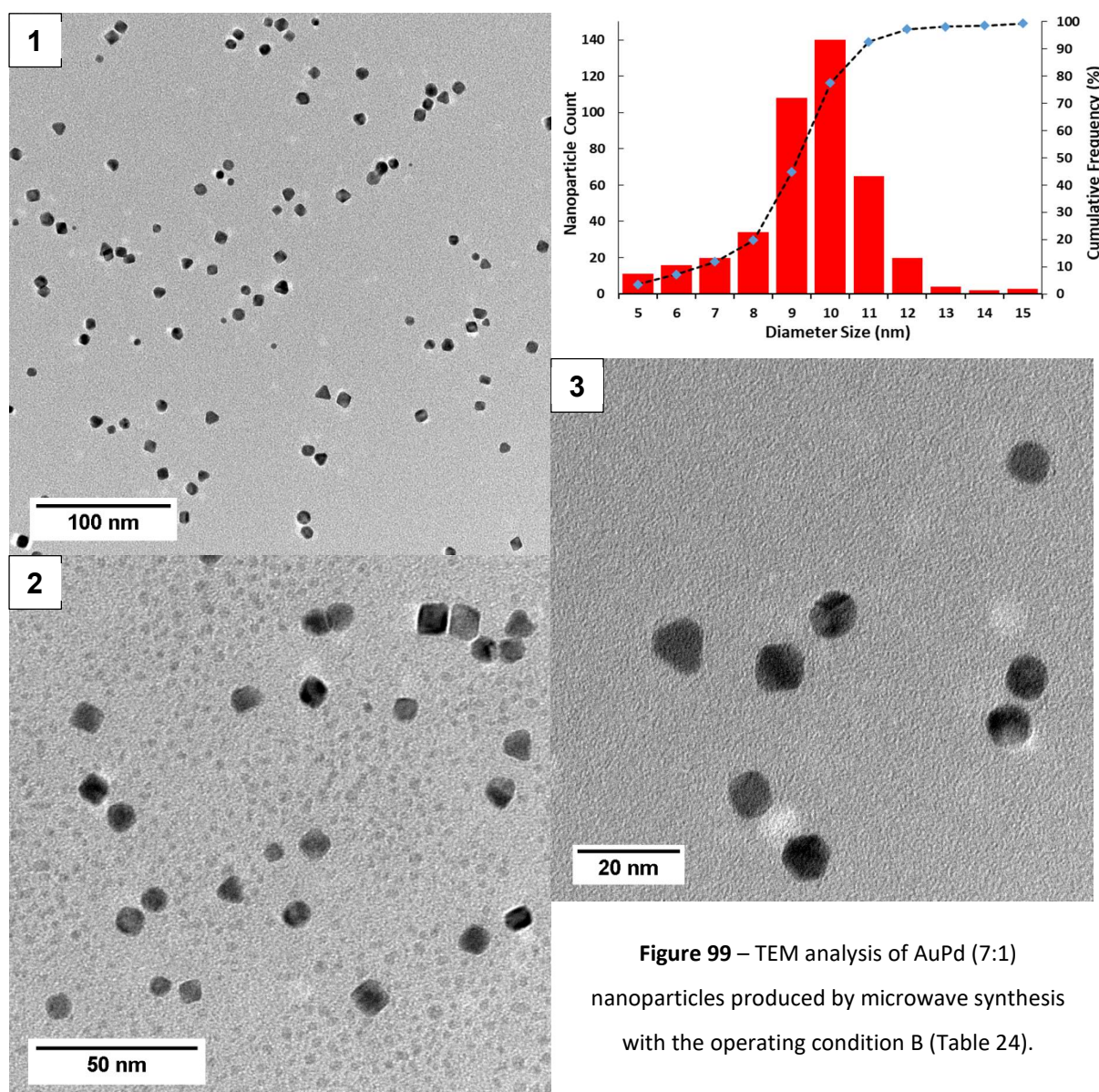


Figure 99 – TEM analysis of AuPd (7:1) nanoparticles produced by microwave synthesis with the operating condition B (Table 24).

Synthesis of Metal Nanoparticles by Microwave

3.5 Metal Nanoparticles Production under Batch Regime

Only one type of AuPd nanoparticles was observed with the TEM analysis for the Au 7:1 Pd sample. This is consistent with the formation of an alloy. However, in order to completely rule out the production of two types of metal nanoparticles, pure Au nanoparticles and pure Pd nanoparticles, high-resolution TEM (STEM/HAADF mode) analysis would also have to be performed, similar to what was done to the Au 1:1 Pd sample in Figure 97. In any case, the TEM analysis confirmed the production of large nanoparticles with an average size of 9.0 ± 1.8 nm, closer to the average size of Au nanoparticles in section 3.5.1 (12 ± 3.9 nm) than to the average size of Pd nanoparticles in section 3.5.2 (3.3 ± 0.8 nm).

The TEM analysis of the Au 3:1 Pd sample is shown in Figure 100. As predicted by DLS analysis the average size decreased from 9.0 ± 1.8 nm with Au 7:1 Pd to 4.7 ± 1.1 nm, a value much closer to the average size of Pd nanoparticles in section 3.5.2 (3.3 ± 0.8 nm).

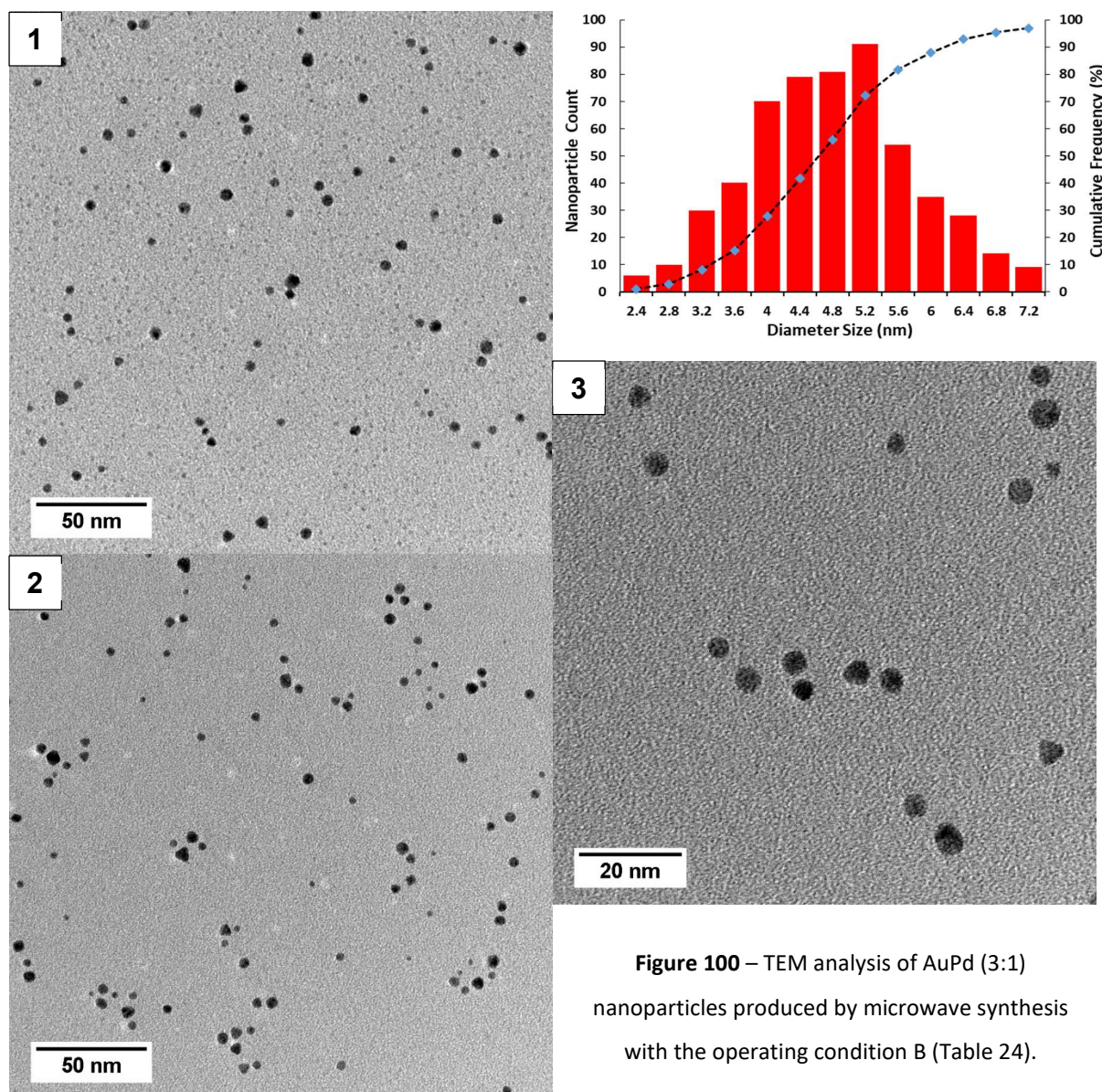


Figure 100 – TEM analysis of AuPd (3:1) nanoparticles produced by microwave synthesis with the operating condition B (Table 24).

Synthesis of Metal Nanoparticles by Microwave

3.5 Metal Nanoparticles Production under Batch Regime

Further TEM analysis to the sample Au 1:3 Pd in Figure 101 and sample Au 1:7 Pd in Figure 102 indicated average sizes of 3.2 ± 0.7 nm and 3.3 ± 0.8 nm respectively, very similar to the average size obtained for Au 1:1 Pd (3.0 ± 0.6 nm). Again, these average sizes are consistent with what had been predicted by DLS analysis.

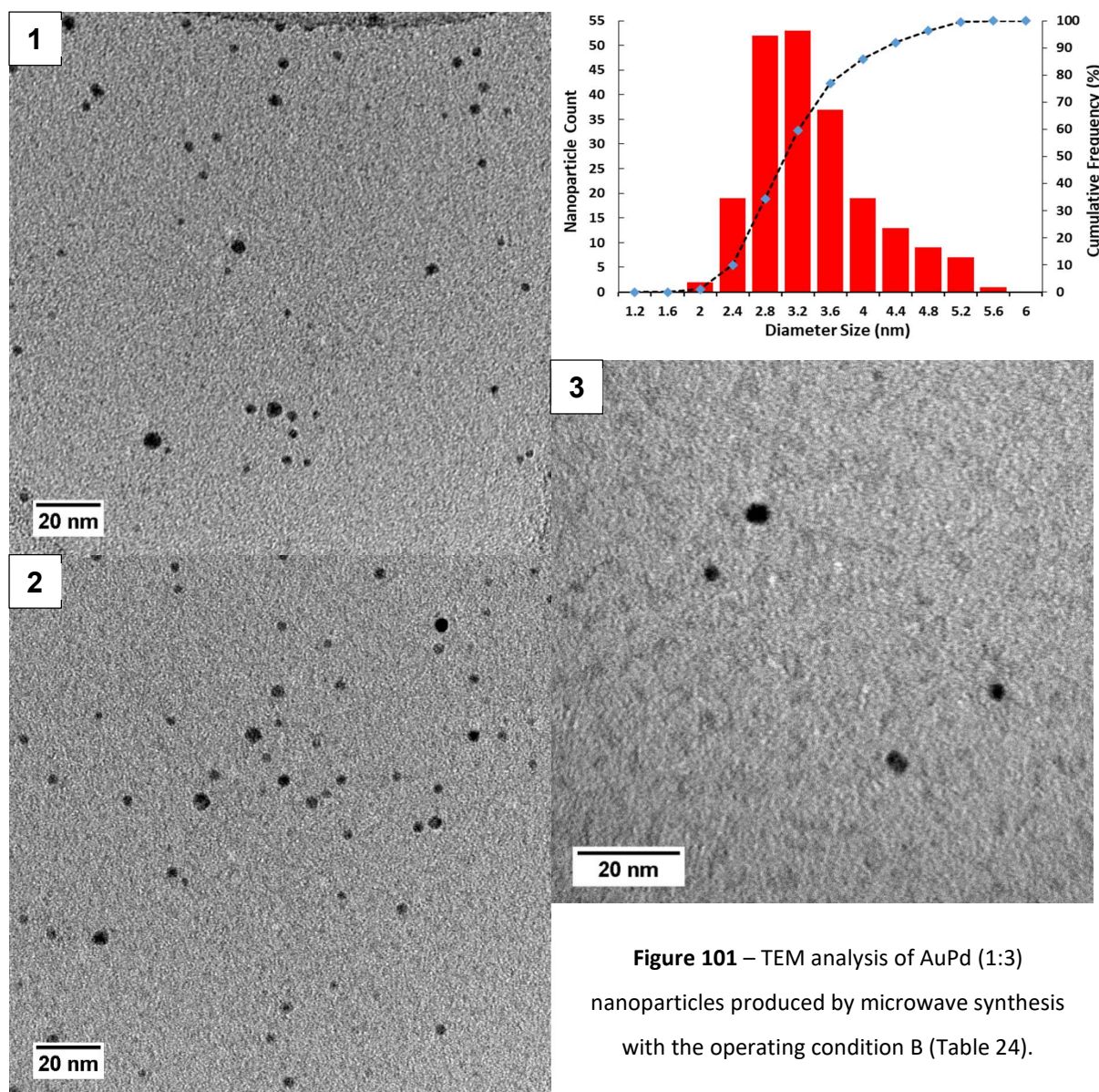


Figure 101 – TEM analysis of AuPd (1:3) nanoparticles produced by microwave synthesis with the operating condition B (Table 24).

Synthesis of Metal Nanoparticles by Microwave

3.5 Metal Nanoparticles Production under Batch Regime

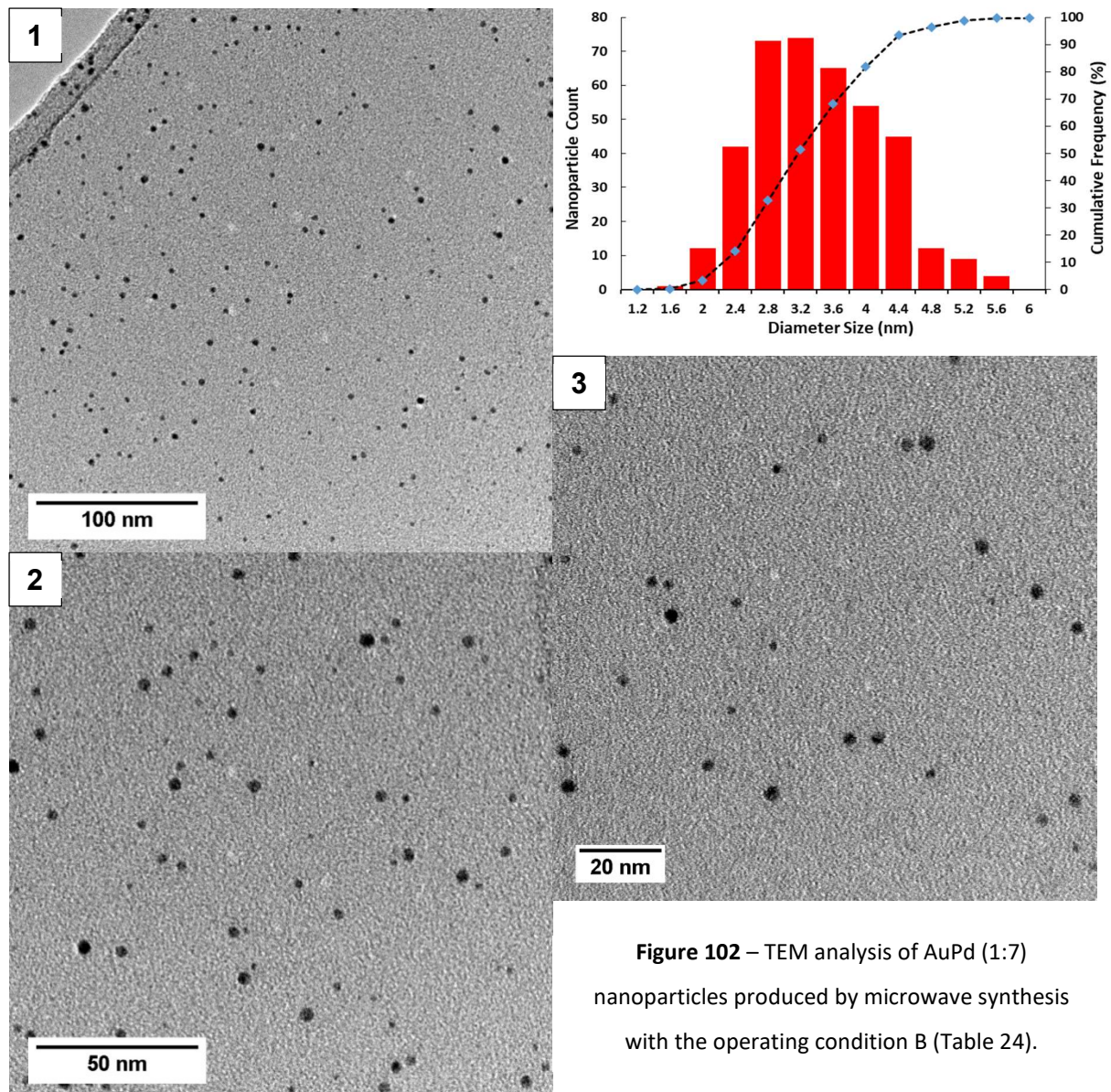


Figure 102 – TEM analysis of AuPd (1:7) nanoparticles produced by microwave synthesis with the operating condition B (Table 24).

3.6 Metal Nanoparticles Production under Continuous Flow Regime

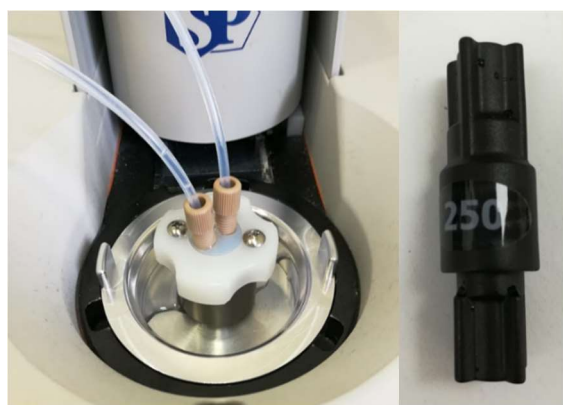
As mentioned in section 1.5, the production of metal nanoparticles can be increased when moving from batch synthesis to continuous flow synthesis. Moreover, continuous flow synthesis allows to manipulate and control additional parameters not possible under batch regime. This can result in higher heat and mass transfer coefficients which can then offer a better control over the metal nanoparticles average size, size distribution and shape.

The continuous flow reactor used was of the CSTR type and the experimental set-up was previously introduced in Figure 28 in section 2.3. Similar to the previous sections each sample was characterised with UV-Vis and DLS analysis and photos of the metal colloids were taken. The characterisation was further completed using TEM analysis with two selected images being presented for each sample.

Metal nanoparticles of Au and Pd were prepared using the operating condition B from Table 24 as this was the selected operating condition that in general produced smaller metal nanoparticles average sizes and narrower size distributions under batch regime as shown in section 3.5. The holding time of 5 min was converted to a residence time by manipulating the flow rate of the feeding metal solution which was set at 2.0 mL min^{-1} .

Unfortunately, production of metal nanoparticles was compromised due to the fouling phenomenon inside the experimental set-up tubing and the 10 mL vessel. This phenomenon was caused by the accumulation of metal nanoparticles on the walls. This has promoted heterogenous nucleation and interfered with the delicate balance between the mechanisms of reduction, nucleation and growth as explained by the LaMer plot, mentioned in section 1.4.1, and contributed to the production of large metal nanoparticles with a broad size distribution and of irregular shape. The experimental results for the production of Au nanoparticles are presented in section 3.6.1 and for the production of Pd nanoparticles in section 3.6.2.

There were also issues related to the quality of the flow cell supplied by the microwave manufacturer which may have compromised the experimental results. As shown in Figure 103



(left) the connection between the inlet/outlet tubing and the 10 mL vessel presented leaks. Also, the backflow valve shown in Figure 103 (right) was not working properly as prevented any flow and had to be removed. This left the entire system exposed to atmospheric pressure which resulted in the formation of bubbles due to the high synthesis temperature of $150 \text{ }^{\circ}\text{C}$.

Figure 103 – Microwave flow cell connection (left) and backflow valve (right).

Synthesis of Metal Nanoparticles by Microwave

3.6 Metal Nanoparticles Production under Continuous Flow Regime

3.6.1 Au Nanoparticles

The UV-Vis and DLS spectra obtained when trying to produce Au nanoparticles under continuous flow regime with the selected operating condition B are presented in Figure 104.

Samples were collected for UV-Vis analysis at the beginning of the synthesis and 30 and 60 min afterwards with the spectra being very similar to one another, an indication of a steady synthesis over time. However, when compared with the UV-Vis spectrum obtained under batch regime the Au nanoparticles production, average size and size distribution are expected to be very different as the plasmon peak absorbance has now decreased from 0.52 to around 0.30, the plasmon peak wavelength has now increased from 535 nm to around 580 nm and the wavelength range has now increased from 70 nm to around 130 nm.

The DLS analysis of the samples collected at the beginning of the synthesis and 60 min afterwards were also very similar with a calculated average size of around 110 ± 41 nm, a value much higher than the 5.4 ± 2.0 nm obtained under batch regime.

In order to show that different residence times could also influence the production of Au nanoparticles the flow rate was decreased at $t=60$ min to 1.0 mL min^{-1} which caused the residence time to increase from 5 min to 10 min and a sample was collected at $t=70$ min. As observed in Figure 104 the UV-Vis spectrum indicates that the experimental results became even worse. This outcome is according to the expected as the holding time and temperature optimisation tests in section 3.2.3 (Table 16) showed that the agglomeration effect can be enhanced as the holding time is increased at a fixed temperature. The fact that a lower flow rate resulted in a less turbulent flow was not important on this occasion and might even have contributed to enhancement of the fouling phenomenon, previously mentioned in section 3.6. Tests at higher flow rates/lower residence times could not be performed due to heating limitations as even when using the maximum power of 300 W the microwave device was unable to provide a temperature of $150 \text{ }^\circ\text{C}$ inside the 10 mL vessel.

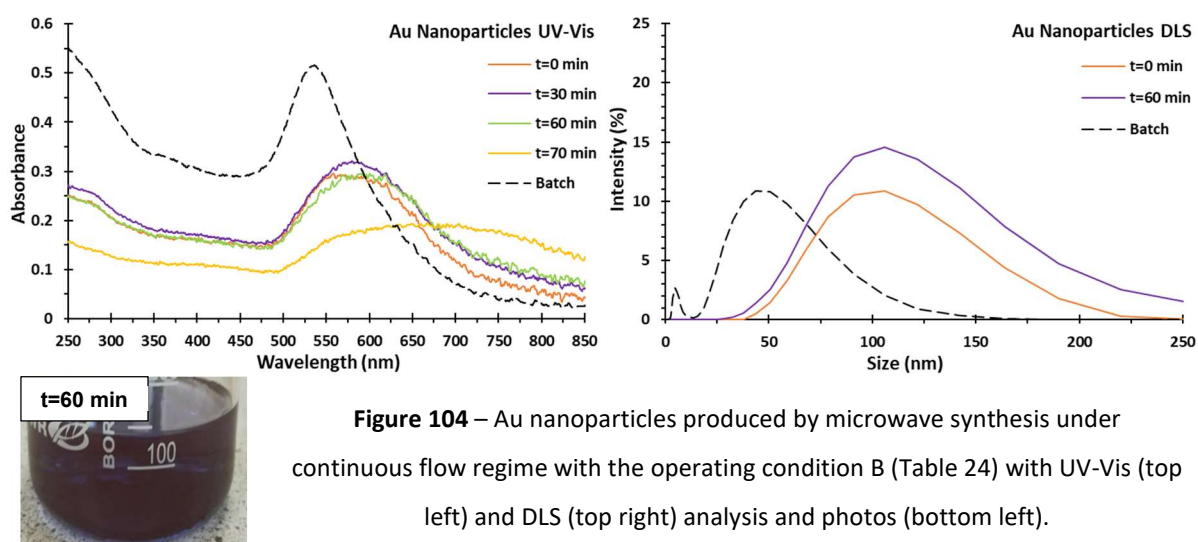


Figure 104 – Au nanoparticles produced by microwave synthesis under continuous flow regime with the operating condition B (Table 24) with UV-Vis (top left) and DLS (top right) analysis and photos (bottom left).

Synthesis of Metal Nanoparticles by Microwave

3.6 Metal Nanoparticles Production under Continuous Flow Regime

The TEM analysis of the samples collected at the beginning of the synthesis and 60 min afterwards is shown in Figure 105 and confirmed that the produced Au nanoparticles were very different from the ones obtained under batch regime and shown in Figure 65. They present large sizes, are of irregular shape and were not well dispersed on the TEM grid.

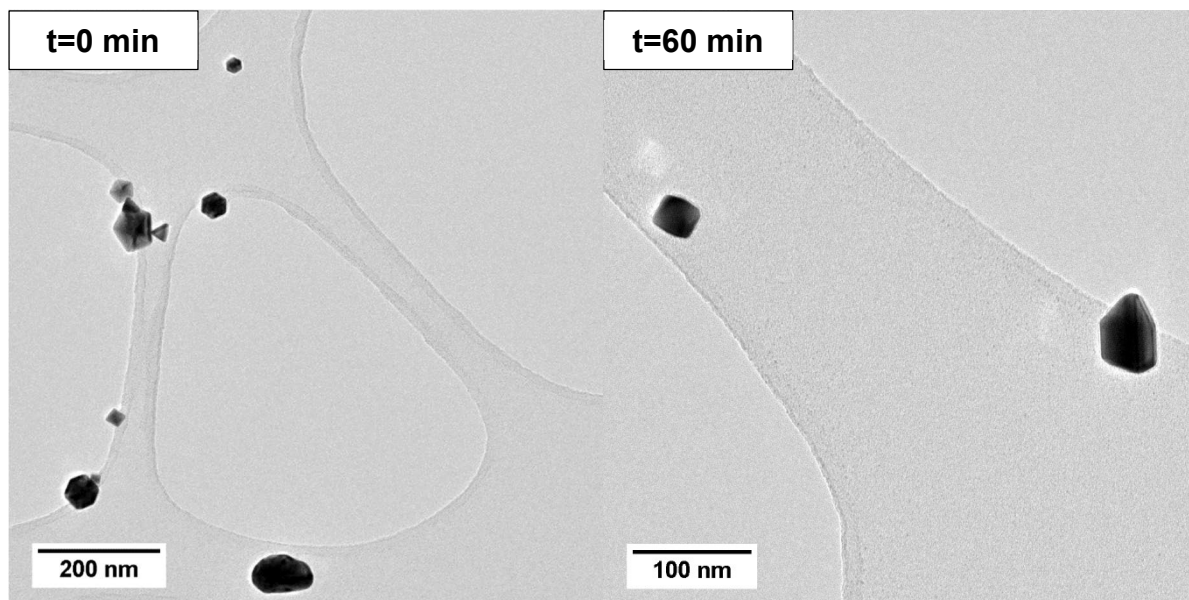


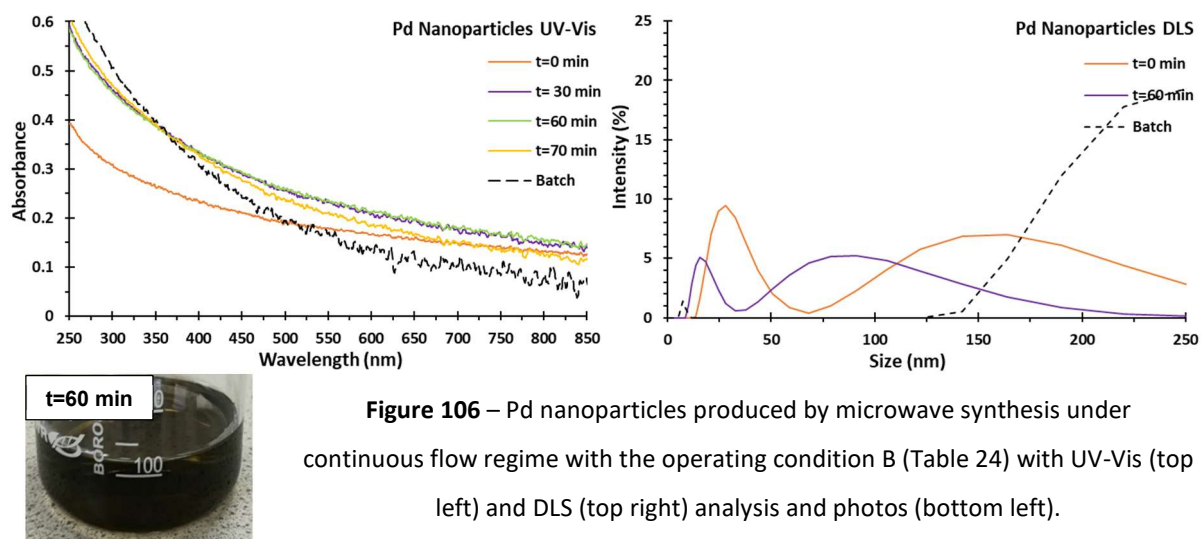
Figure 105 – TEM analysis of Au nanoparticles produced by microwave synthesis under continuous flow regime with the operating condition B (Table 24) at t=0 min (left) and t=60 min (right).

3.6.2 Pd Nanoparticles

The UV-Vis spectra of Pd nanoparticles does not present a plasmon peak. However, it has been previously demonstrated in section 3.5.2 that it is still possible to correlate changes in the UV-Vis spectrum with the production of Pd nanoparticles of different features. Therefore, similar to Au nanoparticles in section 3.6.1, the UV-Vis spectra of Pd nanoparticles produced under continuous flow regime and shown in Figure 106 is consistent with worse experimental results for the Pd nanoparticles production, average size and size distribution when compared to what was obtained under batch regime. Furthermore, the UV-Vis spectrum at t=0 min is very different from the UV-Vis spectra for the samples collected 30 and 60 min afterwards, which indicates that steady state was only achieved between t=0 min and t=30 min.

The DLS analysis also supports this hypothesis with the sample collected at the beginning of the synthesis presenting an average size of 30.0 ± 9.8 nm and the sample collected 60 min afterwards presenting an average size of 17.6 ± 5.1 nm, values higher than the 7.7 ± 1.2 nm obtained under batch regime. The higher value of 30.0 ± 9.8 nm is according to the fact that steady state had not yet been achieved at t=0 min.

Similar to Au nanoparticles in section 3.6.1, the flow rate at t=60 min was also decreased to 1.0 mL min^{-1} which caused the residence time to increase from 5 min to 10 min and a sample was collected at t=70 min. Small UV-Vis changes consistent with an enhanced agglomeration effect were observed. This outcome is according to the expected as the Au holding time and temperature optimisation tests in section 3.2.3 (Table 16) showed that the agglomeration effect can be enhanced as the holding time is increased at a fixed temperature. The fact that a lower flow rate resulted in a less turbulent flow was not important on this occasion and might even have contributed to enhancement of the fouling phenomenon, previously mentioned in section 3.6. Again, for the same reasons as with Au, tests at higher flow rates/lower residence times could not be performed.



Synthesis of Metal Nanoparticles by Microwave

3.6 Metal Nanoparticles Production under Continuous Flow Regime

The TEM analysis of the samples collected at the beginning of the synthesis and 60 min afterwards is shown in Figure 107. The images confirm that large Pd nanoparticles and of irregular shapes were produced. These Pd nanoparticles are very different from the ones obtained under batch regime and shown in Figure 73.

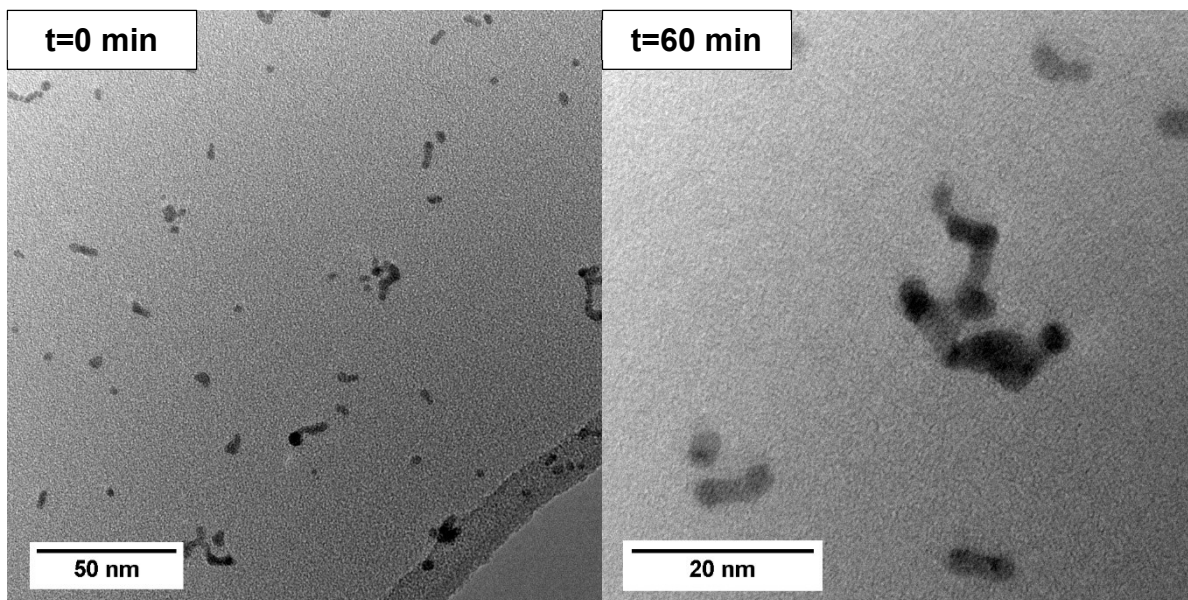


Figure 107 – TEM analysis of Pd nanoparticles produced by microwave synthesis under continuous flow regime with the operating condition B (Table 24) at t= 0 min (left) and t= 60 min (right).

3.7 Conclusions

Monometallic metal nanoparticles of Au, Pd, Ir and bimetallic metal nanoparticles of the alloy type of AuPd at different molar ratios (7:1, 3:1, 1:1, 1:3, 1:7) were successfully synthesised using microwave heating. It was also verified that Ag nanoparticles production was possible but the experimental results were compromised due to incomplete reduction. All metal nanoparticles were analysed by UV-Vis, DLS and TEM in order to assess production, average size, size distribution and shape. The AuPd (1:1) nanoparticles were further analysed with high-resolution TEM (STEM/HAADF mode) and EDX which confirmed that they were of the alloy type and presenting the expected composition.

Three selected operating conditions have been identified by taking into consideration the Au optimisation experimental results from section 3.2 and the mechanistic studies from section 3.3. The Au optimisation tests aimed to understand the effect of stirrer, metal concentration, holding time and temperature, acid/base addition, type of solvent, solvent composition and type and concentration of stabilizer. The mechanistic studies aimed to deliver an insight on the influence of heating, NaOH addition, stabilizer, solvent and Au oxidation state on the metal nanoparticles formation mechanism (metal reduction, nucleation and growth).

The best experimental results were obtained with the operating condition B, which used ethylene glycol as the reducing agent and PVP as the stabilizer. Even though the minimum Au nanoparticles average size that could be obtained was of only 12 ± 3.9 nm, overall the experimental results were in line with the best experimental results found in the literature, in particular if having in consideration that the metal nanoparticles are meant to be used for catalytic purposes and an excess of stabilizer is highly undesirable.

It is remarkable that in the case of Ir nanoparticles the operating condition A, without any stabilizer, could produce such small Ir nanoparticles, a result very different from what was obtained for the other metal nanoparticles. It is also remarkable that NaOH addition could lead to an enhanced effect for production of metal nanoparticles which in the case of Cu, previously shown to not be reduced, could even result now in the production of Cu nanoparticles.

The work with continuous flow synthesis did not produce the expected results. This was due to a fouling phenomenon and issues related to the experimental set-up. However, it can still be said that this work demonstrated that metal nanoparticles can be produced using similar conditions to the ones used under batch regime and that the experimental results were also promising as there is easily room for improvement, for example by adopting a different reactor configuration or by changing the tubing material.

4 Synthesis of Metal Nanoparticles by Ultrasound

4.1 Overview

This chapter presents all the experimental results associated with the ultrasound synthesis of metal nanoparticles, namely Au, Pd and bimetallic alloys of AuPd at a molar ratio of 1:1. The working principle of the ultrasound synthesis is presented in section 1.4.4 and the ultrasound synthesis experimental procedure is described in section 2.4.

Most of the produced metal nanoparticles were characterised by UV-Vis, DLS and TEM analysis. All samples analysed by TEM were also analysed by EDX in order to rule out any contamination. Detailed information about these techniques can be found in section 2.2. The metal nanoparticles identified as having the potential to produce good catalytic results for the reactions presented in chapter 1 were further characterised and analysed after being supported as shown in chapter 5.

In section 4.2 the ultrasound standard operating conditions are defined based on the traditional sol-immobilization protocol (section 1.4.2.1) and the work previously developed with the microwave synthesis (chapter 3) and work found in the literature. The next step consisted in optimising the operating conditions for the production of Au nanoparticles. The optimisation tests studied the effect of wave amplitude, metal concentration, sonication time, solvent composition and type and concentration of stabilizer. Usually for each test only one operating condition was varied and all the others were kept at standard operating conditions. When compared to other metals Au is a good starting model to understand new experimental protocols (see section 3.1 for more details).

In section 4.3 the best ultrasound synthesis operating conditions are defined by having in consideration the Au optimisation experimental results from section 4.2. The stability and reproducibility of ultrasound synthesis was also analysed.

In section 4.4 the experimental results of all the metal nanoparticles produced at the best ultrasound synthesis operating conditions are presented and analysed.

As mentioned in section 2.4, due to safety/technical reasons the ultrasound operation was limited. This has seriously reduced the number of ultrasound experiments undertaken, in particular the ones necessary for a correct optimisation procedure, similar to what was done with the microwave. Despite this major limitation, it was still possible to observe, register and analyse interesting experimental results during the 1-year operation of the ultrasound.

Synthesis of Metal Nanoparticles by Ultrasound

4.2 Au Optimisation Tests

4.2 Au Optimisation Tests

Some of the standard operating conditions adopted for microwave synthesis were based on the traditional sol-immobilization protocol (section 1.4.2.1). Therefore, the volume of 400 mL was scaled down to 75 mL, a significant increase from the 20 mL used for microwave synthesis. The metal concentration was kept at 0.025 g L^{-1} or 0.13 mM. The microwave Au optimisation test in section 3.2.2 has shown this concentration to be a good compromise between metal production and average size and size distribution as the agglomeration effect was progressively enhanced above this concentration.

The reducing action of several solvents was tested with microwave synthesis as shown in section 3.2.5 and best experimental results were obtained with ethylene glycol. For this reason, ethylene glycol was also chosen for ultrasound synthesis. In addition, temperatures of $150 \text{ }^\circ\text{C}$ are not used, as it happens with the microwave synthesis, but the cavitation phenomenon, explained in section 1.4.4, is able to cause the bulk of the liquid to increase its temperature with preliminary trials indicating final temperatures after 15 min of sonication in the range of $70\text{--}90 \text{ }^\circ\text{C}$. This temperature would be enough to expose the surrounding staff to solvent vapours if low boiling compounds such as methanol or ethanol were used as the sound box does not provide enough protection and is too big to be placed inside a fume hood. The use of ethylene glycol is also supported by ultrasound work found in the literature. This was the case of Kan *et al.*¹¹⁷ who have produced bimetallic AuPd nanoparticles of different structures and Nemamcha *et al.*¹¹⁸ who have produced Pd nanoparticles.

As shown in Equation 13, sonication of water generates hydrogen radicals capable of reducing metal ions. Some authors have adopted water as the synthesis solvent. This was the case of Mizukoshi *et al.*¹¹⁹ who have produced AuPd nanoparticles of the core-shell type and of Anandan and Ashokkumar¹²⁰ who have produced Au nanoparticles. However, as expected the required sonication times are very long due to the weak reducing power of water, 66 hours were even observed (production of 0.04 mg Au nanoparticles/hour),¹²⁰ which compares with a microwave synthesis time of only 5 min (production of 6 mg Au nanoparticles/hour). Moreover, it is not clear how much of the reducing power can be attributed only to water as sodium dodecyl sulphate¹¹⁹ and 1-propanol¹²⁰ were also employed.

A mixed solution can then be adopted by combining ethylene glycol and water. This was the case of Jhuang and Cheng¹²¹ who have worked with a 20/80 % water/ethylene glycol mixture to produce Ag nanoparticles. Moving metal nanoparticles production to greener and more economic conditions by decreasing the amount of ethylene glycol are also important targets. Also, if the trials were carried out with pure ethylene glycol a regular 2.5 L bottle would only be enough for 33 optimisation trials whereas with microwave this number was of 125. The adopted standard operating conditions have been set at 75/25 % water/ethylene glycol.

Synthesis of Metal Nanoparticles by Ultrasound

4.2 Au Optimisation Tests

It has been previously shown with the microwave optimisation tests in section 3.2 that the use of stabilizers in mixtures of water and ethylene glycol was associated with worse experimental results, particularly when working with PVA as a bimodal distribution was even observed. Eventually, this was linked to differences in the solubility of the stabilizers in water and ethylene glycol, with PVA being much less soluble in ethylene glycol than PVP, even when applying moderate heating. This solubility effect has then in temporary water rich regions of the mixture enhanced the stabilizers reduction mechanism, shown in Equation 9 for the PVA and in Equation 10 for the PVP. However, as mentioned already, a major difference between microwave and ultrasound synthesis is the working temperature (150 °C vs. 70-90 °C). In order for the stabilizers to act as reducing agents a high temperature is necessary. Therefore, it is expected that during ultrasound synthesis no reducing action can be attributed to the stabilizers. Preliminary tests of Au in water with a stabilizer/metal weight ratio of 6.5 indicated that after 15 min of sonication no changes to the Au solution UV-Vis spectrum were observed. This confirmed that with the ultrasound synthesis the stabilizers are not able to reduce the metal ions the same way they were with microwave synthesis.

Moreover, similar to what was done with the microwave mechanistic study in section 3.3.4.4, a preliminary test of PVA in ethylene glycol confirmed that no new NMR peaks were produced after 15 min of sonication and no degradation of PVA is expected with the ultrasound synthesis. This is also the result of the lower working temperature for the ultrasound synthesis.

Therefore, after having in consideration the previous points the adopted stabilizer has been chosen to be PVA, same as in the traditional sol-immobilization protocol. The PVA also offers a smaller protective factor than PVP, which means it is less likely to leave residues on the surface of the catalyst and compromise the catalytic activity by hindering the access of the substrate to the active sites. In connection to this point, it was also decided to work with a standard PVA/metal weight ratio of only 0.65, same as in the traditional sol-immobilization protocol, even though the microwave stabilizer optimisation test in section 3.2.7 indicated better experimental results at higher stabilizer/metal weight ratios.

The ultrasound device operates at a fixed wave frequency of 20 kHz but the wave amplitude can be tuned, from a relative scale of 50 % to a maximum 100 %. According to Equation 11 the energy intensity of the ultrasound wave is proportional to the square of the wave amplitude, *i.e.* the energy intensity at 100 % amplitude is 4x higher than at 50 % amplitude. For instance, the same energy can be delivered during the ultrasound synthesis by operating at 50 % amplitude for 20 min or at 100 % amplitude for 5 min.

However, assuming a constant overall heat transfer coefficient from the mixture to the surroundings, higher temperatures are expected to be obtained when working at 100 % amplitude than at 50 % amplitude. As a result experimental results at 100 % amplitude are

Synthesis of Metal Nanoparticles by Ultrasound

4.2 Au Optimisation Tests

expected to be worse because the metal nanoparticles growth rate is strongly dependent on the temperature than the metal nanoparticles nucleation rate as suggested by Figure 12. For this reason, the standard amplitude has been set at 50 %. The associated sonication time has been fixed at 15 min, an increase from the microwave synthesis time of 5 min. This increase was to offset the lower amount of energy delivered when compared to what would be delivered at a 100 % amplitude and related to the fact that the volume composition of ethylene glycol, main reducing agent, was of only 25 %. The ultrasound standard operating conditions selected for the Au nanoparticles optimisation tests are summarized in Table 29.

Table 29 – Standard operating conditions for the Au nanoparticles ultrasound optimisation.

Parameter	Value
Amplitude	50 %
Solvent (v/v)	75 % Water + 25 % Ethylene Glycol
Sonication Time	15 min
Volume of Mixture	75 mL
PVA/Au Weight Ratio	0.65
Au Concentration	0.025 g L ⁻¹ or 0.13 mM
Precursor	HAuCl ₄

The UV-Vis spectra of three trials performed at the ultrasound standard operating conditions are presented in Figure 108 with average values for the plasmon peak absorbance (0.18), plasmon peak wavelength (540 nm) and wavelength range (87 nm) calculated.

Photos of the three produced colloids are also shown, with small colour differences observed between trials. As explained in section 3.2, the environmental light can affect the colour perception in each photo rendering comparisons based in colour alone inaccurate. For this reason, the metal colloids photos should serve merely as an indication and only UV-Vis comparisons are reliable enough.

One of the trials was characterised by DLS. An average DLS size distribution having two peaks was calculated with average size for the first peak of 10 ± 3.4 nm and for the second peak of 129 ± 79 nm. This is similar to what was observed with the citrate protocol (section 1.4.2.2) and with the microwave synthesis (chapter 3). It is not clear why two peaks were observed but as mentioned in section 2.2.2 the DLS results are affected by the presence of a stabilizer, the nanoparticles shape and the nanoparticles degree of aggregation. Moreover, the first peak is the most relevant as DLS is an intensity-weighted particle size measurement instead of a mass or number weighted particle size measurement with the amount of scattered light strongly proportional to the particle size. In this chapter only the first DLS peak is reported.

Synthesis of Metal Nanoparticles by Ultrasound

4.2 Au Optimisation Tests

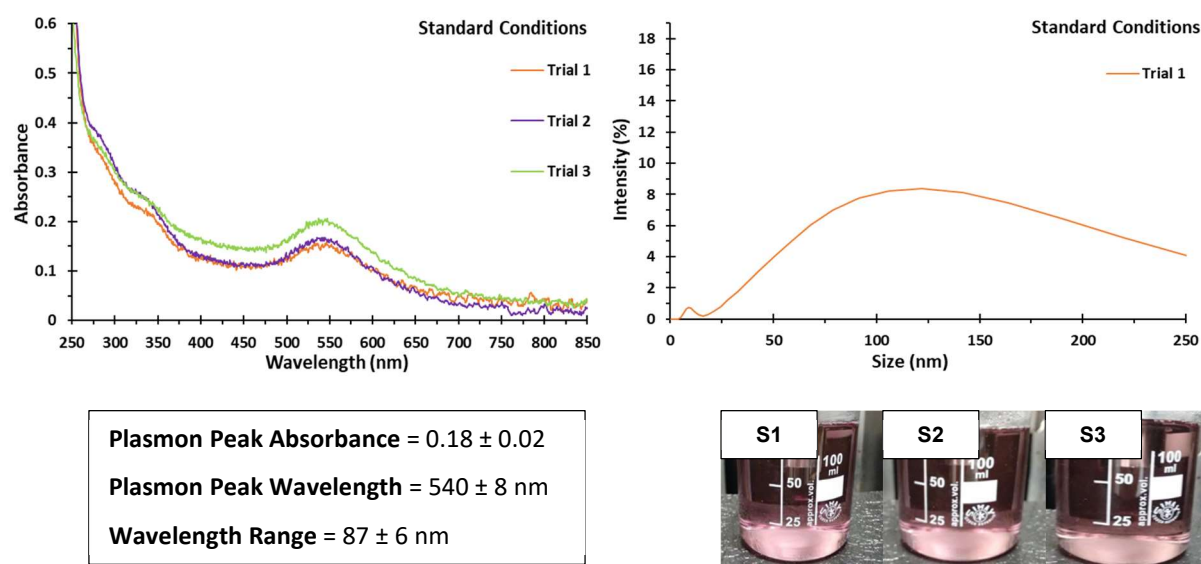


Figure 108 – Au nanoparticles produced at standard operating conditions with UV-Vis (top left) and DLS (top right) analysis and photos for the different trials (bottom).

The average plasmon peak wavelength of 540 nm and the wavelength range of 87 nm are similar to the values observed when working with the microwave synthesis. However, direct comparisons should be avoided as with the microwave synthesis the solvent used was pure ethylene glycol whereas with the ultrasound synthesis the solvent was a mixture of water and ethylene glycol and according to Equation 1, the extinction cross section σ_{ext} , a measure of the light absorbance and scattering, is dependent on the solvent dielectric constant (see section 3.2 for more details). Therefore, it can only be said that the expected average size for the Au nanoparticles produced with the ultrasound synthesis should be of the same order of magnitude than what was observed with the microwave synthesis.

It is remarkable that the plasmon peak absorbance of 0.18 is significantly lower than what was observed with the microwave synthesis (0.52). The expected UV-Vis spectra differences due to different dielectric constants are not enough to explain this gap. Upon addition of NaBH_4 to the UV-Vis cuvette major changes were observed. It is clear that the Au solution had not been fully reduced, an indication already that the energy intensity associated with the wave amplitude of 50 % is not enough and will have eventually to be increased. This is further analysed in the wave amplitude optimisation test.

Other tests were performed in order to understand the effect of metal concentration, sonication time, solvent composition and type and concentration of stabilizer. Usually, for each test only one parameter was varied and all others were kept as shown in Table 29. The results were compared with the average of the three UV-Vis spectra and with the DLS spectrum presented in Figure 108 and with the photo of trial 2 (S2). However, DLS analysis was not performed to all trials as it is not able to detect small trends in the nanoparticles average size.

Synthesis of Metal Nanoparticles by Ultrasound

4.2 Au Optimisation Tests

4.2.1 Wave Amplitude

In total three other wave amplitudes (60, 70 and 80 %) were compared to the standard wave amplitude of 50 %. The UV-Vis spectra in Figure 109 show that the production of Au nanoparticles can be greatly improved when increasing the wave amplitude. This is related to better reduction of the Au ions due to higher supply of energy leading to a higher concentration of radical species. According to Equation 11 the energy intensity of the ultrasound wave is proportional to the square of the wave amplitude. Full reduction was only achieved at a wave amplitude of at least 70 %. This was confirmed with the NaBH₄ addition test.

The experimental results continuously improved as the wave amplitude increased. As shown in Table 30 the Au nanoparticles production indicated by the plasmon peak absorbance went from 0.18 to 0.64. Likewise, the Au nanoparticles average size indicated by the plasmon peak wavelength went from 540 to 533 nm and the Au nanoparticles size distribution indicated by the wavelength range went from 87 to 63 nm. No trials were performed at wave amplitudes higher than 80 % due to safety reasons as the loud noise produced during the ultrasound operation became even worse and an undesired mixture temperature of 90 °C had already been achieved. The DLS analysis was also according with the UV-Vis trend with calculated DLS average sizes of 10 ± 3.4 nm for the standard condition, 6.1 ± 2.9 nm for the 60 % amplitude, 5.4 ± 2.4 nm for the 70 % amplitude and 3.6 ± 1.1 nm for the 80 % amplitude.

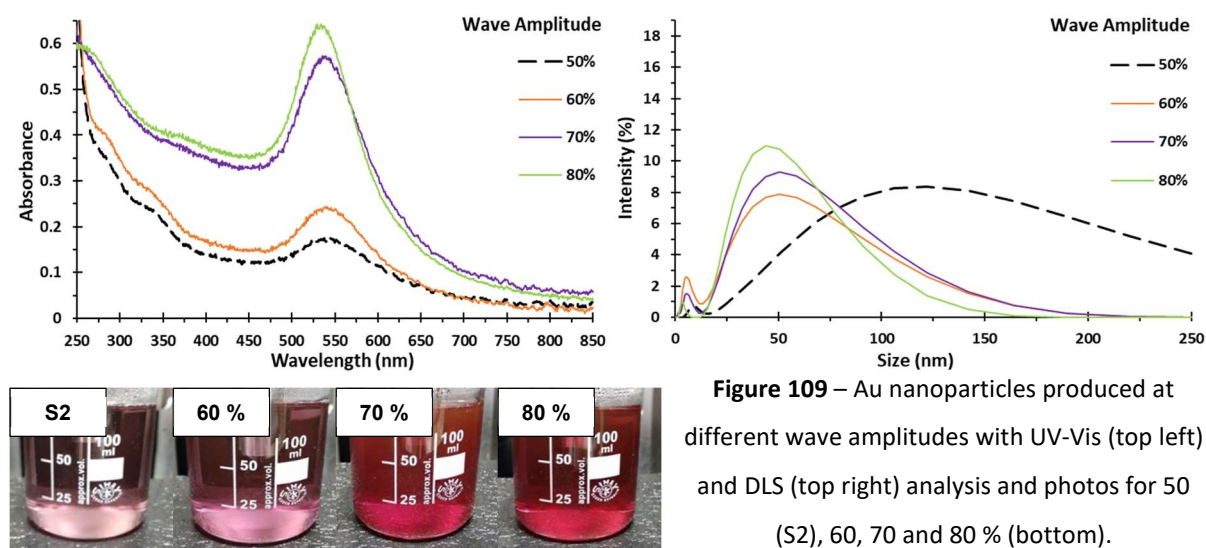


Figure 109 – Au nanoparticles produced at different wave amplitudes with UV-Vis (top left) and DLS (top right) analysis and photos for 50 (S2), 60, 70 and 80 % (bottom).

Table 30 – Au nanoparticles experimental results at different wave amplitudes.

Wave Amplitude %	Plasmon Peak Absorbance	Plasmon Peak Wavelength (nm)	Wavelength Range (nm)
50 (standard)	0.18	540	87
60	0.24	540	77
70	0.57	539	72
80	0.64	533	63

Synthesis of Metal Nanoparticles by Ultrasound

4.2 Au Optimisation Tests

4.2.2 Metal Concentration

Two additional Au solutions of different concentrations were tested. Compared to the standard condition of 0.13 mM one solution presented a lower concentration (0.065 mM) and the other presented a higher concentration (0.26 mM). As shown in Figure 110 (left) both concentrations have UV-Vis spectra consistent with the production of larger Au nanoparticles with a broader size distribution. The experimental results in Table 31 show higher plasmon peak wavelengths of 568 and 570 nm and higher wavelength ranges of 117 and 156 nm. The plasmon peak absorbances are according to the ratios due to differences in the concentration of the Au solutions, half and double of 0.13 mM.

It was previously observed with the microwave optimisation test in section 3.2.2 that increasing the Au concentration above 0.13 mM eventually resulted in worse experimental results. This was linked to a progressive enhancement of the agglomeration effect as the metal concentration increases because the metal nanoparticles growth rate is strongly dependent on the metal concentration, with an order of reaction higher than the metal nanoparticles nucleation rate. However, with the ultrasound synthesis for the trial at a lower concentration (0.065 mM) worse experimental results were also observed. As shown with the mechanistic study in section 3.3.2 and according to the LaMer principle of burst nucleation (Figure 11) the nucleation step is only triggered after a certain amount of Au^{3+} is reduced and a concentration threshold is reached for the individual Au^0 reduced atoms. Therefore, it might be the case that due to the ultrasound synthesis temperature of only 70-90 °C the concentration threshold necessary to trigger the nucleation step is higher than at the microwave synthesis temperature of 150 °C. This could make more difficult the production of Au nanoparticles as the Au solution concentration decreases below 0.13 mM, in this case to 0.065 mM.

The previous optimisation test with the wave amplitude in section 4.2.1 confirmed that working at a wave amplitude of 50 % was not enough to achieve full reduction of the Au ions. For this reason, the Au solution concentration test was also performed under a full reduction scenario, after increasing the wave amplitude from 50 % to 80 %. This would allow to understand if the previous trend was independent of the degree of reduction. The UV-Vis spectra in Figure 110 (right) confirmed this to be the case with both concentrations also having spectra consistent with the production of larger Au nanoparticles with a broader size distribution. The experimental results in Table 31 continue to show higher plasmon peak wavelengths of 560 and 557 nm and higher wavelength ranges of 145 and 200 nm. The only difference relates to the plasmon peak absorbances, a measure of the metal production, which now do not follow the same ratios as the differences in the concentration of the Au solutions. This is according to the expected if there is full reduction and according to what was previously observed with the microwave optimisation test in section 3.2.2.

Synthesis of Metal Nanoparticles by Ultrasound

4.2 Au Optimisation Tests

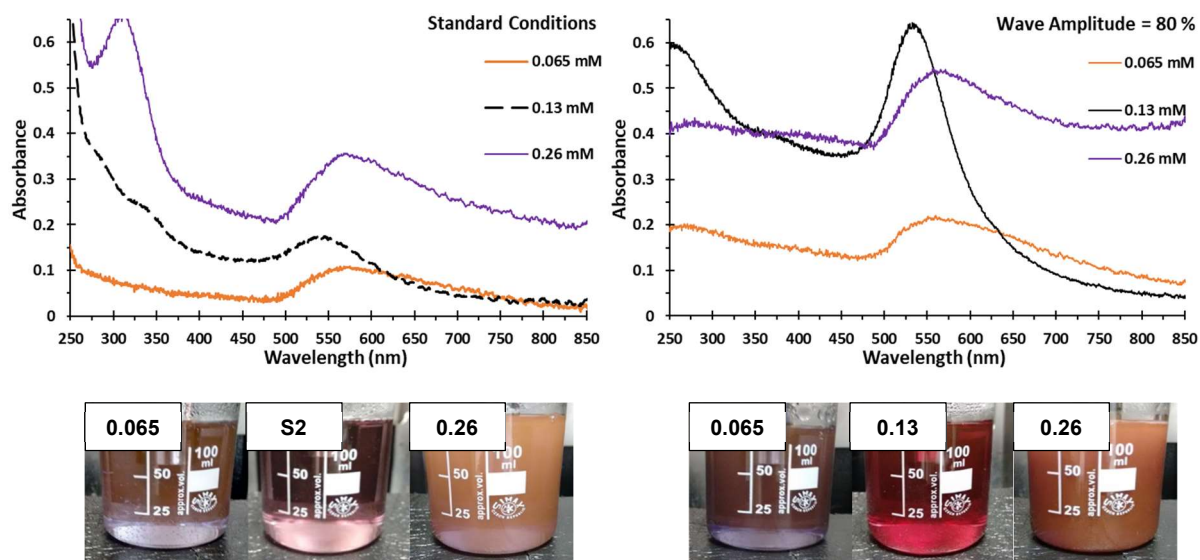


Figure 110 – Au nanoparticles produced at different Au concentrations with UV-Vis analysis at standard conditions (left) and at a wave amplitude of 80 % (right) and photos for 0.065, 0.13 and 0.26 mM at standard conditions (bottom left) and at a wave amplitude of 80 % (bottom right).

Table 31 – Au nanoparticles experimental results at different Au concentrations.

	Au Concentration (mM)	Plasmon Peak Absorbance	Plasmon Peak Wavelength (nm)	Wavelength Range (nm)
50 %	0.065	0.11	568	117
	0.13 (standard)	0.18	540	87
	0.26	0.36	570	156
80 %	0.065	0.22	560	145
	0.13	0.64	533	63
	0.26	0.54	557	200

Synthesis of Metal Nanoparticles by Ultrasound

4.2 Au Optimisation Tests

4.2.3 Sonication Time

As mentioned in section 4.2, the same amount of energy can be delivered by varying either the sonication time or the energy intensity (wave amplitude). For instance, the same energy can be delivered during the ultrasound synthesis by operating at 50 % amplitude for 20 min or at 100 % amplitude for 5 min. The test presented in this section aimed to show the amount of delivered energy effect on the experimental results by changing the sonication time. In total three other sonication times were tested, namely 5, 10 and 20 min.

As shown in Figure 111 (left) when decreasing the sonication time from 15 min to 5 and 10 min the production of Au nanoparticles was compromised as indicated by the UV-Vis spectra. This was according to the expected and related to a lower reduction of the Au ions due to lower supply of energy leading to a lower concentration of radical species. Likewise, when increasing the sonication time to 20 min the opposite was observed. The experimental values presented in Table 32 confirm that the results continuously improved as the sonication time increased with the Au nanoparticles production indicated by the plasmon peak absorbance increasing from 0.07 to 0.30, with the Au nanoparticles average size indicated by the plasmon peak wavelength decreasing from 540 to 539 nm and with the Au nanoparticles size distribution indicated by the wavelength range decreasing from 87 to 71 nm.

Even though the best experimental result was obtained at a 20 min sonication time the NaBH_4 test indicated that full reduction had not yet been achieved. Eventually, increasing the sonication time above 20 min would also result in full reduction. However, one of the targets defined for this PhD was to work with synthesis protocols characterised by reduced synthesis time which led to the decision of not performing work above the 20 min mark. The standard synthesis time of 15 min is already 3x higher than the microwave synthesis time. Therefore, similar to the previous optimisation test with the metal concentration in section 4.2.2 the wave amplitude was also changed to 80 % in order to understand the effect of higher sonication times after full reduction had been achieved. The UV-Vis spectra in Figure 111 (right) also indicate that the Au nanoparticles synthesis continuously improved as the sonication time increased from 5 to 15 min. However, after reaching full reduction with 15 min sonication the trial with 20 min sonication presented worse experimental results for the Au nanoparticles average size and size distribution. All the experimental results are presented in Table 32.

Choice of a minimum sonication time at a fixed wave amplitude is paramount for the synthesis of Au nanoparticles, but above a certain threshold, in this case above 15 min at a wave amplitude of 80 %, the experimental results start to get worse. This is an indication that the agglomeration effect is progressively enhanced when working at higher sonication times and a finding very similar to what had been reached with the microwave Au holding time and temperature optimisation test in section 3.2.3.

Synthesis of Metal Nanoparticles by Ultrasound

4.2 Au Optimisation Tests

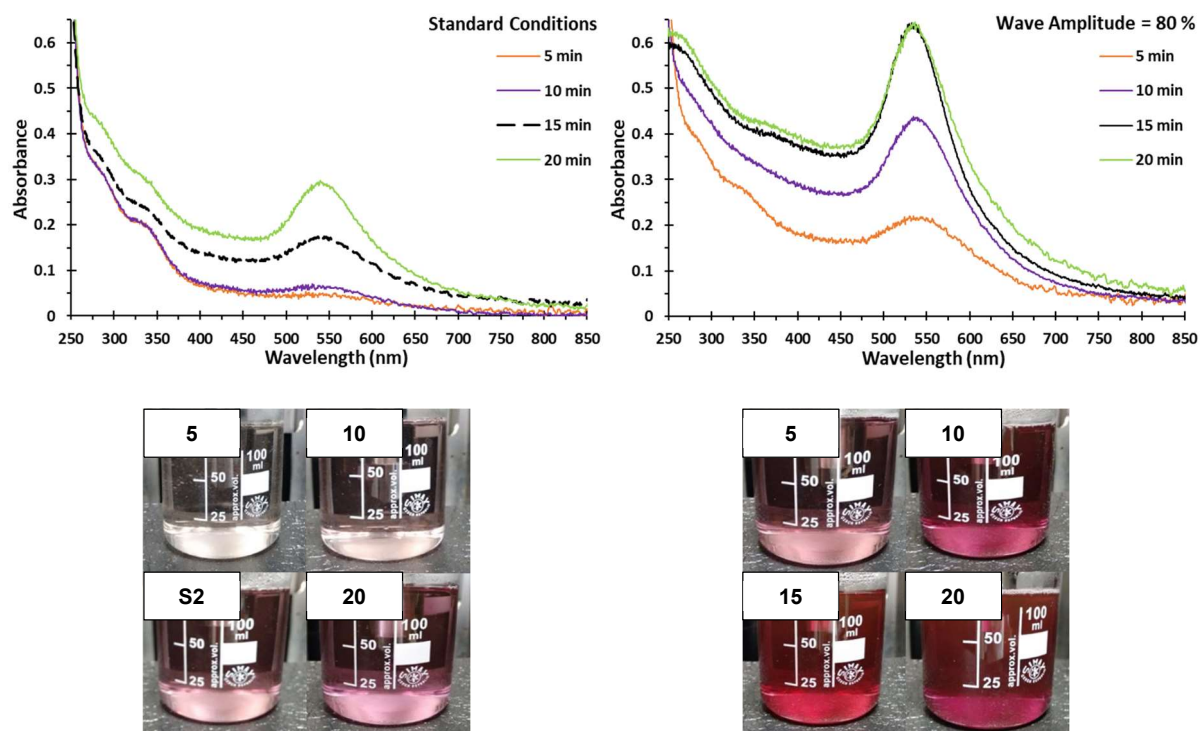


Figure 111 – Au nanoparticles produced at different sonication times with UV-Vis analysis at standard conditions (left) and at a wave amplitude of 80 % (right) and photos for 5, 10, 15 and 20 min at standard conditions (bottom left) and at a wave amplitude of 80 % (bottom right).

Table 32 – Au nanoparticles experimental results at different sonication times.

	Sonication Time (min)	Plasmon Peak Absorbance	Plasmon Peak Wavelength (nm)	Wavelength Range (nm)
50 %	5	0.07	-	-
	10	0.08	-	-
	15 (standard)	0.18	540	87
	20	0.30	539	71
80 %	5	0.22	535	114
	10	0.44	535	79
	15	0.64	533	63
	20	0.65	536	69

4.2.4 Solvent Composition

Interaction between ethylene glycol and water was studied at different mixture compositions of 25, 50 and 100 % (Vol. H₂O/Vol. Glycol) and compared to the standard scenario of 75 % water and 25 % ethylene glycol (75 %). The objective was to understand if by increasing the composition of ethylene glycol full reduction could now be achieved with a wave amplitude of 50 %. According to the UV-Vis spectra in Figure 112 as the composition in ethylene glycol increased from 25 % to 50 % full reduction was now observed (sample 75% to sample 50%). This was confirmed by performing the NaBH₄ test. This is according to the principle that increasing the composition of ethylene glycol will lead to a higher concentration of radical species, thus increasing the rate of reduction.

A further increase in the ethylene glycol composition to 75 % (sample 25%) showed no major differences to the previous trial with a 50 % composition. The small UV-Vis spectra differences can be attributed to the different mixture dielectric constants. Contrary to the previous optimisation test with the sonication time in section 4.2.3 the agglomeration effect is not enhanced after a certain threshold for ethylene glycol is reached. Therefore, increasing the amount of ethylene glycol has a neutral effect after a certain threshold. This was expected as there is no correlation between the amount of ethylene glycol and the working temperature. All the experimental results are presented in Table 33.

A major difference between this ultrasound optimisation test and the equivalent test performed for microwave synthesis in section 3.2.6 relates to the non-existence of a bimodal distribution. As explained in chapter 3 and section 4.2 it was the differences in the solubility of the stabilizers in water and ethylene glycol together with their reducing action that caused the bimodal distribution. Preliminary tests of Au in water with a PVA/metal weight ratio of 6.5, previously mentioned in section 4.2, indicated that after 15 min of sonication no changes had been observed. These preliminary tests were performed at two wave amplitudes of 50 % and 80 % and at a much higher stabilizer concentration than 0.65xPVA. The UV-Vis spectrum in Figure 112 of the trial with 100 % water confirms again that the PVA stabilizer was unable to cause any reduction as there were no changes between the Au solution and after sonication. All these experimental results clearly demonstrate that the working temperatures obtained during ultrasound synthesis are not enough to cause the PVA to act as a reducing agent and mixing ethylene glycol and water is possible for all desired range of compositions. This finding can also be extrapolated to the PVP stabilizer, which had been shown during the microwave work in chapter 3 to not impact the experimental results as much as PVA due to no major solubility issues and to a smaller reducing power.

Synthesis of Metal Nanoparticles by Ultrasound

4.2 Au Optimisation Tests

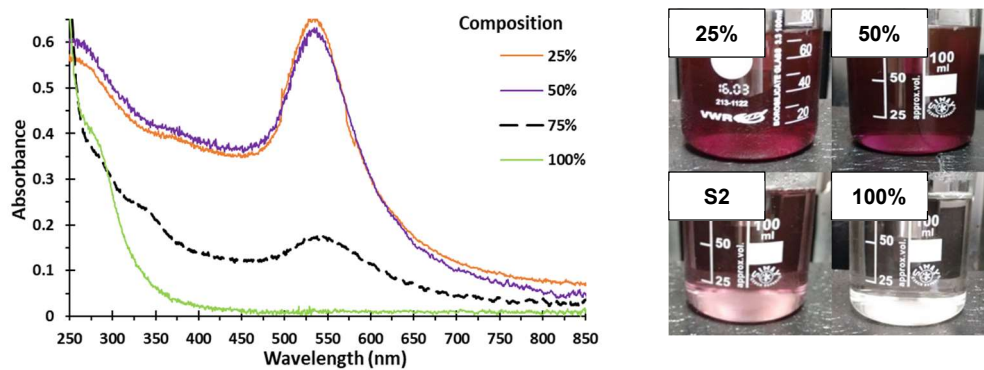


Figure 112 - Au nanoparticles produced at different compositions of water and ethylene glycol with UV-Vis analysis (left) and photos for 25, 50, 75 (S2) and 100 % (Vol. H₂O/Vol. Glycol) (right).

Table 33 – Au nanoparticles experimental results at different water compositions.

Water Composition % (v/v)	Plasmon Peak Absorbance	Plasmon Peak Wavelength (nm)	Wavelength Range (nm)
25	0.66	533	67
50	0.63	534	69
75 (standard)	0.18	540	87
100	-	-	-

Synthesis of Metal Nanoparticles by Ultrasound

4.2 Au Optimisation Tests

4.2.5 Stabilizer

The effect of the PVA concentration was tested at different PVA/metal weight ratios of 0.325, 3.25 and 6.50 and compared to the standard scenario of 0.65 and also when no stabilizer is used. As shown in Figure 113 major UV-Vis spectra changes are observed as the PVA/metal weight ratio is increased. The Au nanoparticles production indicated by the plasmon peak absorbance continuously increased from 0.16 with the 0.325xPVA trial to 0.40 with the 6.50xPVA trial. However, there was not a clear trend for the plasmon peak wavelength and wavelength range.

A trial without any stabilizer was also performed. Contrary to what had been observed with the equivalent test for microwave synthesis in section 3.2.7 better experimental results were obtained without any stabilizer and a higher production and a smaller Au nanoparticles average size and size distribution are expected. All the experimental results are compared in Table 34.

A similar trend was observed with the different DLS size distributions:

- 2.6 nm for no stabilizer trial;
- 13 ± 3.3 nm for the 0.325xPVA trial;
- 10 ± 3.4 nm for the 0.65xPVA trial (standard conditions);
- 4.8 ± 3.0 nm for the 3.25xPVA trial;
- 2.0 ± 1.4 nm for the 6.50xPVA trial;

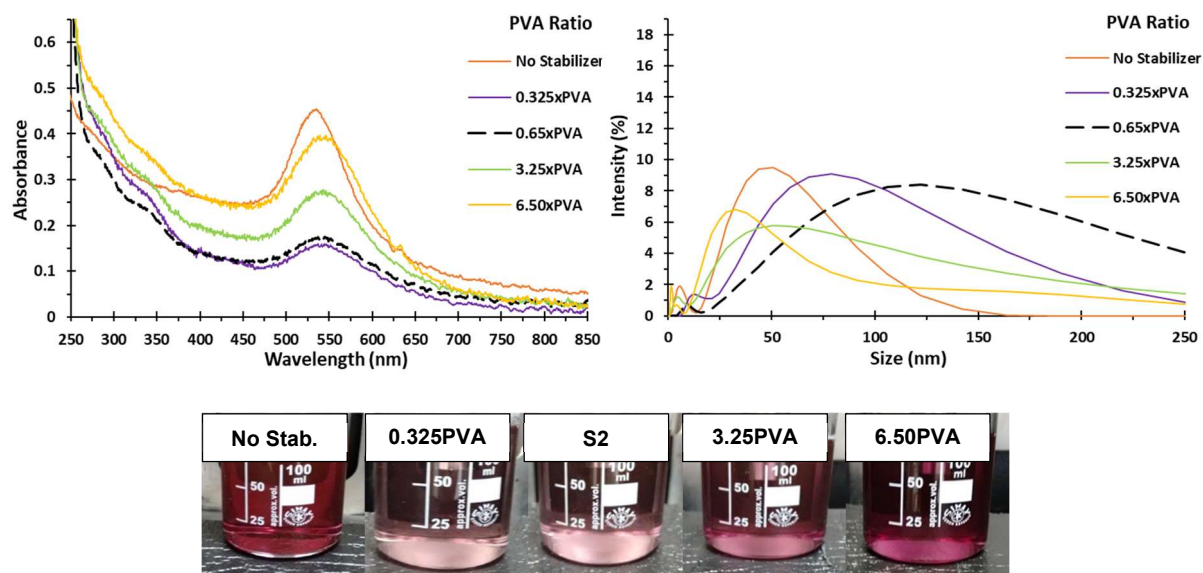


Figure 113 – Au nanoparticles produced at different PVA/metal weight ratios with UV-Vis (top left) and DLS (top right) analysis and photos for no stabilizer, 0.325xPVA, 0.65xPVA (S2), 3.25xPVA and 6.50xPVA (bottom).

Synthesis of Metal Nanoparticles by Ultrasound

4.2 Au Optimisation Tests

It is not clear why better experimental results were obtained when no stabilizer was used. For this reason, it was also investigated the effect of the stabilizer under full reduction conditions by increasing the wave amplitude to 80 %. As shown in Figure 114 (left) it appears that increasing the amount of PVA continues to bring benefits to the production of Au nanoparticles, but only when considering the 0.325xPVA trial. The UV-Vis spectra of the 0.65xPVA, 3.25xPVA and 6.50xPVA trials were very similar to one another. The plasmon peak wavelength and wavelength range also indicated no correlation with the amount of stabilizer, same finding as before with the wave amplitude set at 50 %.

The trial without any stabilizer on this occasion has returned the worst results for the Au nanoparticles production. Moreover, when comparing this trial with the equivalent at a wave amplitude of 50 %, shown in Figure 113, the Au nanoparticles production has also decreased. The plasmon peak wavelength and wavelength range did not show major differences.

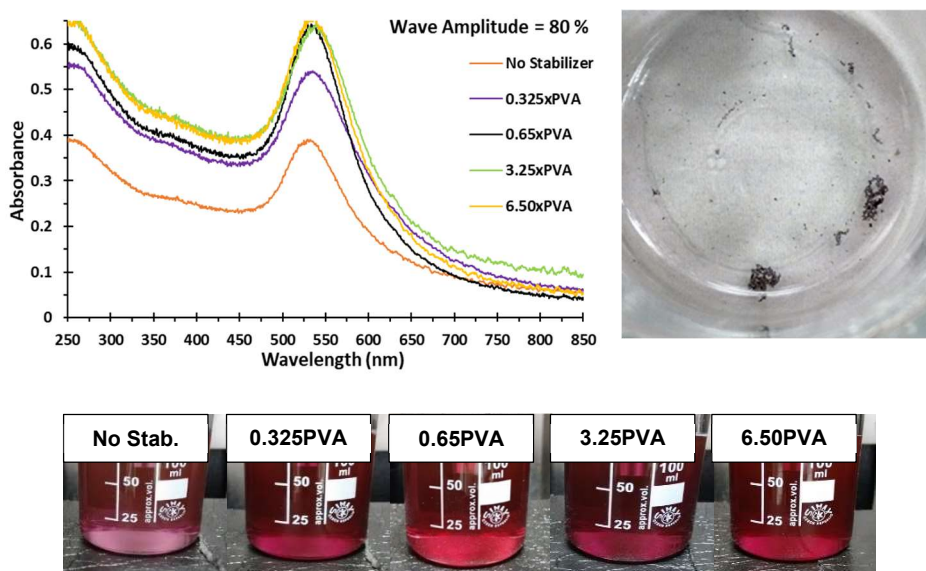


Figure 114 – Au nanoparticles produced at different PVA/metal weight ratios and at a wave amplitude of 80 % with UV-Vis analysis (top left), synthesis beaker for no stabilizer trial (top right) and photos for no stabilizer, 0.325xPVA, 0.65xPVA, 3.25xPVA and 6.50xPVA (bottom).

As shown in Figure 114 (right), the synthesis beaker for the trial without any stabilizer was analysed and agglomerated Au nanoparticles were observed at the bottom. It seems that a significant part of the produced Au nanoparticles ended up agglomerated at the bottom of the beaker but it also seems that another significant part of the produced Au nanoparticles remained stable in the colloid. This would explain why UV-Vis analysis indicated a lower Au nanoparticles production but no major changes to the Au nanoparticles average size and size distribution. The trial with 0.325xPVA also showed to a smaller degree a similar agglomeration.

Synthesis of Metal Nanoparticles by Ultrasound

4.2 Au Optimisation Tests

It is not clear if the working temperature of 90 °C, an increase from 70 °C when moving from a wave amplitude of 50 % to 80 %, is enough to explain this phenomenon on its own. This phenomenon was never observed with the microwave work where a temperature of 150 °C was used. However, with microwave the synthesis time was of only 5 min, whereas with ultrasound the synthesis time was of 15 min. More trials would be necessary to fully understand if the working temperature is the only variable responsible for this phenomenon.

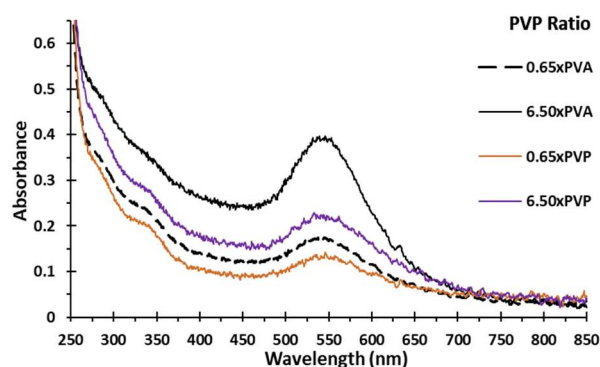


Figure 115 – UV-Vis analysis of Au nanoparticles produced at different stabilizer/metal weight ratios.

It was also investigated the PVA substitution by PVP at two PVP/metal weight ratios of 0.65 and 6.50. The UV-Vis spectra are shown in Figure 115 and compared to the standard scenario of 0.65xPVA and to the 6.50xPVA trial from Figure 113. Contrary to what had been observed with the equivalent test for microwave synthesis in section 3.2.7 the best experimental results were achieved when working with PVA instead of PVP. This is consistent with the principle that with the

microwave synthesis the PVP was only advantageous over PVA as both stabilizers presented reducing action due to the high working temperature of 150 °C but only PVA presented major solubility issues with ethylene glycol, situation that is not verified with the ultrasound synthesis.

Table 34 – Au nanoparticles experimental results at different stabilizer conditions.

	Condition	Plasmon Peak Absorbance	Plasmon Peak Wavelength (nm)	Wavelength Range (nm)
50 %	No stabilizer	0.46	535	62
	0.325xPVA	0.16	545	89
	0.65xPVA (standard)	0.18	540	87
	3.25xPVA	0.28	542	77
	6.50xPVA	0.40	544	83
	0.65xPVP	0.14	546	79
	6.50xPVP	0.23	534	94
80 %	No stabilizer	0.39	531	68
	0.325xPVA	0.54	535	81
	0.65xPVA	0.64	533	63
	3.25xPVA	0.65	534	68
	6.50xPVA	0.66	534	67

Synthesis of Metal Nanoparticles by Ultrasound

4.3 Selected Operating Conditions, Stability and Reproducibility

4.3 Selected Operating Conditions, Stability and Reproducibility

This section aims to identify the best ultrasound synthesis operating conditions for the production of metal nanoparticles in light of the targets defined for this PhD, *i.e.* reduced synthesis time, improved production, minimal operation cost, minimal use of toxic reagents and controlled size and shape. The best ultrasound synthesis operating conditions were defined by taking into consideration the Au optimisation experimental results from section 4.2. The main conclusions drawn from that section can be summarised as follows:

- a) A wave amplitude of 50 % is not enough to achieve full reduction of the Au solution and increasing the sonication time above 15 min is not desirable;
- b) Mixing water and ethylene glycol did not compromise the experimental results;
- c) Better experimental results when using PVA instead of PVP and work without any stabilizer at a wave amplitude of 50 % also produced promising results;
- d) At a wave amplitude of 80 % the Au nanoparticles agglomerated at the bottom of the beaker, but this phenomenon can be minimized by increasing the stabilizer/metal weight ratio. However, too much stabilizer can hinder the catalytic activity as it blocks the substrate access to the metal nanoparticles, which are the active sites;
- e) Working at higher metal concentrations resulted in worse experimental results;
- f) At a wave amplitude of 80 % a minimum sonication time of 15 min is necessary to achieve full reduction of the Au solution;

As shown in Table 35 two operating conditions have been identified and can be compared to the standard ultrasound operating conditions shown in Table 29:

- a) The operating condition A uses no stabilizer;
- b) The operating condition B uses a wave amplitude of 80 % and the PVA/metal weight ratio increases from 0.65 to 3.25. This increase is to provide a safety margin so that the agglomeration phenomenon is avoided when producing other metal nanoparticles;

Table 35 – Selected operating conditions for the metal nanoparticles ultrasound synthesis.

Parameter	Operating Condition A	Operating Condition B
Amplitude	50 %	80 %
Solvent (v/v)	75 % Water + 25 % Ethylene Glycol	75 % Water + 25 % Ethylene Glycol
Sonication Time	15 min	15 min
Volume of Mixture	75 mL	75 mL
Stabilizer/Metal Weight Ratio	0	3.25xPVA
Metal Concentration	0.025 g L ⁻¹ or 0.13 mM	0.025 g L ⁻¹ or 0.13 mM

Synthesis of Metal Nanoparticles by Ultrasound

4.3 Selected Operating Conditions, Stability and Reproducibility

The Au nanoparticles colloid produced at these two selected operating conditions were also checked for their stability over time using UV-Vis spectroscopy. They were first checked immediately after having been produced (Day 1) and then stored in glass vials with repeated UV-Vis measurements performed regularly, namely at Days 3, 8, 19, 26 and 52. This was exactly the same analysis that had been performed for the three selected operating conditions for microwave synthesis in section 3.4. The findings for ultrasound were exactly the same as the findings with microwave (see Figure 61), *i.e.* the Au nanoparticles produced with the operating condition A started to agglomerate and deposit at the bottom of the glass vial whereas the Au nanoparticles colloid produced with the operating condition B was stable over time with no major changes to the UV-Vis spectrum observed.

These stability tests were extremely important as they allow to understand how fast after synthesis the produced metal colloids should be supported without undergoing changes. As explained in section 2.5 the support addition stage for microwave and ultrasound only takes place after the production of several batches have rendered a reasonable volume. Therefore, for the first produced batch several hours can pass between the synthesis and the moment the metal nanoparticles are supported. Moreover, these stability tests also allow to understand the viability of storing and shipping colloidal metal nanoparticles to external research groups.

The reproducibility of the three selected operating conditions for microwave synthesis in section 3.4 was checked by producing several trials and calculating for the six most reproducible trials the standard deviations for the plasmon peak absorbance, plasmon peak wavelength and plasmon peak range. However, with ultrasound only a limited number of trials could be performed and it was not possible to check the reproducibility of the two selected operating conditions. As explained in section 2.4, due to safety/technical reasons the ultrasound operation was limited. This has seriously reduced the number of ultrasound experiments undertaken.

It can be said that the main objective of this section was to narrow down to a reasonable number of selected operating conditions all the possible ultrasound parameters combinations. The two presented operating conditions were then extended to the synthesis of other metal nanoparticles, namely Pd and bimetallic AuPd at a molar ratio of 1:1. All the produced metal nanoparticles are presented and analysed in more detail in section 4.4, in particular with TEM, a more reliable technique to perform size measurements and that also allows to understand the metal nanoparticles shape.

Synthesis of Metal Nanoparticles by Ultrasound

4.4 Metal Nanoparticles Production under Batch Regime

4.4 Metal Nanoparticles Production under Batch Regime

The ultrasound synthesis of metal nanoparticles using the two selected operating conditions from section 4.3 is presented and analysed in detail in this section and compared to some of the ultrasound work found in the literature. The considered metal nanoparticles were Au, Pd and bimetallic alloys of AuPd at a molar ratio of 1:1.

Similar to section 4.2 each sample was characterised with UV-Vis and DLS analysis and photos of the metal colloids were taken. The characterisation was further completed using TEM analysis with three selected images and the metal nanoparticles size distribution histogram being presented for each sample. The TEM histogram also provides information about the total nanoparticles count and the cumulative frequency.

Contrary to Au nanoparticles no plasmon peak in the UV-Vis region is observed for Pd and AuPd nanoparticles. Therefore, for those metal nanoparticles it is not possible to directly correlate the UV-Vis spectra with their average sizes. However, UV-Vis is still a useful technique as it is possible to observe trends as operating conditions change, quickly check for the method reproducibility and observe the metal nanoparticles stability over time.

An overview of the average sizes calculated by DLS and TEM analysis for the metal nanoparticles produced at these two selected operating conditions is shown in Table 36. The calculated DLS average sizes are related to the first peak, which is the most relevant as DLS is an intensity-weighted particle size measurement as explained in more detail in section 2.2.2.

Overall it can be said that both DLS and TEM analysis are in agreement. When metal nanoparticles are calculated to be small by TEM the DLS also indicates a small size, for example AuPd nanoparticles produced with the operating condition B. When TEM analysis shows a decrease on the average size by moving from the operating condition A to the operating condition B the DLS analysis also indicates the same trend.

Table 36 – TEM and DLS average sizes of metal nanoparticles produced by ultrasound synthesis with the two selected operating conditions (Table 35).

Metal	Operating Condition	TEM Average Size (nm)	DLS Average Size (nm)
Au	A	30 ± 13	5.2 ± 2.6
Au	B	12 ± 5.0	3.5 ± 0.8
Pd	A	10 ± 3.8	117 ± 44
Pd	B	2.7 ± 0.7	14 ± 2.9
AuPd 1:1	A	9.9 ± 1.2	22 ± 5.4
AuPd 1:1	B	2.9 ± 1.1	14 ± 3.1

Synthesis of Metal Nanoparticles by Ultrasound

4.4 Metal Nanoparticles Production under Batch Regime

A separated and more detailed discussion for each type of metal nanoparticles can be found in the respective subsections. Further to the points aforementioned it is also discussed:

a) Use of high-resolution transmission electron microscopy analysis (STEM/HAADF mode), a technique with a lower detection limit than regular TEM, in order to demonstrate that produced bimetallic AuPd nanoparticles with a molar ratio of 1:1 were in fact an alloy;

b) The production of bimetallic AuPd nanoparticles alloys with a molar ratio of 1:1 at different conditions from operating conditions A and B in an attempt to understand why a minor degree of agglomeration was observed when working with the operating condition B;

Synthesis of Metal Nanoparticles by Ultrasound

4.4 Metal Nanoparticles Production under Batch Regime

4.4.1 Au Nanoparticles

The UV-Vis and DLS spectra and photos of the Au nanoparticles produced with the two selected operating conditions are compared in Figure 116.

The plasmon peak wavelengths and wavelength ranges obtained for the two types of Au nanoparticles are very similar indicating that average size and size distribution should also be very similar. However, the plasmon peak absorbances are significantly different indicating that the Au nanoparticles production should also be significantly different (see Table 34). As explained in the Au optimisation tests in section 4.2, a wave amplitude of 50 % is not enough to achieve full reduction and compromised the maximum Au production that could be achieved. A further increase of the wave amplitude when no stabilizer is used has been shown to cause the Au nanoparticles to agglomerate at the bottom of the beaker (see Figure 114).

The DLS analysis indicated a smaller average size for the Au nanoparticles produced with operating condition B with the two calculated DLS average sizes reported in Table 36.

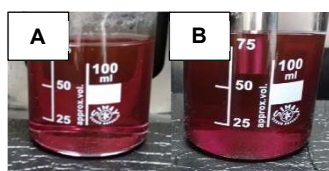
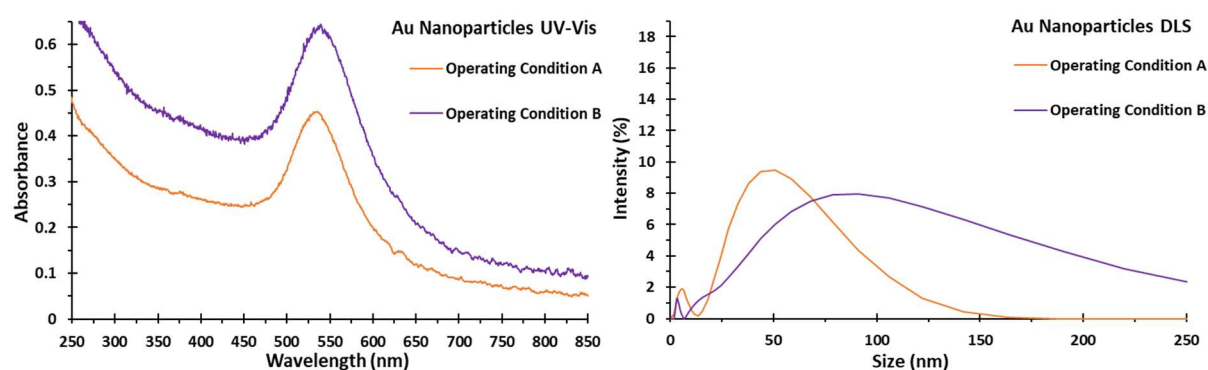
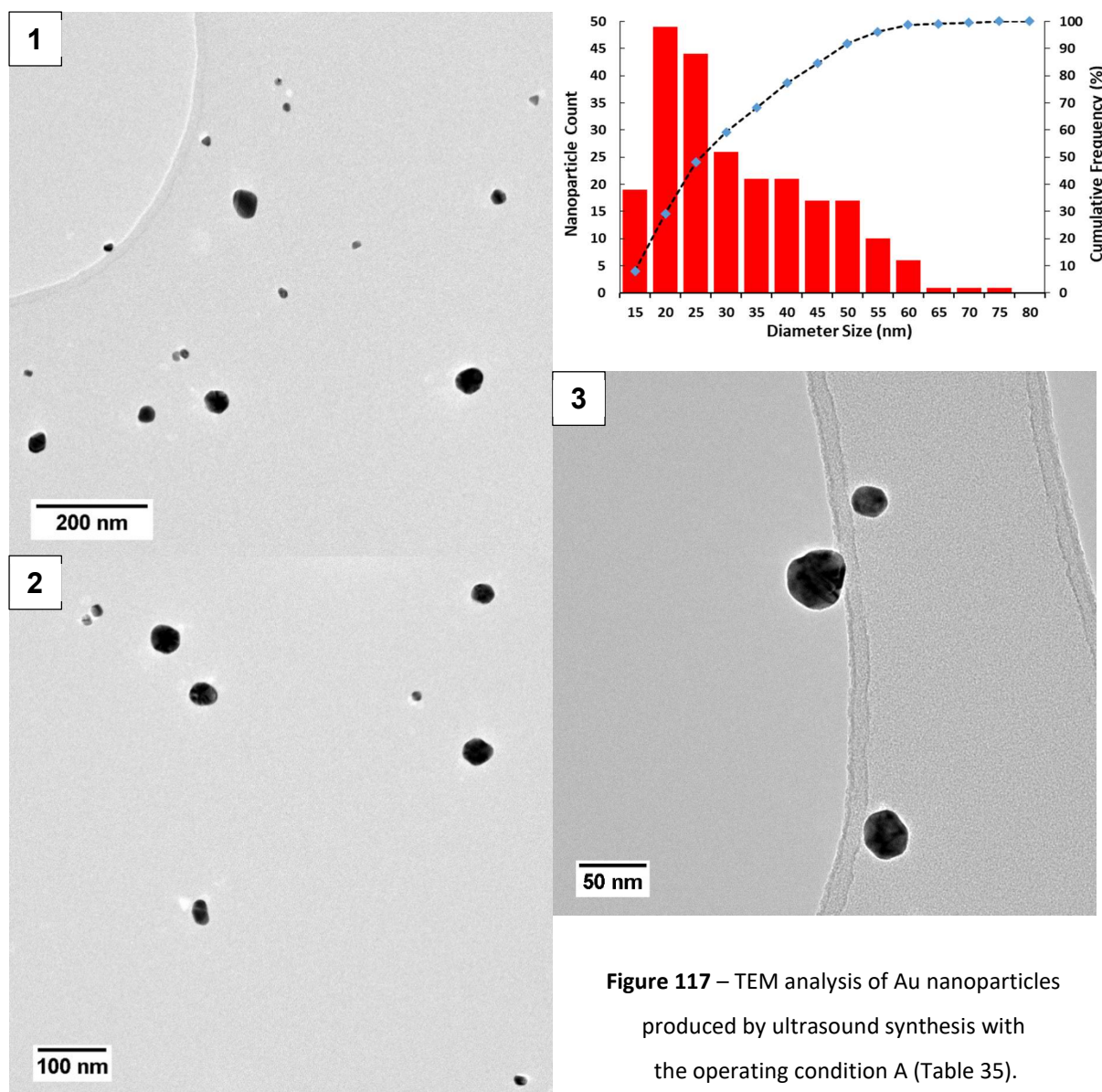


Figure 116 – Au nanoparticles produced by ultrasound synthesis with the two selected operating conditions (Table 35) with UV-Vis (top left) and DLS (top right) analysis and photos (bottom left).

The TEM analysis for the Au nanoparticles produced with the operating condition A is shown in Figure 117. The produced Au nanoparticles were circular and larger than expected when having in consideration the UV-Vis (535 nm) and DLS (5.2 ± 2.6 nm) analysis with a reported TEM average size of 30 ± 13 nm. The incomplete reduction of the Au solution may have affected the DLS analysis. In any case, when compared to the equivalent microwave operating condition when no stabilizer was used (operating condition A in Figure 64) it is remarkable that a smaller average size could be obtained, 30 ± 13 nm vs. 50 ± 14 nm, and that no degree of aggregation or agglomeration could be observed. The different working temperatures, 70 °C with ultrasound and 150 °C with microwave, could explain the different average sizes as the growth rate is strongly dependent on the temperature (Figure 12).

Synthesis of Metal Nanoparticles by Ultrasound

4.4 Metal Nanoparticles Production under Batch Regime



The TEM analysis of Au nanoparticles produced with the operating condition B is shown in Figure 118. A major decrease on the Au nanoparticles average size was observed, from 30 ± 13 nm with the operating condition A to 12 ± 5.0 nm with the operating condition B. The DLS analysis had also given an average size decrease indication, from 5.2 ± 2.6 nm with the operating condition A to 3.5 ± 0.8 nm with the operating condition B. Circular nanoparticles continued to be clearly dominant and no relevant degree of aggregation or agglomeration was observed. The produced Au nanoparticles were very similar to what had been obtained with the equivalent microwave operating condition, when a PVP/metal weight ratio of 3.25 was used (operating condition B in Figure 65), 12 ± 5.0 nm vs. 12 ± 3.9 nm.

Synthesis of Metal Nanoparticles by Ultrasound

4.4 Metal Nanoparticles Production under Batch Regime

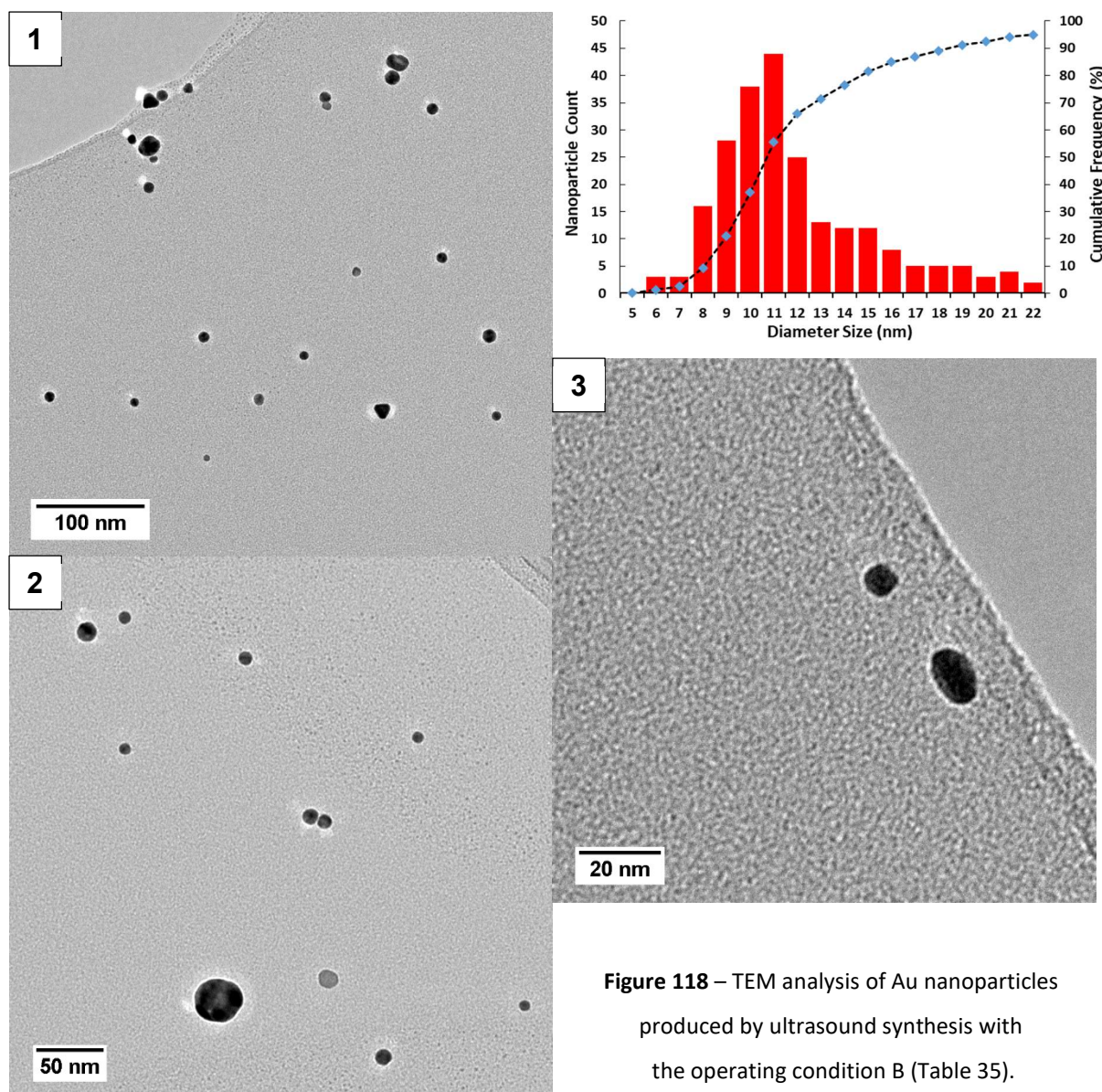


Figure 118 – TEM analysis of Au nanoparticles produced by ultrasound synthesis with the operating condition B (Table 35).

Similar to what had been observed with microwave synthesis in section 3.5.1, the average sizes of the produced Au nanoparticles were still considerable higher than what could be obtained when working with the traditional sol-immobilization protocol, around 3 nm. Again, this difference on the average sizes can be explained by having in consideration that with the ultrasound synthesis the reducing agent action is much weaker than when sodium borohydride is employed. Furthermore, with ultrasound synthesis the Au nanoparticles are subject to higher temperatures and the growth step is favoured. The reducing agent and temperature effects on the metal nanoparticles formation mechanism is explained in more detail in section 1.4.1.

An interesting work from Okitsu *et al.*¹²² has been able to verify the previous point by correlating the reduction rate of the Au solution with the produced Au nanoparticles average size as reported by TEM analysis. As expected, the average size decreased as the reduction rate increased. The previous authors have controlled the reduction rate by changing the

Synthesis of Metal Nanoparticles by Ultrasound

4.4 Metal Nanoparticles Production under Batch Regime

energy intensity of the ultrasound wave, similar to what had been done with the wave amplitude optimisation test in section 4.2.1. However, instead of changing the energy intensity of the ultrasound wave by changing the wave amplitude the previous authors have changed the frequency. The reported TEM average sizes were in the 15-30 nm range and synthesis was carried out at a controlled temperature of 21 °C. The synthesis time was not reported, but it is expected to be much higher than 15 min as only water was used as the solvent. Moreover, the amount of used stabilizer was not disclosed. All these points clearly show the advantage of adopting the optimised operating condition B developed for this PhD which delivered a smaller average size of 12 ± 5.0 nm, with the possibility of obtaining an even smaller size if the synthesis temperature could also be controlled at 21 °C (experimental set-up limitations).

It was still possible to find in the literature the production of Au nanoparticles by ultrasound synthesis with sizes smaller than 12 ± 5.0 nm. This was the case of Anandan and Ashokkumar¹²⁰ who claimed to have produced Au nanoparticles with sizes as small as 5 nm as shown in Figure 119 (left). However, these results should be read with caution as the previous authors were not able to deliver an average size and size distribution and no Au nanoparticles with a 5 nm size could be observed by TEM analysis after supporting the sample on TiO_2 as shown in Figure 119 (right). Moreover, the synthesis time was not reported, but it is expected to be much higher than 15 min as only water was used as the solvent. Also, the stabilizer/metal weight ratio used was of 25, much higher than the 3.25 used with the operating condition B.

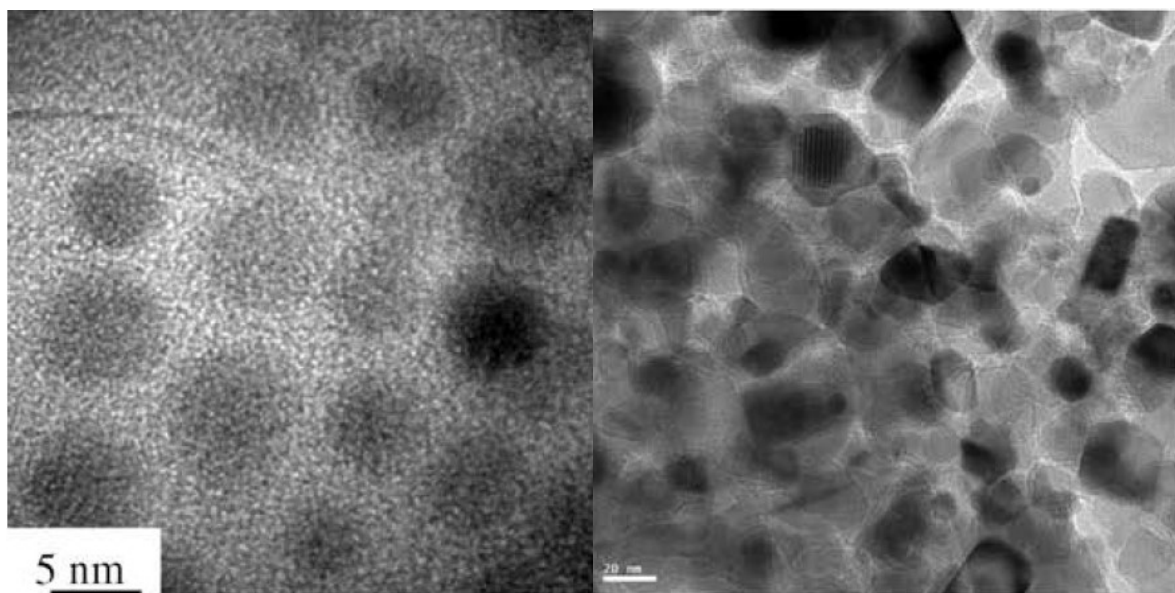


Figure 119 – Au nanoparticles produced by Anandan and Ashokkumar¹²⁰ with TEM analysis as found in the literature of the colloid (left) and after being supported on TiO_2 (right).

Synthesis of Metal Nanoparticles by Ultrasound

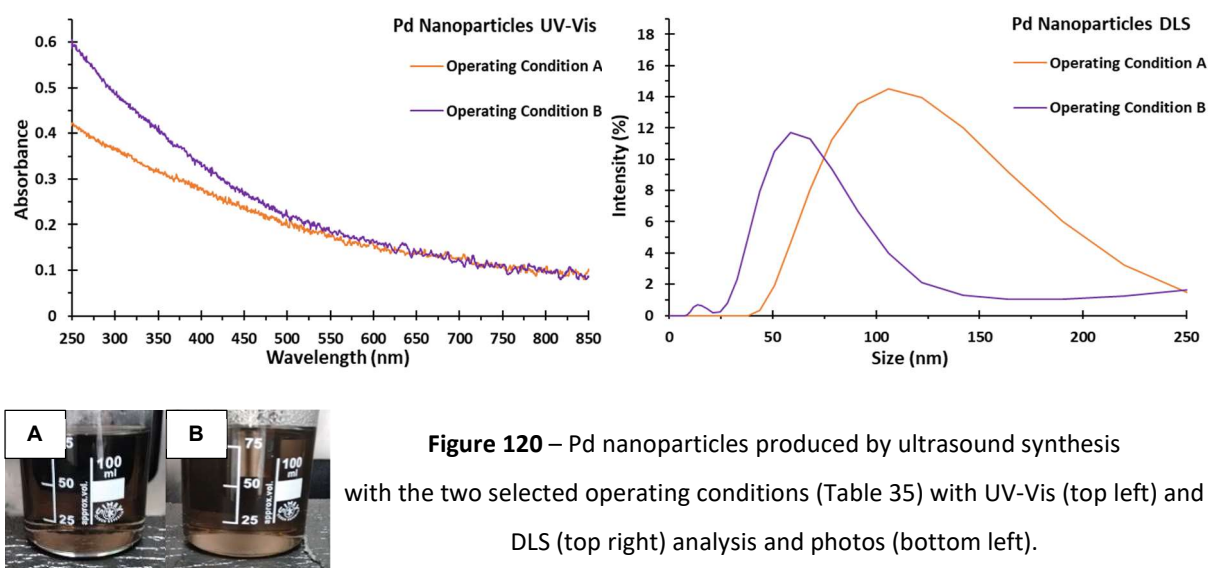
4.4 Metal Nanoparticles Production under Batch Regime

4.4.2 Pd Nanoparticles

The UV-Vis and DLS spectra and photos of the Pd nanoparticles produced with the two selected operating conditions are compared in Figure 120.

As explained in section 1.2 not all metal nanoparticles present a plasmon peak. However, even though Pd nanoparticles do not present a plasmon peak in this region of the electromagnetic spectrum it is still possible to observe that the two UV-Vis spectra are different from each other. This is a strong indication that two types of Pd nanoparticles were produced.

The UV-Vis spectrum of Pd nanoparticles produced with the operating condition B is actually almost identical to the UV-Vis spectra of Pd nanoparticles produced by microwave synthesis with the equivalent operating condition shown in Figure 71 and of Pd nanoparticles produced with the traditional sol-immobilization protocol shown in Figure 15 (middle). These Pd nanoparticles present average sizes of around 3 nm. Therefore, it can also be formulated the hypothesis that Pd nanoparticles produced by ultrasound synthesis with the operating condition B have similar average size. The calculated DLS average size of 14 ± 2.9 nm also supports this hypothesis.



The TEM analysis of Pd nanoparticles produced with the operating condition A is shown in Figure 121. The produced Pd nanoparticles were mainly circular, but some different shapes were also observed (triangular and square). The calculated TEM average size of 10 ± 3.8 nm was considerable smaller than the 117 ± 44 nm calculated with the DLS analysis. However, the size distribution histogram is very far from following the expected normal Gaussian distribution curve.

Synthesis of Metal Nanoparticles by Ultrasound

4.4 Metal Nanoparticles Production under Batch Regime

In any case, it is remarkable that contrary to what had been observed with the equivalent microwave operating condition when no stabilizer was used (operating condition A in Figure 72) with the ultrasound synthesis no major agglomeration was observed. This improvement when moving from microwave synthesis to ultrasound synthesis without stabilizer was also observed with Au nanoparticles in section 4.4.1. Again, different working temperatures, 70 °C with ultrasound and 150 °C with microwave, could explain the different average sizes as the growth rate is strongly dependent on the temperature (Figure 12).

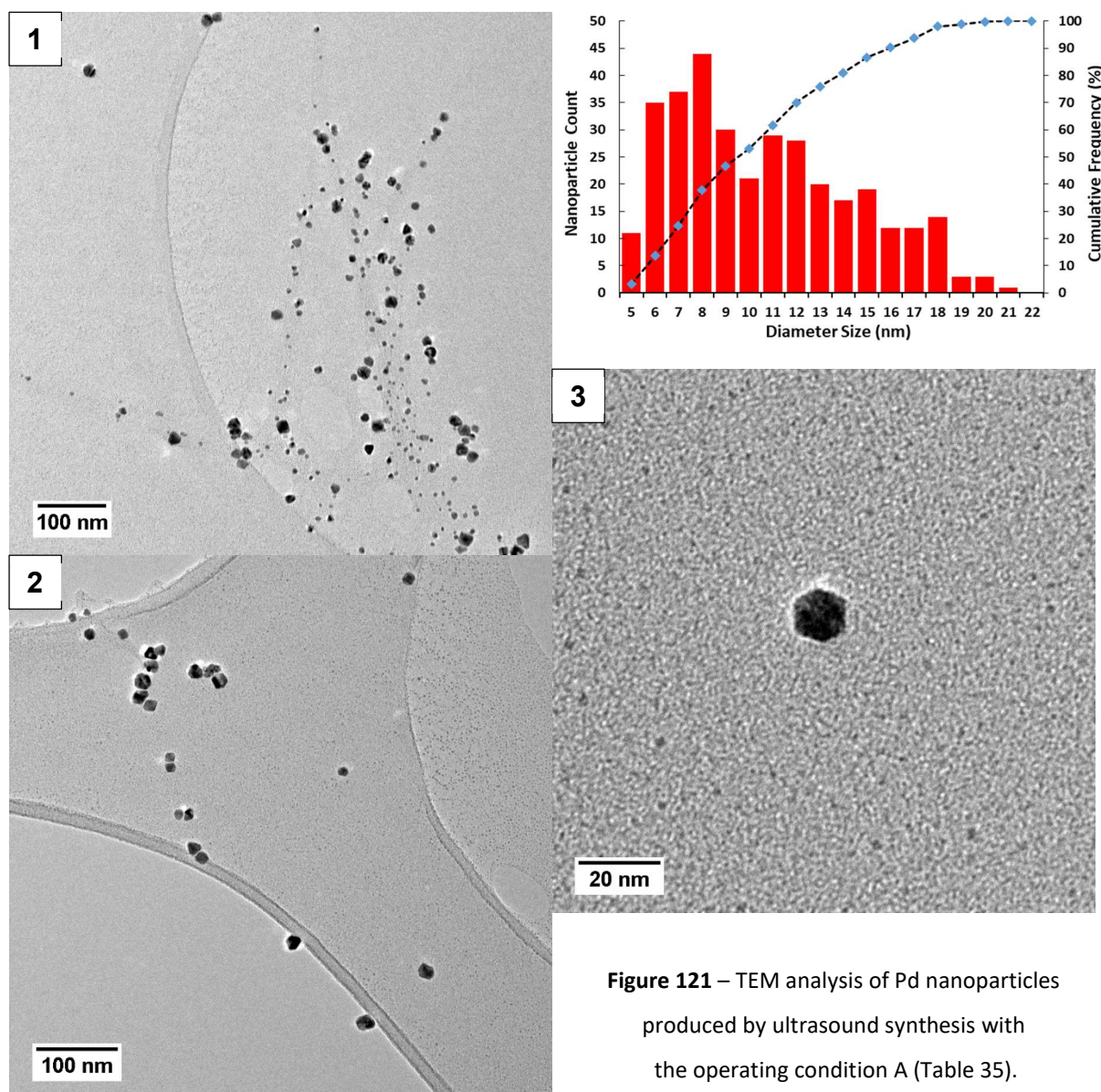


Figure 121 – TEM analysis of Pd nanoparticles produced by ultrasound synthesis with the operating condition A (Table 35).

The TEM analysis shown in Figure 122 validated the hypothesis that the produced Pd nanoparticles with the operating condition B were in the same range of sizes obtained when working with the traditional sol-immobilization protocol and with the equivalent microwave operating condition. Overall, the produced Pd nanoparticles were circular with a calculated

Synthesis of Metal Nanoparticles by Ultrasound

4.4 Metal Nanoparticles Production under Batch Regime

average size of 2.7 ± 0.7 nm. A minor degree of agglomeration was observed but it was not enough to compromise the expected size distribution histogram. This result is comparable to what is found in the literature with Nemamcha *et al.*¹¹⁸ working with pure ethylene glycol and PVP achieving average sizes in the 3-6 nm range, depending on the concentration of the Pd solution. Similar to what was done in section 4.3 the produced Pd nanoparticles were stored in a glass vial and UV-Vis spectrum was checked over time with no major changes detected.

When the traditional sol-immobilization protocol is employed both average sizes for Au and Pd nanoparticles are around 3 nm. However, with microwave and ultrasound synthesis this is no longer valid and the minimum average size that could be obtained for Au nanoparticles was around 12 nm. As explained in more detail in section 3.5.2 some of the factors that could explain this disparity include the stabilizer interaction with the Pd nanoparticles being stronger than with the Au nanoparticles and the reduction rate of Pd^{2+} being higher than the reduction rate of Au^{3+} .

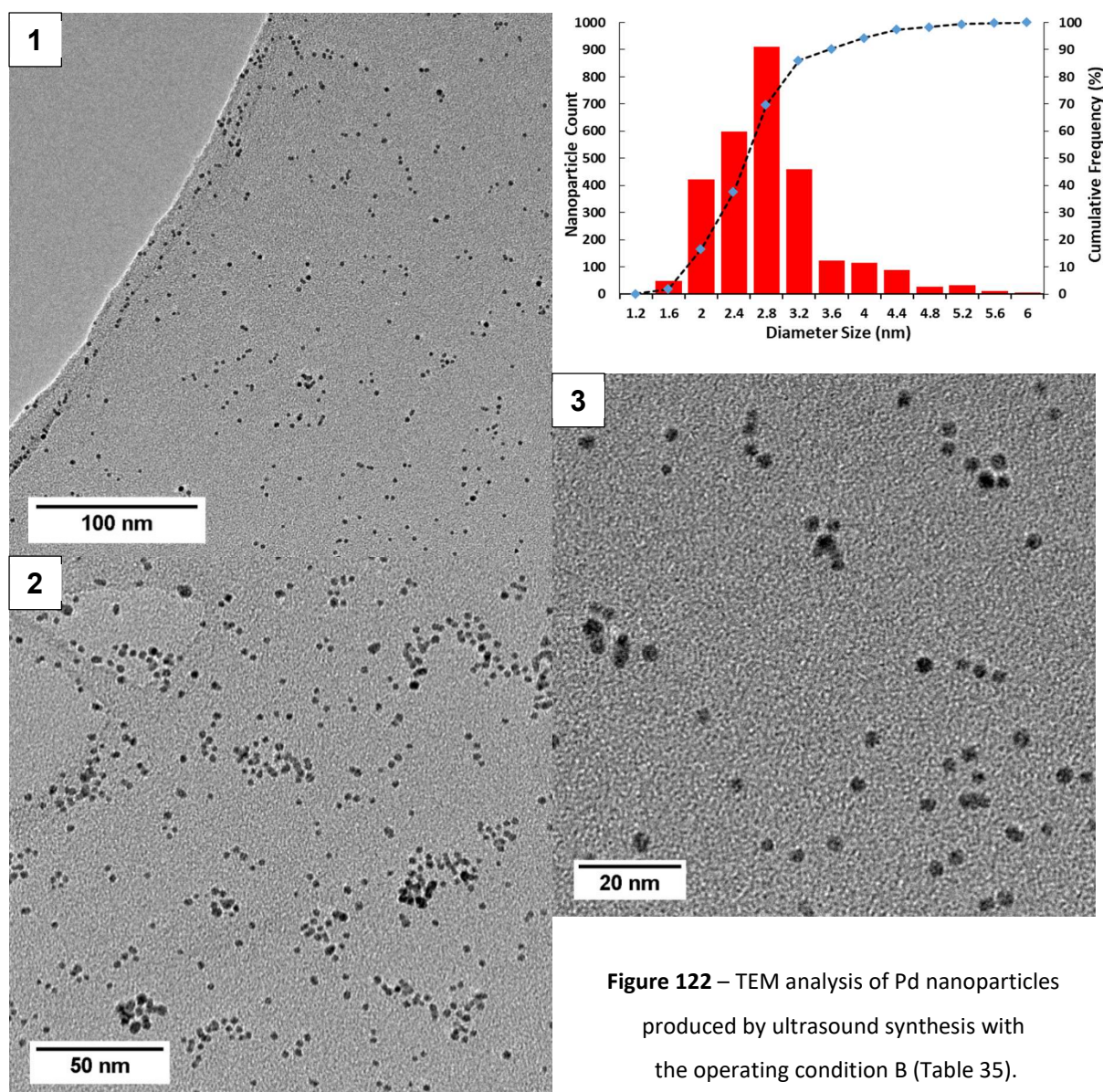


Figure 122 – TEM analysis of Pd nanoparticles produced by ultrasound synthesis with the operating condition B (Table 35).

Synthesis of Metal Nanoparticles by Ultrasound

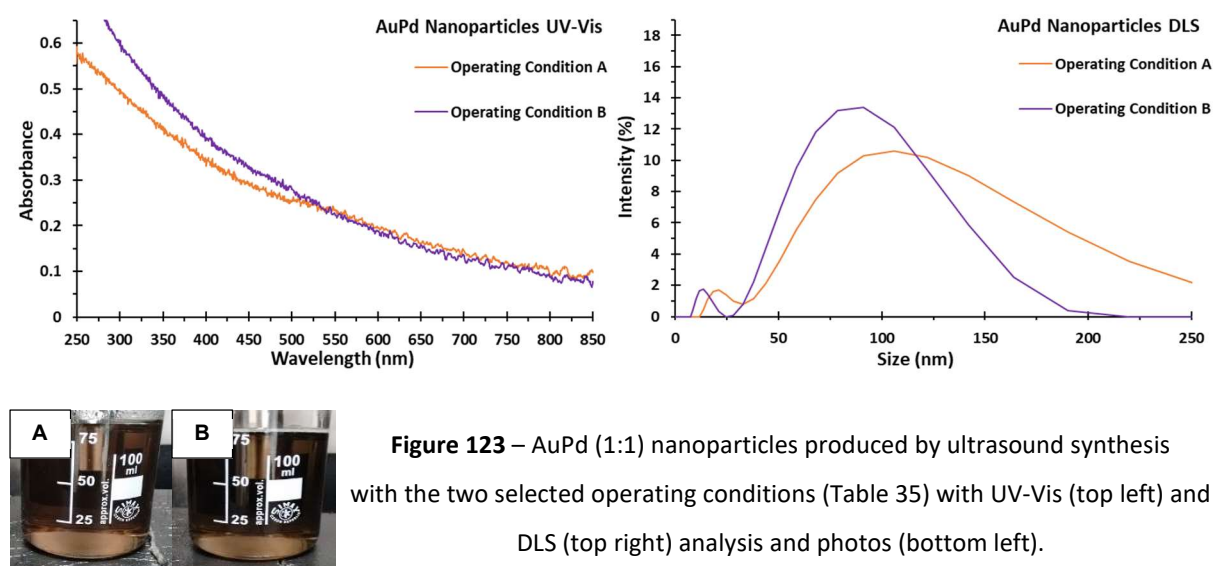
4.4 Metal Nanoparticles Production under Batch Regime

4.4.3 AuPd Nanoparticles

The UV-Vis and DLS spectra and photos of the AuPd (1:1 molar) nanoparticles produced with the two selected operating conditions are compared in Figure 123.

As expected, these AuPd nanoparticles do not present a plasmon peak. Similar to Pd nanoparticles produced in the previous section 4.4.2 it is also possible to observe differences in the UV-Vis spectra for the two selected operating conditions A and B. This is a strong indication that two types of AuPd nanoparticles were produced. However, unlike what had been observed with microwave synthesis in section 3.5.6, with ultrasound synthesis these two UV-Vis spectra are not very different.

The UV-Vis spectrum of AuPd (1:1 molar) nanoparticles produced with the operating condition B is actually almost identical to the UV-Vis spectra of Pd nanoparticles produced with the operating condition B shown in Figure 120, of AuPd/Pd nanoparticles produced by microwave synthesis with the equivalent operating condition shown in Figure 71/Figure 93 and of AuPd/Pd nanoparticles produced with the traditional sol-immobilization protocol shown in Figure 15. All these metal nanoparticles present average sizes of around 3 nm. Therefore, it can also be formulated the hypothesis that AuPd nanoparticles produced by ultrasound synthesis with the operating condition B have similar average size. The calculated DLS average size of 14 ± 3.1 nm also supports this hypothesis.



The TEM analysis of AuPd nanoparticles produced with the operating condition A is shown in Figure 124. The produced AuPd nanoparticles were mainly circular, but some different shapes were also observed (triangular and square). The calculated TEM average size of 9.9 ± 1.2 nm was smaller than the 22 ± 5.4 nm calculated with the DLS analysis and the size distribution histogram followed the expected normal Gaussian distribution curve.

Synthesis of Metal Nanoparticles by Ultrasound

4.4 Metal Nanoparticles Production under Batch Regime

These experimental results are even better than what was obtained for the Pd nanoparticles produced with the operating condition A in section 4.4.2 as they present more circular nanoparticles, smaller average size, a narrower size distribution following a Gaussian shape and TEM and DLS analysis more in agreement. Once more, it is remarkable that contrary to what had been observed with the equivalent microwave operating condition when no stabilizer was used (operating condition A in Figure 94) with the ultrasound synthesis no major agglomeration was observed. This improvement when moving from microwave synthesis to ultrasound synthesis without stabilizer was also observed with Au nanoparticles in section 4.4.1. Again, different working temperatures, 70 °C with ultrasound and 150 °C with microwave, could explain the different average sizes as the growth rate is strongly dependent on the temperature (Figure 12).

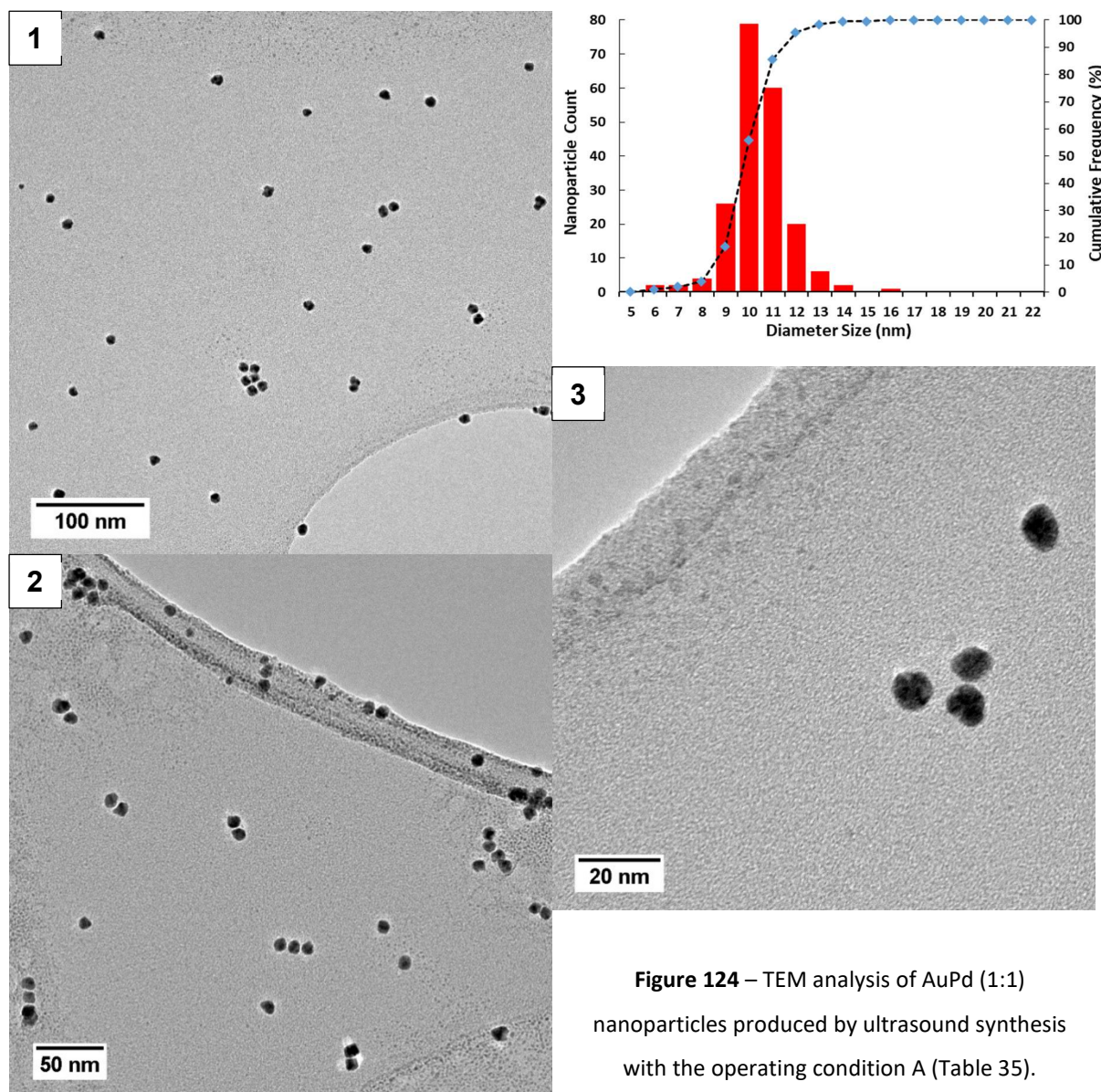


Figure 124 – TEM analysis of AuPd (1:1) nanoparticles produced by ultrasound synthesis with the operating condition A (Table 35).

Synthesis of Metal Nanoparticles by Ultrasound

4.4 Metal Nanoparticles Production under Batch Regime

The TEM analysis of AuPd (1:1 molar) nanoparticles produced with the operating condition B is shown in Figure 125 and confirmed the production of nanoparticles of small sizes with a calculated TEM average size of 2.9 ± 1.1 nm. Overall, the produced AuPd nanoparticles were circular. This result is superior to what is found in the literature with Kan *et al.*¹¹⁷ working with pure ethylene glycol and PVP and reporting average sizes in the 5-9 nm range and Mizukoshi *et al.*¹¹⁹ working with water and sodium dodecyl sulphate and reporting average sizes of around 7 nm. Moreover, the previous authors struggled to produce alloys under simultaneously reduction conditions, obtaining instead AuPd bimetallic nanoparticles of the core-shell type, with Pd being the shell and Au being the core. Also, one of the works has reported a broad size distribution whereas the other work has failed to deliver any size distribution. In both cases the synthesis time largely exceeded the 15 min. All these points clearly show the advantage of adopting the optimised operating condition B developed for this PhD.

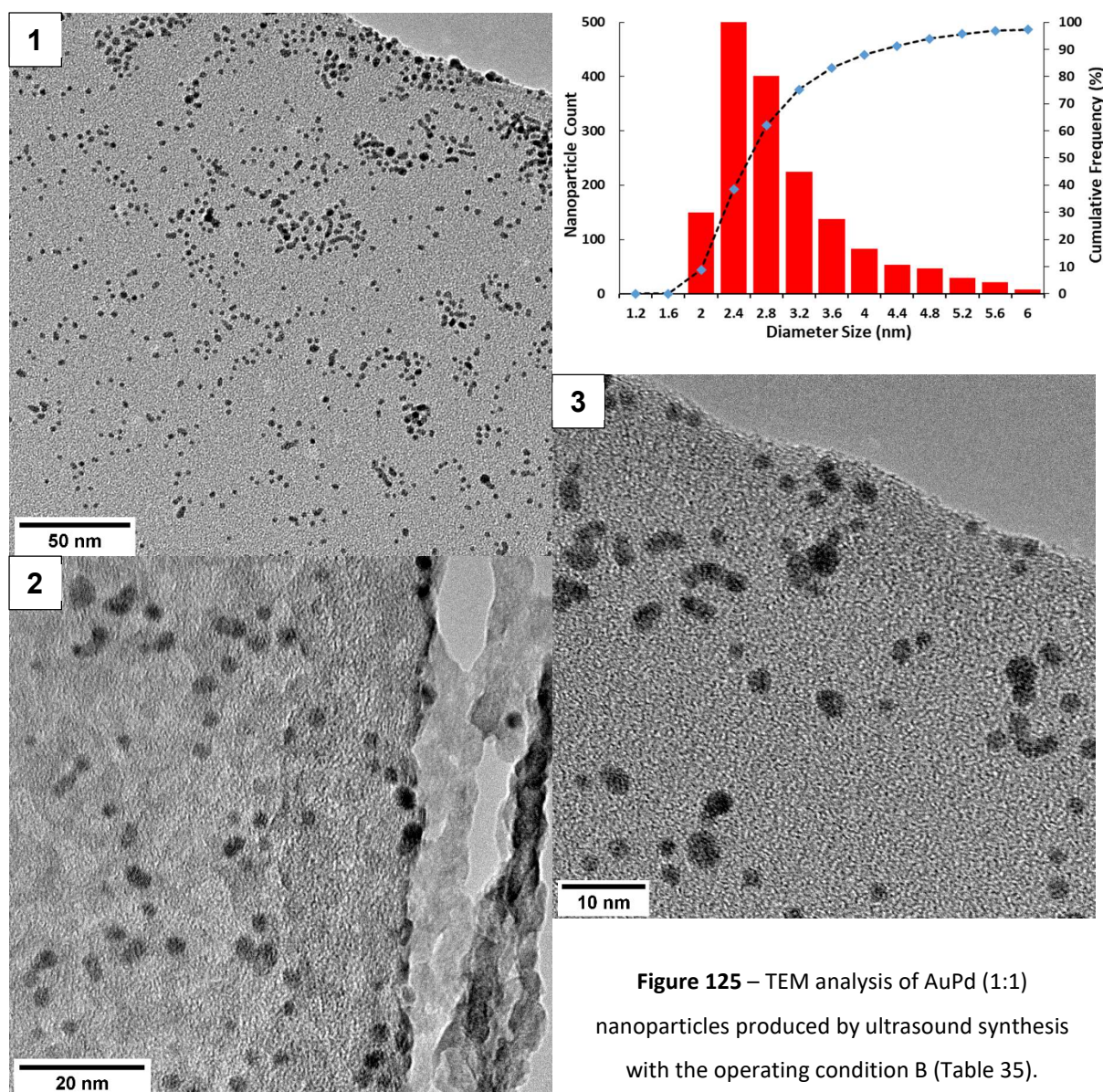


Figure 125 – TEM analysis of AuPd (1:1) nanoparticles produced by ultrasound synthesis with the operating condition B (Table 35).

Synthesis of Metal Nanoparticles by Ultrasound

4.4 Metal Nanoparticles Production under Batch Regime

Similar to AuPd (1:1) nanoparticles produced by the equivalent microwave operating condition in section 3.5.6, analysis with high-resolution TEM (STEM/HAADF mode) was also performed in order to confirm that the bimetallic nanoparticles were of the alloy type and that no individual Au or Pd nanoparticles had been produced. This high-resolution technique allowed to isolate individual nanoparticles and check their composition with EDX with compositions consistent with a 1:1 molar alloy observed. Two of the images obtained with HRTEM are shown in Figure 126.

Moreover, lattice-fringe spacing was also according to the expected with a value of 0.232 nm calculated, between that of pure Au (0.237 nm) and that of pure Pd (0.226 nm). This lattice-fringe spacing analysis looks into creating diffraction patterns that can be observed by TEM which can then be used to estimate distance between atoms in one nanoparticle.¹¹⁵⁻¹¹⁶

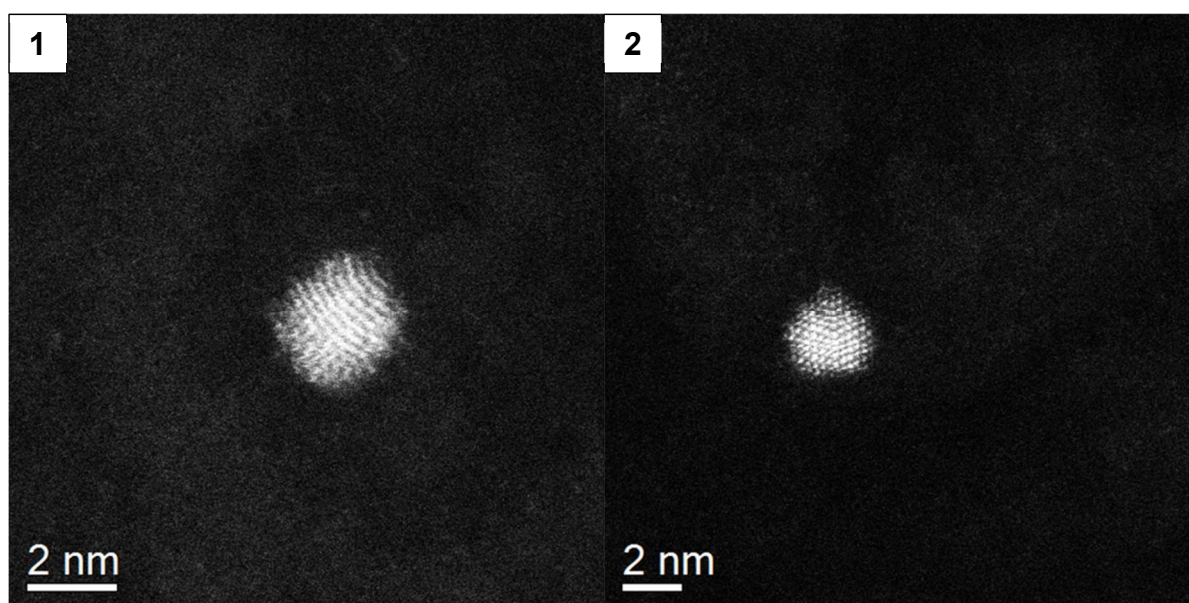


Figure 126 – High-resolution TEM (STEM/HAADF mode) analysis of AuPd (1:1) nanoparticles produced by ultrasound synthesis with the operating condition B (Table 35).

A minor degree of agglomeration was observed when producing Pd nanoparticles as illustrated in Figure 122. This was again verified with the AuPd nanoparticles as shown in Figure 125. Three trials with AuPd (1:1) were also performed at different operating conditions in an attempt to link this agglomeration to the amount of stabilizer or working temperature. Compared to the operating condition B, one trial was performed at 1.2xPVA vs. 3.25xPVA, one trial was performed at 0.65xPVA vs. 3.25xPVA and one trial was performed at a wave amplitude of 50 % vs. 80 %.

UV-Vis and DLS spectra of the previous three trials were very similar to one another and to the one presented in Figure 123 with operating condition B and no trends could be identified. TEM analysis also revealed average sizes very similar to the 2.9 ± 1.1 nm of operating condition B.

Synthesis of Metal Nanoparticles by Ultrasound

4.4 Metal Nanoparticles Production under Batch Regime

However, small changes could be observed by TEM. One image for each one of the three trials and the corresponding histograms can be found in Figure 127. It seems that decreasing the amount of PVA to 1.2xPVA resulted in more agglomeration. Further reduction to 0.65xPVA confirmed this trend. When moving from a wave amplitude of 80 % to 50 % (lower working temperature) full reduction was still achieved and agglomeration decreased.

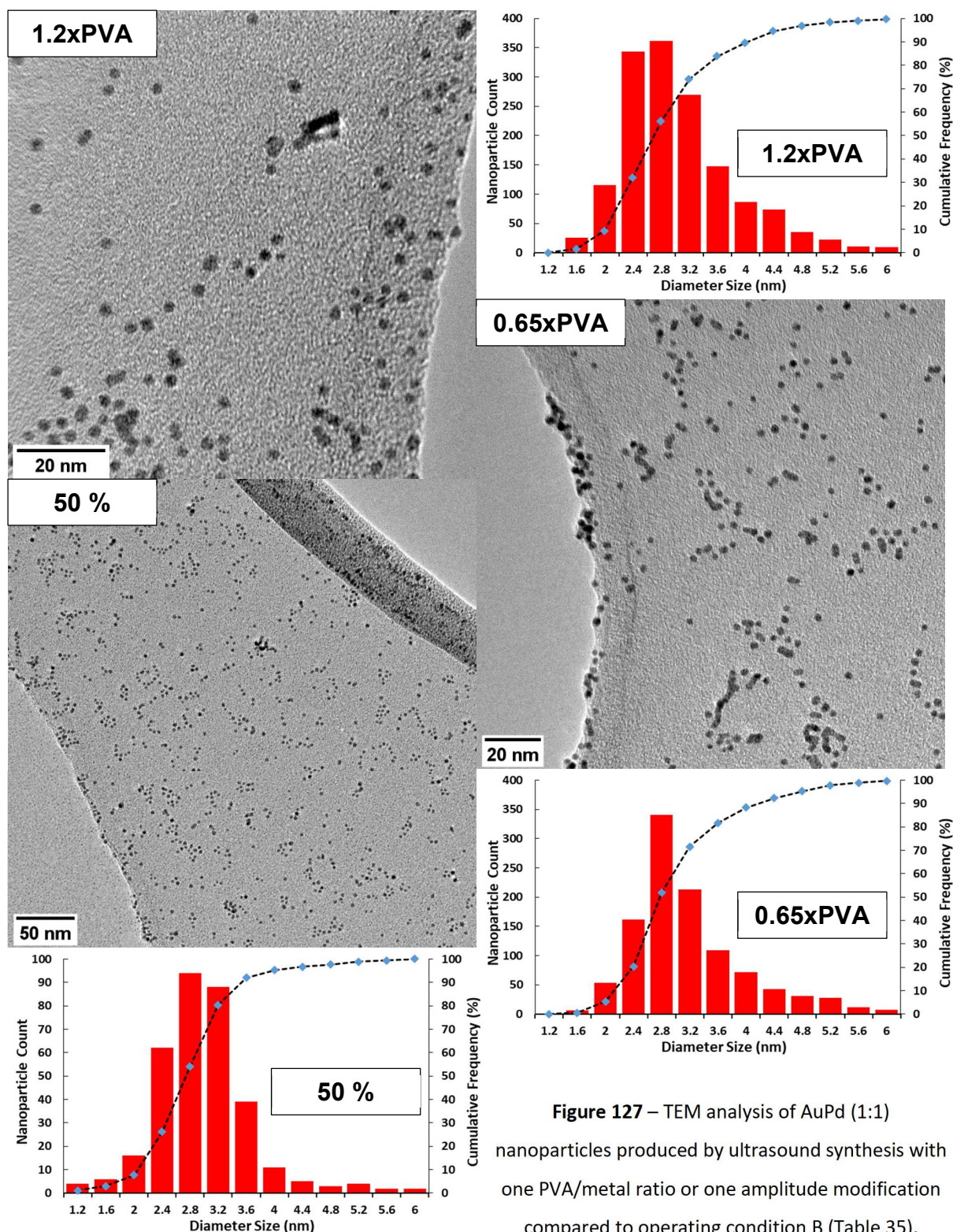


Figure 127 – TEM analysis of AuPd (1:1) nanoparticles produced by ultrasound synthesis with one PVA/metal ratio or one amplitude modification compared to operating condition B (Table 35).

Synthesis of Metal Nanoparticles by Ultrasound

4.5 Conclusions

4.5 Conclusions

Monometallic metal nanoparticles of Au, Pd and bimetallic metal nanoparticles of the alloy type of AuPd at a molar ratio of 1:1 were successfully synthesised using ultrasound effect. All metal nanoparticles were analysed by UV-Vis, DLS and TEM in order to assess production, average size, size distribution and shape. The AuPd nanoparticles with a molar ratio of 1:1 were further analysed with high-resolution TEM (STEM/HAADF mode) and EDX which confirmed that they were of the alloy type and presenting the expected composition.

Two selected operating conditions have been identified by taking into consideration the Au optimisation experimental results from section 4.2. This Au optimisation tests aimed to understand the effect of wave amplitude, metal concentration, sonication time, composition and type and concentration of stabilizer.

The best experimental results were obtained with the operating condition B, which used a mixture of 75 % water and 25 % ethylene glycol (v/v) as the reducing agent and PVA as the stabilizer. Even though the minimum Au nanoparticles average size that could be obtained was of only 12 ± 5.0 nm, overall the experimental results were superior to what is found in the literature, in particular if having in consideration that the metal nanoparticles are meant to be used for catalytic purposes and an excess of stabilizer is highly undesirable.

It is remarkable that in the case of metal nanoparticles produced with operating condition A, without any stabilizer, small metal nanoparticles could be produced. A result very different from what had been observed with microwave synthesis in chapter 3, in particular for Pd and AuPd. The different working temperatures, 70 °C with ultrasound and 150 °C with microwave, could explain the different results. The amount of stabilizer was also shown to play an important role in the ultrasound synthesis, in line with the expected.

At a wave amplitude of 50 % a higher degree of reduction is observed for the Au solution when no stabilizer is used vs. when a stabilizer is used. Moreover, it seems that without any stabilizer when increasing the wave amplitude to 80 % a significant part of the produced Au nanoparticles ended up agglomerated at the bottom of the synthesis beaker. Also, a minor degree of agglomeration was observed with the operating condition B. These observations could not be clearly explained and more trials would be necessary.

5 Catalysts Characterisation

5.1 Overview

A selected series of metal colloids produced in the previous chapters were supported on TiO₂, C and CeO₂ and further characterised by TEM, SEM/EDX, XPS and DRIFTS techniques. FEG-SEM analysis was also performed whenever the TEM analysis was poor due to the bad contrast between the metal nanoparticles and the support as it happened when analysing metal nanoparticles supported on TiO₂ with sizes larger than 10-12 nm. The support addition stage was carefully controlled in order to achieve a total metal weight ratio of 1 wt. % as explained in more detail in section 2.5 and detailed information about these techniques can be found in section 2.2. Many of the supported metal nanoparticles were also subject to heat treatments and characterised again.

The characterisation techniques were also extended to Au, Pd and bimetallic metal nanoparticles of the alloy type of AuPd (1:1) produced by the traditional sol-immobilization protocol and supported on TiO₂ and to a 5% Pd/C commercial catalyst. These supported metal nanoparticles were used for benchmarking purposes.

The main objective of this chapter is to present and explain in detail some of the supported metal nanoparticles characteristics (size, shape, loading, composition, traces of stabilizer and oxidation state). These supported metal nanoparticles were then used as catalysts in the several reactions presented in chapter 1 and their catalytic activity was linked to these characteristics. As mentioned in section 2.2.3 the characteristics that should be linked to the catalytic activity are the ones obtained for the supported metal nanoparticles as during the support addition stage some of the metal nanoparticles can be excluded because of their size/shape and changes can happen during the drying and heat treatments stages.

Each microwave/ultrasound preparation rendered a catalyst amount of 100 to 500 mg. Most of the catalyst was used in the several reactions presented in chapter 1 and in heat treatments. Therefore, an important limiting factor was related to the available amount of catalyst that could be used for characterisation, in particular with DRIFTS which could easily require an amount in the range of 100 to 150 mg. Even though DRIFTS is a non-destructive technique it was decided to not recover any of the analysed catalysts in order to avoid any contamination in further analysis or reaction testing. In any case, even if not all the catalysts were characterised by all the techniques, it was still possible to observe trends, analyse them and draw conclusions. All characterisation results can be found in the following subsections.

Catalysts Characterisation

5.2 Transmission Electron Microscopy

5.2 Transmission Electron Microscopy (TEM)

All the catalysts analysed by TEM are presented in Table 37. Some of the catalysts had to be analysed by FEG-SEM due to bad contrast when using TEM as the metal nanoparticles presented sizes larger than 10-12 nm, same order of magnitude as the TiO₂ particles. Details of the *Traditional* protocol can be found in section 1.4.2.1, details of the *Microwave B* protocol can be found in section 3.4 and details of the *Ultrasound A* and *Ultrasound B* protocols (including modifications) can be found in sections 4.3 and 4.4.3.

Table 37 – TEM and FEG-SEM average sizes of supported metal nanoparticles produced at different operating conditions.

Metal	Support	Protocol	Average Size (nm)	Comments
Au	TiO ₂	Traditional	3.8 ± 1.1	Colloid with 2-3 nm ³⁴
Au	TiO ₂	Traditional	8.4 ± 2.1	Calci. – 400 °C/3 h + Red. – 300 °C/3 h
Au	TiO ₂	Microwave B	13 ± 3.4	Colloid with 12 ± 3.9 nm in Figure 80
Au	TiO ₂	Microwave B	15 ± 6.0	Calci. – 400 °C/3 h + Red. – 300 °C/3 h
Au	TiO ₂	Ultrasound A	33 ± 14	Colloid with 30 ± 13 nm in Figure 132
Au	TiO ₂	Ultrasound A	43 ± 11	Calci. – 400 °C/3 h + Red. – 300 °C/3 h
Au	TiO ₂	Ultrasound B	13 ± 6.4	Colloid with 12 ± 5.0 nm in Figure 133
Au	TiO ₂	Ultrasound B	15 ± 8.5	Calci. – 400 °C/3 h + Red. – 300 °C/3 h
Pd	TiO ₂	Traditional	3.8 ± 1.0	Expected average size of 2-3 nm ³⁷
Pd	TiO ₂	Traditional	5.1 ± 1.5	Calci. – 400 °C/3 h + Red. – 300 °C/3 h
Pd	TiO ₂	Microwave B	2.9 ± 0.5	Colloid with 3.3 ± 0.8 nm in Figure 88
Pd	TiO ₂	Microwave B	3.5 ± 0.8	Calci. – 400 °C/3 h + Red. – 300 °C/3 h
Pd	TiO ₂	Ultrasound B	2.7 ± 0.6	Colloid with 2.7 ± 0.7 nm in Figure 137
Pd	C	Commercial	2.6 ± 0.5	Sigma-Aldrich (25680)
AuPd (1:1)	TiO ₂	Traditional	3.0 ± 0.8	Expected average size of 4 nm ³⁶
AuPd (1:1)	TiO ₂	Traditional	5.4 ± 1.1	Calci. – 400 °C/3 h + Red. – 300 °C/3 h
AuPd (1:1)	TiO ₂	Microwave B	3.1 ± 0.5	Colloid with 3.0 ± 0.6 nm in Figure 111
AuPd (1:1)	TiO ₂	Microwave B	4.3 ± 1.0	Calci. – 400 °C/3 h + Red. – 300 °C/3 h
AuPd (1:1)	C	Microwave B	3.0 ± 0.5	Colloid with 3.0 ± 0.6 nm in Figure 111
AuPd (1:1)	TiO ₂	Ultrasound A	10 ± 2.7	Colloid with 9.9 ± 1.2 nm in Figure 139
AuPd (1:1)	TiO ₂	Ultrasound A	12 ± 4.7	Calci. – 200 °C/3 h + Red. – 300 °C/3 h
AuPd (1:1)	TiO ₂	Ultrasound A	12 ± 5.9	Calci. – 300 °C/3 h + Red. – 300 °C/3 h
AuPd (1:1)	TiO ₂	Ultrasound A	13 ± 5.0	Calci. – 400 °C/3 h + Red. – 300 °C/3 h
AuPd (1:1)	TiO ₂	Ultrasound 0.65xPVA	2.8 ± 0.6	Colloid with 3.0 ± 0.8 nm in Figure 142
AuPd (1:1)	TiO ₂	Ultrasound 0.65xPVA	3.3 ± 1.2	Calci. – 200 °C/3 h + Red. – 300 °C/3 h
AuPd (1:1)	TiO ₂	Ultrasound 0.65xPVA	3.9 ± 1.6	Calci. – 300 °C/3 h + Red. – 300 °C/3 h
AuPd (1:1)	TiO ₂	Ultrasound 0.65xPVA	5.0 ± 1.5	Calci. – 400 °C/3 h + Red. – 300 °C/3 h

Catalysts Characterisation

5.2 Transmission Electron Microscopy

Metal	Support	Protocol	Average Size (nm)	Comments
AuPd (1:1)	TiO ₂	Ultrasound 1.2xPVA	2.9 ± 0.6	Colloid with 2.9 ± 0.8 nm in Figure 142
AuPd (1:1)	TiO ₂	Ultrasound 1.2xPVA	4.4 ± 1.1	Calci. – 400 °C/3 h + Red. – 300 °C/3 h
AuPd (1:1)	TiO ₂	Ultrasound B	2.7 ± 0.6	Colloid with 2.9 ± 0.8 nm in Figure 140
AuPd (1:1)	TiO ₂	Ultrasound B	3.0 ± 0.8	Calci. – 200 °C/3 h + Red. – 300 °C/3 h
AuPd (1:1)	TiO ₂	Ultrasound B	3.1 ± 0.8	Calci. – 300 °C/3 h + Red. – 300 °C/3 h
AuPd (1:1)	TiO ₂	Ultrasound B	4.5 ± 1.0	Calci. – 400 °C/3 h + Red. – 300 °C/3 h
AuPd (1:1)	C	Ultrasound B	2.8 ± 0.7	Colloid with 3.0 ± 0.8 nm in Figure 142
AuPd (1:1)	TiO ₂	Ultrasound 50 %	2.5 ± 0.6	Colloid with 2.7 ± 0.7 nm in Figure 142
AuPd (1:1)	TiO ₂	Ultrasound 50 %	4.0 ± 1.0	Calci. – 400 °C/3 h + Red. – 300 °C/3 h

Ir	CeO ₂	Microwave A	< 1-2 nm	Colloid with < 1-2 nm in Figure 100
Ir	CeO ₂	Microwave B	< 1-2 nm	Colloid with < 1-2 nm in Figure 101
Ir	CeO ₂	Microwave A+NaOH	< 1-2 nm	Colloid with < 1-2 nm in Figure 104

a) Calci. stands for calcination;

b) Red. stands for reduction;

It can be said that the metal nanoparticles average sizes and size distributions remained unchanged after being supported, regardless of the support used and regardless of the type of metal nanoparticles. Overall, there was not a clear trend and any observed differences were very small, within the error indicated by the standard deviation. Some of the supported metal nanoparticles had their average size increased after being supported, for example the AuPd (1:1) nanoparticles produced by microwave synthesis with the operating condition B had a colloid average size of 3.0 nm, which increased to 3.1 nm after being supported on TiO₂. Other metal nanoparticles had their average size decreased after being supported, for example the AuPd (1:1) nanoparticles produced by ultrasound synthesis with the operating condition B had a colloid average size of 2.9 nm, which decreased to 2.7 nm after being supported on TiO₂.

As expected, all metal nanoparticles that were heat treated had their average size increased and the more severe the heat treatment conditions the higher the degree of agglomeration observed. This was the case for the AuPd (1:1) nanoparticles produced by ultrasound synthesis with the operating condition B, but using a PVA/metal weight ratio of 0.65 instead of the 3.25 indicated in Table 35. The original average size of 2.8 nm increased to 3.3 nm after applying a mild heat treatment with a calcination temperature of only 200 °C. However, as the calcination temperature increased the average size continued to increase. Thus, when the calcination temperature was of 300 °C the average size increased from 2.8 nm to 3.9 nm and when the calcination temperature was of 400 °C the average size increased from 2.8 nm to 5.0 nm.

Catalysts Characterisation

5.2 Transmission Electron Microscopy

Once more the heat treatments and the TEM analysis confirmed the importance of the amount of stabilizer used during the metal nanoparticles synthesis. When the PVA/metal weight ratio increased from 0.65 to 3.25 (operating condition B) it was still possible to observe that any heat treatment would cause an increase in the average size and that the more severe the heat treatment conditions the higher the degree of agglomeration. However, because of the higher amount of stabilizer used the agglomeration was less severe when compared to the equivalent heat treatment conditions when only a PVA/metal weight ratio of 0.65 was employed. Thus, when the calcination temperature was of 200 °C the average size increased from 2.7 nm to 3.0 nm, when the calcination temperature was of 300 °C the average size increased from 2.7 nm to 3.1 nm and when the calcination temperature was of 400 °C the average size increased from 2.7 nm to 4.5 nm.

The previous analysis also allowed to understand that the filtration/washing step during the support addition stage is not enough to completely remove stabilizer traces from the catalyst surface. This is a very important observation as it demonstrates that some of the literature methods previously mentioned in chapters 3 and 4 are not suitable for the production of metal nanoparticles meant to be used as catalysts as they employ amounts of stabilizer much higher than the maximum stabilizer/metal weight ratio of 3.25 used for this PhD. As previously explained, too much stabilizer can hinder the catalytic activity as it blocks the substrate access to the metal nanoparticles, which are the active sites. This observation is further verified when using XPS analysis in section 5.4.

A minor degree of agglomeration could be observed with the ultrasound synthesis when using the operating condition B for the production of Pd and AuPd (1:1) nanoparticles as shown in Figure 122 and Figure 125 respectively. However, the TEM analysis indicates that the supported metal nanoparticles only present the expected circular shape and the minor degree of agglomeration was no longer observed. It is possible that the metal nanoparticles affected by the minor degree of agglomeration and presenting a non-circular shape were excluded during the support addition stage.

TEM analysis of Ir/CeO₂ catalysts did not show any nanoparticles. This is consistent with what was observed with the TEM analysis of the colloids shown in Figure 85, Figure 86 and Figure 89. This was because the small Ir nanoparticles were similar to the TEM detection limit. Therefore, it can only be said that smaller than 1-2 nm Ir nanoparticles have been supported. In order to make sure that they had been supported the filtrate was checked after the support addition stage and SEM/EDX and XPS analysis was performed.

TEM images of all the supported metal nanoparticles can be found on the next pages.

Catalysts Characterisation

5.2 Transmission Electron Microscopy

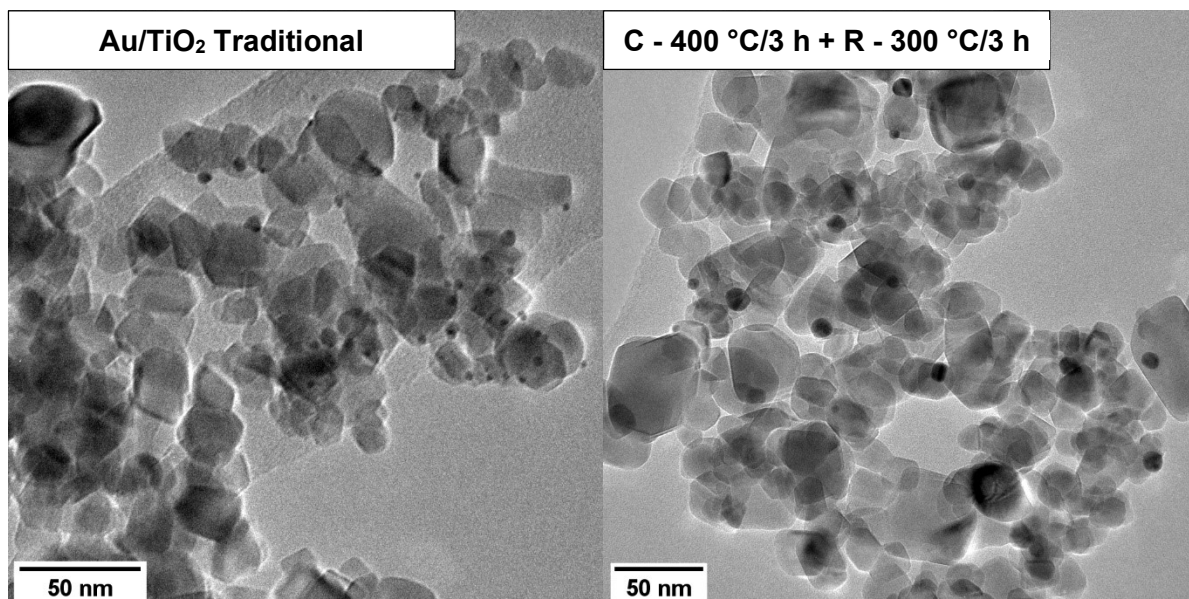
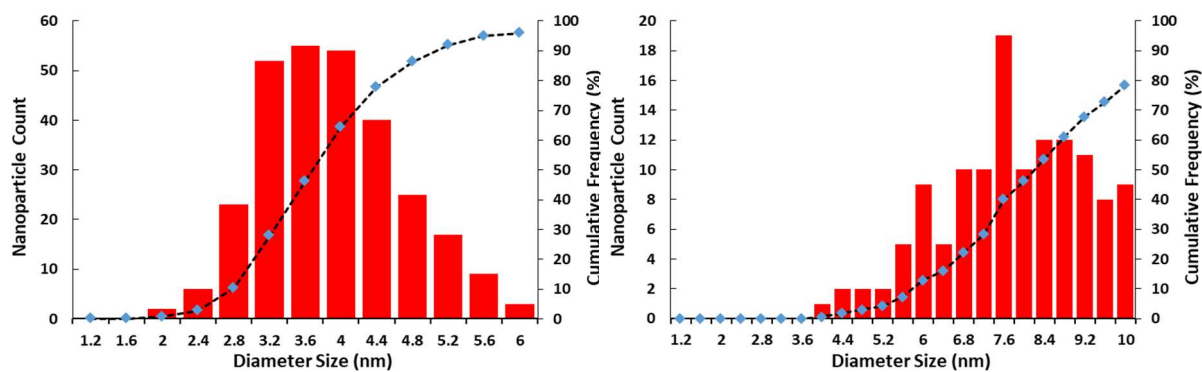


Figure 128 – TEM analysis of TiO₂ supported Au nanoparticles produced with the traditional sol-immobilization protocol without heat treatment (left) and after heat treatment (right).

Catalysts Characterisation

5.2 Transmission Electron Microscopy

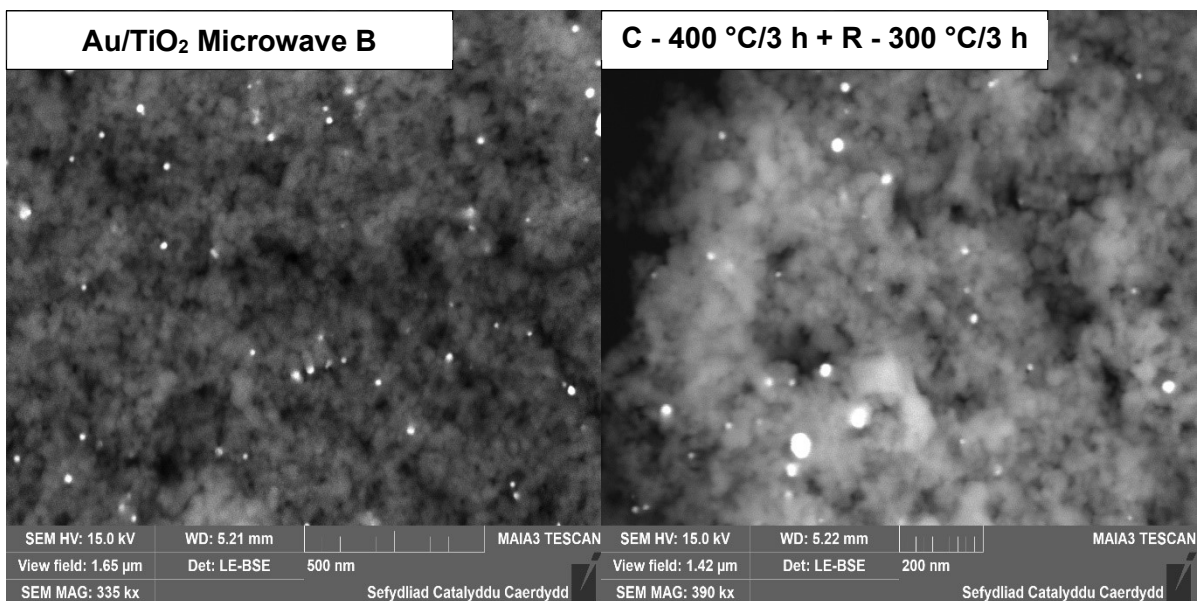
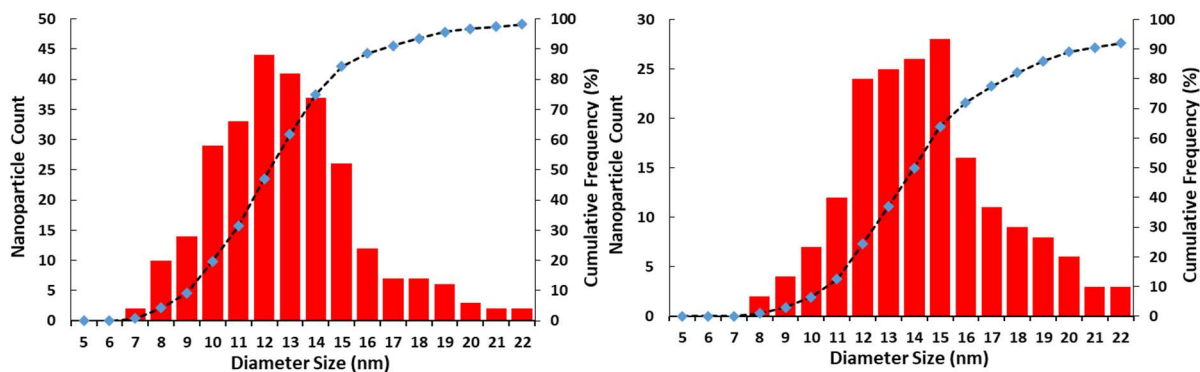


Figure 129 – FEG-SEM analysis of TiO₂ supported Au nanoparticles produced by microwave synthesis with the operating condition B without heat treatment (left) and after heat treatment (right).

Catalysts Characterisation

5.2 Transmission Electron Microscopy

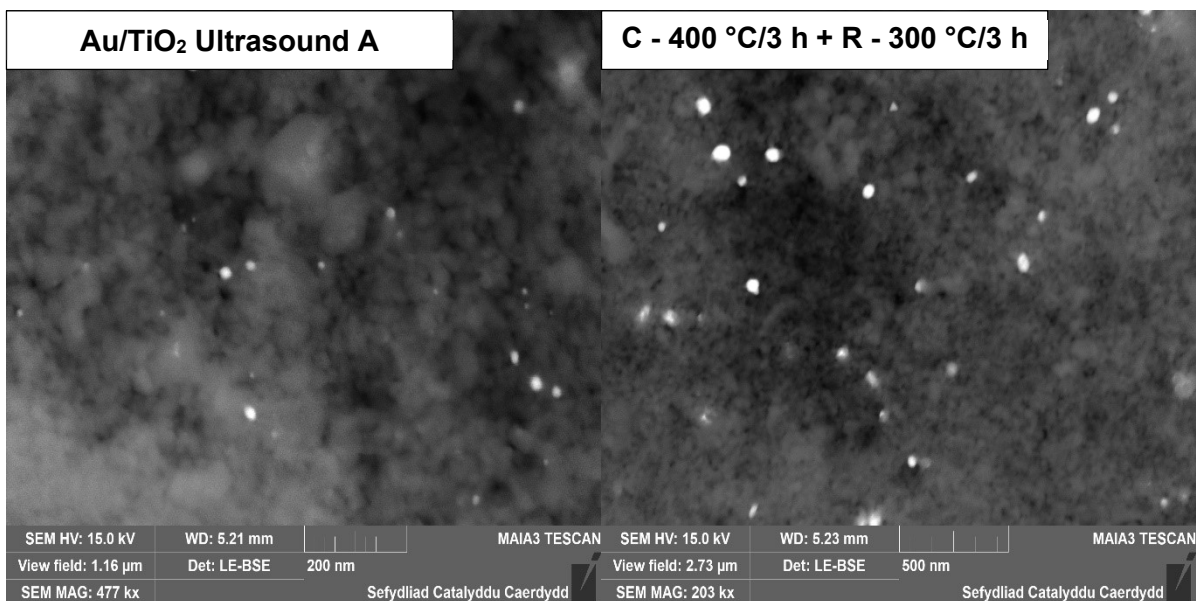
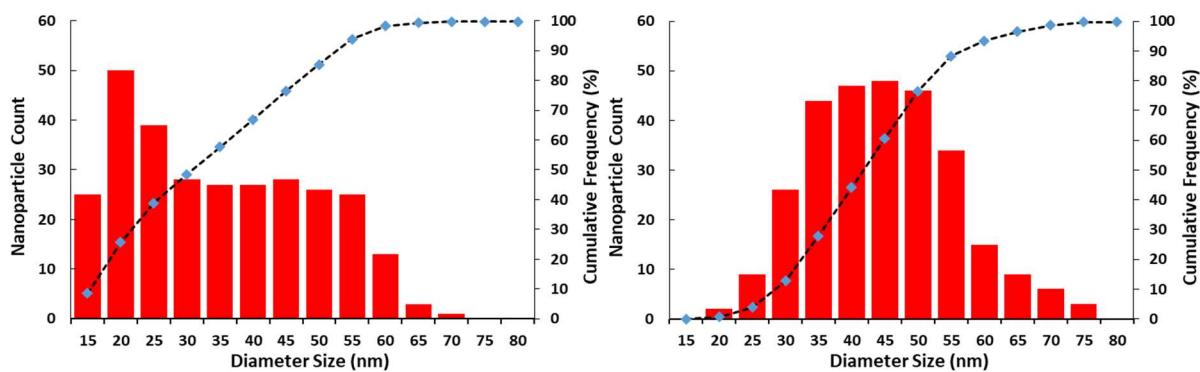


Figure 130 – FEG-SEM analysis of TiO₂ supported Au nanoparticles produced by ultrasound synthesis with the operating condition A without heat treatment (left) and after heat treatment (right).

Catalysts Characterisation

5.2 Transmission Electron Microscopy

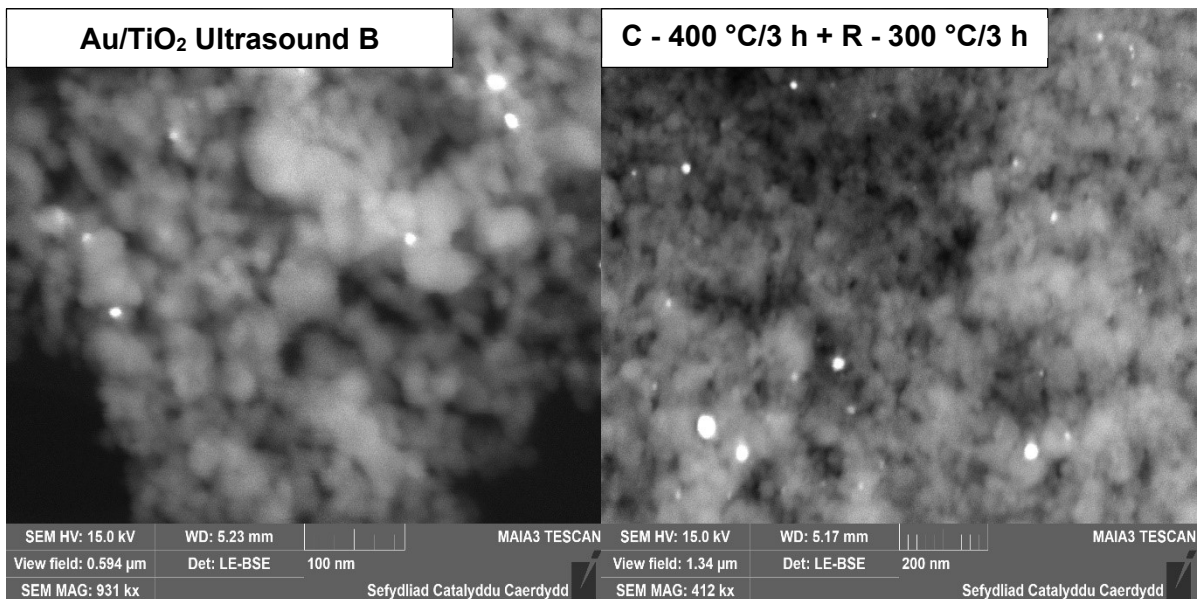
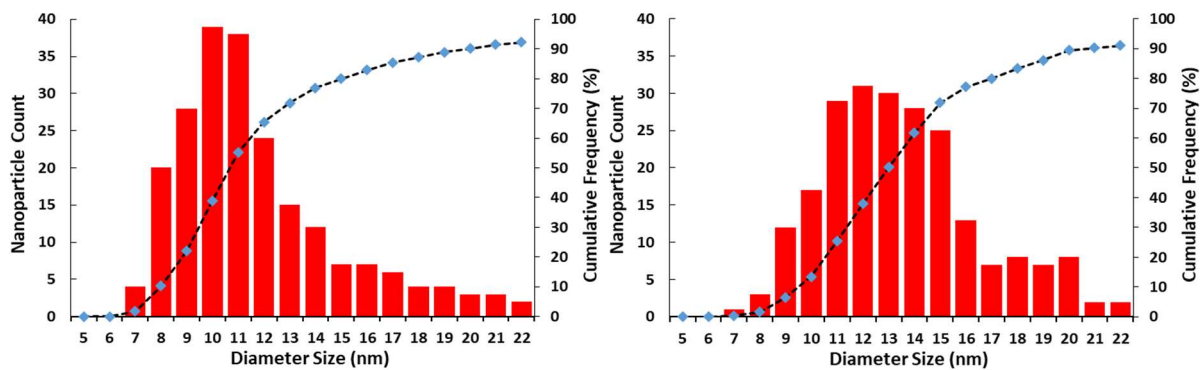


Figure 131 – FEG-SEM analysis of TiO₂ supported Au nanoparticles produced by ultrasound synthesis with the operating condition B without heat treatment (left) and after heat treatment (right).

Catalysts Characterisation

5.2 Transmission Electron Microscopy

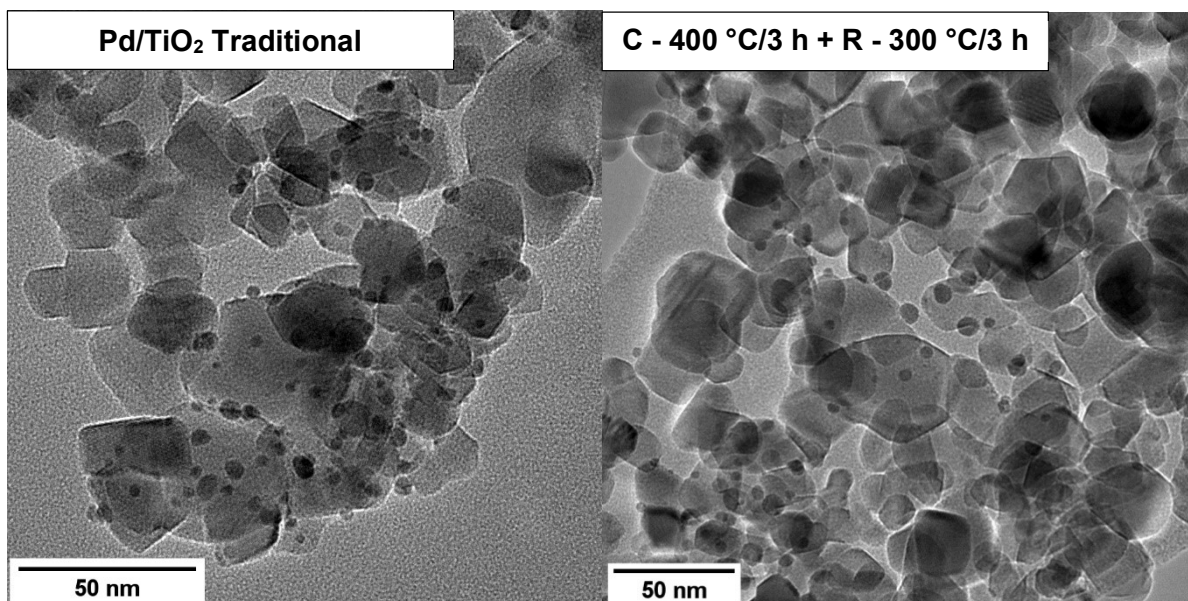
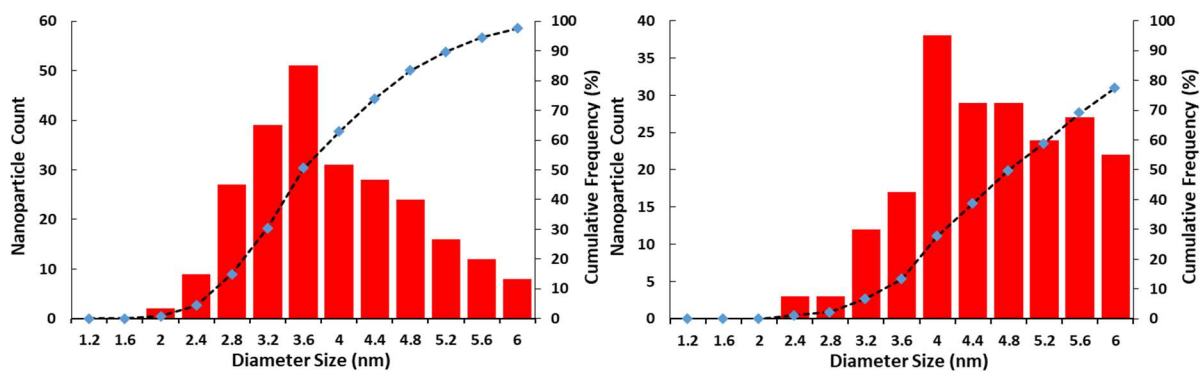


Figure 132 – TEM analysis of TiO₂ supported Pd nanoparticles produced with the traditional sol-immobilization protocol without heat treatment (left) and after heat treatment (right).

Catalysts Characterisation

5.2 Transmission Electron Microscopy

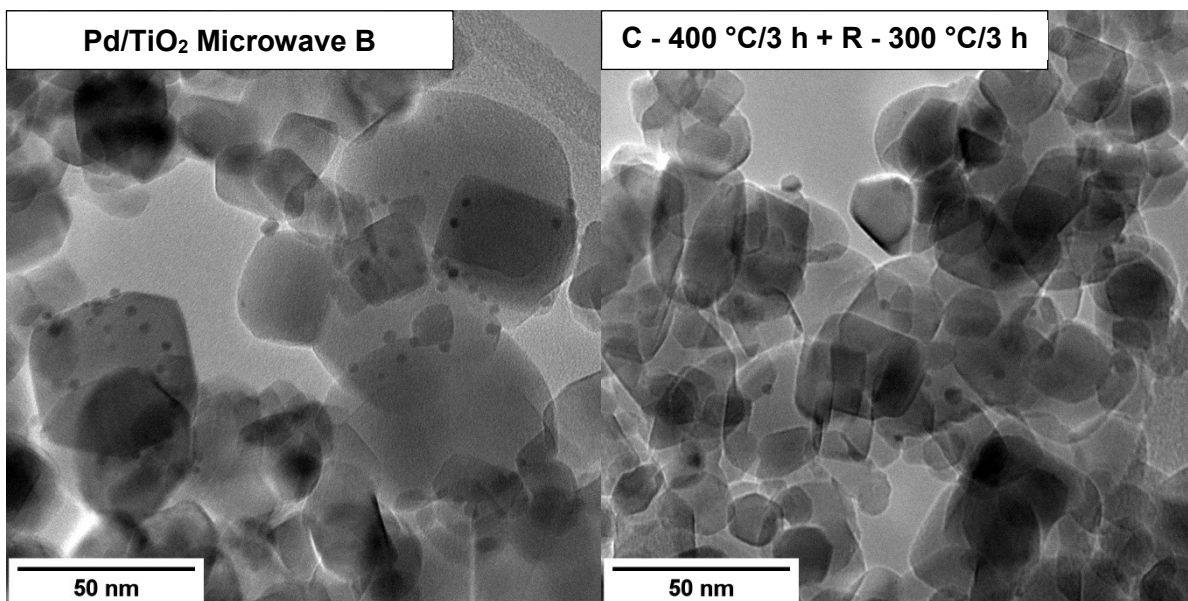
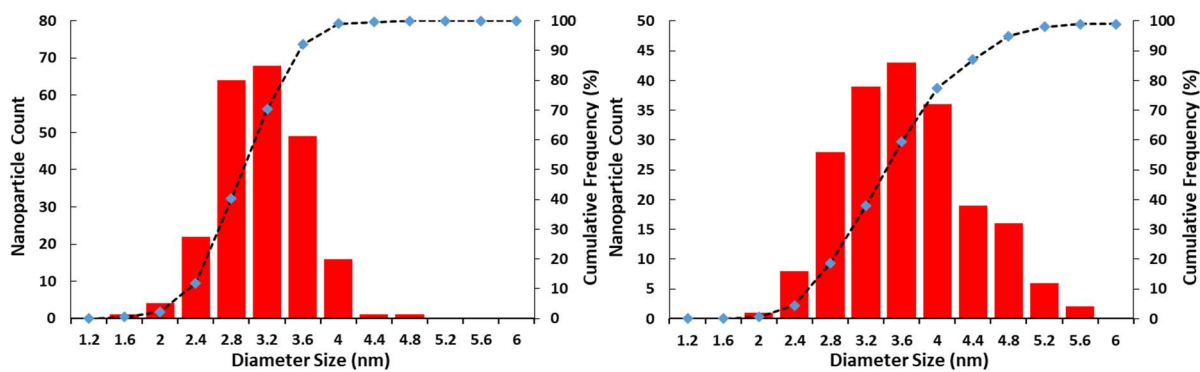


Figure 133 – TEM analysis of TiO₂ supported Pd nanoparticles produced by microwave synthesis with the operating condition B without heat treatment (left) and after heat treatment (right).

Catalysts Characterisation

5.2 Transmission Electron Microscopy

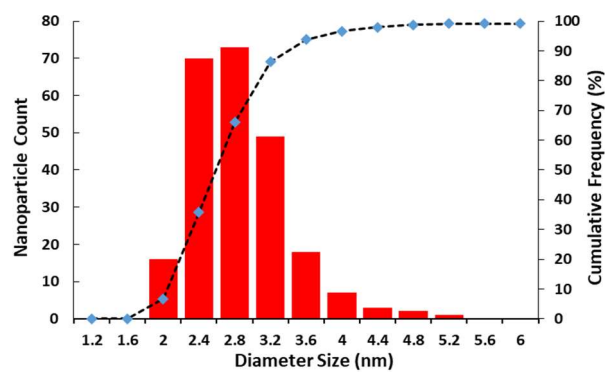
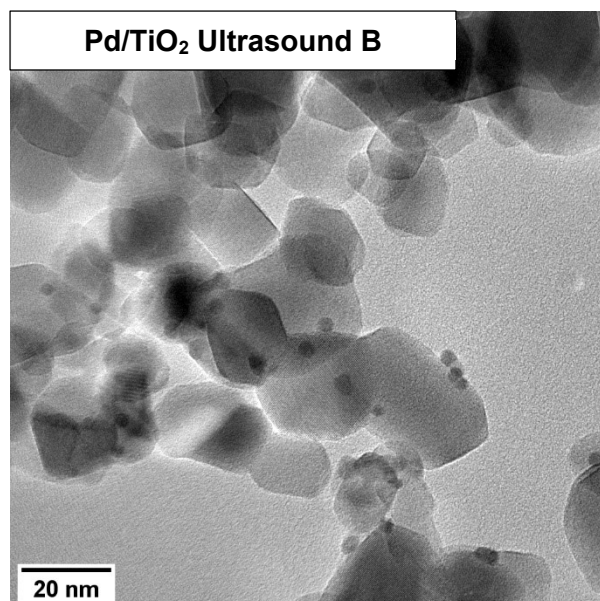


Figure 134 – TEM analysis of TiO₂ supported Pd nanoparticles produced by ultrasound synthesis with the operating condition B without heat treatment.

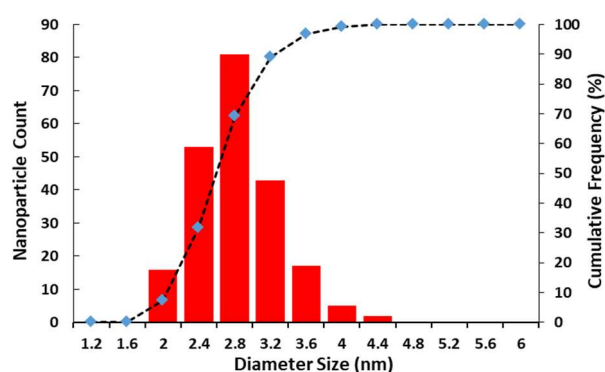
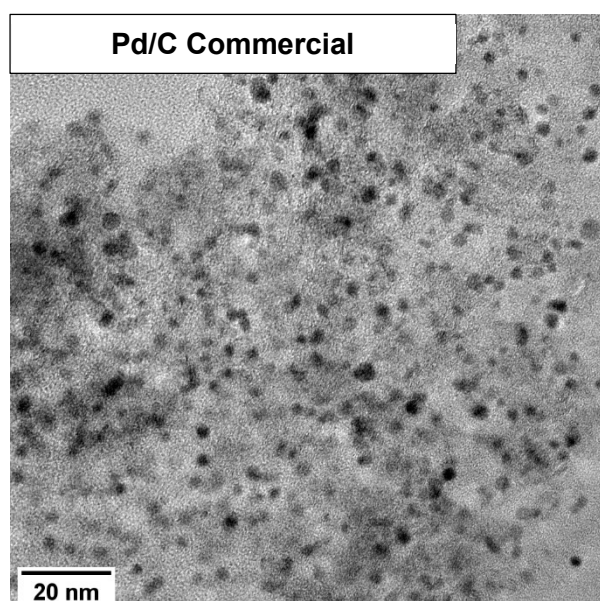


Figure 135 – TEM analysis of commercial carbon supported Pd nanoparticles.

Catalysts Characterisation

5.2 Transmission Electron Microscopy

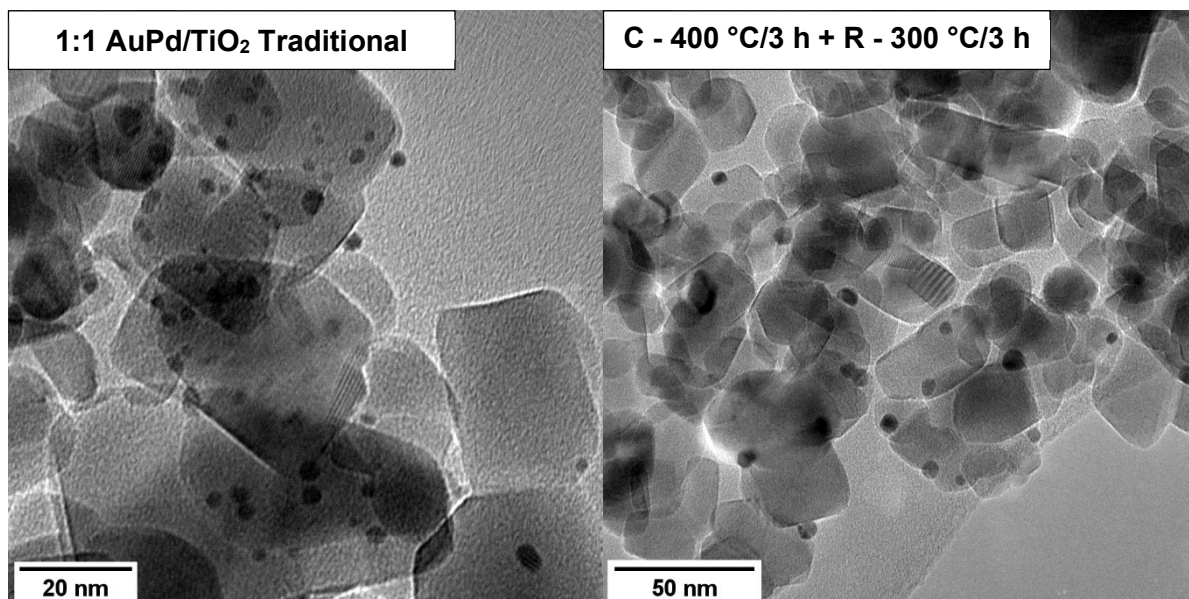
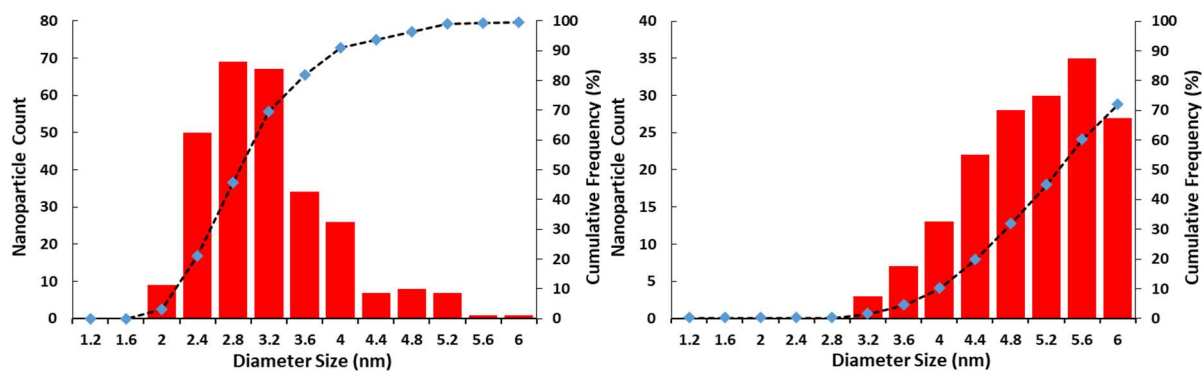


Figure 136 – TEM analysis of TiO₂ supported AuPd (1:1) nanoparticles produced with the traditional sol-immobilization protocol without heat treatment (left) and after heat treatment (right).

Catalysts Characterisation
5.2 Transmission Electron Microscopy

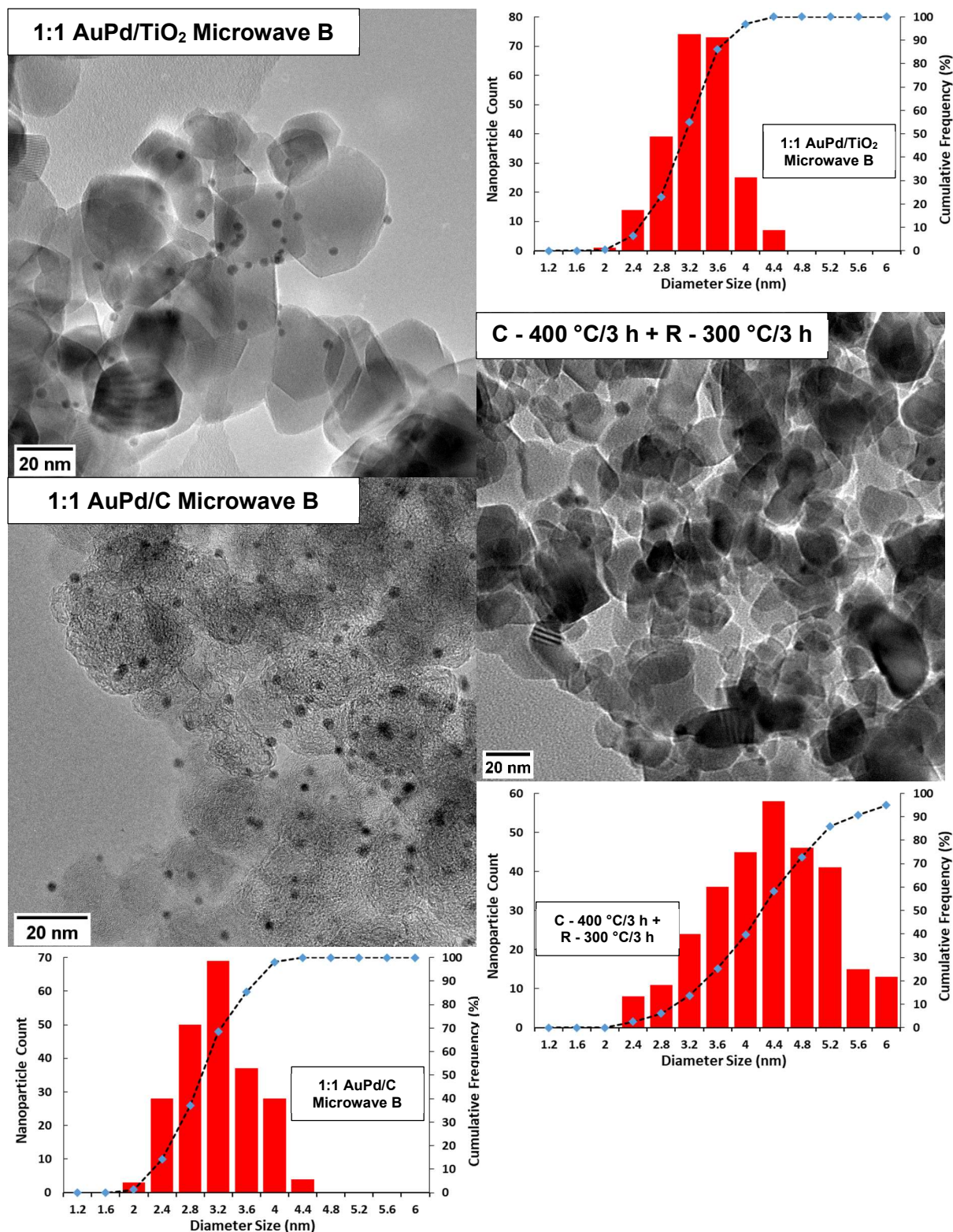


Figure 137 – TEM analysis of TiO₂ supported AuPd (1:1) nanoparticles produced by microwave synthesis with the operating condition B without heat treatment (top left) and after heat treatment (middle right) and of carbon supported of the same AuPd (1:1) nanoparticles (bottom left).

Catalysts Characterisation

5.2 Transmission Electron Microscopy

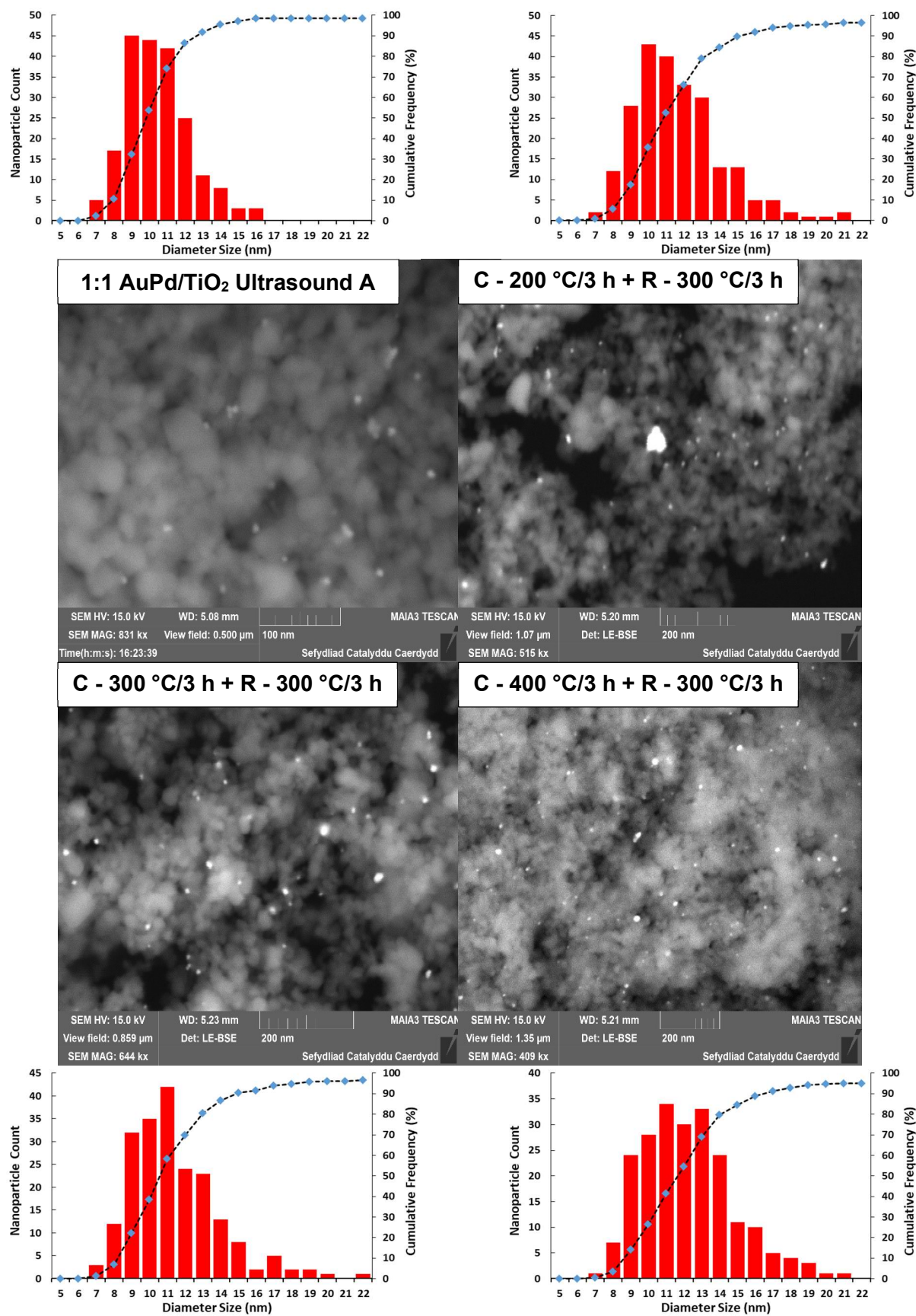


Figure 138 – FEG-SEM analysis of TiO₂ supported AuPd (1:1) nanoparticles produced by ultrasound synthesis with the operating condition A without heat treatment and after heat treatment at different conditions.

Catalysts Characterisation

5.2 Transmission Electron Microscopy

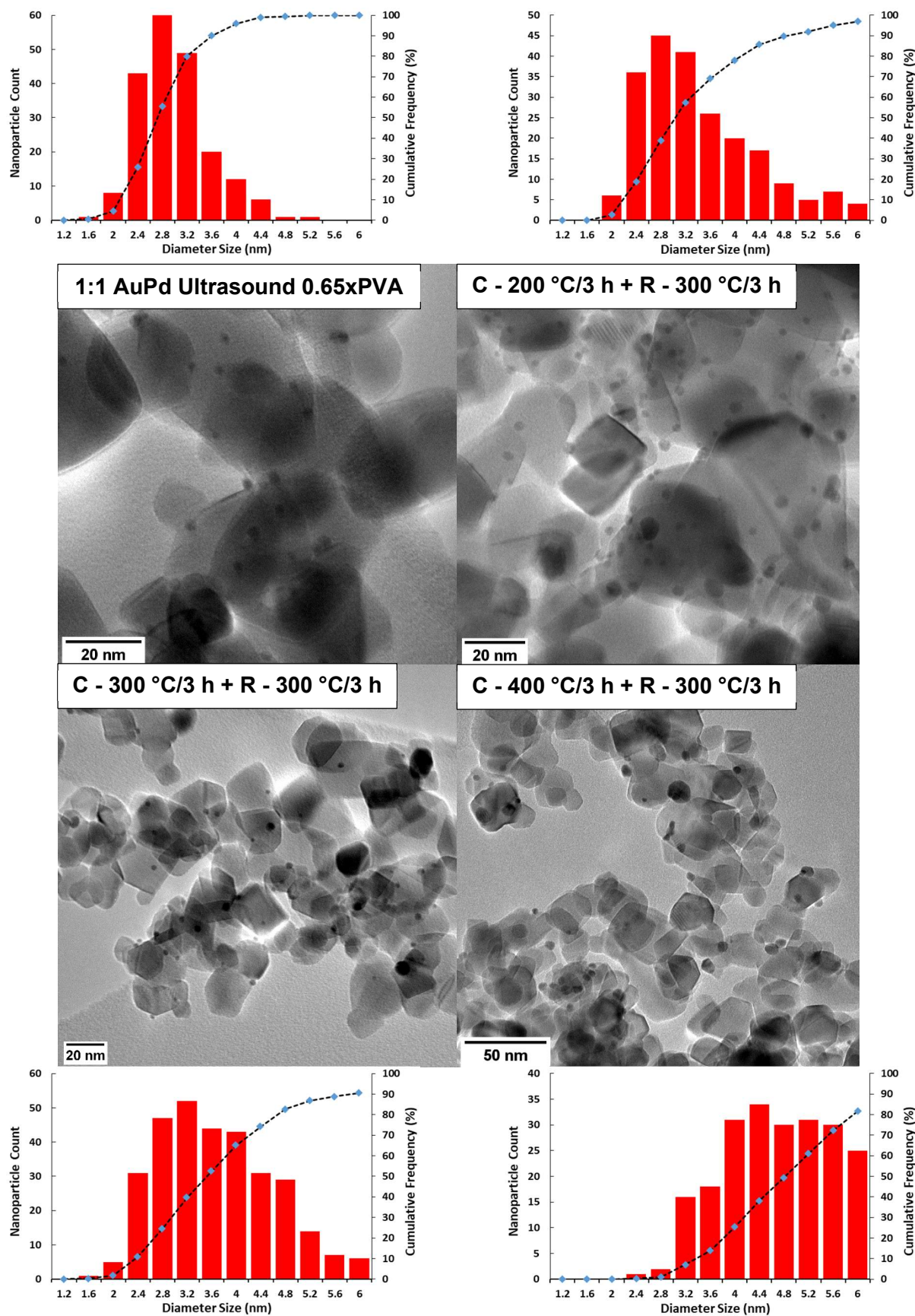


Figure 139 – TEM analysis of TiO₂ supported AuPd (1:1) nanoparticles produced by ultrasound synthesis with 0.65xPVA without heat treatment and after heat treatment at different conditions.

Catalysts Characterisation

5.2 Transmission Electron Microscopy

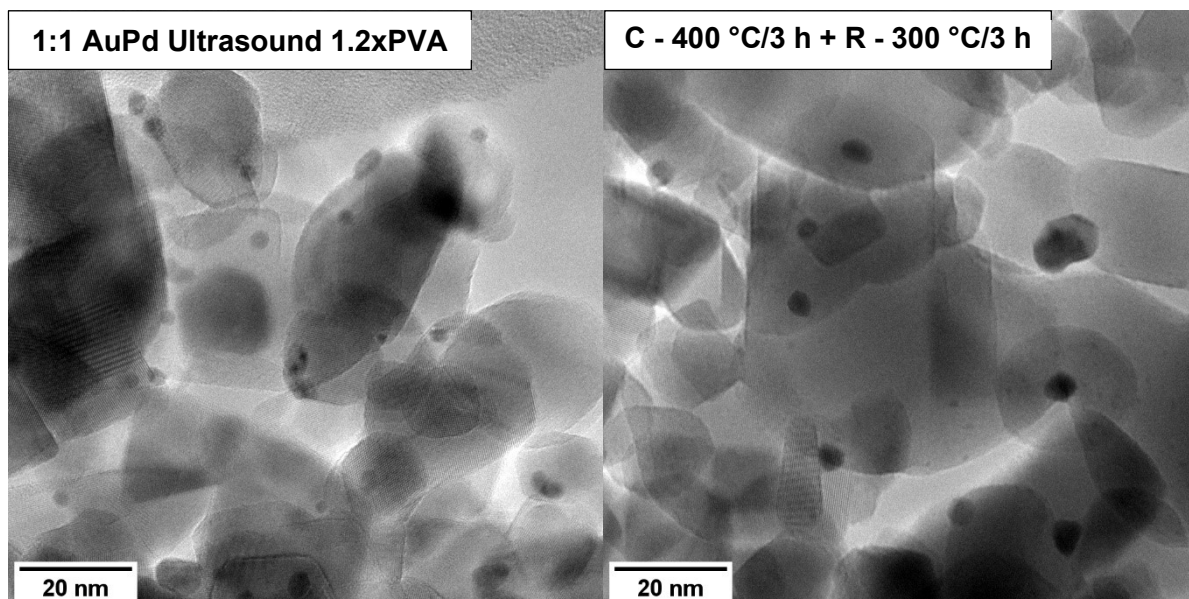
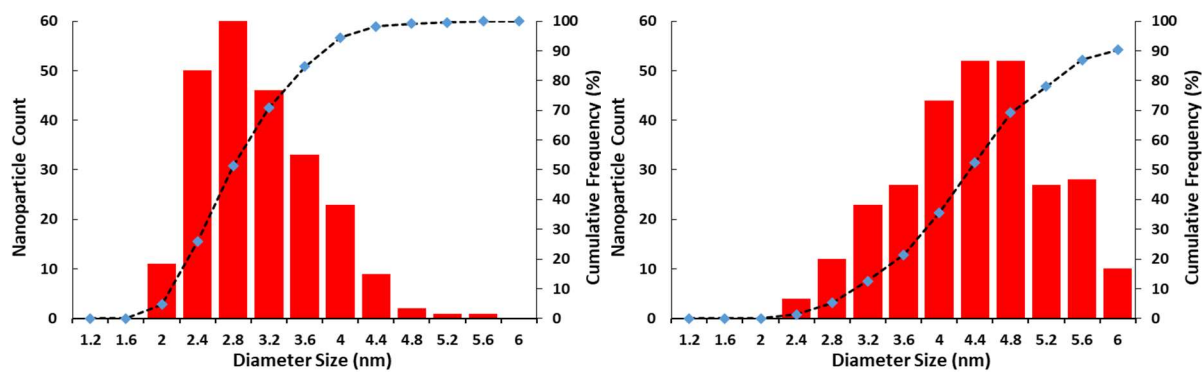
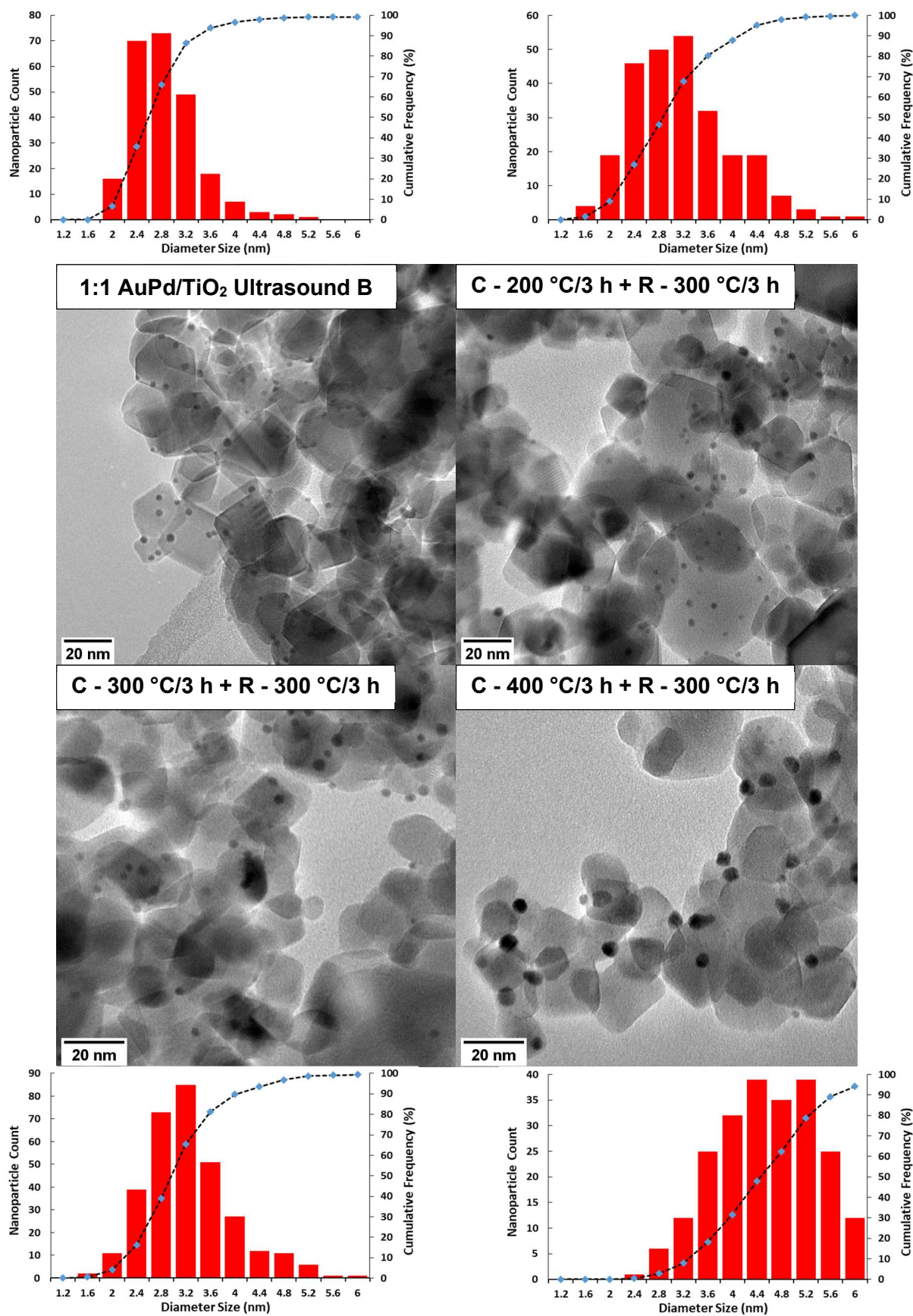


Figure 140 – TEM analysis of TiO₂ supported AuPd (1:1) nanoparticles produced by ultrasound synthesis with 1.2xPVA without heat treatment (left) and after heat treatment (right).

Catalysts Characterisation

5.2 Transmission Electron Microscopy



Catalysts Characterisation
5.2 Transmission Electron Microscopy

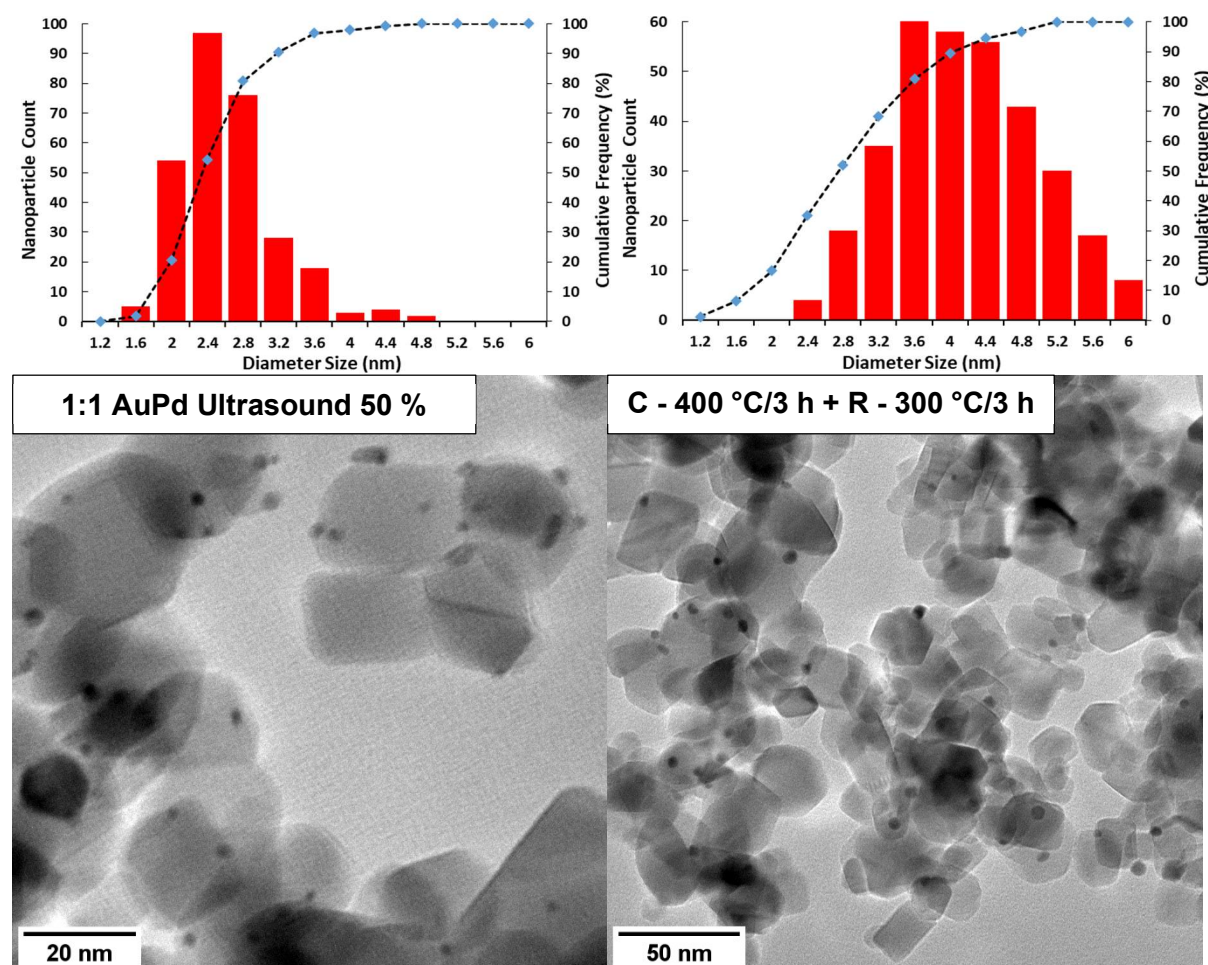
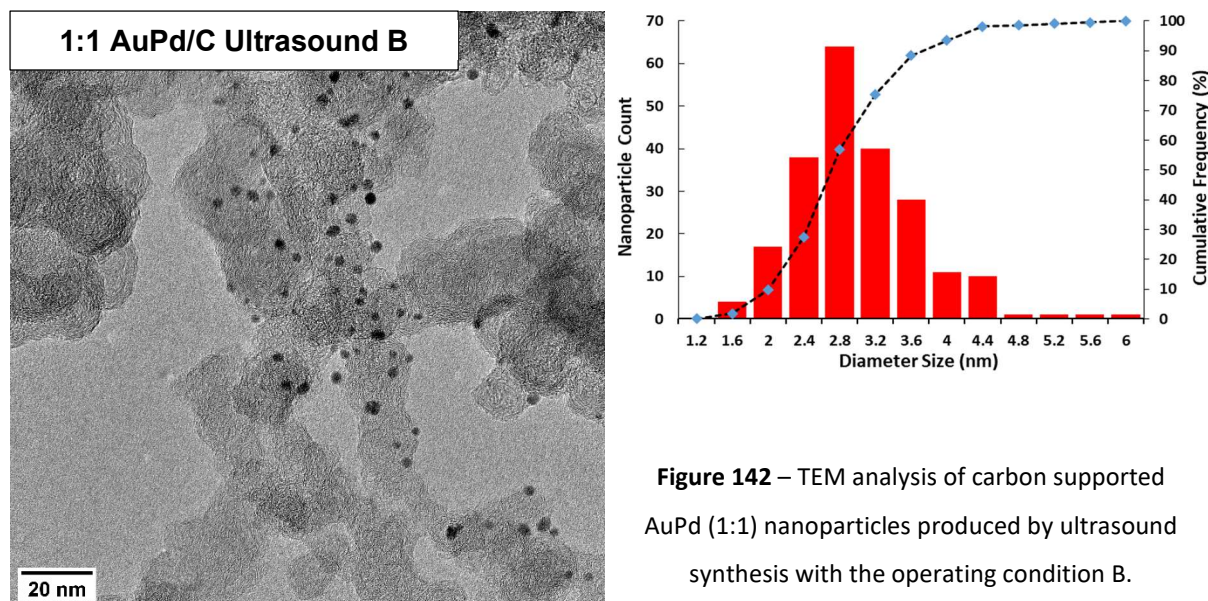


Figure 143 – TEM analysis of TiO₂ supported AuPd (1:1) nanoparticles produced by ultrasound synthesis with 50 % without heat treatment (left) and after heat treatment (right).

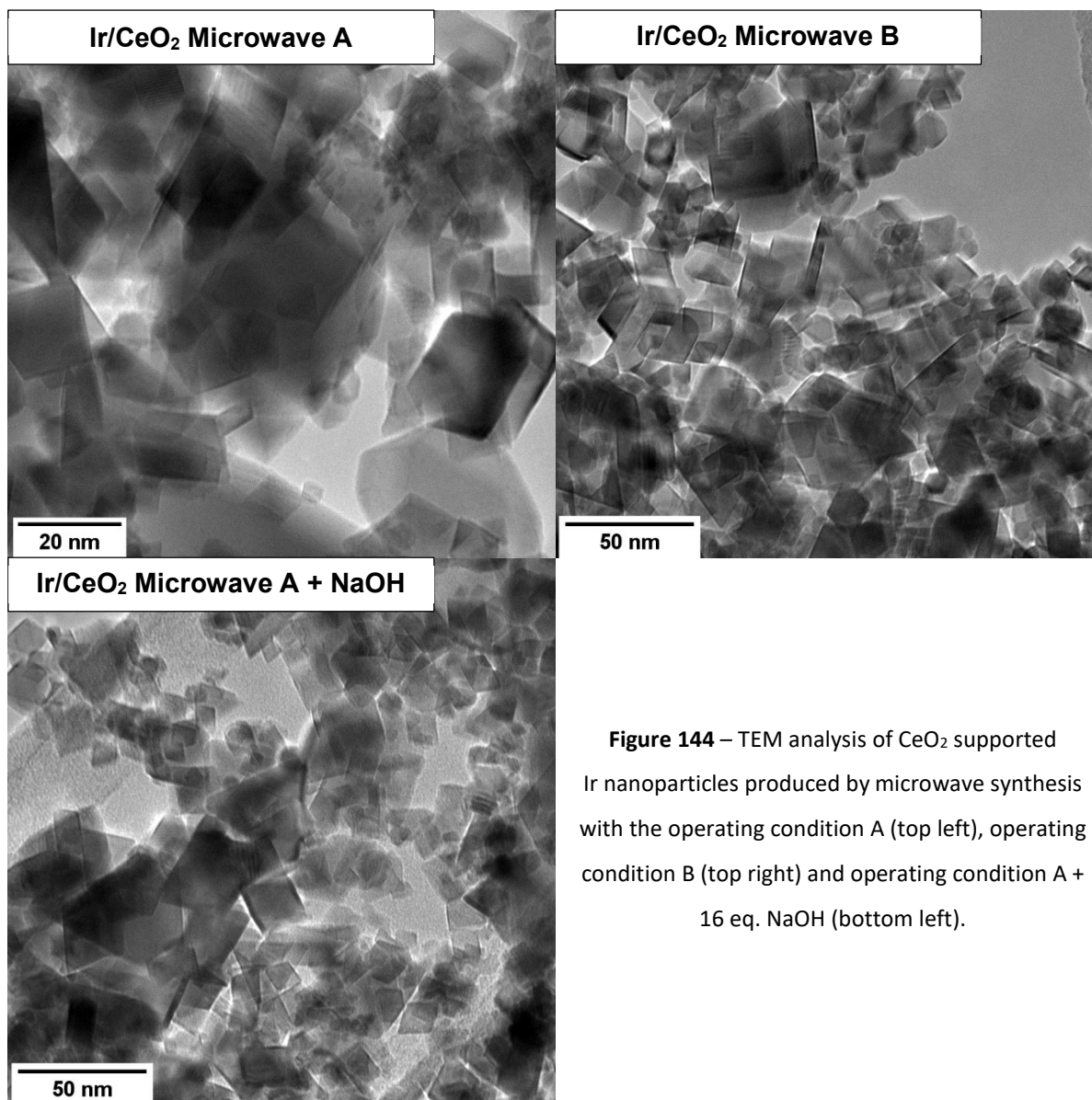


Figure 144 – TEM analysis of CeO₂ supported Ir nanoparticles produced by microwave synthesis with the operating condition A (top left), operating condition B (top right) and operating condition A + 16 eq. NaOH (bottom left).

Catalysts Characterisation

5.3 Scanning Electron Microscopy and Energy Dispersive X-ray

5.3 Scanning Electron Microscopy and Energy Dispersive X-ray (SEM/EDX)

All the catalysts analysed by SEM/EDX can be found in Table 38. Details of the *Traditional* protocol can be found in section 1.4.2.1, details of the *Microwave B* protocol can be found in section 3.4 and details of the *Ultrasound A* and *Ultrasound B* protocols (including modifications) can be found in sections 4.3 and 4.4.3.

Overall, it can be said that SEM/EDX analysis confirmed that the metal nanoparticles were correctly supported and presented total metal loadings close to the expected 1.0 wt. %. This is according to what had been observed during the support addition stage as the filtrate was always checked by UV-Vis spectroscopy in order to ensure that no metal nanoparticles had been lost during the process. The only exception was the Ir/CeO₂ catalysts, which presented metal loadings significantly lower than the expected 1.0 wt. %. Moreover, the Ir/CeO₂ catalysts also presented CeO₂ composition slightly higher than 100 wt. %. This is an indication that there would be a lack of oxygen if all the Ce was present as Ce(IV), with the support being only CeO₂. However, it is very likely that Ce is also present as Ce(III), with the support being also made of Ce₂O₃.

The SEM/EDX analysis also indicated some contamination with carbon. It is interesting that this carbon contamination could be observed for all the catalysts except for the AuPd (1:1) catalysts. This carbon contamination could not be linked to the amount of stabilizer used during the metal nanoparticles synthesis, for example the Au nanoparticles produced by ultrasound synthesis with the operating condition A, without any stabilizer, and supported on TiO₂ had a carbon composition of 1.8 ± 0.3 wt. % whereas the AuPd nanoparticles produced by ultrasound synthesis with the operating condition B and supported on TiO₂ did not present any carbon contamination. This carbon contamination could also not be linked to the ethylene glycol used during the metal nanoparticles synthesis, for example the Au nanoparticles produced by the traditional sol-immobilization protocol, without any ethylene glycol, and supported on TiO₂ had a carbon composition of 2.2 ± 0.5 wt. %.

It was not possible to identify the source of this bulk carbon contamination in the catalysts. However, it is possible that this carbon contamination could be due only to external contamination during sample preparation. Other common contaminants were also checked, namely sodium, sulphur, potassium and chlorine, but no significant amount could be detected.

Catalysts Characterisation

5.3 Scanning Electron Microscopy and Energy Dispersive X-ray

Table 38 – SEM/EDX bulk mass composition of supported metal nanoparticles produced at different operating conditions.

Metal	Support	Protocol	Metal (wt. %)	Support (wt. %)	Carbon (wt. %)	Other (wt. %)
Au	TiO ₂	Traditional	0.8 ± 0.1	89 ± 2	2.2 ± 0.5	0
Au	TiO ₂	Microwave B	0.8 ± 0.1	98 ± 3	2.4 ± 0.4	0
Au	TiO ₂	Ultrasound A	0.9 ± 0.04	88 ± 2	1.8 ± 0.3	0
Au	TiO ₂	Ultrasound B	0.8 ± 0.1	92 ± 3	1.9 ± 0.2	0
Pd	TiO ₂	Traditional	0.7 ± 0.1	95 ± 5	0.1 ± 0.1	0.3 ± 0.2
Pd	TiO ₂	Microwave B	0.5 ± 0.1	95 ± 6	0.3 ± 0.4	0.1 ± 0.04
Pd	TiO ₂	Ultrasound A	0.9 ± 0.1	94 ± 4	0.5 ± 0.3	0
Pd	TiO ₂	Ultrasound B	0.9 ± 0.1	93 ± 2	0.5 ± 0.4	0
AuPd (1:1)	TiO ₂	Traditional	Au - 0.7 ± 0.1 Pd - 0.4 ± 0.03	93 ± 2	0	0
AuPd (1:1)	TiO ₂	Microwave B	Au - 0.5 ± 0.03 Pd - 0.3 ± 0.02	94 ± 1	0	0.2 ± 0.02
AuPd (1:1)	C	Microwave B	Au - 0.8 ± 0.1 Pd - 0.5 ± 0.1	99 ± 0.1	N/A	0
AuPd (1:1)	TiO ₂	Ultrasound A	Au - 0.6 ± 0.04 Pd - 0.3 ± 0.1	96 ± 2	0	0
AuPd (1:1)	TiO ₂	Ultrasound 0.65xPVA	Au - 0.8 ± 0.1 Pd - 0.4 ± 0.04	87 ± 5	0	0
AuPd (1:1)	TiO ₂	Ultrasound 1.2xPVA	Au - 0.7 ± 0.04 Pd - 0.4 ± 0.02	94 ± 4	0	0
AuPd (1:1)	TiO ₂	Ultrasound B	Au - 0.6 ± 0.1 Pd - 0.4 ± 0.03	95 ± 2	0	0
AuPd (1:1)	C	Ultrasound B	Au - 0.8 ± 0.03 Pd - 0.5 ± 0.1	99 ± 0.1	N/A	0
AuPd (1:1)	TiO ₂	Ultrasound 50 %	Au - 0.6 ± 0.1 Pd - 0.4 ± 0.04	96 ± 3	0	0
Ir	CeO ₂	Microwave A	0.2 ± 0.1	102 ± 1	1.7 ± 0.1	0.1 ± 0.03
Ir	CeO ₂	Microwave B	0.4 ± 0.2	102 ± 1	2.1 ± 0.3	0.1 ± 0.04
Ir	CeO ₂	Microwave A+NaOH	0.4 ± 0.1	101 ± 1	1.8 ± 0.1	0.1 ± 0.03

5.4 X-ray Photoelectron Spectroscopy (XPS)

All catalysts analysed by XPS are presented in Table 39. Details of the *Traditional* protocol can be found in section 1.4.2.1, details of the *Microwave B* protocol can be found in section 3.4 and details of the *Ultrasound A* and *Ultrasound B* protocols (including modifications) can be found in sections 4.3 and 4.4.3.

The XPS peaks were analysed as described in section 2.2.5. All XPS peak fittings presented a residual standard deviation very close to 1.0, an indication that the fitting assumptions were correct. Figure 145 shows typical XPS peak fittings for some of the metal nanoparticles supported catalysts.

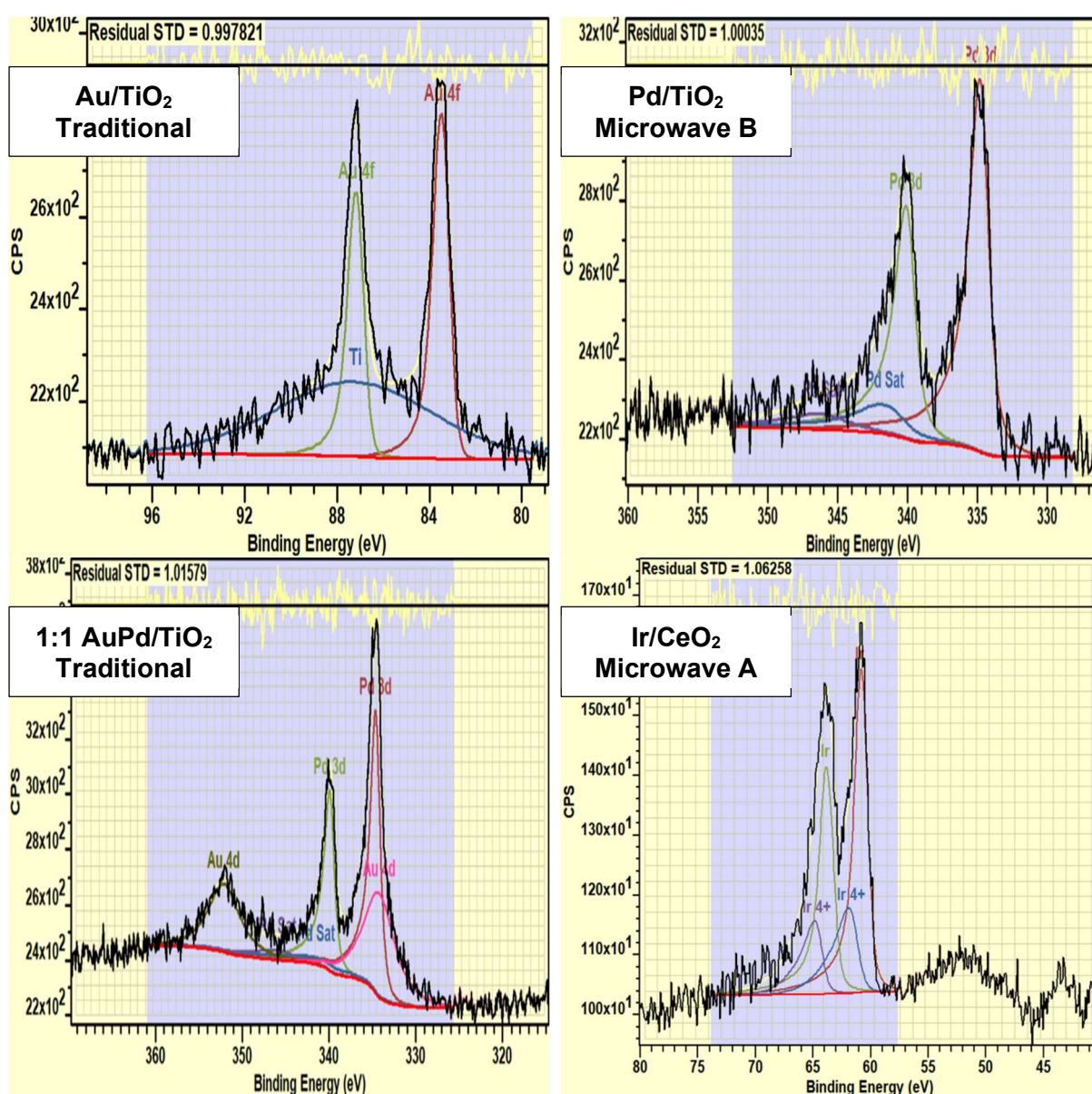


Figure 145 – Typical XPS peak fittings of supported metal nanoparticles produced at different operating conditions.

Catalysts Characterisation

5.4 X-ray Photoelectron Spectroscopy

As observed in Figure 145 correct fittings could be implemented despite interference from other chemical species. The Au 4f region presented some interference from the TiO₂ support. When analysing Pd catalysts the Pd fitting took into consideration the existence of Pd²⁺, Pd⁰ and other unknown forms of Pd (Pd Sat.). When analysing AuPd catalysts the Pd fitting did not consider anymore the existence of Pd²⁺, but there was now interference from Au 4d. The Ir fitting considered the existence of Ir⁰ and Ir⁴⁺.

Overall, it can be said that XPS analysis indicated that the compositions of the metal nanoparticles on the surface of the catalysts were higher than 1.0 wt. %. Only the Au catalysts presented compositions similar to 1.0 wt. %. When considering the metal composition average of all the untreated catalysts in Table 39 a value of 2.3 wt. % is achieved, with the highest metal composition of 7.2 wt. % observed for the Ir/CeO₂ catalyst produced by microwave synthesis with the operating condition A + 16 eq. NaOH.

This result was the expected, as during the support addition stage it is easier to have the metal nanoparticles immediately supported on the surface than to have them diffusing through a porous support and only after supported. No correlation could be established between the metal nanoparticles average size and the surface composition. Actually, as shown by TEM analysis, the Au nanoparticles presented the largest average sizes but that has not interfered with the porous diffusion as the Au catalysts were the only ones to present surface compositions similar to 1.0 wt. %. In any case, as shown in section 5.3 the metal bulk compositions of all the catalysts were similar to the theoretical value of 1.0 wt. %.

Surprisingly, for the 1:1 AuPd/TiO₂ catalysts the average Au/Pd mass composition ratio was of only 1.3, considerably lower than the theoretical mass ratio of 1.85. This was independent of the synthesis protocol. It is not clear why this ratio has decreased when changing from the SEM/EDX analysis to the XPS analysis. For the 1:1 AuPd/C catalyst produced by microwave synthesis with the operating condition B this ratio was even lower. However, there might have been a problem with the XPS analysis/fitting of this sample as the Pd 3d region presented an unusual interference, probably from overlap with carbon peak(s).

From the XPS analysis around 80 % of the Pd was present as Pd⁰ and the remaining as Pd²⁺. The Pd/TiO₂ produced with the traditional sol-immobilization protocol presented a lower value of around 60 %, but this might have been the result of a larger delay between this catalyst synthesis and the XPS analysis when compared to what happened with the other Pd catalysts. This would have allowed more time for the Pd nanoparticles to be oxidised due to contact with the atmosphere.

Catalysts Characterisation

5.4 X-ray Photoelectron Spectroscopy

From the XPS analysis around 70-80 % of the Ir was present as Ir⁰ and the remaining as Ir⁴⁺. There was also indication that around 10 % of the support was Ce₂O₃ instead of CeO₂. This confirms the result obtained with the SEM/EDX analysis in section 5.3.

The XPS analysis also indicated some contamination with carbon. Contrary to the SEM/EDX analysis in section 5.3 it was possible to link this carbon contamination to the amount of stabilizer used during the metal nanoparticles synthesis. Thus, the highest carbon compositions (4-5 wt. %) were obtained for the catalysts which used protocols with a stabilizer/metal weight ratio of 3.25.

Moreover, when the previous catalysts were subject to heat treatments, therefore removing traces of stabilizer, the carbon composition also decreased as expected. The only exception was the 1:1 AuPd/TiO₂ catalyst produced by ultrasound synthesis with the operating condition B, but using a PVA/metal weight ratio of 0.65 instead of the 3.25, which for the calcination temperature of 300 °C had a significant increase in the carbon composition. There might have been some external contamination with this sample.

However, it can be said that there is always some residual carbon even when no stabilizer was used, for example the 1:1 AuPd/TiO₂ catalyst produced by ultrasound synthesis with the operating condition A presented a carbon composition of 2.4 wt. %. This is consistent with what was observed with the SEM/EDX analysis in section 5.3.

Again, as mentioned with the TEM analysis in section 5.2, the XPS analysis allowed to understand that the filtration/washing step during the support addition stage is not enough to completely remove stabilizer traces from the catalyst surface. This is a very important observation as it demonstrates that some of the literature methods previously mentioned in chapters 3 and 4 are not suitable for the production of metal nanoparticles meant to be used as catalysts as they employ amounts of stabilizer much higher than the maximum stabilizer/metal weight ratio of 3.25 used for this PhD. As previously explained, too much stabilizer can hinder the catalytic activity as it blocks the substrate access to the metal nanoparticles, which are the active sites.

Catalysts Characterisation

5.4 X-ray Photoelectron Spectroscopy

Table 39 – XPS surface mass composition of supported metal nanoparticles produced at different operating conditions.

	Metal (wt. %)	Support (wt. %)	Carbon (wt. %)	Other (wt. %)
Au/TiO₂ Traditional				
No Heat Treatment	1.0	88	2.8	1.7
Calci. – 400 °C/3 h + Red. – 300 °C/3 h	0.9	91	2.1	1.2
Au/TiO₂ Microwave B				
No Heat Treatment	0.6	88	4.1	0.5
Calci. – 400 °C/3 h + Red. – 300 °C/3 h	0.7	91	2.8	0.7
Au/TiO₂ Ultrasound B				
No Heat Treatment	0.7	88	3.4	0.9
Calci. – 400 °C/3 h + Red. – 300 °C/3 h	0.7	91	1.8	1.1
Pd/TiO₂ Traditional				
No Heat Treatment	Pd – 2.6 Pd ⁰ = 60 %	86	3.2	1.9
Calci. – 400 °C/3 h + Red. – 300 °C/3 h	Pd – 2.5 Pd ⁰ = 82 %	89	2.2	1.3
Pd/TiO₂ Microwave B				
No Heat Treatment	Pd – 1.6 Pd ⁰ = 83 %	88	4.8	0
Calci. – 400 °C/3 h + Red. – 300 °C/3 h	Pd – 1.8 Pd ⁰ = 75 %	89	2.8	0.6
Pd/TiO₂ Ultrasound B				
No Heat Treatment	Pd – 2.6 Pd ⁰ = 84 %	86	4.2	0.6
AuPd/TiO₂ Traditional				
No Heat Treatment	Au – 1.7 Pd – 1.4	86	3.1	1.7
Calci. – 400 °C/3 h + Red. – 300 °C/3 h	Au – 1.1 Pd – 1.6	90	1.8	0.9
1:1 AuPd/TiO₂ Microwave B				
No Heat Treatment	Au – 1.1 Pd – 0.8	85	4.6	1.1
Calci. – 400 °C/3 h + Red. – 300 °C/3 h	Au – 0.9 Pd – 0.7	90	2.4	0.5

Catalysts Characterisation
5.4 X-ray Photoelectron Spectroscopy

	Metal (wt. %)	Support (wt. %)	Carbon (wt. %)	Other (wt. %)
7:1 AuPd/TiO₂ Microwave B				
No Heat Treatment	Au – 1.3 Pd – 0.2	89	3.0	0.7
3:1 AuPd/TiO₂ Microwave B				
No Heat Treatment	Au – 1.3 Pd – 0.4	88	4.0	0.9
1:3 AuPd/TiO₂ Microwave B				
No Heat Treatment	Au – 0.6 Pd – 1.2	88	4.0	0.2
1:7 AuPd/TiO₂ Microwave B				
No Heat Treatment	Au – 0.3 Pd – 1.7	86	5.5	0.3
1:1 AuPd/C Microwave B				
No Heat Treatment	Au – 1.0 Pd – 2.2	94	N/A	0
1:1 AuPd/TiO₂ Ultrasound A				
No Heat Treatment	Au – 0.7 Pd – 0.9	90	2.4	0.7
Calci. – 200 °C/3 h + Red. – 300 °C/3 h	Au – 0.6 Pd – 0.6	90	2.0	0.6
Calci. – 300 °C/3 h + Red. – 300 °C/3 h	Au – 0.7 Pd – 0.6	91	1.7	0.8
Calci. – 400 °C/3 h + Red. – 300 °C/3 h	Au – 0.5 Pd – 0.8	89	2.5	0.7
1:1 AuPd/TiO₂ Ultrasound 0.65xPVA				
No Heat Treatment	Au – 1.6 Pd – 1.3	88	2.6	0
Calci. – 200 °C/3 h + Red. – 300 °C/3 h	Au – 1.4 Pd – 1.0	89	2.7	0.85
Calci. – 300 °C/3 h + Red. – 300 °C/3 h	Au – 1.3 Pd – 1.2	82	7.1	1.2
Calci. – 400 °C/3 h + Red. – 300 °C/3 h	Au – 1.2 Pd – 1.0	91	1.5	0.3

Catalysts Characterisation
5.4 X-ray Photoelectron Spectroscopy

	Metal (wt. %)	Support (wt. %)	Carbon (wt. %)	Other (wt. %)
1:1 AuPd/TiO₂ Ultrasound 1.2xPVA				
No Heat Treatment	Au – 1.5 Pd – 1.1	88	2.6	0.6
Calci. – 400 °C/3 h + Red. – 300 °C/3 h	Au – 1.1 Pd – 1.0	90	1.9	0.9
1:1 AuPd/TiO₂ Ultrasound B				
No Heat Treatment	Au – 1.7 Pd – 1.0	85	4.7	1.0
Calci. – 200 °C/3 h + Red. – 300 °C/3 h	Au – 1.5 Pd – 1.2	87	4.0	1.3
Calci. – 300 °C/3 h + Red. – 300 °C/3 h	Au – 1.5 Pd – 1.2	87	3.8	1.2
Calci. – 400 °C/3 h + Red. – 300 °C/3 h	Au – 1.0 Pd – 1.1	88	4.2	0.9
1:1 AuPd/TiO₂ Ultrasound 50 %				
No Heat Treatment	Au – 1.5 Pd – 1.4	86	3.9	0.2
Calci. – 400 °C/3 h + Red. – 300 °C/3 h	Au – 1.1 Pd – 1.1	90	1.9	0.9
Ir/CeO₂ Microwave A				
No Heat Treatment	Ir – 2.3 Ir ⁰ = 71 %	CeO ₂ - 78 Ce ₂ O ₃ - 11	0	0
Ir/CeO₂ Microwave A + 16 Eq. NaOH				
No Heat Treatment	Ir – 7.2 Ir ⁰ = 81 %	CeO ₂ - 72 Ce ₂ O ₃ - 10	0	0.8

a) Calci. stands for calcination;

b) Red. stands for reduction;

Catalysts Characterisation

5.5 Diffuse Reflectance Infrared Fourier Transform Spectroscopy

5.5 Diffuse Reflectance Infrared Fourier Transform Spectroscopy (DRIFTS)

The Au/TiO₂ and Pd/TiO₂ catalysts analysed by DRIFTS can be found in Figure 146 and Figure 147 respectively. The DRIFTS analysis of the 1:1 AuPd/TiO₂ catalysts is shown in Figure 148, including for a catalyst heat-treated at standard conditions and prepared by the traditional sol-immobilization protocol. The AuPd molar composition ratio influence on DRIFTS analysis is highlighted in Figure 149 for the catalysts prepared by microwave synthesis with the operating condition B. Details of the *Traditional* protocol can be found in section 1.4.2.1, details of the *Microwave B* protocol can be found in section 3.4 and details of the *Ultrasound A* and *Ultrasound B* protocols (including modifications) can be found in sections 4.3 and 4.4.3.

Overall, the peaks observed during the DRIFTS analysis were affected by carbon monoxide vibrational-rotational transitions and also by the different metal configurations (facet, edge or corner).

All the Au/TiO₂ catalysts presented a carbon monoxide adsorption spectrum very similar to the TiO₂ support. This spectrum indicates a linear carbon monoxide adsorption to the Au nanoparticles (2040-2120 cm⁻¹). It appears that there was no correlation between the type of adsorption and the average size of the Au nanoparticles and/or the synthesis protocol.

The Pd/TiO₂ catalysts presented a new infrared peak (1910-2000 cm⁻¹) consistent with a bridge carbon monoxide adsorption to the Pd nanoparticles. There was still some degree of linear carbon monoxide adsorption but much less than what had been observed with the Au nanoparticles. Again, it appears that there was no correlation between the type of adsorption and the average size of the Pd nanoparticles and/or the synthesis protocol.

The 1:1 AuPd/TiO₂ catalysts presented peaks consistent with a bridge and linear carbon monoxide adsorption to the AuPd (1:1) nanoparticles. Moreover, the catalyst prepared by ultrasound synthesis with the operating condition B also presented a peak consistent with hollow adsorption (1800-1900 cm⁻¹). It was the only catalyst to present this feature. Therefore, it appears that the synthesis protocol adopted can play an important role on the metal nanoparticles configuration. Also, it appears that the AuPd (1:1) nanoparticles average size has influence on the type of adsorption. After being subject to heat treatment the traditional catalyst had the average size increased from 3.0 ± 0.8 nm to 5.4 ± 1.1 nm which caused the infrared spectrum to change (less linear adsorption and higher bridge adsorption).

When analysing the effect of the AuPd molar ratio at a fixed protocol (microwave B) it was not possible to observe any trends. The only interesting observation is that even the small addition of Pd (Au 7:1 Pd) is enough to promote a bridge adsorption.

Catalysts Characterisation

5.5 Diffuse Reflectance Infrared Fourier Transform Spectroscopy

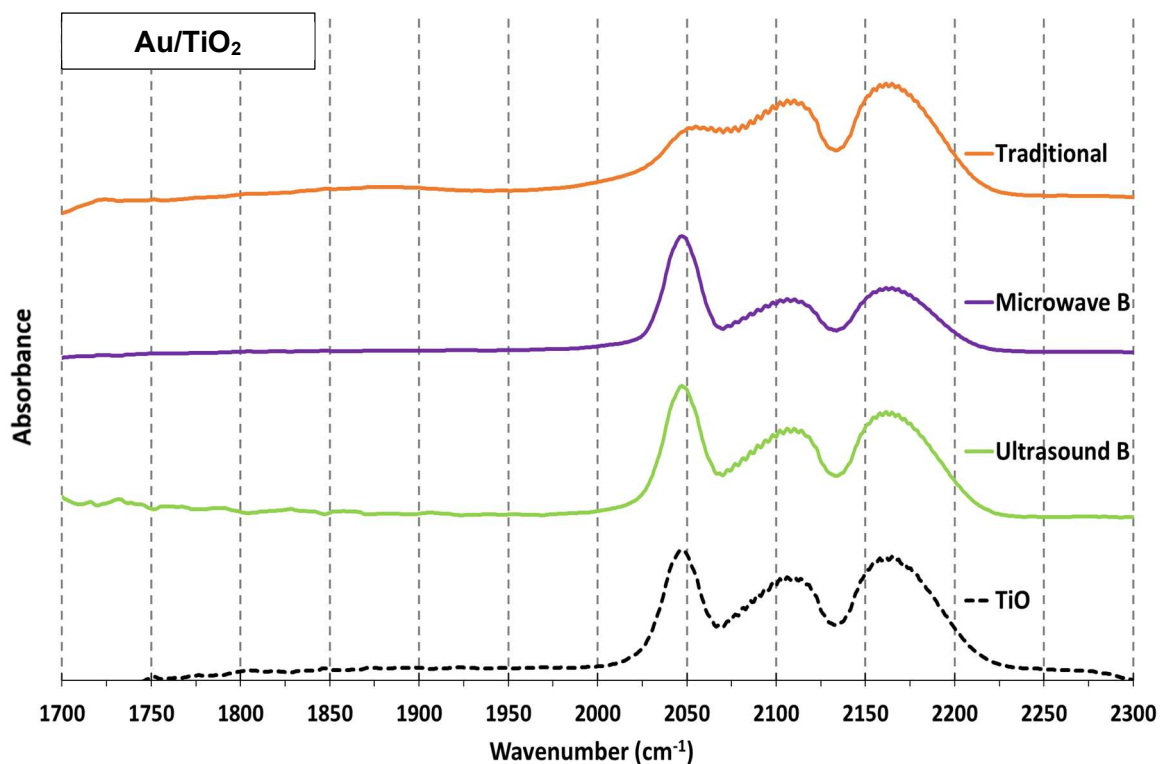


Figure 146 – DRIFTS analysis of Au/TiO₂ catalysts produced at different operating conditions and of the TiO₂ support.

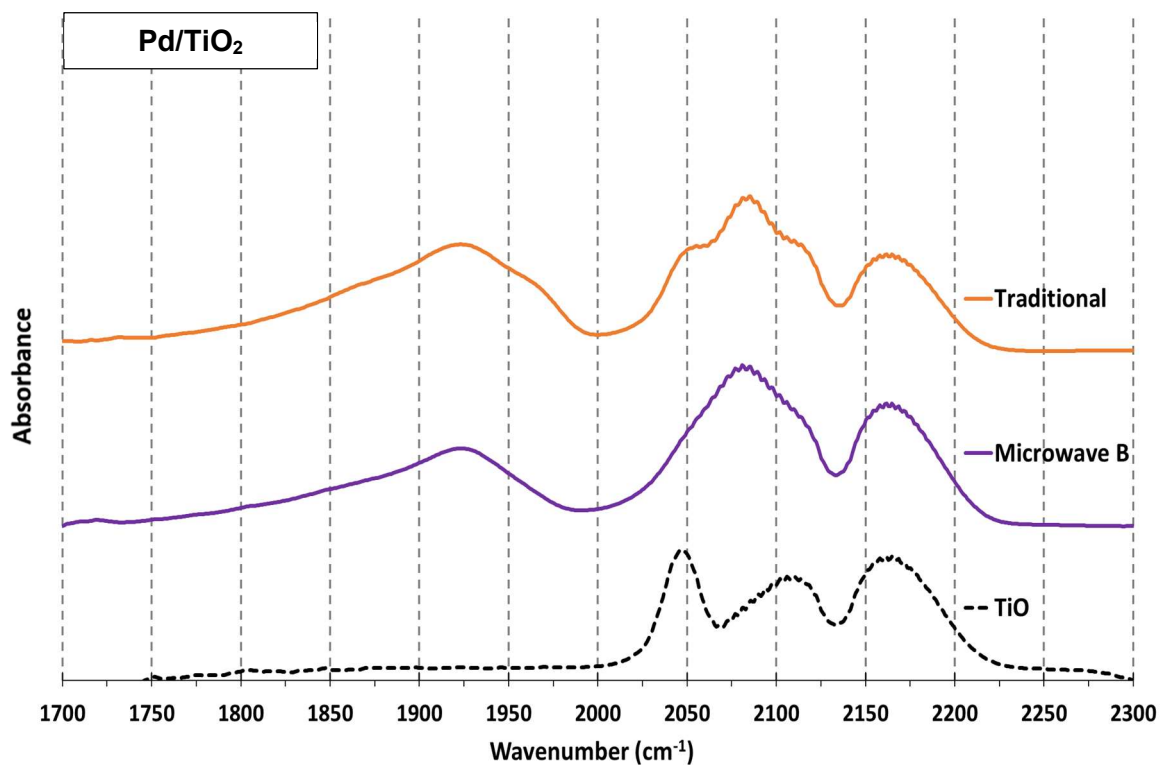


Figure 147 – DRIFTS analysis of Pd/TiO₂ catalysts produced at different operating conditions and of the TiO₂ support.

Catalysts Characterisation

5.5 Diffuse Reflectance Infrared Fourier Transform Spectroscopy

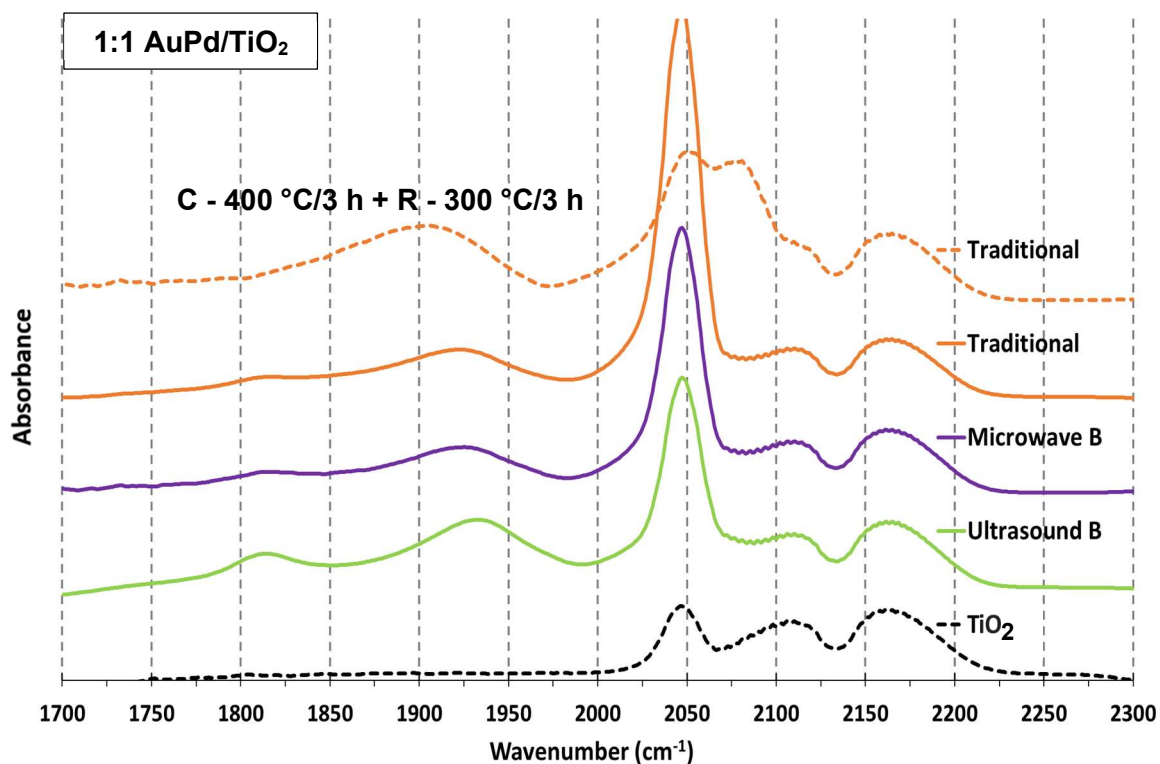


Figure 148 – DRIFTS analysis of AuPd/TiO₂ catalysts produced at different operating conditions and of the TiO₂ support.

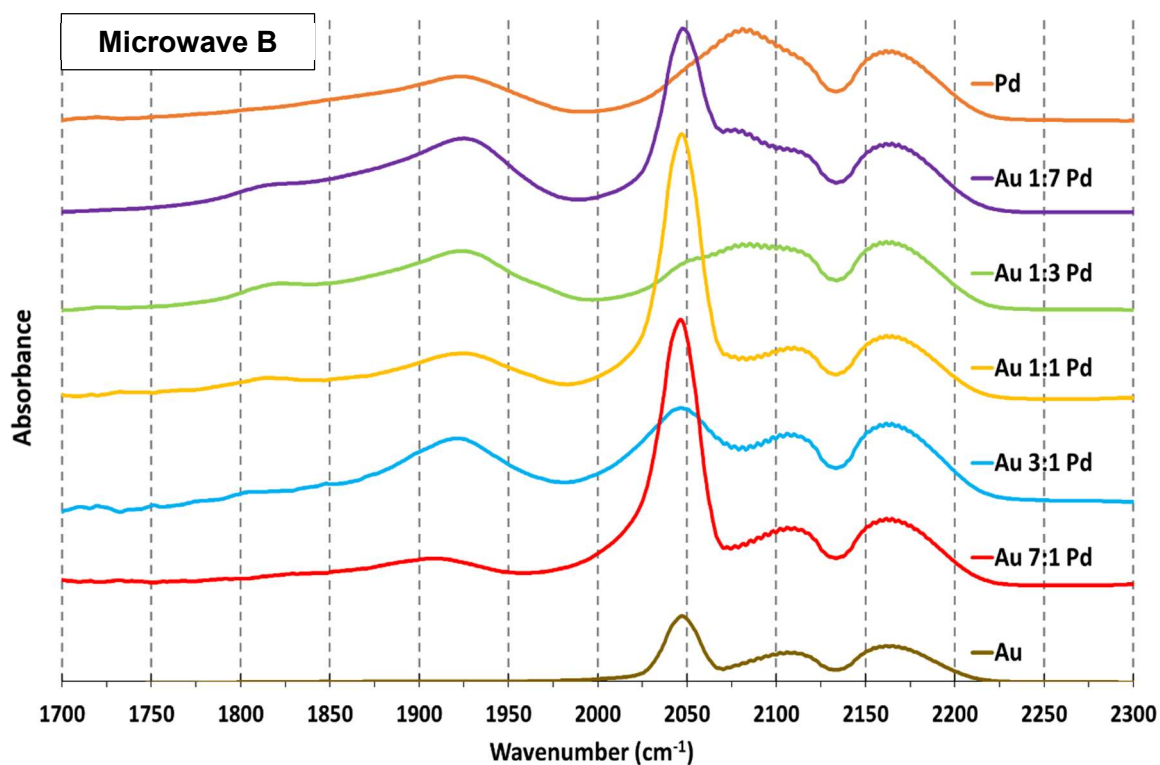


Figure 149 – DRIFTS analysis of different catalysts produced by microwave synthesis with the operating condition B (Au/TiO₂, Pd/TiO₂ and AuPd/TiO₂ at different molar ratios).

6 Model Reactions Experimental Results

6.1 Overview

The metal nanoparticles supported and characterised in chapter 5 were used as heterogeneous catalysts in liquid/gas phase reactions. In total seven reactions were tested. All experimental results are presented in this chapter. An overview for each one of these reactions can be found in section 1.6, where the reaction schemes are presented and their importance in light of the targets defined for this PhD is described, and the experimental procedures can be found in section 2.7.

The seven reactions were only used as model reactions. The objective was never to optimise the reactions operating conditions, but rather to use the reactions as a tool to catalytically characterise the produced metal nanoparticles, in this case by calculating conversions and selectivities. The catalysts characterisation in chapter 5 allow to explain the different conversions and selectivities in terms of the metal nanoparticles average size, size distribution, loading, composition, shape, oxidation state, contamination and type of metal active site. Ultimately, the catalytic activity results can give insight into which one of the developed microwave and ultrasound sol-immobilization protocols for the synthesis of metal nanoparticles are more interesting and where future research should focus on.

Some of the reactions were tested by other research colleagues. This was the case of the propane total oxidation, which was tested by Parag Shah, and of the hydrazine decomposition, which was tested by Davide Motta. The 4-nitrophenol reduction was carried out with the help of Briony Munslow and the formic acid decomposition with the help of Thomas Hall. The furfural hydrogenation was carried out in an external university (Universita degli Studi di Milano) within Dr. Alberto Villa research group who have optimised the operating conditions.

Similar to what happened with the catalysts characterisation in chapter 5 there were limitations due to the amount of available catalyst as each microwave/ultrasound preparation rendered a catalyst amount of 100 to 500 mg. In addition to having to spread the catalyst through seven different reactions, some of the trials had to be repeated in order to check for reproducibility. Also, important amounts of catalyst were used in heat treatments. Therefore, it was not possible to test all the catalyst in all the reactions. Priority was given to 1:1 AuPd/TiO₂ catalysts produced by microwave synthesis with the operating condition B and by ultrasound synthesis with the operating condition B. In any case, even if not all the catalysts were tested, for each reaction it was still possible to observe trends, analyse them and draw conclusions.

Model Reactions Experimental Results

6.2 4-Nitrophenol Reduction

6.2 4-Nitrophenol Reduction

All catalysts tested in the 4-nitrophenol reduction reaction can be found in Table 40. Details of the *Traditional* protocol can be found in section 1.4.2.1, details of the *Microwave B* protocol can be found in section 3.4 and details of the *Ultrasound A* and *Ultrasound B* protocols (including modifications) can be found in sections 4.3 and 4.4.3.

Table 40 – List of the catalysts tested in the 4-nitrophenol reduction.

Metal	Support	Protocol	Comments
Au	TiO ₂	Traditional	No Heat Treatment
Au	TiO ₂	Microwave B	No Heat Treatment
Au	TiO ₂	Microwave B	Calci. – 400 °C/3 h + Red. – 300 °C/3 h
Au	TiO ₂	Ultrasound A	No Heat Treatment
Au	TiO ₂	Ultrasound A	Calci. – 400 °C/3 h + Red. – 300 °C/3 h
Au	TiO ₂	Ultrasound B	No Heat Treatment
Au	TiO ₂	Ultrasound B	Calci. – 400 °C/3 h + Red. – 300 °C/3 h
Pd	TiO ₂	Traditional	No Heat Treatment
Pd	TiO ₂	Microwave B	No Heat Treatment
Pd	TiO ₂	Microwave B	Calci. – 400 °C/3 h + Red. – 300 °C/3 h
Pd	TiO ₂	Ultrasound A	No Heat Treatment
Pd	TiO ₂	Ultrasound A	Calci. – 400 °C/3 h + Red. – 300 °C/3 h
Pd	TiO ₂	Ultrasound B	No Heat Treatment
AuPd (1:1)	TiO ₂	Traditional	No Heat Treatment
AuPd (1:1)	TiO ₂	Microwave B	No Heat Treatment
AuPd (1:1)	TiO ₂	Microwave B	Calci. – 400 °C/3 h + Red. – 300 °C/3 h
AuPd (1:1)	C	Microwave B	No Heat Treatment
AuPd (1:1)	TiO ₂	Ultrasound A	No Heat Treatment
AuPd (1:1)	TiO ₂	Ultrasound A	Calci. – 200 °C/3 h + Red. – 300 °C/3 h
AuPd (1:1)	TiO ₂	Ultrasound A	Calci. – 300 °C/3 h + Red. – 300 °C/3 h
AuPd (1:1)	TiO ₂	Ultrasound A	Calci. – 400 °C/3 h + Red. – 300 °C/3 h
AuPd (1:1)	TiO ₂	Ultrasound 0.65xPVA	No Heat Treatment
AuPd (1:1)	TiO ₂	Ultrasound 0.65xPVA	Calci. – 200 °C/3 h + Red. – 300 °C/3 h
AuPd (1:1)	TiO ₂	Ultrasound 0.65xPVA	Calci. – 300 °C/3 h + Red. – 300 °C/3 h
AuPd (1:1)	TiO ₂	Ultrasound 0.65xPVA	Calci. – 400 °C/3 h + Red. – 300 °C/3 h
AuPd (1:1)	TiO ₂	Ultrasound 1.2xPVA	No Heat Treatment
AuPd (1:1)	TiO ₂	Ultrasound 1.2xPVA	Calci. – 400 °C/3 h + Red. – 300 °C/3 h
AuPd (1:1)	TiO ₂	Ultrasound B	No Heat Treatment
AuPd (1:1)	TiO ₂	Ultrasound B	Calci. – 200 °C/3 h + Red. – 300 °C/3 h
AuPd (1:1)	TiO ₂	Ultrasound B	Calci. – 300 °C/3 h + Red. – 300 °C/3 h
AuPd (1:1)	TiO ₂	Ultrasound B	Calci. – 400 °C/3 h + Red. – 300 °C/3 h

Model Reactions Experimental Results

6.2 4-Nitrophenol Reduction

The first catalysts to be tested were the TiO₂ catalysts prepared with the traditional sol-immobilization protocol. The reproducibility was checked by performing several trials with fresh catalysts from different batches at 30 °C. As observed in Figure 150 the trials with the Pd/TiO₂ catalyst were very similar to one another. However, when moving to the trials with the AuPd/TiO₂ catalyst the reproducibility started to be compromised. The reproducibility was further compromised with the Au/TiO₂ catalysts.

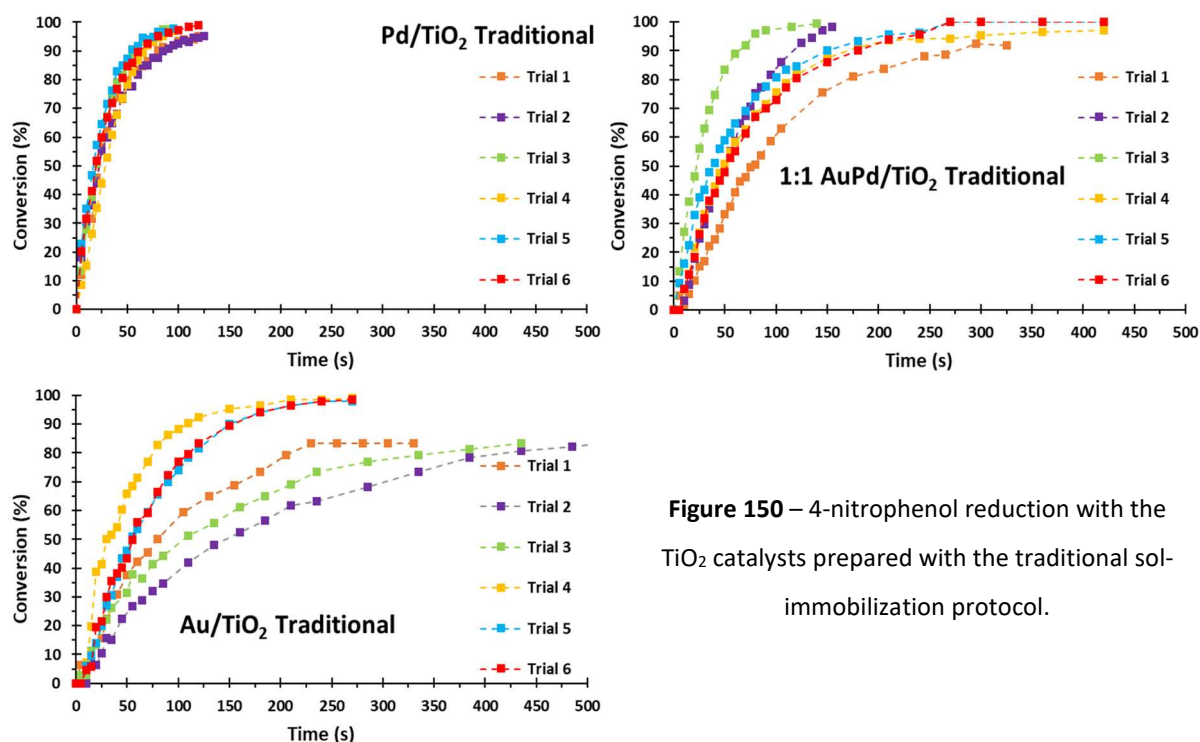


Figure 150 – 4-nitrophenol reduction with the TiO₂ catalysts prepared with the traditional sol-immobilization protocol.

After initial trials with the TiO₂ catalysts prepared with the traditional sol-immobilization protocol the work moved to the catalysts prepared by the protocols developed in this PhD. However, it was observed that all the untreated TiO₂ catalysts produced by microwave and ultrasound synthesis were inactive to the 4-nitrophenol reduction. Moreover, upon addition of NaBH₄ not only the catalysts were inactive as they also started to leach. This was verified by UV-Vis analysis and by visually inspecting the UV-Vis cuvette.

As explained in section 2.7.1 before addition of the NaBH₄ the 4-nitrophenol peak is observed at around 325 nm. Upon addition of NaBH₄ the medium changes to basic conditions which causes an instantaneous change of 4-nitrophenol to 4-nitrophenolate, with the peak shifting to around 400 nm. This peak is expected to gradually decrease as the reaction proceeds and the 4-nitrophenolate is being reduced. In Figure 151 the UV-Vis spectra associated with the trial with the 1:1 AuPd/TiO₂ catalyst produced by ultrasound synthesis with the operating condition B is presented.

Model Reactions Experimental Results

6.2 4-Nitrophenol Reduction

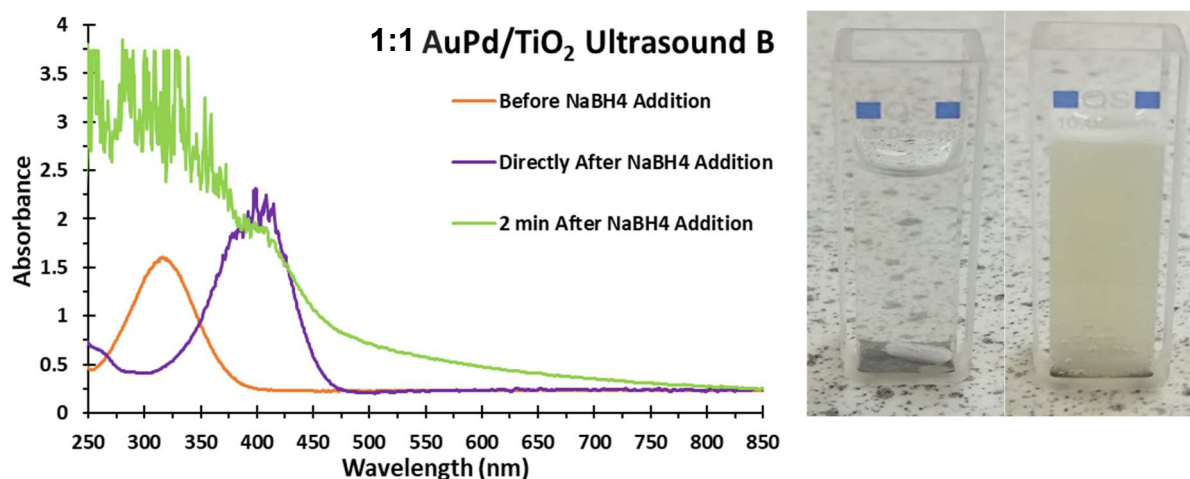


Figure 151 – 4-nitrophenol reduction with the 1:1 AuPd/TiO₂ catalyst produced by ultrasound synthesis with the operating condition B with UV-Vis analysis (left) and photos of the UV-Vis cuvette before adding the NaBH₄ and 2 min after adding the NaBH₄ (right).

The 4-nitrophenolate peak did not decrease as expected, instead it appears that the metal nanoparticles started to leach from the support into the reaction solution with a UV-Vis spectrum consistent with AuPd nanoparticles in solution being produced 2 min after the addition of the NaBH₄. This UV-Vis spectrum is similar to the ones presented for the AuPd colloids in chapters 3 and 4. The photo of the UV-Vis cuvette 2 min after the NaBH₄ addition also indicates a turbid reaction solution consistent with leaching of the metal nanoparticles from the support. This photo also shows a yellow colour for the reaction solution, which indicates that the 4-nitrophenolate did not react at all. These observations could be extended to all trials with untreated TiO₂ catalysts produced by microwave and ultrasound synthesis.

Several trials were performed in order to understand why the catalysts produced by ultrasound and microwave synthesis presented this leaching problem whereas the untreated TiO₂ catalysts prepared with the traditional sol-immobilization protocol were free of such problem. The main conclusions reached are as follows:

- The leaching problem was not related to the stirrer setting in the UV-Vis cuvette;
- The leaching problem was related only to TiO₂ as the metal nanoparticles prepared by microwave synthesis but supported on carbon worked fine. However, this catalyst is difficult to use with this experimental procedure as the carbon accumulates evenly along the UV-Vis cuvette and interferes with the UV-Vis analysis;

Model Reactions Experimental Results

6.2 4-Nitrophenol Reduction

c) The leaching problem was not related to the solvent used as another polar solvent was also tested (ethylene glycol) and the leaching problem was observed;

d) The leaching problem was not related to NaBH_4 itself but rather to the change of the medium conditions to basic conditions as it was observed that the addition of NaOH instead of NaBH_4 resulted in the same leaching problem;

After taking into consideration the previous conclusions it was formulated the hypothesis that the leaching problem was associated with a weak interaction between the metal nanoparticles and the TiO_2 support during the support addition stage. The formation of this weak interaction could only be explained by the different synthesis conditions when compared to the traditional sol-immobilization protocol, most likely due to the presence of the ethylene glycol. In order to validate this hypothesis different heat-treated catalysts were tested as they should present stronger metal-support interaction.

As observed in Figure 152 heat-treated catalysts were now active as expected. This was verified for the 1:1 AuPd/TiO_2 catalysts produced by ultrasound synthesis with the operating condition A and operating condition B. It was also observed a positive trend between activity and calcination temperature. The higher the calcination temperature the more active the catalyst was. This is also according to the expected as the higher the calcination temperature the stronger the metal-support interaction should be. However, even if the heat-treated catalysts were now active the activity was still lower than what could be obtained for the equivalent catalyst produced with the traditional sol-immobilization protocol. The average of the trials from Figure 150 is also presented for benchmarking purposes.

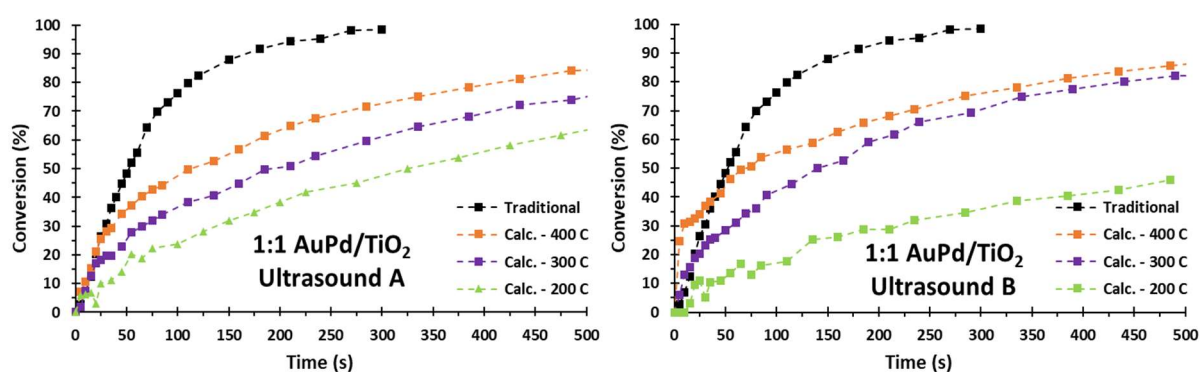


Figure 152 – 4-nitrophenol reduction with the 1:1 AuPd/TiO_2 catalysts prepared by ultrasound synthesis with the operating condition A (left) and operating condition B (right) and heat-treated at different calcination temperatures.

Model Reactions Experimental Results

6.2 4-Nitrophenol Reduction

The activity of all the 1:1 AuPd/TiO₂ and Pd/TiO₂ catalysts heat-treated at the standard conditions (Calc. – 400 °C/3 h + Red. – 300 °C/3 h) is presented in Figure 153 and compared to the average of the trials from Figure 150 for the equivalent catalyst produced with the traditional sol-immobilization protocol.

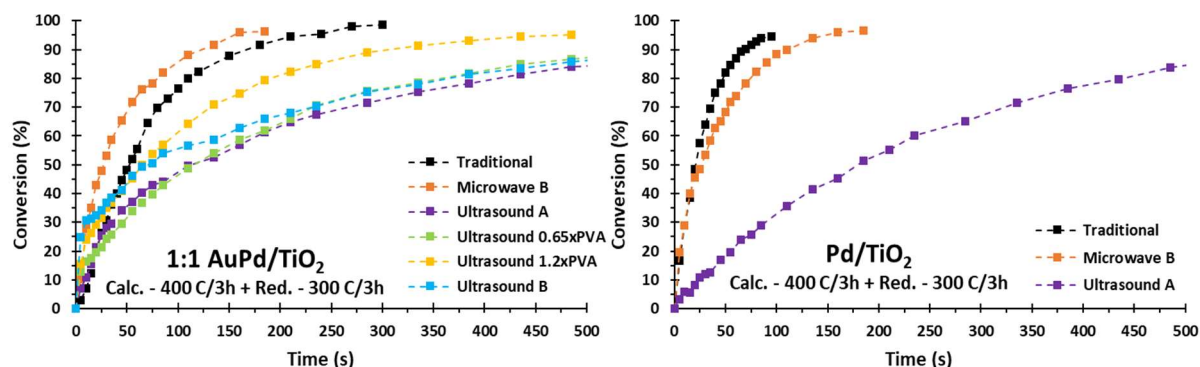


Figure 153 – 4-nitrophenol reduction with 1:1 AuPd/TiO₂ and Pd/TiO₂ catalysts produced by microwave and ultrasound synthesis at different operating conditions and heat-treated at standard conditions.

1:1 AuPd/TiO₂ and Pd/TiO₂ presented the highest activity for catalysts produced by microwave synthesis with the operating condition B, with conversions very similar to what had been obtained with the catalysts produced with the traditional sol-immobilization protocol.

The lowest activity for the Pd/TiO₂ catalysts was observed for the catalyst produced by ultrasound synthesis with the operating condition A. This can be explained by the larger Pd nanoparticles average size as shown in section 4.4 (10 ± 3.8 nm).

The lowest activity for the 1:1 AuPd/TiO₂ catalysts was obtained when working with ultrasound catalysts (A, B and 0.65xPVA very similar to one another). It is likely that the smaller AuPd (1:1) nanoparticles average size for operating conditions B and 0.65xPVA when compared to Ultrasound A was offset by the PVA contamination on the catalyst surface as supported by the XPS analysis. The excessive PVA contamination on the surface could also explain why the activity of the Ultrasound 1.2xPVA catalyst was higher than the Ultrasound B catalyst even though they presented very similar average sizes (around 4.5 nm).

All heat-treated Au/TiO₂ catalysts no longer presented the leaching problem mentioned in Figure 151. However, they continued to show no activity for the 4-nitrophenol reduction. These catalysts presented average sizes larger than 15 nm as seen in section 5.2. Similar to what was observed with the AuPd and Pd catalysts, it appears that the activity for this reaction is strongly dependent on the Au nanoparticles average size.

Model Reactions Experimental Results

6.3 Carbon Monoxide Oxidation

6.3 Carbon Monoxide Oxidation

All catalysts tested for carbon monoxide oxidation reaction can be found in Table 41. Details of the *Traditional* protocol can be found in section 1.4.2.1, details of the *Microwave B* protocol can be found in section 3.4 and details of the *Ultrasound A* and *Ultrasound B* protocols (including modifications) can be found in sections 4.3 and 4.4.3.

Table 41 – List of the catalysts tested for the carbon monoxide oxidation.

Metal	Support	Protocol	Comments
Au	TiO ₂	Traditional	No Heat Treatment
Au	TiO ₂	Traditional	Calci. – 400 °C/3 h + Red. – 300 °C/3 h
Au	TiO ₂	Microwave B	No Heat Treatment
Au	TiO ₂	Microwave B	Calci. – 400 °C/3 h + Red. – 300 °C/3 h
Au	TiO ₂	Ultrasound A	No Heat Treatment
Au	TiO ₂	Ultrasound A	Calci. – 400 °C/3 h + Red. – 300 °C/3 h
Pd	TiO ₂	Traditional	No Heat Treatment
Pd	TiO ₂	Traditional	Calci. – 400 °C/3 h + Red. – 300 °C/3 h
Pd	TiO ₂	Microwave B	No Heat Treatment
Pd	TiO ₂	Microwave B	Calci. – 400 °C/3 h + Red. – 300 °C/3 h
Pd	TiO ₂	Ultrasound A	No Heat Treatment
Pd	TiO ₂	Ultrasound A	Calci. – 400 °C/3 h + Red. – 300 °C/3 h
AuPd (1:1)	TiO ₂	Traditional	No Heat Treatment
AuPd (1:1)	TiO ₂	Traditional	Calci. – 400 °C/3 h + Red. – 300 °C/3 h
AuPd (1:1)	TiO ₂	Microwave B	No Heat Treatment
AuPd (1:1)	TiO ₂	Microwave B	Calci. – 400 °C/3 h + Red. – 300 °C/3 h
AuPd (1:1)	TiO ₂	Ultrasound A	No Heat Treatment
AuPd (1:1)	TiO ₂	Ultrasound A	Calci. – 400 °C/3 h + Red. – 300 °C/3 h
AuPd (1:1)	TiO ₂	Ultrasound 0.65xPVA	No Heat Treatment
AuPd (1:1)	TiO ₂	Ultrasound 0.65xPVA	Calci. – 200 °C/3 h + Red. – 300 °C/3 h
AuPd (1:1)	TiO ₂	Ultrasound 0.65xPVA	Calci. – 300 °C/3 h + Red. – 300 °C/3 h
AuPd (1:1)	TiO ₂	Ultrasound 0.65xPVA	Calci. – 400 °C/3 h + Red. – 300 °C/3 h
AuPd (1:1)	TiO ₂	Ultrasound 1.2xPVA	No Heat Treatment
AuPd (1:1)	TiO ₂	Ultrasound 1.2xPVA	Calci. – 400 °C/3 h + Red. – 300 °C/3 h
AuPd (1:1)	TiO ₂	Ultrasound B	No Heat Treatment
AuPd (1:1)	TiO ₂	Ultrasound B	Calci. – 200 °C/3 h + Red. – 300 °C/3 h
AuPd (1:1)	TiO ₂	Ultrasound B	Calci. – 300 °C/3 h + Red. – 300 °C/3 h
AuPd (1:1)	TiO ₂	Ultrasound B	Calci. – 400 °C/3 h + Red. – 300 °C/3 h
AuPd (1:1)	TiO ₂	Ultrasound 50 %	No Heat Treatment
AuPd (1:1)	TiO ₂	Ultrasound 50 %	Calci. – 400 °C/3 h + Red. – 300 °C/3 h

Model Reactions Experimental Results

6.3 Carbon Monoxide Oxidation

In total 13 untreated catalysts were initially tested at 30 °C, including the ones produced with the traditional sol-immobilization protocol. All of them showed no activity even after running the reaction for approximately 2 hours. The same results were obtained when increasing the temperature from 30 °C to 50 °C.

The lack of any activity for the untreated catalysts is similar to what was observed with the 4-nitrophenol reduction in section 6.2. This was caused by metal leaching from the support and could be solved after submitting the catalysts to heat treatments. For the carbon monoxide oxidation the inactivity was not caused by metal leaching as the reaction is carried out in the gas phase and even the catalysts prepared with the traditional sol-immobilization protocol were now affected. However, the same heat treatment approach was also followed in order to enhance the metal-support interaction.

As observed in Figure 154 heat-treated catalysts were now active as expected. This was verified at both 30 °C and 50 °C for the 1:1 AuPd/TiO₂ catalysts produced by ultrasound synthesis with the operating conditions B and with a PVA/metal weight ratio of 0.65 instead of 3.25. Only the trials at 50 °C are presented in Figure 154.

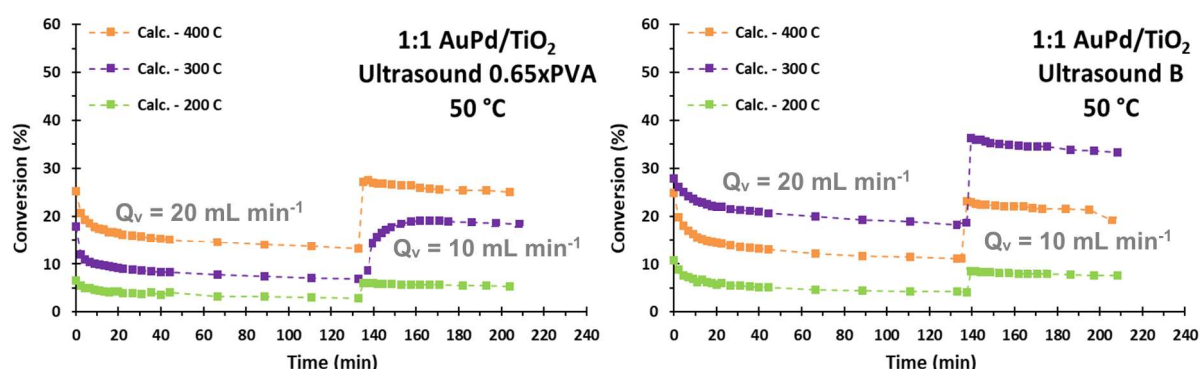


Figure 154 – Carbon monoxide oxidation with 1:1 AuPd/TiO₂ catalysts produced by ultrasound synthesis with the operating condition 0.65xPVA (left) and operating condition B (right) and heat-treated at different calcination temperatures. (Flow rate = Q_v)

Contrary to what had been observed with the 4-nitrophenol reduction a mixed trend was observed between activity and calcination temperature for the two catalysts.

The catalytic activity of the 1:1 AuPd/TiO₂ Ultrasound 0.65xPVA catalyst gradually increased as the calcination temperature increased with the most active catalyst being the one heat treated at the standard condition of 400 °C. The TEM average sizes for the 200, 300 and 400 °C catalysts were 3.3 ± 1.2 nm, 3.9 ± 1.6 nm and 5.0 ± 1.5 nm respectively. Despite the larger nanoparticles average size at 400 °C the enhanced metal-support interaction attained by working at a higher calcination temperature together with a very low carbon content were the most important factors.

Model Reactions Experimental Results

6.3 Carbon Monoxide Oxidation

The catalytic activity of the 1:1 AuPd/TiO₂ Ultrasound B catalyst was mixed. The highest catalytic activity was obtained for the 300 °C catalyst. The carbon content was not an important factor as the XPS analysis indicated values very similar for the 200, 300 and 400 °C catalysts. The TEM average sizes for the 200, 300 and 400 °C catalysts were 3.0 ± 0.8 nm, 3.1 ± 0.8 nm and 4.5 ± 1.0 nm respectively. As explained in section 5.2 due to the high PVA amount of 3.25 at 300 °C the average size had only increased to 3.1 ± 0.8 nm, still very close to the size observed for the untreated catalyst. On this occasion the small nanoparticles average size at 300 °C played a more important role than the enhanced metal-support interaction at 400 °C. However, it can still be observed the importance of a strong metal-support interaction as the 200 °C catalyst was almost inactive.

From the trials shown in Figure 154 it was also observed that the activity over time was not a constant as the conversion gradually decreased over time. The poison of the active sites by carbon monoxide could be an explanation to this phenomenon. It might be the case that after applying the heat treatments the adsorption energy was now too strong and some carbon monoxide was irreversibly adsorbed. According to the Sabatier principle, previously illustrated in Figure 3, the interaction of the substrate/product to the active sites should not be too strong otherwise their desorption could become compromised. After approximately 2 hours the flow rate was halved from 20 mL min⁻¹ to 10 mL min⁻¹ causing the activity to immediately double as expected. The decrease of the activity over time continued to be observed, thus confirming not to be dependent on the flow rate.

The activity at both 30 °C and 50 °C of all the 1:1 AuPd/TiO₂ catalysts heat-treated at standard conditions (Calc. – 400 °C/3 h + Red. – 300 °C/3 h) is presented in Figure 155 and compared to the equivalent catalyst produced with the traditional sol-immobilization protocol.

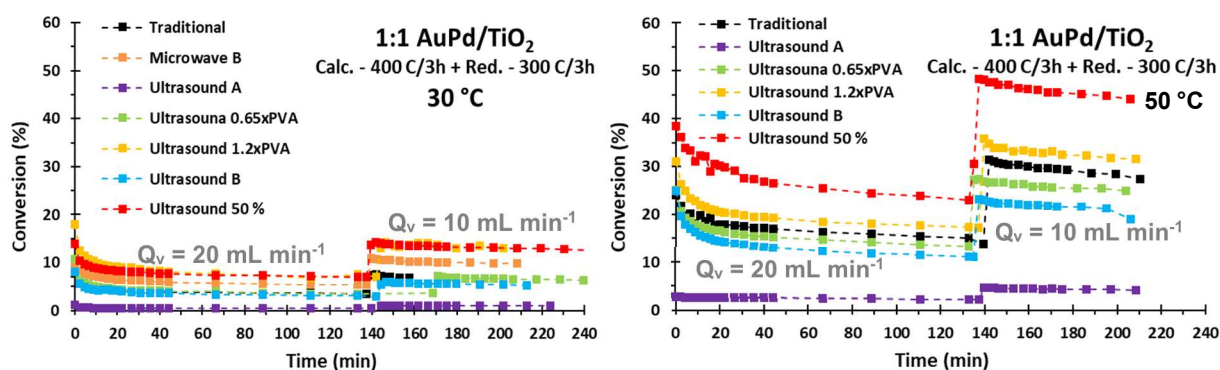


Figure 155 – Carbon monoxide oxidation at 30 °C (left) and 50 °C (right) with 1:1 AuPd/TiO₂ catalysts produced by microwave and ultrasound synthesis at different operating conditions and heat-treated at standard conditions. (Flow rate = Q_v)

Model Reactions Experimental Results

6.3 Carbon Monoxide Oxidation

The activity at both 30 °C and 50 °C of all the Pd/TiO₂ catalysts heat-treated at standard conditions (Calci. – 400 °C/3 h + Red. – 300 °C/3 h) is presented in Figure 156 and compared to the equivalent catalyst produced with the traditional sol-immobilization protocol.

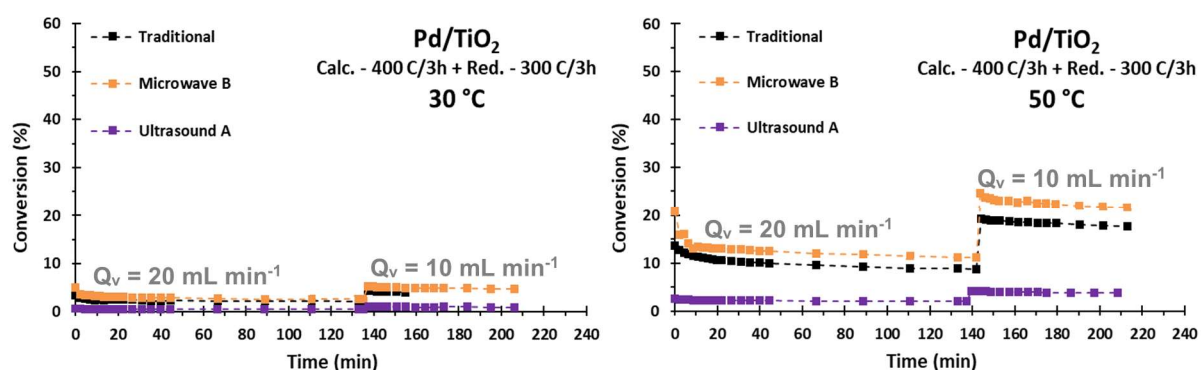


Figure 156 – Carbon monoxide oxidation at 30 °C (left) and 50 °C (right) with Pd/TiO₂ catalysts produced by microwave and ultrasound synthesis at different operating conditions and heat-treated at standard conditions. (Flow rate = Q_v)

The activity at both 30 °C and 50 °C of all the Au/TiO₂ catalysts heat-treated at standard conditions (Calci. – 400 °C/3 h + Red. – 300 °C/3 h) is presented in Figure 157 and compared to the equivalent catalyst produced with the traditional sol-immobilization protocol.

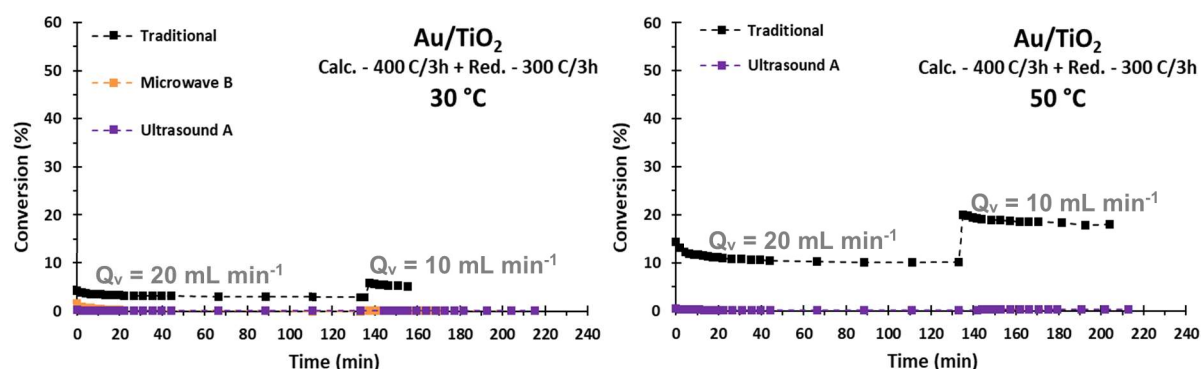


Figure 157 – Carbon monoxide oxidation at 30 °C (left) and 50 °C (right) with Au/TiO₂ catalysts produced by microwave and ultrasound synthesis at different operating conditions and heat-treated at standard conditions. (Flow rate = Q_v)

When moving from 30 °C to 50 °C the activity trends were kept constant but there was a better resolution between the activity of the different catalysts.

Overall, it was possible to observe that the highest activity was obtained when working with 1:1 AuPd/TiO₂ catalysts, in particular with the catalyst produced by ultrasound synthesis with the operating condition 50 %. As seen in sections 5.2 and 5.4 this catalyst presented the smallest average size with 4.0 ± 1.0 nm and a very low carbon content on the surface with a value of 1.9 wt. %.

Model Reactions Experimental Results

6.3 Carbon Monoxide Oxidation

Once more, similar to what happened with the 4-nitrophenol reduction in section 6.2, the Ultrasound 1.2xPVA catalyst was more active than the Ultrasound B catalyst even though they present very similar average sizes (around 4.5 nm). This was due to PVA contamination as indicated by the higher carbon content for the Ultrasound B catalyst (4.2 vs. 1.9 wt. %).

Some of the 1:1 AuPd/TiO₂ and Pd/TiO₂ catalysts were more active than the catalysts produced with the traditional sol-immobilization protocol. This was observed for the catalysts prepared by microwave synthesis with the operating condition B and by ultrasound synthesis with the operating conditions 50 % and 1.2xPVA. These results are in agreement with what was observed for the 4-nitrophenol reduction.

The importance of the metal nanoparticles average size was once more verified with this reaction. The tested Au/TiO₂ catalysts prepared by microwave and ultrasound synthesis presenting average sizes larger than 15 nm were inactive. Furthermore, it appears that when compared to the 4-nitrophenol reduction with the carbon monoxide oxidation the metal nanoparticles average size plays a bigger role on the catalytic activity as even the 1:1 AuPd/TiO₂ and Pd/TiO₂ catalysts prepared by ultrasound synthesis with the operating condition A were now almost inactive.

Model Reactions Experimental Results

6.4 Propane Total Oxidation

6.4 Propane Total Oxidation

All catalysts tested for propane total oxidation reaction can be found in Table 42. Details of the *Traditional* protocol can be found in section 1.4.2.1, details of the *Microwave B* protocol can be found in section 3.4 and details of the *Ultrasound A* and *Ultrasound B* protocols can be found in section 4.3.

Table 42 – List of the catalysts tested for the propane total oxidation.

Metal	Support	Protocol	Comments
Au	TiO ₂	Traditional	No Heat Treatment
Au	TiO ₂	Traditional	Calci. – 400 °C/3 h + Red. – 300 °C/3 h
Au	TiO ₂	Microwave B	No Heat Treatment
Au	TiO ₂	Ultrasound A	No Heat Treatment
Pd	TiO ₂	Traditional	No Heat Treatment
Pd	TiO ₂	Traditional	Calci. – 400 °C/3 h + Red. – 300 °C/3 h
Pd	TiO ₂	Microwave B	No Heat Treatment
Pd	TiO ₂	Microwave B	Calci. – 400 °C/3 h + Red. – 300 °C/3 h
AuPd (1:1)	TiO ₂	Traditional	No Heat Treatment
AuPd (1:1)	TiO ₂	Traditional	Calci. – 400 °C/3 h + Red. – 300 °C/3 h
AuPd (1:1)	TiO ₂	Microwave B	No Heat Treatment
AuPd (1:1)	TiO ₂	Ultrasound B	No Heat Treatment

In total 8 untreated and 4 treated catalysts were tested at different temperatures with activity and CO₂ selectivity for the 1:1 AuPd/TiO₂ catalysts shown in Figure 158, for the Pd/TiO₂ catalysts shown in Figure 159 and for the Au/TiO₂ catalysts shown in Figure 160.

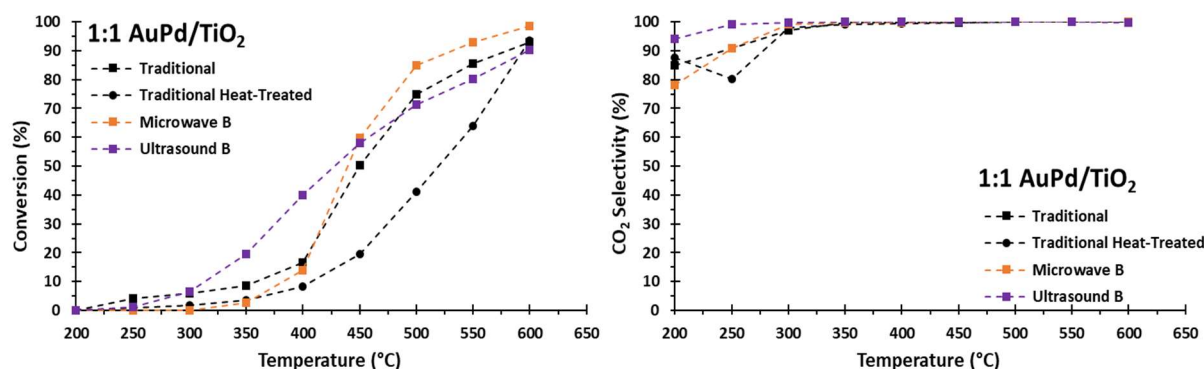


Figure 158 – Activity (left) and CO₂ selectivity (right) at different temperatures of the propane total oxidation with 1:1 AuPd/TiO₂ catalysts produced at different operating conditions.

Model Reactions Experimental Results

6.4 Propane Total Oxidation

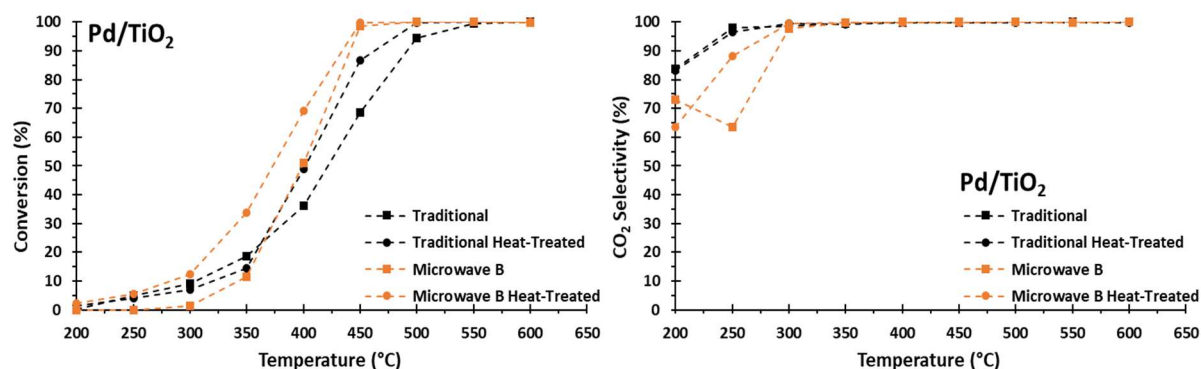


Figure 159 – Activity (left) and CO₂ selectivity (right) at different temperatures of the propane total oxidation with Pd/TiO₂ catalysts produced at different operating conditions.

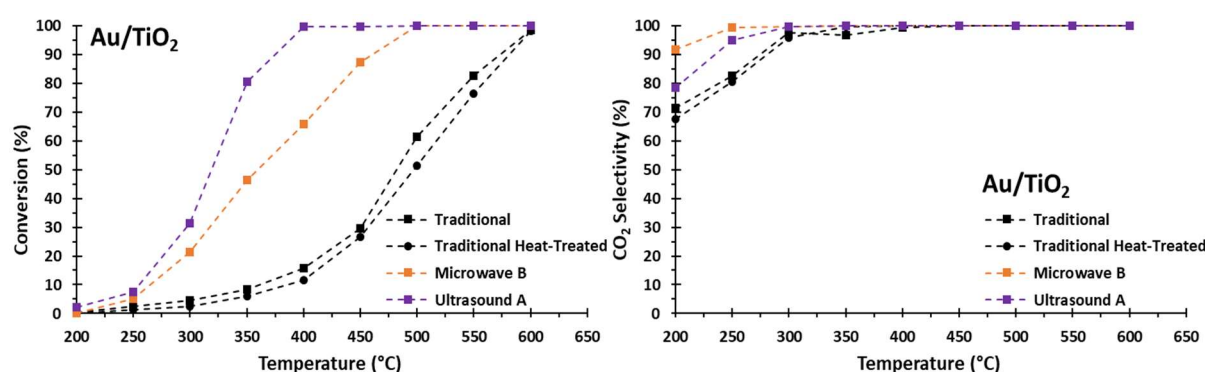


Figure 160 – Activity (left) and CO₂ selectivity (right) at different temperatures of the propane total oxidation with Au/TiO₂ catalysts produced at different operating conditions.

Overall, no trends could be detected for CO₂ selectivity with values in the 60-100 % range for a temperature equal or lower than 250 °C and values very close to 100 % when the temperature was equal or higher than 300 °C.

Once more the 1:1 AuPd/TiO₂ and Pd/TiO₂ catalysts produced by microwave synthesis with the operating condition B were more active than the equivalent catalyst produced with the traditional sol-immobilization protocol. Surprisingly, with this reaction this could also be observed with the Au/TiO₂ catalyst, a result very different from what had been observed with the 4-nitrophenol reduction and the carbon monoxide oxidation.

In fact, the most active catalyst was Au/TiO₂ produced by ultrasound synthesis with operating condition A, with nanoparticles presenting a considerable large average size of 33 ± 14 nm. It seems that large Au nanoparticles (Microwave B and Ultrasound A) were much more active than small Au nanoparticles (Traditional). However, it was not possible to definitely link activity to metal nanoparticles average size, for instance with Au the heat-treated catalyst had a lower activity, with Pd the heat-treated catalysts had a higher activity and with AuPd (1:1) the heat-treated catalyst had again a lower activity. More trials are necessary in order to draw conclusions for the correlation between activity and metal nanoparticles average size.

Model Reactions Experimental Results

6.5 Furfural Hydrogenation

6.5 Furfural Hydrogenation

All catalysts tested for furfural hydrogenation reaction can be found in Table 43. Details of the *Traditional* protocol can be found in section 1.4.2.1, details of the *Microwave B* protocol can be found in section 3.4 and details of the *Ultrasound B* protocol can be found in section 4.3.

Table 43 – List of the catalysts tested for the furfural hydrogenation.

Metal	Support	Protocol	Comments
Au	TiO ₂	Traditional	No Heat Treatment
Au	TiO ₂	Microwave B	No Heat Treatment
Pd	TiO ₂	Traditional	No Heat Treatment
Pd	TiO ₂	Microwave B	No Heat Treatment
AuPd (1:1)	TiO ₂	Traditional	No Heat Treatment
AuPd (7:1)	TiO ₂	Microwave B	No Heat Treatment
AuPd (3:1)	TiO ₂	Microwave B	No Heat Treatment
AuPd (1:1)	TiO ₂	Microwave B	No Heat Treatment
AuPd (1:3)	TiO ₂	Microwave B	No Heat Treatment
AuPd (1:7)	TiO ₂	Microwave B	No Heat Treatment
AuPd (1:1)	TiO ₂	Ultrasound B	No Heat Treatment

In total 11 catalysts were tested, all of them being untreated, with activity for the 1:1 AuPd/TiO₂ catalysts shown in Figure 161 and for the Pd/TiO₂ catalysts shown in Figure 162. The Au/TiO₂ catalysts presented little to no activity. As mentioned in section 1.6.4 the main products formed in this reaction are furfuryl alcohol (FA) and 2-tetrahydrofurfuryl alcohol (THFA). Therefore, for all the trials their selectivity is also presented.

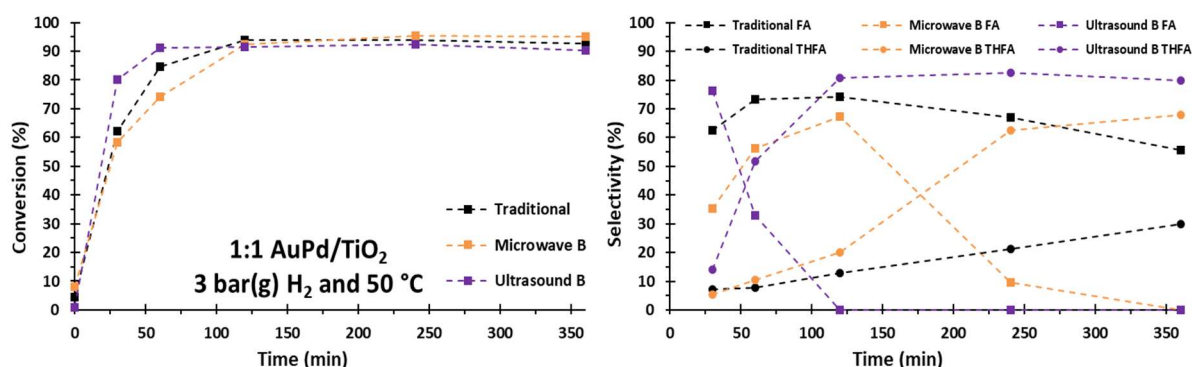


Figure 161 – Activity (left) and FA and THFA selectivity (right) of the furfural hydrogenation with 1:1 AuPd/TiO₂ catalysts produced at different operating conditions.

Model Reactions Experimental Results

6.5 Furfural Hydrogenation

The activity of the different 1:1 AuPd/TiO₂ catalysts was very similar to one another. However, the THFA selectivity was much higher for the catalyst prepared by ultrasound synthesis with the operating condition B, in particular when compared to the traditional sol-immobilization protocol. The TEM and XPS analysis cannot provide an explanation to the differences in selectivity. Contrary to this, the DRIFTS analysis presented in section 5.5 provides an explanation in terms of the type of metal active site as the Ultrasound B was the only catalyst to present a XPS peak consistent with hollow adsorption.

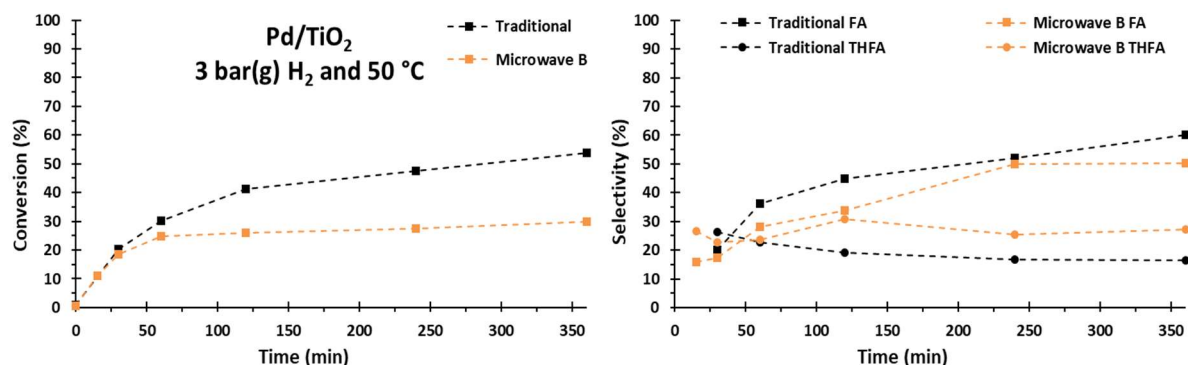


Figure 162 – Activity (left) and FA and THFA selectivity (right) of the furfural hydrogenation with Pd/TiO₂ catalysts produced at different operating conditions.

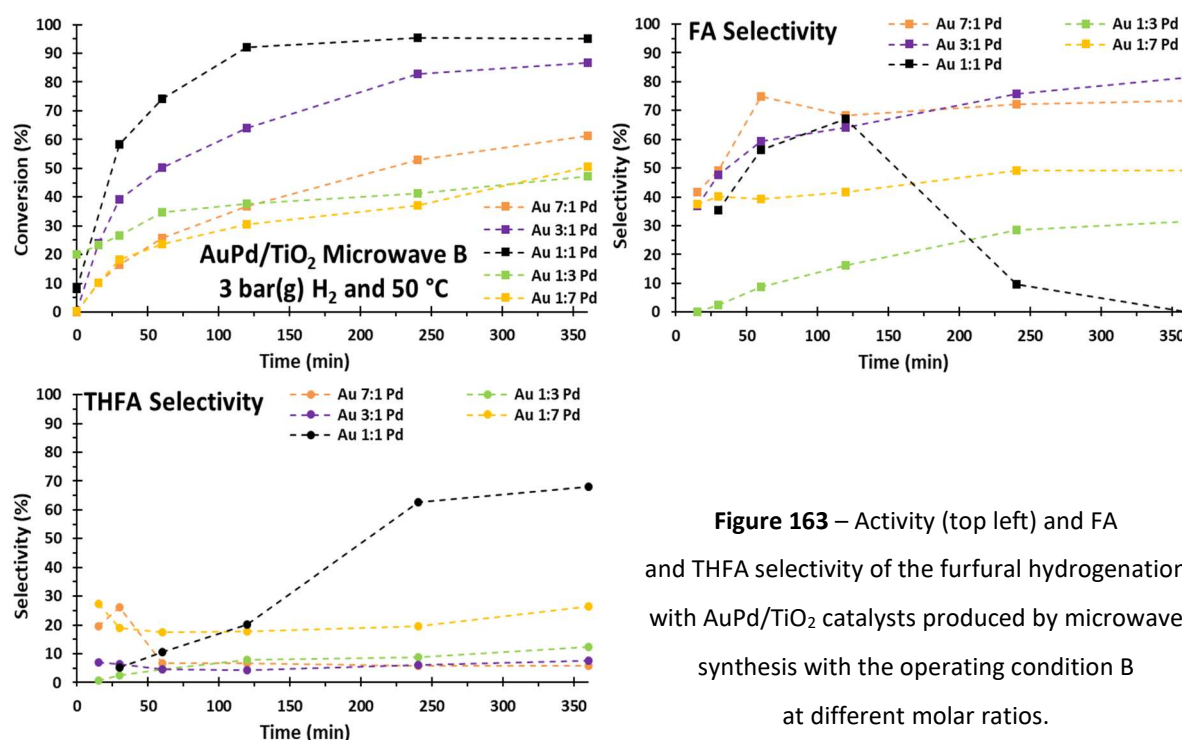
The Pd/TiO₂ catalyst produced with the traditional sol-immobilization protocol was more active than the Microwave B catalyst. As indicated by TEM and XPS analysis this catalyst presented a larger nanoparticles average size (3.8 nm vs. 2.9 nm), a lower carbon content (3.2 vs. 4.8 wt. %) and a lower content of Pd⁰ (60 % vs. 83 %). For this reaction any of these three parameters or a combination of them might explain the differences in activity. It should also be noted that the Microwave B catalyst appears to become inactive during the reaction. More trials and characterisation of the used catalyst would be necessary to fully understand why as there are several factors to take into consideration, for example poisoning, leaching or change of the oxidation state.

Despite the aforementioned TEM and XPS differences the selectivity profiles over time of the two Pd/TiO₂ catalysts were very similar. At the same time, the DRIFTS analysis indicated almost no differences between the type of metal active sites, with only bridge and linear adsorption being observed. This further supports the conclusion that it was the different types of metal active sites observed with the 1:1 AuPd/TiO₂ catalysts that caused the differences in selectivity.

Model Reactions Experimental Results

6.5 Furfural Hydrogenation

Further catalytic tests were performed by fixing the operating condition (Microwave B) and changing the AuPd molar ratio (7:1, 3:1, 1:3 and 1:7). The activity and selectivity are presented in Figure 163 and compared to 1:1 molar ratio, previously presented in Figure 161.



It was possible to observe a trend between activity and the molar ratio. The AuPd/TiO₂ catalyst with a molar ratio of 7:1 presented a low activity when compared to the molar ratio of 1:1. This is consistent with the composition of this catalyst being the closest to pure Au, which was shown to present little to no activity for the furfural hydrogenation. As the Pd molar ratio increased from 7:1 to 3:1 the activity increased, eventually reaching a maximum when the molar ratio was 1:1. As the Pd molar ratio continued to increase to 1:3 and 1:7 the activity dropped again, close to the values observed with the pure Pd catalyst as shown in Figure 162.

However, it should also be noted that as the AuPd molar ratio changes the metal nanoparticles average size also changes as shown in section 3.5, in particular for the molar ratios of 7:1 and 3:1 (9.0 ± 1.8 nm and 4.7 ± 1.1 nm). Therefore, it is not possible to definitely conclude that the 7:1 and 3:1 catalysts are less active than 1:1 catalyst.

When considering the selectivity, it was not possible to detect any trends. It seems that the 1:1 catalyst was the only one to present low selectivity towards FA and high selectivity towards THFA. All the other catalysts presented low selectivity towards THFA and mixed selectivity towards FA, in particular the 1:3 catalyst. For this catalyst when adding the THFA and FA selectivities a total value of around 40 % is obtained. This means that there was 60 % conversion towards some of the other compounds presented in Equation 17.

Model Reactions Experimental Results

6.6 Cinnamaldehyde Hydrogenation

6.6 Cinnamaldehyde Hydrogenation

The catalytic results for the cinnamaldehyde hydrogenation after a reaction time of 2 h can be found in Table 44. As mentioned in section 1.6.5 the main products formed in this reaction are 3-phenyl-1-propanol (PPA) and hydrocinnamaldehyde (HCAL). Therefore, for all the trials their selectivity is also presented.

Details of the *Traditional* protocol can be found in section 1.42.1, details of the *Microwave B* protocol can be found in section 3.4 and details of the *Ultrasound A* and *Ultrasound B* protocols (including modifications) can be found in sections 4.3 and 4.4.3.

Table 44 – Activity and selectivity of catalysts produced at different operating conditions for the cinnamaldehyde hydrogenation at 100 °C after a reaction time of 2 h with a hydrogen pressure of 1 bar(g).

	Conversion (%)	PPA (%)	HCAL (%)	Others (%)
Traditional				
Au/TiO ₂	3	0	0	100
Pd/TiO ₂	100	9	82	9
1:1 AuPd/TiO ₂	86	50	42	8
Microwave B				
Au/TiO ₂	0	0	0	0
Pd/TiO ₂	89	28	67	5
1:1 AuPd/TiO ₂	28	37	61	2
1:1 AuPd/C	8	8	74	18
1:1 AuPd/TiO ₂ (Calci. – 400 °C/3 h + Red. – 300 °C/3 h)	8	19	75	6
Ultrasound A				
Au/TiO ₂	8	0	0	100
Pd/TiO ₂	100	14	64	22
1:1 AuPd/TiO ₂	58	27	73	0
Ultrasound 0.65xPVA				
1:1 AuPd/TiO ₂	80	35	62	3
Ultrasound 1.2xPVA				
1:1 AuPd/TiO ₂	70	45	53	2
Ultrasound B				
Pd/TiO ₂	100	6	92	2
1:1 AuPd/TiO ₂	44	42	57	1

Model Reactions Experimental Results

6.6 Cinnamaldehyde Hydrogenation

	Conversion (%)	PPA (%)	HCAL (%)	Others (%)
Ultrasound 50 %				
1:1 AuPd/TiO₂	72	31	67	2
Commercial				
Pd/C	100	14	83	3

Similar to what had been observed with the furfural hydrogenation in section 6.5 the Au/TiO₂ catalysts presented little to no activity. When comparing results at the same operating condition the Pd/TiO₂ catalysts were more active and in general more selective towards HCAL than the equivalent 1:1 AuPd/TiO₂ catalysts.

The 1:1 AuPd/TiO₂ catalyst produced with the traditional sol-immobilization protocol was more active (86 %) than the other 1:1 AuPd/TiO₂ catalysts, in particular the one produced by microwave synthesis with the operating condition B (28 %). This can be explained by taking into consideration the XPS analysis in section 5.4. The carbon contamination, an indication of residual stabilizer on the catalyst surface, was significantly lower for the Traditional catalyst when compared to the Microwave B catalyst (3.1 vs. 4.6 wt. %) and to the Ultrasound B catalyst (3.1 vs. 4.7 wt. %). This trend is better observed with the ultrasound catalysts. As the PVA amount increased (0.65, 1.2 and 3.25) the activity also decreased (80 %, 70 % and 44 %). The Ultrasound A catalyst presented low activity (58 %) even though no PVA was used for synthesis. In this case this was due to the large nanoparticles average size (10 ± 2.7 nm).

The Microwave B catalyst was subject to heat treatment at standard conditions in order to understand if the catalytic activity could be improved by further removing traces of the stabilizer. This turned out to be an unsuccessful approach as the activity dropped to 8 %. It seems that the increase on the nanoparticles average size after the heat treatment offset any removal from the stabilizer. A different support, carbon, was also tested. However, the activity remained low at only 8 % conversion as the excess of stabilizer continued to hinder adsorption. The carbon support itself can be ruled out as the case for this low activity as the Pd/C commercial catalyst presented a very high activity.

It is remarkable that for this reaction small traces of stabilizer were able to cause major differences in the catalytic activity. This had not been observed with the furfural hydrogenation in section 6.5 and with the formic acid decomposition in section 6.7. This can be explained by the different solvents. The previous two reactions used polar solvents, 2-propanol and water, whereas with the cinnamaldehyde hydrogenation a non-polar solvent was used, toluene. A polar solvent is able to easily interact with the stabilizer thus allowing a better adoption to the active sites and as a result a higher catalytic activity, closer to the free stabilizer scenario.

Model Reactions Experimental Results

6.6 Cinnamaldehyde Hydrogenation

Overall, the Pd/TiO₂ catalysts had conversions of 100 %. The only exception was the Microwave B catalyst with a conversion of 89 %. Again, this result is consistent with interference from the stabilizer as this catalyst had the highest carbon content (4.8 wt. %). Moreover, it was the catalyst that used PVP as stabilizer instead of PVA. As mentioned in previous sections, the PVP offers a higher protective factor than PVA, which means it is more likely to compromise the catalytic activity.

In order to better understand differences in the activity between the different Pd/TiO₂ catalysts the reaction time was decreased to 1 h as shown in Table 45. Some of the previous 1:1 AuPd/TiO₂ catalysts were also tested again as well as more heat-treated catalysts.

Table 45 – Activity and selectivity of catalysts produced at different operating conditions for the cinnamaldehyde hydrogenation at 100 °C after a reaction time of 1 h with a hydrogen pressure of 1 bar(g).

	Conversion (%)	PPA (%)	HCAL (%)	Others (%)
Traditional				
Pd/TiO ₂	100	9	83	8
1:1 AuPd/TiO ₂	66	47	48	5
Microwave B				
Pd/TiO ₂	53	8	91	1
Ultrasound A				
Pd/TiO ₂	90	10	81	9
1:1 AuPd/TiO ₂	40	27	72	3
1:1 AuPd/TiO ₂ (Calci. – 200 °C/3 h + Red. – 300 °C/3 h)	19	17	83	0
1:1 AuPd/TiO ₂ (Calci. – 300 °C/3 h + Red. – 300 °C/3 h)	17	14	85	1
1:1 AuPd/TiO ₂ (Calci. – 400 °C/3 h + Red. – 300 °C/3 h)	17	16	82	2
Ultrasound 0.65xPVA				
1:1 AuPd/TiO ₂	63	37	60	3
1:1 AuPd/TiO ₂ (Calci. – 200 °C/3 h + Red. – 300 °C/3 h)	40	12	80	8
1:1 AuPd/TiO ₂ (Calci. – 300 °C/3 h + Red. – 300 °C/3 h)	33	14	77	9
1:1 AuPd/TiO ₂ (Calci. – 400 °C/3 h + Red. – 300 °C/3 h)	22	12	81	7
Ultrasound 1.2xPVA				
1:1 AuPd/TiO ₂	55	34	64	2
1:1 AuPd/TiO ₂ (Calci. – 400 °C/3 h + Red. – 300 °C/3 h)	18	20	65	5

Model Reactions Experimental Results

6.6 Cinnamaldehyde Hydrogenation

	Conversion (%)	PPA (%)	HCAL (%)	Others (%)
Ultrasound B				
Pd/TiO₂	99	7	93	0
1:1 AuPd/TiO₂	26	37	59	4
1:1 AuPd/TiO₂ (Calci. – 200 °C/3 h + Red. – 300 °C/3 h)	26	13	73	14
1:1 AuPd/TiO₂ (Calci. – 300 °C/3 h + Red. – 300 °C/3 h)	20	14	67	19
1:1 AuPd/TiO₂ (Calci. – 400 °C/3 h + Red. – 300 °C/3 h)	21	18	70	12
Ultrasound 50 %				
1:1 AuPd/TiO₂	57	32	67	1
Commercial				
Pd/C	100	14	85	1

The catalytic trends remained very similar to the reaction time of 2 h:

a) The Pd/TiO₂ catalysts were more active and in general more selective towards HCAL than the equivalent 1:1 AuPd/TiO₂ catalysts;

b) The effect of the carbon contamination was once more verified. The 1:1 AuPd/TiO₂ catalyst produced with the traditional sol-immobilization protocol was more active (66 %) than the other 1:1 AuPd/TiO₂ catalysts, in particular the one produced by ultrasound synthesis with the operating condition B (26 %). Again, this trend could be better observed with the ultrasound catalysts. As the PVA amount increased (0.65, 1.2 and 3.25) the catalytic activity also decreased (63 %, 55 % and 26 %);

c) The Ultrasound A catalyst continued to present low activity (40 %) due to the large nanoparticles average size (10 ± 2.7 nm) even though no PVA was used for synthesis;

d) The removal of traces of stabilizer by subjecting the catalysts to heat treatments was not enough to bring conversions closer to the same value observed with the traditional sol-immobilization protocol (66 %). It seems that the increase on the nanoparticles average size after the heat treatment offset any removal from the stabilizer;

The reaction time of 1 h was now enough to better understand differences in the activity between the different Pd/TiO₂ catalysts. Again, the Microwave B catalyst was the least active (PVP contamination) with 53 % conversion followed by the Ultrasound A catalyst (larger nanoparticles average size of 10 ± 3.8 nm) with 90 % conversion. The Commercial and Traditional catalysts remained very active with a conversion of 100 % being achieved.

Model Reactions Experimental Results

6.7 Formic Acid Decomposition

6.7 Formic Acid Decomposition

All catalysts tested in the formic acid decomposition reaction can be found in Table 46. Details of the *Traditional* protocol can be found in section 1.4.2.1, details of the *Microwave B* protocol can be found in section 3.4 and details of the *Ultrasound A* and *Ultrasound B* protocols (including modifications) can be found in sections 4.3 and 4.4.3.

Table 46 – List of the catalysts tested in the formic acid decomposition.

Metal	Support	Protocol	Comments
Pd	TiO ₂	Traditional	No Heat Treatment
Pd	TiO ₂	Microwave B	No Heat Treatment
Pd	TiO ₂	Ultrasound A	No Heat Treatment
AuPd (1:1)	TiO ₂	Traditional	No Heat Treatment
AuPd (1:1)	TiO ₂	Microwave B	No Heat Treatment
AuPd (1:1)	TiO ₂	Microwave B	Calci. – 400 °C/3 h + Red. – 300 °C/3 h
AuPd (1:1)	C	Microwave B	No Heat Treatment
AuPd (1:1)	TiO ₂	Ultrasound A	No Heat Treatment
AuPd (1:1)	TiO ₂	Ultrasound A	Calci. – 400 °C/3 h + Red. – 300 °C/3 h
AuPd (1:1)	TiO ₂	Ultrasound 0.65xPVA	No Heat Treatment
AuPd (1:1)	TiO ₂	Ultrasound 0.65xPVA	Calci. – 400 °C/3 h + Red. – 300 °C/3 h
AuPd (1:1)	TiO ₂	Ultrasound B	No Heat Treatment
AuPd (1:1)	TiO ₂	Ultrasound B	Calci. – 400 °C/3 h + Red. – 300 °C/3 h
AuPd (1:1)	C	Ultrasound B	No Heat Treatment

In total 10 untreated and 4 treated catalysts were tested at 50 °C with the activity for the untreated 1:1 AuPd/TiO₂ and Pd/TiO₂ catalysts shown in Figure 164.

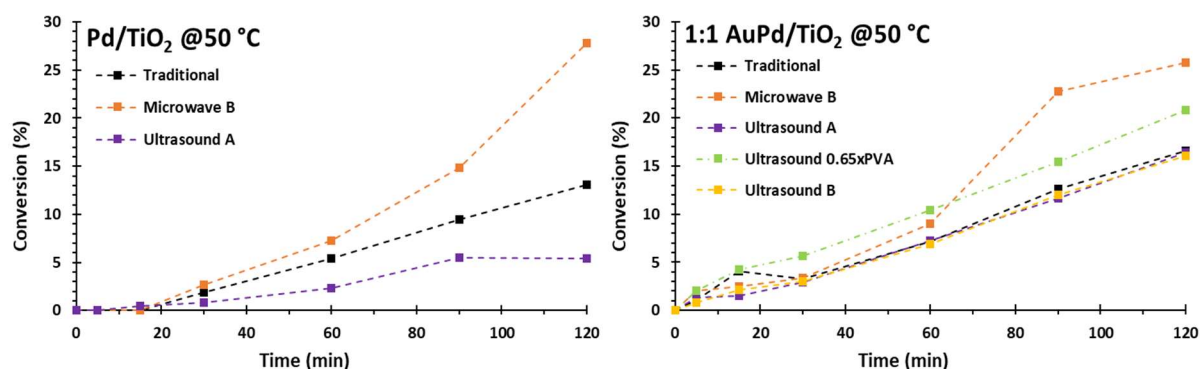


Figure 164 – Formic acid decomposition with Pd/TiO₂ (left) and 1:1 AuPd/TiO₂ (right) catalysts produced at different operating conditions.

Model Reactions Experimental Results

6.7 Formic Acid Decomposition

When considering the Pd/TiO₂ and 1:1 AuPd/TiO₂ catalysts produced by microwave synthesis with the operating condition B they were more active than the equivalent catalyst produced with the traditional sol-immobilization protocol, in line with what had been observed for the 4-nitrophenol reduction, the carbon monoxide oxidation and the propane total oxidation. As expected, the Ultrasound A catalysts were among the least active catalysts due to the large nanoparticles average size, also in line with previous reactions.

The effect of the support on the activity of AuPd (1:1) nanoparticles was also tested by changing the support from TiO₂ to C for the Microwave B and Ultrasound B protocols. No major differences could be detected for the conversion over time with values very similar to what are presented in Figure 164 (right) for the equivalent catalysts supported on TiO₂.

Similar to what happened with the cinnamaldehyde hydrogenation, after subjecting the 1:1 AuPd/TiO₂ catalysts to heat treatment at standard conditions the activity decreased. Once more, it seems that the increase on the nanoparticles average size after the heat treatment offset any removal from the stabilizer. The only exception was the Ultrasound B catalyst which was slightly more active after being subject to the heat treatment. The activity of the different catalysts is compared in Figure 165 with the untreated catalysts shown on the left and the heat-treated catalysts at standard conditions shown on the right.

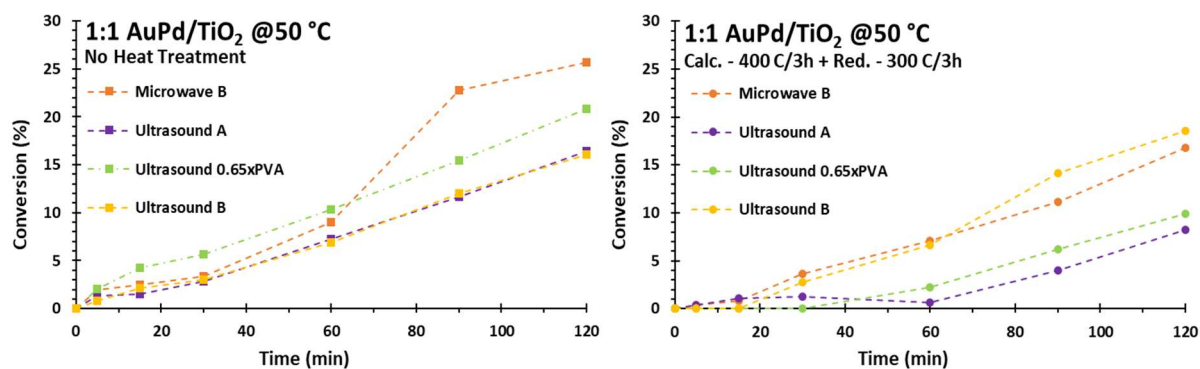


Figure 165 – Formic acid decomposition with untreated (left) and heat-treated at standard conditions (right) 1:1 AuPd/TiO₂ catalysts produced at different operating conditions.

Model Reactions Experimental Results

6.8 Hydrazine Decomposition

6.8 Hydrazine Decomposition

Three Ir/CeO₂ catalysts were tested for the hydrazine decomposition reaction with the activity being expressed by the amount of produced gas (cm³). As shown in Figure 166 the most active catalyst was the one produced with the addition of 16 eq. of NaOH (see section 3.5.4 for more details). According to the TEM analysis this was the colloid that presented the smallest average size (< 1-2 nm). The TEM analysis also indicated similar average sizes for the Microwave A and Microwave B colloids. However, the Microwave A catalyst appears to be more active than the Microwave B catalyst. This is according to what was observed in the previous reactions as the Microwave A catalyst was free of any stabilizer contamination whereas the Microwave B catalyst used a PVP/metal weight ratio of 3.25 during synthesis.

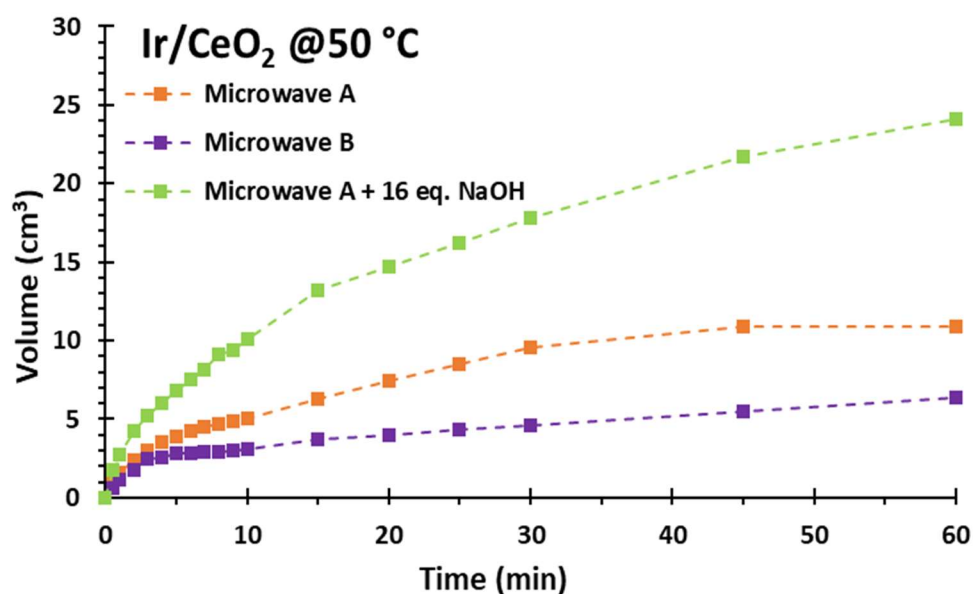


Figure 166 – Hydrazine decomposition with Ir/CeO₂ catalysts produced at different operating conditions.

As mentioned in section 1.6.7 both hydrazine and formic acid present two possible decomposition pathways. Similar to the formic acid decomposition it was not possible to calculate the selectivity towards hydrogen, only activity. However, it should be noted that with the formic acid decomposition the activity was expressed by the conversion values, calculated based on the concentration of formic acid, whereas with the hydrazine decomposition the activity is inferred from the volume of produced gas. It is therefore an apparent activity as it is possible to have the same conversion but different values for the volume of produced gas if the selectivities are also different from one catalyst to the other (not likely in this specific case as the catalysts are very similar to one another).

7 Conclusions and Future Work

This PhD has covered the production of different metal nanoparticles (Au, Pd, Ag, Ir, Cu and AuPd) by adopting the sol-immobilization method and producing stabilized colloids. Water, organic solvents or a mixture of both have been used as the synthesis medium, with ethylene glycol being the main organic solvent and PVA and PVP being used as stabilizers. Some of the produced metal nanoparticles were supported on TiO₂, C and CeO₂ and used as catalysts in gas/liquid phase reactions. Several techniques were employed to characterise the produced metal colloids and the supported metal nanoparticles. Whenever possible attempts were made to link the catalytic results with the characterisation results.

Different protocols have been developed and tested using microwave, ultrasound and continuous flow synthesis. Adoption of these three non-conventional synthesis methods has allowed to address challenging issues in the areas of green chemistry, catalysis and materials design. This positive outcome offers a potential impact in future projects relating to water purification, biomass transformation and hydrogen storage and production.

Overall, the PhD research could be divided into four areas:

a) The first area (chapter 3) focused on the microwave synthesis of monometallic metal nanoparticles of Au, Pd, Ag, Ir and Cu and bimetallic metal nanoparticles of the alloy type of AuPd at different molar ratios (7:1, 3:1, 1:1, 1:3, 1:7). This included work carried out under batch and continuous flow regime;

b) The second area (chapter 4) focused on the ultrasound synthesis of monometallic metal nanoparticles of Au, Pd and bimetallic metal nanoparticles of the alloy type of AuPd at a molar ratio of 1:1. All work was carried out under batch regime;

c) The third area (chapter 5) saw the application of several characterisation techniques (TEM, SEM/EDX, XPS and DRIFTS) to selected metal nanoparticles produced by microwave and ultrasound synthesis and supported on TiO₂, C and CeO₂. This provided important information regarding the metal nanoparticles average size, shape, loading, composition, traces of stabilizer and oxidation state;

d) The fourth area (chapter 6) focused on the catalytic testing of some of the supported metal nanoparticles using them as heterogeneous catalysts in liquid/gas phase reactions. In total seven reactions were tested, namely 4-nitrophenol reduction, carbon monoxide oxidation, propane total oxidation, furfural hydrogenation, cinnamaldehyde hydrogenation, formic acid decomposition and hydrazine decomposition;

Conclusions and Future Work

The majority of the metal colloids produced by microwave and ultrasound synthesis were also characterized by TEM, UV-Vis and DLS spectroscopy. Comparisons were made with results that could be obtained from the literature. Comparisons were also made with equivalent metal nanoparticles produced by sol-immobilization, but using more conventional approaches, in particular the traditional sol-immobilization protocol, which employs NaBH_4 as the reducing agent (section 1.4.2). A commercial Pd/C catalyst was also used for benchmarking purposes.

When considering in more detail the first research area of this PhD (chapter 3) metal nanoparticles could be successfully synthesised using microwave heating. In total, three batch protocols have been developed by taking into consideration the Au optimisation experimental results from section 3.2 and the mechanistic studies from section 3.3. The Au optimisation tests aimed to understand the effect of stirrer, metal concentration, holding time and temperature, acid/base addition, type of solvent, solvent composition and type and concentration of stabilizer. The mechanistic studies aimed to deliver an insight on the influence of heating, NaOH addition, stabilizer, solvent and Au oxidation state on the nanoparticles formation mechanism (metal reduction, nucleation and growth).

The best experimental results were obtained with the protocol using ethylene glycol as the solvent/reducing agent and PVP as the stabilizer at a stabilizer/metal weight ratio of 3.25. Overall the experimental results were in line with the best experimental results found in the literature, in particular if having in consideration that the metal nanoparticles are meant to be used for catalytic purposes and an excess of stabilizer is highly undesirable. The produced Au nanoparticles had an average size of 12 ± 3.9 nm, the produced Pd nanoparticles had an average size of 3.3 ± 0.8 nm, the produced Ag nanoparticles had an average size of 13 ± 14 nm, the produced AuPd (1:1) nanoparticles had an average size of 3.0 ± 0.6 nm and it is estimated that the produced Ir nanoparticles had an average size below 1-2 nm.

The correct production of Ag nanoparticles was compromised due to an incomplete reduction. This was worse with the Cu solution as no reduction could even be observed. However, it was verified that NaOH addition could lead to an enhanced effect which in the case of Ag nanoparticles resulted in complete reduction and in the case of Cu solution could even result now in the production of Cu nanoparticles.

The work with continuous flow synthesis did not produce the expected results. This was due to a fouling phenomenon and issues related to the experimental set-up. However, it can still be said that this work demonstrated that metal nanoparticles can be produced using similar conditions to the ones used under batch regime and that the experimental results were also promising as there is easily room for improvement, for example by adopting a different reactor configuration or by changing the tubing material.

Conclusions and Future Work

When considering in more detail the second research area of this PhD (chapter 4) metal nanoparticles could be successfully synthesised using ultrasound effect. In total, two batch protocols have been developed by taking into consideration the Au optimisation experimental results from section 4.2. This Au optimisation tests aimed to understand the effect of wave amplitude, metal concentration, sonication time, composition and type and concentration of stabilizer.

The best experimental results were obtained with the protocol using a mixture of 75 % water and 25 % ethylene glycol (v/v) as the solvent/reducing agent and PVA as the stabilizer at a stabilizer/metal weight ratio of 3.25x. Overall the experimental results were superior to what is found in the literature, in particular if having in consideration that the metal nanoparticles are meant to be used for catalytic purposes and an excess of stabilizer is highly undesirable. The produced Au nanoparticles had an average size of 12 ± 5.0 nm, the produced Pd nanoparticles had an average size of 2.7 ± 0.7 nm and the produced AuPd (1:1) nanoparticles had an average size of 2.9 ± 1.1 nm.

Compared to the traditional sol-immobilization protocol the adoption of microwave and ultrasound synthesis has eliminated the need to use a toxic reducing agent (NaBH_4). This is in line with one of the targets defined for this PhD. The synthesis time has also been reduced from 30 min to 5 min with microwave and to 15 min with ultrasound. This is also in line with another target defined for this PhD. Moving production from batch to continuous flow regime has also been attempted in order to improve production, another one of the PhD targets.

Moreover, this PhD research demonstrated how flexible the production of metal nanoparticles of different sizes and shapes can be by changing the different operating conditions. To this end the microwave and ultrasound synthesis have been shown to be unique methods as they are able to unlock additional operating conditions and offer better control over size and shape. In the case of microwave synthesis there are thermal advantages by having a rapid and more homogeneous way of heating. In the case of ultrasound synthesis the cavitation effect is able to create regions of extreme temperature and pressure (hotspots) leading to the production of radical species. This cavitation effect can be tuned by changing the wave amplitude or the wave frequency. Another unique feature of ultrasound synthesis is that the reducing effect can instantaneously be turned on/off by controlling the sonication time as the hotspots regions have a very short lifetime.

Conclusions and Future Work

It is remarkable that with ultrasound synthesis small Pd and AuPd (1:1) nanoparticles could also be produced without employing any stabilizer, very different from what had been observed with microwave synthesis where only agglomeration could be observed. The different working temperatures, 70 °C with ultrasound and 150 °C with microwave, could explain the different results as the growth rate is strongly dependent on the temperature. The lower ultrasound working temperature has also allowed the use of PVA in conjugation with ethylene glycol without creating an undesired bimodal distribution. This was because PVA is not able to act as a reducing agent at a temperature of only 70 °C.

Overall, it was verified with TEM analysis that the metal nanoparticles average sizes and size distributions remained unchanged after the support addition stage, regardless of the support used and regardless of the type of metal nanoparticles. It could also be observed from the TEM analysis that the amount of stabilizer employed during the metal nanoparticles synthesis had a direct impact on the average size after applying any heat treatment. The more severe the heat treatment conditions the higher the degree of agglomeration. However, the higher the amount of used stabilizer the less severe this agglomeration was for the equivalent heat treatment. From this analysis it could be inferred that the filtration/washing step during the support addition stage is not enough to completely remove stabilizer traces from the catalyst surface, which can end up compromising the catalytic activity.

The SEM/EDX analysis confirmed that metal nanoparticles were correctly supported and presented total metal loadings close to the expected 1.0 wt. %. As expected, the XPS analysis indicated that the surface composition was almost always higher than 1.0 wt. %. From the XPS analysis it was also possible to understand that around 80 % of the Pd was present as Pd⁰ and the remaining as Pd²⁺ and that around 70-80 % of the Ir was present as Ir⁰ and the remaining as Ir⁴⁺. There was also indication that around 10 % of the support was Ce₂O₃ instead of CeO₂. The XPS analysis also confirmed some contamination with carbon which could be linked to the amount of stabilizer used during the metal nanoparticles synthesis.

The DRIFTS analysis probed the adsorption of CO to the different metal nanoparticles, an indication of the type of active sites that had been produced. The Au/TiO₂ catalysts only presented linear adsorption and no correlation between the type of adsorption and the average size of the Au nanoparticles and/or the synthesis protocol could be detected. The same conclusion was valid for the Pd/TiO₂ catalysts even though they also presented bridge adsorption in addition to linear adsorption. However, the 1:1 AuPd/TiO₂ catalysts indicated that the synthesis protocol may have an important role as the catalyst prepared by ultrasound synthesis was the only one to present a peak consistent with hollow adsorption.

Conclusions and Future Work

The catalysts prepared by microwave and ultrasound synthesis were successfully tested in all the reactions considered in chapter 6. However, this was not without limitations. In the case of the 4-nitrophenol reduction it was observed that upon addition of NaBH₄ not only were the catalysts inactive, they also started to leach. This could be linked to leaching from the TiO₂ supported under basic conditions and could eventually be solved by subjecting the catalyst to heat treatment. This was probably caused by the presence of ethylene glycol during the support addition stage. In the case of the carbon monoxide oxidation it was also necessary to submit the catalysts to heat treatment, but this was not exclusive to the microwave and ultrasound catalysts. Also the catalyst prepared by the traditional sol-immobilization protocol needed to follow the same procedure.

Overall, it could be observed that many of the catalysts produced by microwave and ultrasound synthesis were more active than the equivalent catalysts produced by the traditional sol-immobilization protocol. Catalytic trends were as expected *i.e.* less activity as the metal nanoparticle average size increases and also as the amount of stabilizer used during synthesis increases. The latter trend was particularly visible during the cinnamaldehyde hydrogenation which used a non-polar solvent, toluene. Toluene is less likely to interact with the stabilizers and offers a catalytic activity closer to the free stabilizer scenario.

Furfural hydrogenation was an important reaction in demonstrating the advantages of adopting alternative synthesis methods for synthesis of metal nanoparticles. The selectivity could be completely shifted towards THFA due to the different types of AuPd (1:1) active sites produced when using ultrasound synthesis as the DRIFTS analysis indicated CO adsorption consistent with hollow configuration, the only catalyst to present this feature.

This PhD research gives an insight into which of the developed microwave and ultrasound sol-immobilization protocols for the synthesis of metal nanoparticles are more interesting and where future research should focus on.

In the short term it would be important for future research to continue the catalytic testing of the different reactions presented in chapter 6, potentially extending the tests to other similar reactions, for example limonene dehydrogenation where some initial work has already been developed with Pd/C catalysts. These catalytic tests should now aim to demonstrate as well how resistant to deactivation the produced microwave and ultrasound catalysts are. This can be accomplished by performing several cycles of recovering the used catalyst, performing characterisation and testing the recovered catalyst again.

Conclusions and Future Work

In the short term the developed microwave and ultrasound synthesis protocols should also be extended to the production of other metal nanoparticles, in particular with ultrasound synthesis which only considered the production of monometallic Au and Pd nanoparticles and bimetallic AuPd nanoparticles. In the case of bimetallic nanoparticles, it would be very important to consider not only a molar ratio of 1:1 but also different molar ratios. In addition to this, other types of bimetallic nanoparticles should also be considered, for example AuAg, AuIr, etc... in particular the research should focus on bimetallic nanoparticles that are difficult to produce with conventional protocols. Finally, it would also be very important to consider the production of bimetallic nanoparticles of different structures, not only of the alloy type. It is foreseen that this would require small modifications to the developed microwave and ultrasound protocols, similar to what happens with the traditional sol-immobilization protocol.

In the long term there are still important synthesis hurdles that can be identified and should be addressed. One of them would be to bring the Au nanoparticles average size below 12 nm. Another one would be to complete the ultrasound optimisation tests, similar to what was done with the microwave synthesis. To this end there are some new options to explore, for instance the synthesis and support of metal nanoparticles in only one step. This would further reduce the total production time and would likely reduce the amount of stabilizer necessary therefore increasing the catalysts activity. Another interesting option to explore would be in the case of ultrasound to control the working temperature and bring the synthesis as close as possible to room temperature from the present 70-90 °C range. This should minimise the growth step and deliver smaller average sizes.

Notes and References

- 1 F. P. Zamborini, L. Bao and R. Dasari, *Anal. Chem.* **2012**, *84*, 541-576.
- 2 OV Salata, *Journal of Nanobiotechnology* **2004**, *2*:3.
- 3 C. Zhao, L. He, S. Z. Qiao and A. P. J. Middelberg, *Chemical Engineering Science* **66** (**2011**) 1463-1479.
- 4 E. Roduner, *Chem. Soc. Rev.*, **2006**, *35*, 583-592.
- 5 M. Bowker, *The Basis and Applications of Heterogeneous Catalysis*, **1998**, Oxford Chemistry Primers.
- 6 B. Hvolbæk, T. V. W. Janssens, B. S. Clausen, H. Falsig, C. H. Christensen and J. K. Nørskov, *Nano Today*, **2007**, Vol. 2, 4.
- 7 P. Warriar and A. Teja, *Nanoscale Research Letters*, **2011**, *6*:247.
- 8 G. Schmid and B. Corain, *Eur. J. Inorg. Chem.*, **2003**, 3081-3098.
- 9 M. Haruta, *The Chemical Record*, Vol. 3, 75-87 (**2003**).
- 10 A. S. K. Hashmi and G. J. Hutchings, *Angew. Chem. Int. Ed.*, **2006**, *45*, 7896-7936.
- 11 S. Horikoshi and N. Serpone, *Microwaves in Nanoparticle Synthesis*, **2013**, Wiley VCH.
- 12 J. He, I. Ichinose, T. Kunitake, A. Nakao, Y. Shiraishi and N. Toshima, *J. AM. CHEM. SOC.* **2003**, *125*, 11034-11040.
- 13 K. Mondal and A. Sharma, *RSC Adv.*, **2016**, *6*, 83589-83612.
- 14 T. A. G. Silva, E. Teixeira-Neto, N. Lopez and L. M. Rossi, *Sci. Rep.*, *4*, 5766 (**2014**).
- 15 N. Dimitratos, J. A. Lopez-Sanchez, D. Morgan, A. F. Carley, R. Tiruvalam, C. J. Kiely, D. Bethell and G. J. Hutchings, *Phys. Chem. Chem. Phys.*, **2009**, *11*, 5142-5153.
- 16 M. Hosseini, T. Barakat, R. Cousin, A. Aboukais, B-L. Su and G. De Weireld, *Applied Catalysis B: Environmental*, 111-112 (**2012**) 218-224.
- 17 M. Zhong, **2010**. Light Scattering by Small Particles, PHY4422. [PowerPoint Presentation] Available from: <http://www.phys.ufl.edu/courses/phy4422/spring10/Reports/Light%20Scattering%20by%20Small%20Particles.pdf> [Accessed 24th April 2017].
- 18 S. Link and M. A. El-Sayed, *Annu. Rev. Phys. Chem.*, **2003**. *54*:331-366.
- 19 A. M. Schwartzberg, T. Y. Olson, C. E. Talley and J. Z. Zhang, *J. Phys. Chem. B*, **2006**, *110*, 19935-19944.
- 20 X. Huang and M. A. El-Sayed, *Journal of Advance Research*, (**2010**), *1*, 13-28.
- 21 J. Haber, J. H. Block and B. Delmon, *Pure & Appl. Chem.*, Vol. 67, Nos 8/9, pp. 1257-1306, **1995**.
- 22 F. Moreau, G. C. Bond and A. O. Taylor, *Journal of Catalysis*, *231*, (**2005**), 105-114.
- 23 C. Baltes, S. Vukojevic and F. Schuth, *Journal of Catalysis*, *258*, (**2008**), 334-344.
- 24 W. A. Spieker and J. R. Regalbuto, *Chemical Engineering Science*, *56*, (**2001**), 3491-3504.
- 25 M. Kosmulski, *Journal of Colloids and Interface Science*, *253*, 77-87, (**2002**).
- 26 J. A. Schwarz, C. Contescu and A. Contescu, *Chem. Rev.*, **1995**, *95*, 477-510.
- 27 F. Moreau, G. C. Bond and A. O. Taylor, *Journal of Catalysis*, *231* (**2005**) 105-114.
- 28 A. D. Pomogailo and G. I. Dzhardimalieva, *Nanostructured Materials Preparation via Condensation Ways*, **2014**, Springer.

Notes and References

- 29 A. Patil, M. L. Bari, B. A. Bhanvase, V. Ganvir, S. Mishra and S.H. Sonawane, *Chemical Engineering and Processing* 62 (2012) 69-77.
- 30 J. Polte, *CrystEngComm*, 2015, 17,6809.
- 31 J. Park, J. Joo, S.G. Kwon, Y. Jang, T. Hyeon, *Angew. Chem. Int. Ed.* 2007, 46, 4630-4660.
- 32 D. R. Askeland, P. P. Fulay and W. J. Wright, *The Science and Engineering of Materials Essentials of Materials Science and Engineering*, Sixth Edition, CENGAGE Learning, 2010.
- 33 N. Dimitratos, J. A. Lopez-Sanchez, D. Lennon, F. Porta, L. Prati and A. Villa, *Catalysis Letters*, Vol. 108, Nos. 3-4, 2006.
- 34 N. Dimitratos, J. A. Lopez-Sanchez, D. Morgan, A. Carley, L. Prati and G. J. Hutchings, *Catalysis Today*, 122 (2007) 317-324.
- 35 J. A. Lopez-Sanchez, N. Dimitratos, P. Miedziak, E. Ntainjua, J. K. Edwards, D. Morgan, A. F. Carley, R. Tiruvalam, C. J. Kiely and G. J. Hutchings, *Phys. Chem. Chem. Phys.*, 2008, 10, 1921-1930.
- 36 N. Dimitratos, J. A. Lopez-Sanchez, D. Morgan, A. F. Carley, R. Tiruvalam, C. J. Kiely, D. Bethell and G. J. Hutchings, *Phys. Chem. Chem. Phys.*, 2009, 11, 5142-5153.
- 37 S. Cattaneo, S. J. Freakley, D. J. Morgan, M. Sankar, N. Dimitratos and G. J. Hutchings, *Catal. Sci. Technol.*, 2018, 8, 1677.
- 38 A. Gharatape, S. Davaran, R. Salehi and H. Hamishehkar, *RSC Adv.*, 2016, 6, 111482-111516.
- 39 E. A. Sterling, J. Stolk, L. Hafford and M. Gross, *Metallurgical and Materials Transactions A*, Vol. 40A, 2009.
- 40 S. D. Solomon, M. Bahadory, A. V. Jeyarajasingam, Susan A. Rutkowsky and C. Boritz, *Journal of Chemical Education*, Vol. 84, No. 2, 2007.
- 41 G. N. Glavee, K. J. Klabunde, C. M. Sorensen and G. C. Hadjapanayis, *Langmuir*, 1992, 8, 771-773.
- 42 Q. Xiao, S. Sarina, E. Jaatinen, J. Jia, D. P. Arnold, H. Liu and H. Zhu, *Green Chem.*, 2014, 16, 4272.
- 43 J. Turkevich, P. C. Stevenson and J. A. Hillier, *Discuss. Faraday Soc.*, 1951, 11, 55-75.
- 44 G. Frens, *Nature Phys. Sci.*, 1973, 241, 20-22.
- 45 D. G. Duff, A. Baiker and P. P. Edwards, *Langmuir*, Vol. 9, No. 9, 1993.
- 46 J. L. Hueso, V. Sebastian, A. Mayoral, L. Uson, M. Arruebo and J. Santamaria, *RSC Adv.*, 2013, 3, 10427-10433.
- 47 J. Grunwaldt, C. Kiener, C. Wogerbauer and A. Baiker, *Journal of Catalysis*, 181, 223-232 (1999).
- 48 S. A. Galema, *Chemical Society Reviews*, 1997, Vol. 26, 233-238.
- 49 M. Vollmer, *Physics Education*, 39 (2004).
- 50 F. Kormin, N. H. Abdurahman, R. M. Yunus and M. Rivai, *International Journal of Engineering Science and Innovative Technology*, Vol. 2, No. 5 (2013).
- 51 S. Komarneni, D. Li, B. Newalkar, H. Katsuki and A. S. Bhalla, *Langmuir*, 2002, 18, 5959-5962.
- 52 R. Abargues, R. Gradess, J. Canet-Ferrer and K. Abderrafi, *New J. Chem.*, 2009, 33, 913-917.
- 53 A. Gautam, G. P. Singh and S. Ram, *Synthetic Metals* 157 (2007) 5-10.
- 54 K. M. Koczur, S. Mourdikoudis, L. Polavarapu and S. E. Skrabalak, *Dalton Trans.*, 2015, 44, 17883.
- 55 C. Wu, B. P. Mosher, K. Lyons and T. Zeng, *J. Nanosci. Nanotechnol.* 2010, Vol. 10, No. 4.

Notes and References

- 56 A. Zhang, L. Cai, L. Sui, D. Qian and M. Chen, *Polymer Reviews*, 53:240-276. **2013**.
- 57 D. Purves, G. J. Augustine, D. Fitzpatrick, W. C. Hall, A. LaMantia, J. O. McNmara and S. M. Williams, *Neuroscience*, **2004**, Sinauer.
- 58 L. H. Thompson and L. K. Doraiswamy, *Ind. Eng. Chem. Res.*, **1999**, Vol. 38, 1215-1249.
- 59 J. H. Bang and K. S. Suslick, *Adv. Mater.*, **2010**, 22, 1039-1059.
- 60 A. Gedanken, *Ultrasonics Sonochemistry*, 11 (**2004**) 47-55.
- 61 M. Gutierrez and A. Henglein, *J. Phys. Chem.*, **1990**, 94 (9), 3625-3628.
- 62 R. F. Contamine, A. M. Wilhelm, J. Berlan and H. Delmas, *Ultrasonics Sonochemistry*, 2 (**1995a**), S43-S47.
- 63 T. S. Awad, H. A. Moharram, O. E. Shaltout, D. Asker and M. M. Youssef, *Food Research International*, 48 (**2012**), 410-427.
- 64 Y. Song, J. Hormes and C. S. S. R. Kumar, *Small*, **2008**, 4, No. 6, 698-711.
- 65 H. S. Fogler, *Essentials of Chemical Reaction Engineering*, **2010**, Prentice Hall.
- 66 E.R. Delsman, M.H.J.M. de Croon, G.D. Elzinga, P.D. Cobden, G.J. Kramer and J.C. Schouten, *Chemical Engineering & Technology*, **2005**, 28, No. 3.
- 67 J. Wagner and J. M. Kohler, *Nano Lett.*, **2005**, 5 (4), 685 – 691.
- 68 K. V. Wong and A. Hernandez, *ISRN Mechanical Engineering*, **2012**, 208760.
- 69 R. Ciganda, N. Li, C. Deraedt, S. Gatard, P. Zhao, L. Salmon, R. Hernández, J. Ruiz and D. Astruc, *Chemical Communications*, **2014**, 50, 10126.
- 70 M. A. Newton, D. Ferri, G. Smolentsev, V. Marchionni and M. Nachtegaal, *Nature Communications*, 6, 8675 (**2015**).
- 71 B. Solsona, T. E. Davies, T. Garcia, I. Vazquez, A. Dejoz and S. H. Taylor, *Applied Catalysis B: Environmental*, 84 (**2008**), 176-184.
- 72 M. N. Taylor, W. Zhou, T. Garcia, B. Solsona, A. F. Carley, C. J. Kiely and S. H. Taylor, *Journal of Catalysis*, 285 (**2012**), 103-114.
- 73 T. Werpy and G. Petersen, *Top Value Added Chemicals from Biomass*, U. S. Department of Energy, **2004**.
- 74 S. M. Rogers, C. R. A. Catlow, C. E. Chan-Thaw, A. Chutia, N. Jian, R. E. Palmer, M. Perdjon, A. Thetford, N. Dimitratos, A. Villa and P. P. Wells, *ACS Catal.*, **2017**, 7, 2266-2274.
- 75 N. Gupta, N. Dimitratos, D. Su and A. Villa, *Energy Technol.*, **2018**, 6, 1-9.
- 76 A. S. Nagpure, L. Gurralla, P. Gogoi and S. V. Chilukuri, *RSC Adv.*, **2016**, 6, 44333-44340.
- 77 M. Grasemann and G. Laurenczy, *Energy Environ. Sci.*, **2012**, 5, 8171–8181.
- 78 S. Sharma and S. K. Ghoshal, *Renew. Sustain. Energy Rev.*, **2015**, 43, 1151–1158.
- 79 M. Yadav and Q. Xu, *Energy Environ. Sci.*, **2012**, 5, 9698–9725.
- 80 Y. Cheng, X. Wu and H. Xu, *Sustainable Energy Fuels*, **2019**, 3, 343-365.
- 81 T. Zheng, S. Bott and Q. Huo, *ACS Appl. Mater. Interfaces*, **2016**, 8, 21585-21594.
- 82 P. B. Johnson and R. W. Christy, *Physical Review B*, Vol. 6, No. 12, **1972**.
- 83 W. S. M. Werner, K. Glantschnig and C. Ambrosch-Draxl, *J. Phys. Chem. Ref. Data*, Vol. 38, No. 4, **2009**.
- 84 G. Hass, G. F. Jacobus and W. R. Hunter, *J. Opt. Soc. Am.*, 57, 758-762 (**1967**).

Notes and References

- 85 R.K. Shukla, A. Kumar, U. Srivastava, K. Srivastava and V. S. Gangwar, *Arabian Journal of Chemistry*, (2016), 9, S1357–S1367.
- 86 A. T. Mane and V. B. Patil, *Spectroscopy of Polymer Nanocomposites*, 2016, 452–467.
- 87 M. Che and J. Vedin, *Characterization of Solid Materials and Heterogeneous Catalysts: From Structure to Surface*, 2012, Wiley VCH.
- 88 C. D. Zeinalipour-Yazdi, D. J. Willock, L. Thomas, K. Wilson and A. F. Lee, *Surface Sciences*, 646 (2016) 210–220.
- 89 C. F. Poole, *The Essence of Chromatography*, Elsevier, 2003.
- 90 D. W. Sanchez, *Journal of the Forensic Science Society*, Vol. 10, 1, 1970.
- 91 V. Rao, P. Latha, P. V. Ashokan and M. H. Shridhar, *Polymer Journal*, Vol. 31, No. 10, pp 887–889 (1999).
- 92 E. W. Lemmon and R.T. Jacobsen, *Int. J. Thermophysics*, Vol. 25, No. 1, 2004.
- 93 J. Millat and W. A. Wakeham, *J. Phys. Chem. Ref. Data*, Vol. 18, No. 2, 1989.
- 94 V. Vesovic, W. A. Wakeham, G. A. Olchoway, J. V. Sengers, J. T. R. Watson and J. Millat, *J. Phys. Chem. Ref. Data*, Vol. 19, No. 3, 1990.
- 95 J. V. Sengers and J. T. R. Watson, *J. Phys. Chem. Ref. Data*, Vol. 15, No. 4, 1986.
- 96 D. R. Lide, *Handbook of Chemistry and Physics*, 2004, CRC Press.
- 97 R. Abargues, R. Gradess, J. Canet-Ferrer and K. Abderrafi, *New J. Chem.*, 2009, 33, 913–917.
- 98 W. Tu and H. Liu, *J. Mater. Chem.*, 2000, 10, 2207–2211.
- 99 S. Komarneni, D. Li, B. Newalkar, H. Katsuki and A. S. Bhalla, *Langmuir*, 2002, 18, 5959–5962.
- 100 W. Chen, J. Zhao, J. Lee and Z. Liu, *Chemistry Letters* Vol. 33, No.4 (2004).
- 101 G. Akerlof, *The Journal of the American Chemical Society*, Vol. 54, No. 11, 1932.
- 102 S. Wang, K. Qian, X. Bi and W. Huang, *J. Phys. Chem. C*, 2009, 113 (16), pp 6505–6510.
- 103 V. Etacheri, R. Georgekutty, M. K. Seery and S. C. Pillai, *Mater. Res. Soc. Symp. Proc.*, Vol. 1217, 2010.
- 104 J. W. Gilman, D. L. VanderHart and T. Kashiwagi, *Fire and Polymers II: Materials and Test for Hazard Prevention*, American Chemical Society, ACS Symposium Series 599, August 21–26, 1994.
- 105 S. Pandey, S. K. Pandey, V. Parashar, G. K. Mehrotra and A. C. Pandey, *J. Mater. Chem.*, 2011, 21, 17154.
- 106 Zawadzki, *Journal of Alloys and Compounds*, 439 (2007), 312–320.
- 107 B. Baruwati and R. S. Varma, *ChemSusChem*, 2009, 2, 1041–1044.
- 108 A. N. Grace and K. Pandian, *Materials Chemistry and Physics*, 104 (2007), 191–198.
- 109 K. Patel, S. Kapoor, D. P. Dave and T. Mukherjee, *J. Chem. Sci.*, Vol. 117, No. 4, 2005, 311–316.
- 110A. Pal, S. Shah, D. Chakraborty and S. Devi, *Aust. J. Chem.*, 2008, 61, 833–836.
- 111 W. Zhang, Q. Wang, F. Qin, H. Zhou, Z. Lu and R. Chen, *J. Nanosci. Nanotechnol.*, 2011, Vol. 11, No. 9.
- 112 M. Blosi, S. Albonetti, M. Dondi, C. Martelli and G. Baldi, *J. Nanopart. Res.*, (2011) 13:127–138.
- 113 T. Nakamura, Y. Tsukahara, T. Sakata, H. Mori, Y. Kanbe, H. Bessho and Y. Wada, *Bull. Chem. Soc. Jpn*, Vol. 80, No. 1, 224–232 (2007).
- 114 H. Zhu, C. Zhang and Y. Yin, *Nanotechnology*, 16 (2005) 3079–3083.
- 115 S. C.Y. Tsen, P.A. Crozier and J. Liu, *Ultramicroscopy*, 98 (2003) 63–72.

Notes and References

- 116 Z. R. Dai, J. P. Bradley, D. J. Joswiak, D. E. Brownlee, H. G. M. Hill and M. J. Genge, *Nature*, Vol. 418 (2002).
- 117 C. Kan, W. Cai, C. Li, L. Zhang and H. Hofmeister, *J. Phys. D: Appl. Phys.*, 36 (2003), 1609–1614.
- 118 A. Nemamcha, J. L. Rehspringer and D. Khatmi, *J. Phys. Chem. B*, 2006, 110, 383–387.
- 119 Y. Mizukoshi, T. Fujimoto, Y. Nagata, R. Oshima and Y. Maeda, *J. Phys. Chem. B*, 2000, 104, 6028–6032.
- 120 S. Anandan and M. Ashokkumar, *Ultrasonics Sonochemistry*, 16 (2009), 316–320.
- 121 Y. Jhuang and W. Cheng, *Ultrasonics Sonochemistry*, 28 (2016), 327–333.
- 122 K. Okitsu, M. Ashokkumar and F. Grieser, *J. Phys. Chem. B*, Vol. 109, No. 44, 2005.